Universidad de Barcelona
Facultad de Farmacia
Departamento de Fisicoquímica

Consejo Superior de Investigaciones Científicas
Instituto de Investigaciones Químicas y Ambientales de Barcelona
Departamento de Química de Péptidos y Proteínas

PÉPTIDOS DE FUSIÓN DEL VIRUS DE LA HEPATITIS G: DEFINICIÓN, SÍNTESIS Y CARACTERIZACIÓN BIOFÍSICA

Cristina Larios Paterna
2005

Universidad de Barcelona
Facultad de Farmacia
Departamento de Fisicoquímica

Consejo Superior de Investigaciones Científicas
Instituto de Investigaciones Químicas y Ambientales de Barcelona
Departamento de Química de Péptidos y Proteínas

PÉPTIDOS DE FUSIÓN DEL VIRUS DE LA HEPATITIS G: DEFINICIÓN, SÍNTESIS Y CARACTERIZACIÓN BIOFÍSICA

Programa de doctorado "Aliments, medicaments i salut"
Bienio: 2001-2003

Memoria presentada por Cristina Larios Paterna para optar al título de doctor por la universidad de Barcelona

Dra. Mª Asunción Alsina Esteller

Dra. Isabel Haro Villar

Cristina Larios Paterna

Cristina Larios Paterna
Barcelona, Diciembre de 2005

A Juan

Quisiera agradecer a todas las personas que han colaborado de una manera u otra en la realización de esta tesis doctoral.

En primer lugar a mis directoras de tesis, la Dra. Mª Asunción Alsina y la Dra. Isabel Haro, por haberme permitido realizar esta tesis en ambos departamentos y ayudarme en todo momento durante la realización de ésta.

Al departamento de Péptidos del CSIC. A Emili, Mari y Mª Carmen que siempre me han prestado su ayuda con mucho cariño. A todos los compañeros de laboratorio que he conocido durante todos estos años. A Núria, que me introdujo en la síntesis de péptidos. A Silvia, que siempre me solucionaba mis problemas informáticos. A Tere, siempre dispuesta a ayudar en todo. A Jordi, con el que compartí algunas dificultades con el leakage. A Marisa, que siempre me animaba para ir a comer. Y a María, Ana, Titi e Inma. A Mª José, que me ha ayudado en mi última etapa. Con todos ellos, especialmente Silvia, Tere y Marisa, he compartido mucho más que horas de trabajo.

Al departamento de Fisicoquímica, a mis compañeros, Adrià, Konrad, Alba, Carme, Marta y especialmente a la Dra. Mª Antònia Busquets que me ha ayudado mucho en la parte fisicoquímica. También me gustaría agradecer a las Dras. Marta Espina y Conxita Mestres la ayuda prestada para realizar los cálculos termodinámicos.

Al Servicio de Calorimetría del CSIC, tengo que agradecer a Amèlia López y Josep Carilla la ayuda prestada en los experimentos de DSC.

A Carmen López del Servicio de Microscopía de los Servicios cientificotécnicos de la Universidad de Barcelona.

A la Prof. Rosseneau por permitirme realizar la estancia en Gante. A Bart Christiaens por ayudarme y hacerme más agradable la estancia allí, y a la Dra. Berlinda Vanloo por sus consejos sobre fluorescencia.

Al Dr. José Miñones Trillo por permitirme realizar los experimentos en el departamento de Química Física de la Universidad de Santiago y, especialmente a José Miñones Conde por haberme introducido en la técnica del BAM.

Finalmente, a mi familia, por su apoyo desde siempre, a mis amigos y a Juan que me ha acompañado en los buenos y malos momentos.

ABREVIATURAS

A	Absorbancia
AA	Aminoácido
ADN	Ácido desoxirribonucleico
ARN	Ácido ribonucleico
Anti-E2	Anticuerpos anti proteína E2
ANTS	Ácido 8-aminonaftaleno-1,3,6-trisulfónico
BAM	Microscopía del ángulo de Brewster
CD	Dicroísmo circular
DSC	Calorimetría diferencial de barrido
DIPCDI	N,N-Diisopropiletiletilcarbodiimida
DMF	Dimetilformamida
ΔH	Incremento de entalpía
DPPC	Dipalmitoilfosfatidilcolina
DMPC	Dimiristoilfosfatidilcolina
DMPG	Dimiristoilfosfatidilglicerol
DMTAP	Dimiristoiltrimetilpropilamonio
DPX	Bromuro de N,N'-*p*-xilenobis(piridinio)
$\Delta T_{1/2}$	Amplitud del pico del termograma en el punto medio
ε	Coeficiente de extinción molar
EDT	1,2-Etanoditiol
ELISA	Ensayo inmunoenzimático
Fmoc	9-fluorenilmetoxicarbonil
FTIR	Espectroscopia de infrarrojo por transformada de Fourier
GBV-A	GB virus A
GBV-B	GB virus B
GBV-C/HGV	Hepatitis G virus
HCV	Hepatitis C virus
HEPES	Ácido N-(2-hidroxietil)piperacina-N'-(2-etanosulfónico)
HFIP	Hexafluoroisopropanol
HOBt	1-hidroxibenzotriazol
HPLC	Cromatografía líquida de alta resolución
λ	Longitud de onda
LUVs	Vesículas unilamelares grandes
MLVs	Vesículas multilamelares
MET	Microscopía electrónica de transmisión
NBD-PE	*N*-(7-nitrobenz-2-oxa-1,3-diazol-4-il)–1,2-dihexadecanoil-*sn*-glicero-3-fosfoetanolamina
PBS	Tampón fosfato
PC	Fosfatidilcolina
PFI	Péptido de fusión interno
PG	Fosfatidilglicerol
POPC	Palmitoiloleoilfosfatidilcolina
POPG	Palmitoiloleoilfosfatidilglicerol

PS	Fosfatidilserina
RET	Transferencia de energía por resonancia
Rho-PE	Rodamina B 1,2 –dihexaecanoil-*sn*-glicero-3-fosfoetanolamina
SDS	Dodecil sulfato sódico
SFV	Semliki Forest virus
SIDA	Síndrome de la inmunodeficiencia humana adquirida
SPPS	Síntesis de péptidos en fase sólida
SUVs	Vesículas unilamelares pequeñas
SV	Sendai virus
TBEV	Tick borne encephalitis virus
tBU	Alcohol terc-Butilo
TFA	Ácido trifluoroacético
TFE	2,2,2-trifluoroetanol
TIS	Triisopropilsilano
T_m	Temperatura de transición de gel a cristal líquido
UV	Espectroscopia ultravioleta
HIV	Virus de la inmunodeficiencia humana

Abreviaturas aminoácidos

A	Ala	Alanina
C	Cys	Cisteína
E	Glu	Ácido glutámico
F	Phe	Fenilalanina
G	Gly	Glicina
L	Leu	Leucina
N	Asn	Asparagina
P	Pro	Prolina
Q	Gln	Glutamina
R	Arg	Arginina
S	Ser	Serina
T	Thr	Treonina
V	Val	Valina
W	Trp	Triptófano
Y	Tyr	Tirosina

ÍNDICE

INTRODUCCIÓN

Los virus son parásitos celulares que aunque presentan material genético, necesitan una célula huésped para poderse replicar. Están compuestos por una envuelta proteica denominada cápside y un núcleo formado por material genético, que puede ser ácido desoxiribonucleico (ADN) o ácido ribonucleico (ARN), de doble cadena o de cadena sencilla. Además, ciertos virus presentan una envoltura exterior formada por una bicapa lipídica que obtienen de la célula huésped, la cual contiene glicoproteínas codificadas por el propio virus.

Para que un virus inserte el material genético en la célula huésped para poderse replicar, es necesario que previamente se produzcan una serie de pasos: primero, el virus se aproxima y se adhiere a la célula, a continuación se produce la penetración, y por último, la entrada del genoma en la célula huésped.

Los virus utilizan varios mecanismos para penetrar en la célula, la fusión de su membrana con la membrana celular, la fagocitosis o endocitosis por parte de la célula huésped, e incluso la transferencia directa [1].

La entrada en la célula de los virus con envuelta requiere normalmente una proteína de fusión que se encuentra en la superficie del virión. Algunos virus como el de la gripe [2], el de Semliki Forest [3] (SFV) o el de la encefalitis asociada a ácaros (tick-borne encephalitis virus, TBEV) [4] necesitan condiciones de acidez para activarla. En otros casos, la fusión se produce como resultado de los cambios conformacionales derivados de la unión de la proteína de fusión a los receptores celulares. En este grupo se encuentran el virus de la inmunodeficiencia humana (VIH) [5] o el virus de Sendai (SV) [6].

1 Virus de la familia Flaviviridae

La familia *Flaviviridae* está compuesta por 69 patógenos. Dentro de esta familia se encuentran tres géneros: el Flavivirus, el Hepacivirus y el Pestivirus. Los virus de esta familia presentan envuelta y una cadena de RNA sencilla de polaridad positiva [7].

El género Flavivirus contiene virus de gran importancia clínica como el virus de la fiebre amarilla, el virus de la meningoencefalitis del Nilo occidental, el virus de la encefalitis japonesa, el virus de la encefalitis asociada a ácaros (TBEV) y el virus del dengue [8]. En este género, también se encuentra el virus de la hepatitis G (Figura 1), un virus cuya patogenicidad ha sido cuestionada [9]. En el género Hepacivirus encontramos el virus de la hepatitis C, la principal causa de hepatitis crónica, cirrosis y carcinoma hepatocelular [10]. Dentro del género Pestivirus encontramos virus que infectan a animales como el virus de la de la peste porcina clásica y el virus de la diarrea bovina, pero ningún virus asociado a humanos.

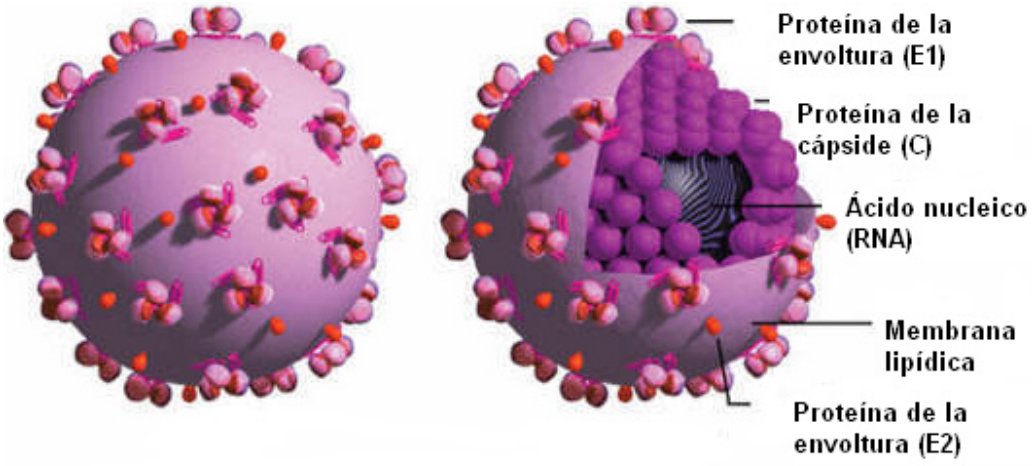

Figura 1. Estructura del virus de la hepatitis G visto desde fuera (izquierda) y con corte transversal (derecha).

1.1 Virus de la hepatitis G

El virus de la hepatitis G fue descubierto simultáneamente en 1996 por dos laboratorios distintos que lo denominaron GB virus C (GBV-C) [11] y hepatitis G virus (HGV) [12], respectivamente. Ambos laboratorios lo descubrieron procedente del plasma de un paciente con hepatitis. El grupo que lo denominó GBV-C lo aisló después de inocular el plasma de dicho paciente a tamarinos. En estos primates también se descubrieron otros virus, denominados GBV-A y GBV-B, que infectan únicamente a esta especie. Los genomas de GBV-C y HGV presentaban una homología del 96% indicando que se trataba de dos cepas de un mismo virus [9;13]. El virus GBV-C/ HGV ha sido identificado tanto en chimpancés como en humanos, aunque en cada especie las cepas son distintas [14].

La organización del genoma del virus GBV-C/ HGV es similar a la de GBV-A, GBV-B y al virus de la hepatitis C, con el cual presenta una homología del 25% en la cadena nucleotídica.

La infección con GBV-C/ HGV en humanos es frecuente y puede identificarse mediante la detección de ARN en el suero [15]. El virus puede permanecer durante muchos años sin ninguna evidencia de síntomas clínicos o enfermedad, tanto en pacientes inmunodeprimidos como en la población sana [16].

La vía principal de transmisión de este virus es a través de la sangre o de sus derivados. Personas con elevada exposición a productos relacionados con la sangre, ya sean pacientes hemodializados [17], con trasplante de órganos [18] o en personas drogadictas [19] tienen un gran riesgo de adquirir el virus de la hepatitis G, siendo del 14-38% la presencia de GBV-C/ HGV o de un 50-70% de anticuerpos anti-E2 [20;21]. Otras posibles vías de infección pueden ser mediante contacto sexual [22] o verticalmente de madre a hijo [23]. La prevalencia del virus en personas que no han estado en contacto con patógenos que puedan transmitirse a través de la sangre es del 1-4% [24;25].

El virus de la hepatitis G contiene una cadena positiva de ARN de 9.4 Kb. La poliproteína codificada presenta dos proteínas estructurales (E1, E2) y cuatro no estructurales (NS). De estas últimas, una helicasa ARN dependiente (NS3), una proteasa (NS4) y una polimerasa ARN dependiente (NS5) (Figura 2). A diferencia del virus de la hepatitis C, en el virus GBV-C/ HGV todavía no se ha identificado una proteína que forme el núcleo (core) [26].

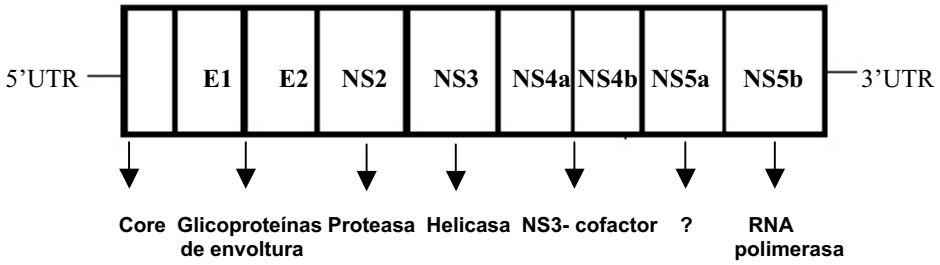

Figura 2. Poliproteína del virus de la hepatitis G que contiene la región no codificada (5'UTR y 3'UTR; UTR=untranslated region) y la región que va a codificar las proteínas: E1, E2, NS2, NS3, NS4a, NS4b, NS5a y N5b.

Las personas con una infección activa de GBV-C/HGV normalmente no presentan anticuerpos contra la proteína estructural E2 [27]. La presencia de estos anticuerpos, es indicativo de la eliminación del virus en sangre, por lo tanto, se puede determinar mediante la técnica del ELISA (ensayo inmunoenzimático) una infección pasada [28]. En donantes de sangre se han encontrado anticuerpos anti-E2 entre un 10 y un 20 % de la población [29]. Finalmente, tras un período de tiempo de unos 10 años se van eliminando los anticuerpos anti-E2 en sangre.

El virus en humanos parece ser asintomático, aunque algunos autores lo han relacionado con hepatitis crónica e incluso con hepatitis fulminante [30;31]. Se ha estudiado el posible efecto de una coinfección con el virus de la hepatitis C, pero la presencia de GBV-C/ HGV no produce ningún cambio respecto a pacientes únicamente infectados con hepatitis C [32]. Debido a su vía de transmisión, GBV-C/ HGV está presente en elevada proporción en personas infectadas con el virus causante del síndrome de la inmunodeficiencia humana adquirida (SIDA). Los estudios realizados hasta el momento, indican que la presencia de GBV-C/ HGV produce una inhibición en la replicación del virus del SIDA. El mecanismo por el cual se produce esta inhibición todavía no es del todo conocido, lo que si parece estar claro es la reducción de la progresión de la enfermedad [33-35].

Se han establecido 5 genotipos distintos para el virus de la hepatitis G distribuidos por todo el mundo. El grupo 1 se encuentra en África, y se piensa que es el ancestro común [36]. Debido a las migraciones se fue extendiendo y diversificando hacia los otros grupos existentes [37]. El grupo 2 se encuentra repartido por Europa, Estados Unidos y América del Sur. En Asia se encuentran los genotipos 3 y 4. El grupo 3 abarca el Norte de Asia y también se encuentra una variante en Sudamérica, probablemente debido a las primeras

colonizaciones. El grupo 4 se encuentra en el Sur asiático. Finalmente, el genotipo 5 se encuentra en Sudáfrica [38].

2 Interacción virus-célula

El primer paso para que se produzca una infección de un virus a una célula, consiste en la unión de las proteínas estructurales del virus con los receptores de membrana específicos de la célula, que pueden ser proteínas, lípidos o carbohidratos. Una vez que se ha producido esta unión, la entrada del virus a la célula puede realizarse mediante endocitosis o bien, por fusión de la envoltura viral con la membrana celular [39]. En este segundo mecanismo, la fusión se produce mediante unas glicoproteínas específicas del virus que, al unirse a la membrana celular, cambian su conformación y se convierten en fusogénicas. La región de la proteína que directamente interacciona con la membrana se ha denominado "péptido de fusión", y es esta región la que desencadena el proceso de entrada en la célula [40]. Los péptidos de fusión de los diferentes virus, tienen características comunes [41]. Además de los denominados péptidos de fusión, existen otras regiones en las glicoproteínas que también intervienen en el proceso de fusión [42-44].

2.1 Glicoproteínas de fusión

Se han definido dos tipos de glicoproteínas de fusión:

-Clase I: las glicoproteínas de la envoltura del virus se sintetizan como precursores inactivos, los cuales una vez escindidos por proteasas de la célula huésped son activos. La nueva región N-terminal que se forma contiene el péptido de fusión. Las proteínas de la envoltura que contienen los péptidos de fusión amino terminales, generalmente presentan estructuras de tipo α-hélice. Se ha descrito que la forma activa de la proteína de fusión es un trímero [45], el cual se coloca perpendicularmente a la membrana celular (Figura 3). La proteína de fusión más estudiada dentro de este grupo es la hemaglutinina del virus de la gripe [46]. También encontramos virus de los géneros retrovirus [47;48], paramixovirus [49] y filovirus [50].

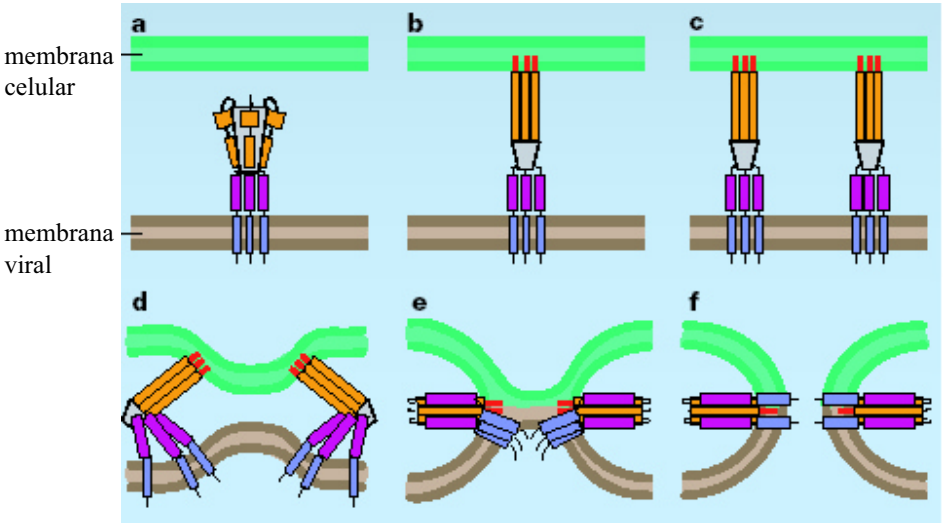

Figura 3. Mecanismo propuesto para las proteínas de fusión de la clase I. (a) Conformación metaestable de la forma trimérica de la proteína. Cada unidad está compuesta por dos dominios helicoidales (en naranja y violeta) y un dominio transmembrana (azul). (b) Después de unirse al receptor celular, la proteína presenta una conformación extendida donde el péptido de fusión se inserta en la membrana. (c) Para que se produzca el proceso de fusión es necesaria la presencia de varios trímeros. (d) La conformación de las proteínas cambia de forma que las bicapas se acercan. (e) Formación del estado de hemifusión en el cual las capas superficiales se mezclan. (f) Fusión de ambas membranas con la formación de la estructura estable de la proteína [41].

-Clase II: las proteínas de fusión de clase II, normalmente, no presentan una estructura de α-hélice, teniendo habitualmente una conformación de tipo lámina β [51]. Esta proteína se sintetiza en forma de un complejo junto a otra proteína estructural (prM en los flavivirus, pE1 en los hepacivirus) que luego se escinde en la forma activa. Generalmente, estas proteínas presentan secuencias de fusión internas (péptidos de fusión internos, PFI) que se caracterizan por tener en el centro de la secuencia un residuo de prolina cuya función es importante para producirse la fusión [52]. Dentro de este grupo, encontramos varios géneros como el rhabdovirus [53], el flavivirus [54] y el alfavirus [55]. La proteína de fusión experimenta un cambio en su conformación al ser activada en el pH ácido de los endosomas. Así, pasa de ser un dímero antiparalelo dispuesto horizontalmente en la forma inactiva a un trímero vertical en la forma activa, en el cual las subunidades permanecen en una diposición paralela (Figura 4) [56;57].

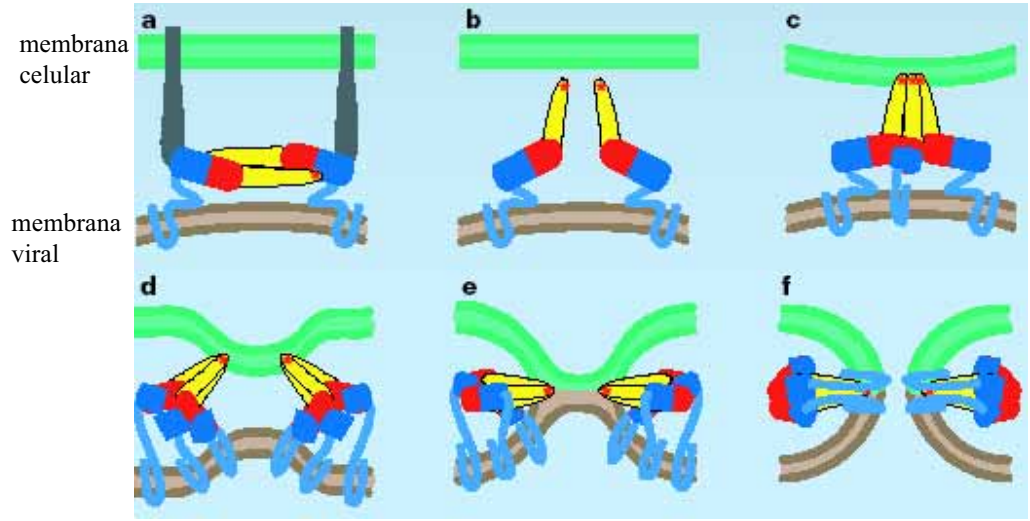

Figura 4. Mecanismo propuesto para las proteínas de fusión de clase II. (a) La proteína en forma de dímero se une al receptor celular (gris) y el virus es internalizado en los endosomas. Cada unidad está formada por tres dominios: I (rojo), II (amarillo) y III (azul). (b) El pH ácido de los endosomas provoca que los monómeros se coloquen verticalmente. (c) El loop fusogénico (puntos rojos) se inserta en la capa externa de la membrana celular, permitiendo la formación del trímero.(d) El dominio III se desplaza permitiendo que las membranas se acerquen. (e) Formación del estado de hemifusión. (f) Fusión de ambas membranas y obtención de la conformación estable de la proteína [41].

Los mecanismos de fusión de los dos tipos de proteínas (I y II) son similares a pesar de las diferencias conformacionales que existen entre ellas, ya que en ambas proteínas la forma activa es un trímero dispuesto perpendicularmente a la membrana lipídica (Figuras 3 y 4) [41].

Los péptidos de fusión suelen estar formados por una secuencia de unos 20 residuos. Los aminoácidos de pequeño tamaño como la alanina y la glicina se encuentran en elevada proporción, lo que confiere a los péptidos de fusión una elevada plasticidad, facilitando de este modo la interacción con las membranas biológicas [58]. Además, contienen una proporción elevada de aminoácidos hidrofóbicos [59]. Los péptidos de fusión se unen a la membrana celular y deshidratan la bicapa externa, consiguiendo reducir la barrera energética al formar un intermediario lipídico más curvado que finalmente deriva en la fusión de las dos membranas.

Debido a la gran importancia de los péptidos de fusión en la penetración celular, se han realizado muchos estudios con péptidos sintéticos, que corresponden al segmento de fusión del virus, con membranas celulares [60] o bien, con modelos de membrana como son los liposomas [61].

2.1.1 Péptidos de fusión de la familia Flaviviridae

Los péptidos de fusión de la familia *Flaviviridae*, se han clasificado dentro de la clase II, es decir son péptidos de fusión internos [62]. Debido a que los virus de esta familia no presentan homología en su secuencia aminoacídica, se han comparado en base a programas de predicción de estructuras secundarias [63].

Péptidos de fusión del género Flavivirus:

En este género encontramos como prototipo el virus de la encefalitis asociada a ácaros (TBEV). La estructura de la proteína de la envoltura E de TBEV se ha observado mediante cristalografía de rayos-X [64]. Se ha descrito un péptido de fusión para este virus, que se encuentra en la región interna de la proteína (región E(98-110)) [54]. En otros virus de este género, como el virus del dengue, también se ha identificado el péptido de fusión interno. La secuencia es prácticamente idéntica a la del TBEV [57;65;66]. Las proteínas de fusión de este género se sintetizan como complejos junto con otra proteína de membrana, prM (precursor de M) [56].

El virus de la hepatitis G pertenece al género Flavivirus, pero tiene una estructura similar al virus de la hepatitis C del género *Hepacivirus*, ya que existe una gran homología entre sus proteínas estructurales (E1 y E2) [67]. Aunque se ha descrito un posible péptido de fusión para el virus de la hepatitis C [63], hasta el inicio de este trabajo para GBV-C/HGV no se habían realizado estudios encaminados a la definición del péptido de fusión.

Péptidos de fusión del género Hepacivirus:

El virus de la hepatitis C es el único componente de este género. Contiene dos proteínas en la envoltura, E1 y E2, que forman un heterodímero. La situación del péptido de fusión en la proteína ha sido controvertida. Inicialmente, se propuso que el péptido de fusión se encontraba en la proteína E1 [68], pero la homología con otras proteínas de fusión de la misma familia puso de manifiesto que el péptido de fusión se localizaba probablemente en la secuencia (476-494) de la proteína E2 [55;63].

Péptidos de fusión del género Pestivirus:

En este género encontramos el virus de la diarrea bovina y el virus de la peste porcina clásica. El péptido de fusión del virus de la diarrea bovina se encuentra en la región (818-828) de la proteína E2. Esta secuencia se encontró por alineación con otras secuencias de virus de la familia F*laviviridae* (TBEV y HCV) [69].

3 Membranas biológicas

El modelo de mosaico fluido que describe las membranas lipídicas fue introducido en 1972 por Singer y Nicholson. En este modelo se muestra la bicapa lipídica como un ambiente dinámico y de aspecto líquido que permite el paso de moléculas a través de su estructura.

La membrana está compuesta básicamente de lípidos (fosfolípidos y colesterol) y proteínas. Los lípidos y las proteínas pueden estar conjugados con otros grupos como los carbohidratos. Los fosfolípidos son los lípidos más abundantes en las membranas celulares. Son componentes esenciales dada su capacidad para formar bicapas espontáneamente cuando son dispersados en agua. Este comportamiento se debe a su estructura anfifílica ya que su molécula consiste en una cabeza polar con un grupo fosfato y una región no polar hidrocarbonada. En contacto con el agua se produce el efecto hidrofóbico, generándose agregados de lípidos con las cabezas polares en contacto con el agua y las colas hidrocarbonadas en el interior (Figura 5). La estructura más favorable es la bicapa lipídica, aunque también se forman micelas y fases hexagonales invertidas.

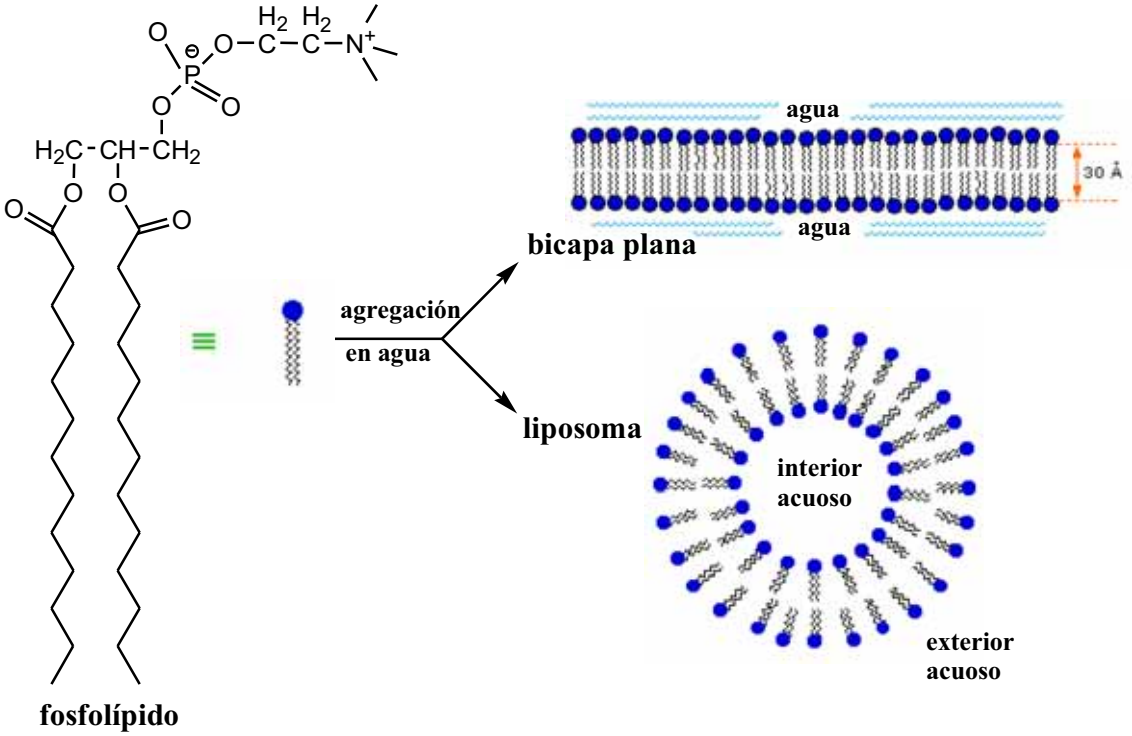

Figura 5. Estructura de los fosfolípidos al dispersarlos en agua. A la izquieda se muestra la estructura química: la molécula de glicerol se encuentra esterificada por dos ácidos grasos (región apolar) y un grupo fosfato esterificado por una base nitrogenada (colina) (región apolar). A la derecha en la parte superior se muestra la bicapa plana y en la parte inferior un liposoma.

Los fosfolípidos se clasifican en dos grupos, los glicerolípidos y los esfingolípidos. Los más abundantes en las membranas biológicas son los glicerolípidos cuya molécula se basa en el grupo glicerol. Dependiendo de los ácidos grasos que se esterifiquen obtendremos los diferentes derivados del ácido sn-glicero-3-fosfatídico [70].

El fosfolípido más utilizado en los estudios de interacciones de membranas es la fosfatidilcolina (phosphatidylcholine, PC), que tiene carácter zwitteriónico y se encuentra presente en las membranas biológicas en elevada proporción. Otros fosfolípidos ampliamente estudiados con carga negativa son el fosfatidilglicerol (phosphatidylglicerol, PG) y la fosfatidilserina (phosphatidylserine, PS), que también se encuentran presentes en

la cara interna de las membranas celulares, estando la PS presente en mayor porcentaje [71].

Existen diferentes fosfolípidos según la longitud de la cadena hidrocarbonada. Los fosfolípidos utilizados en este trabajo son tanto de origen natural como sintético. Los de origen natural consisten en una mezcla de fosfolípidos de diversa longitud de cadena hidrocarbonada y diverso grado de insaturación como la fosfatidilcolina (PC), la fosfatidilserina (PS) y el fosfatidilglicerol (PG). Por otro lado, los fosfolípidos sintéticos empleados son saturados como la dipalmitoilfosfatidilcolina (DPPC C:16, C:16), la dimiristoilfosfatidilcolina (DMPC C:14, C:14) y la 1-palmitoil-2-oleoilfosfatidilcolina (POPC C:16, C:18), todos ellos zwitteriónicos. También se han realizado experimentos con fosfolípidos con carga negativa, como el dimiristoilfosfatidilglicerol (DMPG C:14, C:14) y el 1-palmitoil-2-oleoilfosfatidilglicerol (POPG C:16, C:18), y un fosfolípido con carga positiva (el dimiristoiltrimetilpropilamonio, DMTAP C:14, C:14). El colesterol también se ha utilizado, ya que es un componente presente en las membranas celulares y tiene un efecto rigidificante.

3.1 Modelos de membrana

El estudio de las interacciones entre células y virus es muy complejo, por ese motivo se utilizan modelos simplificados como son los modelos de membranas de distinta complejidad, las monocapas y las bicapas lipídicas. La principal ventaja de estos sistemas es que se puede variar su composición, para determinar qué componentes son más importantes en las interacciones entre los fosfolípidos y las moléculas en estudio [72;73]. Los modelos de membranas utilizados en este trabajo son los siguientes:

Monocapas o capas monomoleculares: la utilización de capas monomoleculares es un método sencillo pero a su vez altamente versátil [74]. Los fosfolípidos se distribuyen formando una capa cuando son dispersados en la interfase aire-agua, situándose la parte polar hacia el agua y la parte apolar hacia el aire. Este modelo de membrana es muy útil ya que permite estudiar las interacciones de otras moléculas (por ejemplo, los péptidos) con los fosfolípidos, y luego extrapolarlo a sistemas más complejos como los liposomas [75]. Además, ésta técnica nos permite evaluar la capacidad de las moléculas en estudio de penetrar en las membranas celulares [76].

Bicapas lipídicas: los liposomas son los modelos de membrana más utilizados ya que la estructura en forma de bicapa lipídica es idéntica a la porción lipídica de las membranas celulares. Los liposomas son estructuras vesiculares submicroscópicas compuestas por moléculas anfifílicas, típicamente fosfolípidos. Al ser dispersados en agua, los fosfolípidos forman bicapas donde las cadenas hidrocarbonadas se organizan de modo que se encuentran protegidas del agua, y así el sistema es termodinámicamente favorable. Las bicapas se unen de manera que dejan en su interior el contenido acuoso. Dependiendo del número de bicapas y del tamaño del liposoma se pueden clasificar de la siguiente manera [77]:

-Liposomas multilamelares (multilamellar vesicles, MLVs): están formados por varias lamelas concéntricas (entre 7 y 10) y su tamaño es muy diverso (de 100 a 1000 nm). La obtención es muy rápida y nos permite estudiar las interacciones entre los fosfolípidos y los péptidos en estudio con técnicas como la calorimetría diferencial de barrido (DSC), la espectroscopia visible o la espectroscopia de infrarrojos por transformada de Fourier (FTIR).

-Liposomas unilamelares grandes (large unilamellar vesicles, LUVs): su tamaño oscila entre 100 y 500 nm. Estos liposomas se caracterizan por tener una tesión superficial muy similar a la de las membranas celulares (30-32 mN/m). Los liposomas unilamelares son los modelos de membrana más estudiados para intentar comprender las propiedades físicas, químicas y mecanísticas de las membranas biológicas. En esta tesis se han empleado en los estudios de fluorescencia.

-Liposomas unilamelares pequeños (small unilamellar vesicles, SUVs): tal como su nombre indica son liposomas de tamaño pequeño, entre 15-50 nm. Estos liposomas tienen una mayor curvatura que los LUVs, lo que les confiere una menor estabilidad. En este trabajo han sido utilizados en técnicas espectrofluorimétricas y en dicroísmo circular, ya que tienen la ventaja respecto a los LUVs de producir poca dispersión de la luz (light scattering).

4 Selección de las secuencias peptídicas

En la presente tesis doctoral se estudian varias secuencias peptídicas pertenecientes a la proteína estructural E2 del virus de la hepatitis G. Dado que la proteína E2 probablemente esté implicada en el proceso de fusión del virus en la célula, el estudio de secuencias peptídicas dentro de su estructura nos puede permitir definir el péptido de fusión de este virus, y por tanto, conocer mejor el mecanismo de fusión.

La selección de los posibles péptidos fusogénicos se realiza a partir del estudio de los siguientes perfiles:

-La escala de accesibilidad de Janin [78] que permite determinar los aminoácidos más expuestos en la proteína o secuencia peptídica.

-La escala de Kyte & Doolittle [79] basada en el cálculo de la hidrofobicidad media y el momento hidrofóbico. Esta escala permite evaluar la hidrofobicidad de una proteína a lo largo de su secuencia aminoacídica.

-La escala de Wimley & White [80] que refleja la capacidad de partición de las secuencias peptídicas en membranas.

-La escala de predicción de estructuras secundarias de Chou & Fasman [81] la cual se utiliza para localizar posibles giros β dentro de la proteína.

Todas estas escalas están basadas en proteínas modelo aunque se utilizan también por extrapolación en péptidos.

5 Síntesis de péptidos en fase sólida

Una vez seleccionadas las secuencias peptídicas, se lleva a cabo la síntesis manual en fase sólida.

La síntesis de péptidos en fase sólida (solid phase peptide synthesis, SPPS), descrita inicialmente por Merrifield [82], está basada en el crecimiento de una cadena peptídica mediante la adición consecutiva de aminoácidos sobre un soporte polimérico o resina al cual permanecen anclados durante toda la síntesis. Los L-α-aminoácidos adicionados se unen a través del grupo carboxilo de éstos, ya que el grupo amino se encuentra protegido temporalmente.

La estrategia utilizada para las distintas síntesis se basa en el uso de grupos protectores de tipo ortogonal: el grupo 9-fluorenilmetoxicarbonil (Fmoc) [83] para las funciones α-amino, lábiles en medio básico moderado, y el grupo terc-butilo (tBu) para las funciones de las cadenas laterales de los aminoácidos que se eliminan al final del proceso sintético en medio ácido. Una de las ventajas de la SPPS es la posibilidad de eliminar excesos de reactivos y productos secundarios mediante la filtración y el lavado del polímero que contiene el péptido en crecimiento. Con la adición de excesos de reactivos se pueden obtener rendimientos prácticamente cuantitativos.

Cada adición de aminoácido presenta el mismo ciclo:

-desprotección del grupo Fmoc mediante la adición de una mezcla de dimetilformamida (DMF) que contiene un 20% de piperidina.

-realización de un test de ninhidrina o test de Kaiser [84] para comprobar la presencia de grupos amino libres.

-adición del aminoácido protegido con el grupo Fmoc junto con los reactivos de acoplamiento, diisopropilcarbodiimida/1-hidroxibenzotriazol (DIPCDI/HOBt), en exceso de tres equivalentes.

-agitación ocasional durante las 3 horas que dura la reacción.

-lavado y test de ninhidrina para comprobar la incorporación del aminoácido.

Finalizada la síntesis se procede al secado de la resina y al desanclaje del péptido de ésta mediante un tratamiento ácido: ácido trifluoroacético (TFA) en presencia de capturadores tales como agua, etanoditiol (EDT) y triisopropilsilano (TIS). En la Figura 6 se puede observar el esquema de síntesis empleado con la estrategia de protección Fmoc/tBu.

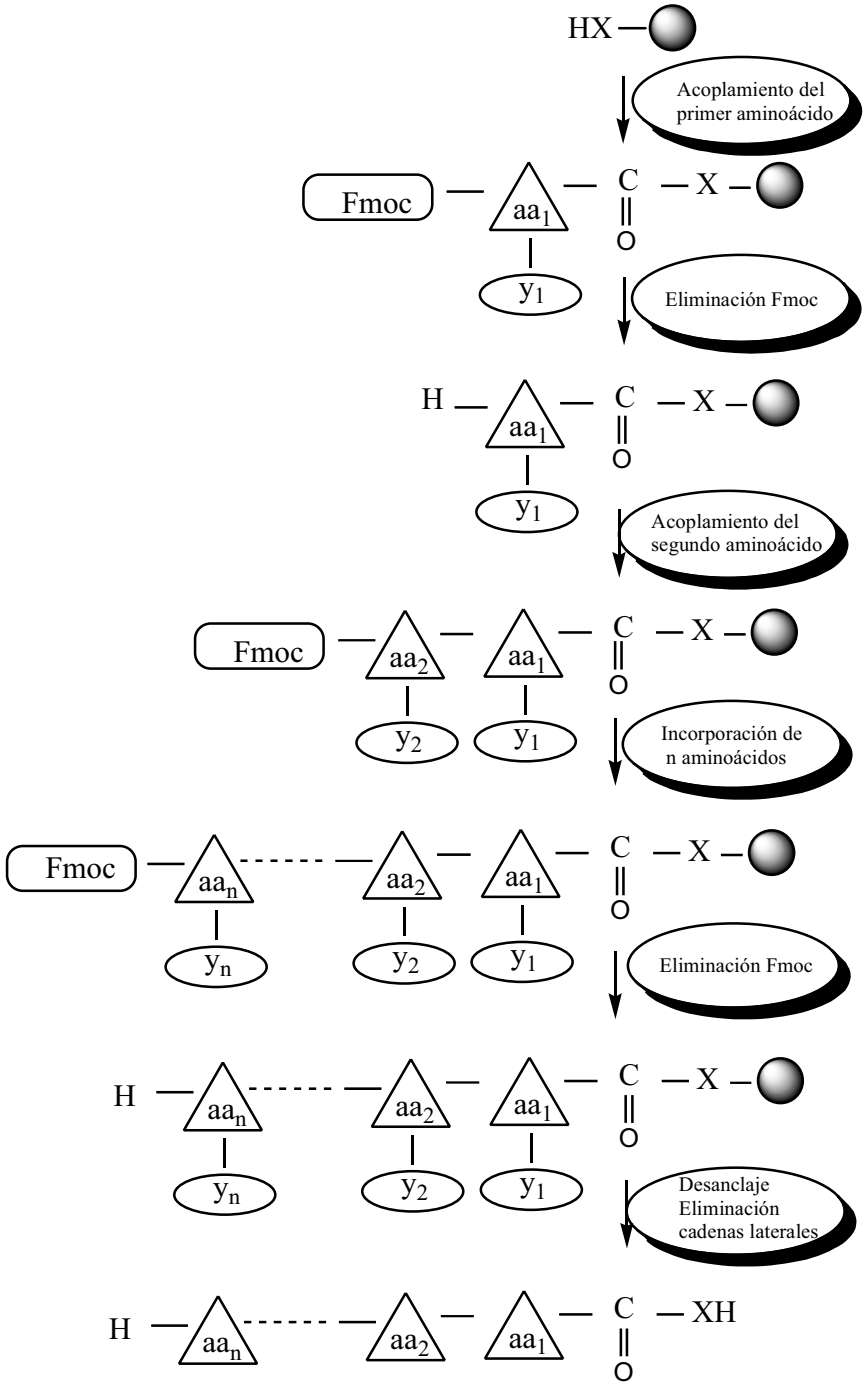

Figura 6. Esquema de síntesis en fase sólida siguiendo una estrategia Fmoc/tBu.

Una vez sintetizados los péptidos, los crudos peptídicos se purifican mediante cromatografía líquida de alta resolución (HPLC). Finalmente, son analizados mediante análisis de aminoácidos, espectrometría de masas y HPLC a escala analítica.

6 Caracterización fisicoquímica

Los péptidos sintetizados se analizan respecto a sus características fisicoquímicas y se estudian las interacciones que se producen con distintos modelos de membrana. Para ello se utilizan técnicas como las isotermas de adsorción y extensión, la calorimetría diferencial de barrido y la fluorescencia entre otras.

6.1 Isotermas de Langmuir

6.1.1 Isotermas de adsorción de Gibbs

Los compuestos anfipáticos tienden a situarse en la interfase aire-agua cuando se depositan en una subfase acuosa formándose una monocapa de adsorción. Esta propiedad produce un aumento en la presión superficial o una disminución en la tensión superficial que proporciona la medida de la actividad superficial de la sustancia. Las moléculas que se encuentran en la interfase están en equilibrio dinámico con las moléculas que se encuentran disueltas en la subfase. Cuando las moléculas se hallan en el equilibrio, el sistema se puede definir mediante la isoterma de adsorción de Gibbs [85], en la cual la cantidad de soluto adsorbido en la interfase aire-agua (Γ) es proporcional a la concentración de soluto en el líquido (c).

$$\Gamma = \frac{1 \cdot \Delta\pi}{RT \cdot \Delta \ln c} \qquad (1)$$

siendo $\Delta\pi$ la variación de la presión superficial, R la constante de los gases y T la temperatura absoluta.

A partir de esta ecuación Langmuir [86] concluyó que las moléculas adsorbidas se comportan en cierta manera como las moléculas de los gases perfectos y adquieren un cierto grado de orientación.

6.1.2 Isotermas de extensión

Cuando sustancias no volátiles o insolubles en disolventes acuosos, se extienden mediante disolventes orgánicos volátiles en la interfase aire-agua, se forman las monocapas de extensión. Para que se extienda bien una monocapa la sustancia tiene que ser anfifílica. Así, los grupos polares se dirigirán hacia la parte acuosa y los grupos apolares se situarán hacia el aire e impedirán que las moléculas difundan hacia la subfase. Al extender un fosfolípido la cabeza polar se dirige hacia la fase acuosa y las cadenas hidrocarbonadas hacia el aire.

La disposición de estas películas monomoleculares es similar a la de las membranas fosfolipídicas, por lo que se utilizan como modelos de membrana.

Una monocapa puede presentar varios estados asemejándose a los tres estados de la materia: sólido, líquido y gas. Al comprimir una monocapa se van mostrando los diferentes estados de ordenación: primero el estado gaseoso, donde las moléculas se encuentran separadas aunque existan interacciones entre ellas. Al comprimir más la monocapa aumentan las fuerzas de Wan deer Waals y las moléculas se encuentran en estado de líquido expandido (primer estado después del gaseoso) seguido del estado de líquido condensado o también conocido como sólido expandido. Finalmente se llega al estado sólido, donde las moléculas tienen una mayor ordenación molecular y ya no pueden moverse libremente [86]. Para una temperatura constante, obtendremos la isoterma de compresión π-A, si representamos el cambio de la presión superficial (mN/m) respecto al área molecular (nm^2/molécula). En la Figura 7 se representa una isoterma de compresión mostrando los diferentes estados de ordenación posibles.

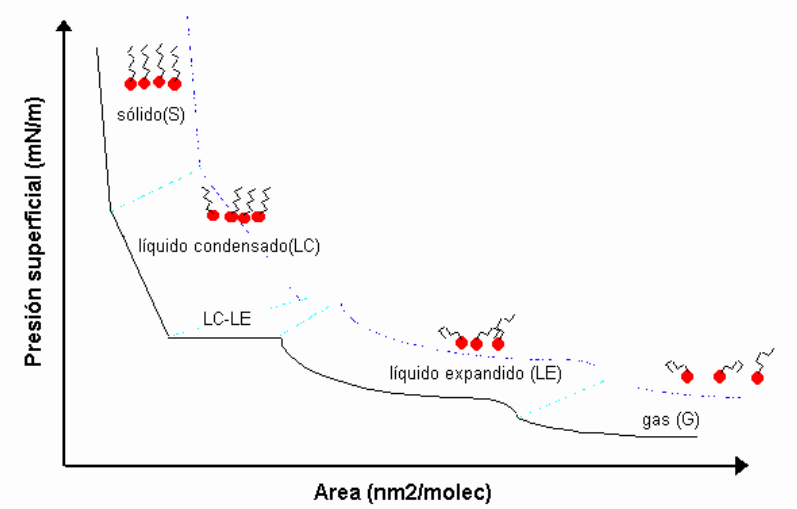

Figura 7. Isoterma de compresión donde se muestran todos los estados que se pueden presentar: estado gaseoso (G), estado de líquido expandido (LE), estado de líquido condensado (LC) y estado sólido (S).

Algunas monocapas son inestables ya que tienden a desorberse. El proceso de desorción viene dado por factores externos tales como el pK, la masa o el balance hidrofílico-lipofílico. Este proceso implica la disolución y la difusión de las moléculas en la subfase.

Otro factor importante en la estabilidad de la monocapa es la presión de colapso [87] que es la presión máxima que se puede ejercer sobre una monocapa sin que se produzca la expulsión de las moléculas que la componen. Si se sobrepasa este valor se produce la destrucción de la monocapa.

A partir de las isotermas de compresión, se puede determinar el estado de la monocapa a las diferentes presiones mediante el cálculo del módulo de compresibilidad (C_s^{-1}) para cada área [88].

$$C_s^{-1} = -A(\partial\pi / \partial A)_T \qquad (2)$$

donde ∂π/∂A es la pendiente de la curva π-A.

El módulo de compresibilidad es cero en agua y se incrementa al aumentar la cantidad de material superficialmente activo. C_s^{-1} también depende del estado de la monocapa siendo mayor para monocapas más condensadas. En función del valor de C_s^{-1} se puede determinar el estado de fase de la monocapa.

Monocapa	**C_s^{-1} (mN/m)**
Superficie limpia	0
Ideal	Π
Proteína	1 a 20
Líquido expandido	12.5 a 50
Líquido condensado	100 a 250
Sólido condensado	1000 a 2000

Polipéptidos que tengan un valor del módulo de compresibilidad entre 12.5-50 mN/m se encuentran en un estado de líquido expandido o bidimensional. Al aumentar el módulo de compresibilidad hasta valores de 100-250 mN/m, se encuentra en forma de líquido condensado y esto nos indica la formación de loops tridimensionales.

6.1.3 Monocapas mixtas

Las monocapas que están formadas por dos o más componentes nos pueden informar del tipo de interacciones que se producen entre ellos y en qué medida. Además, en los sistemas biológicos las monocapas existentes están formadas por más de un componente. Cuando se realiza la mezcla, las monocapas mixtas obtenidas pueden ser de dos tipos, miscibles cuando los componentes se mezclan perfectamente entre si, e inmiscibles cuando se producen separaciones entre ellos [89].

En una monocapa con dos componentes (A_1, A_2), el área ocupado por la mezcla ideal ($A_{1,2}$) a cualquier presión superficial será igual a:

$$A_{1,2} = x_1 A_1 + x_2 A_2 \qquad (3)$$

donde A_1 y A_2 son las áreas ocupadas por los componentes en monocapas puras y x_1, x_2 sus fracciones molares en la monocapa.

En las monocapas reales podemos encontrar las funciones de exceso (a π y a T constantes).

$$A_{ex} = A_{1,2} - (x_1 A_1 + x_2 A_2) \qquad (4)$$

donde $A_{1,2}$ es el área por molécula promedio de la mezcla de 1 y 2.

En una monocapa real, si se representa $A_{1,2}$ frente a la fracción molar y observamos una línea recta querrá decir que los componentes son inmiscibles o miscibles, pero no se producen interacciones específicas. Sin embargo, si hay un desvío indica un comportamiento no ideal, por tanto, existencia de interacciones entre los componentes.

La medida de la presión de colapso, a lo largo de todo el rango de composiciones molares, en las monocapas mixtas es también una prueba de la existencia de miscibilidad entre ellas. Cuando los dos componentes son inmiscibles, las monocapas mixtas colapsan a la misma presión superficial independientemente de la composición molar. Sin embargo, para las monocapas miscibles la presión de colapso varía en función de la composición.

Otra función que nos puede ser de gran ayuda es la energía libre de exceso, que nos sirve para conocer como se desvían del comportamiento ideal las monocapas mixtas. Las ecuaciones aplicadas son derivadas de las de Goodrich y Pagano [90;91].

$$AG_m^{ex} = \Delta G_m - \Delta G_{m(ideal)} \qquad (5)$$

$$AG_m^{ex} = \int_{\pi\to 0}^{\pi} A_{1,2} \cdot d\pi - x_1 \int_{\pi\to 0}^{\pi} A_1 \cdot d\pi - x_2 \int_{\pi\to 0}^{\pi} A_2 \cdot d\pi \qquad (6)$$

donde $A_{1,2}$ es el área por molécula promedio de la monocapa mixta; A_1 y A_2 son las áreas por moléculas media en las monocapas puras de 1 y 2; x_1 y x_2 son las fracciones molares de los componentes puros 1 y 2.

Si la monocapa es ideal $\Delta G_m=0$, pero si el valor obtenido no es igual a cero quiere decir que existen desviaciones del comportamiento ideal. Cuando $\Delta G_{ex}<0$ significa que el tipo de interacción es de atracción electrostática o que las interacciones son mayores que las de los componentes puros. Si $\Delta G_{ex}>0$ indica un predominio de repulsiones electrostáticas entre los componentes o que las atracciones son menores que las existentes en los componentes puros.

Mediante la utilización del microscopio del ángulo de Brewster (BAM) se puede resolver mejor la miscibilidad de los componentes en las monocapas mixtas.

6.2 Microscopía del ángulo de Brewster (BAM)

El estudio de la morfología y del espesor relativo de las monocapas puede realizarse mediante el microscopio del ángulo de Brewster (Brewster angle microscopy, BAM). Se trata de una técnica óptica no invasiva muy utilizada para observar los cambios de fases de las monocapas o la influencia de distintas subfases, entre otras aplicaciones. El principio

del ángulo de Brewster se basa en lo siguiente: al incidir un haz de luz no polarizada sobre una superficie transparente cuyo índice de refracción es mayor al del aire, parte de la luz se refracta y parte se refleja con luz parcialmente polarizada. La intensidad de luz reflejada depende del ángulo de incidencia (θ_i) y de la naturaleza de la interfase. La relación existente entre la intensidad de luz reflejada y la luz incidente es la medida de la reflectancia.

En una interfase Fresnel (interfase plana entre dos medios isotrópicos), donde el índice de refracción es distinto en n_1 (índice de refracción incidente) y n_2 (índice de refracción del segundo medio) la reflectancia se define por las fórmulas de Fresnel:

-reflectancia del rayo reflejado paralelo al plano de incidencia (p-polarizada)

$$R_p = \left[\frac{tg(\theta_i - \theta_r)}{tg(\theta_i + \theta_r} \right]^2 \qquad (7)$$

-reflectancia del rayo reflejado perpendicular al plano de incidencia (s-polarizada)

$$R_s = \left[\frac{sen(\theta_i - \theta_r)}{sen(\theta_i + \theta_r)} \right]^2 \qquad (8)$$

$$n_1 sen\theta_i = n_2 sen\theta_r \qquad (9)$$

El ángulo de incidencia cuando R_p=0 es el ángulo de Brewster. Para que esto suceda: $\theta_i + \theta_r = \pi/2$ (10) y esto significa que los rayos reflejado y refractado son perpendiculares. De las ecuaciones 9 y 10 se puede deducir:

$$\frac{n_2}{n_1} = \frac{sen\theta_i}{sen\theta_r} = \frac{sen\theta_i}{\cos\theta_i} = tg\theta_{Brewster} \qquad (11)$$

Si la luz incidente es p-polarizada , cuando el ángulo de incidencia es el de Brewster (53° para el agua), no hay luz reflejada. Sin embargo, cuando se deposita una monocapa en la interfase, se produce un cambio en el índice de refracción del medio así como del ángulo de Brewster, aumentando la reflectancia (Figura 8). Este aumento en la reflectancia hace que la monocapa pueda visualizarse como una imagen clara, sobre un fondo oscuro que pertenece al agua [92].

Las monocapas pueden visualizarse *in situ*, y por lo tanto, conocer mejor las interacciones y la morfología de las moléculas en estudio. La intensidad de cada punto de la imagen del microscopio depende del espesor (d) y de las propiedades ópticas de la monocapa.

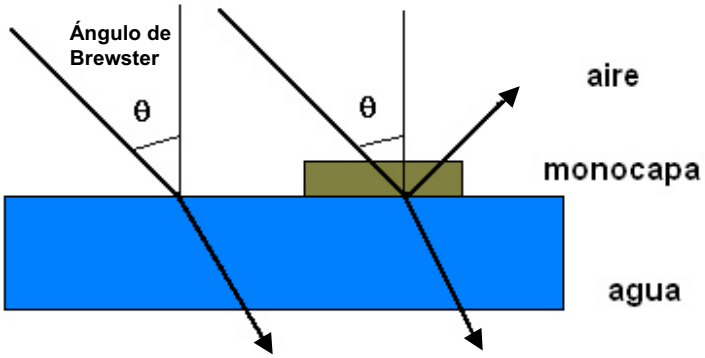

Figura 8. Esquema del cambio de la reflectividad debido a la presencia de una monocapa en la interfase aire/agua.

6.3 Calorimetría diferencial de barrido (DSC)

Las bicapas lipídicas compuestas por fosfolípidos manifiestan una transición calorimétrica principal desde una fase en estado de *gel*, a bajas temperaturas, en la cual las cadenas lipídicas se encuentran rígidas y ordenadas, a una fase de estado fluido o de *cristal-líquido* a elevada temperatura, donde las cadenas tienen un mayor movimiento y el espesor de la bicapa es menor (Figura 9). La transición de fase es un proceso endotérmico que puede ser detectado mediante técnicas físicas al variar la temperatura. En el termograma que se obtiene se observa un pico agudo y el proceso se dice que es cooperativo, es decir, que todas las moléculas tienen el cambio de fase en la temperatura de transición (Tm, temperature melting). El estudio de estas transiciones de fase proporciona un método valioso para caracterizar las propiedades del estado fluido, el cual es el más relevante en las membranas biológicas.

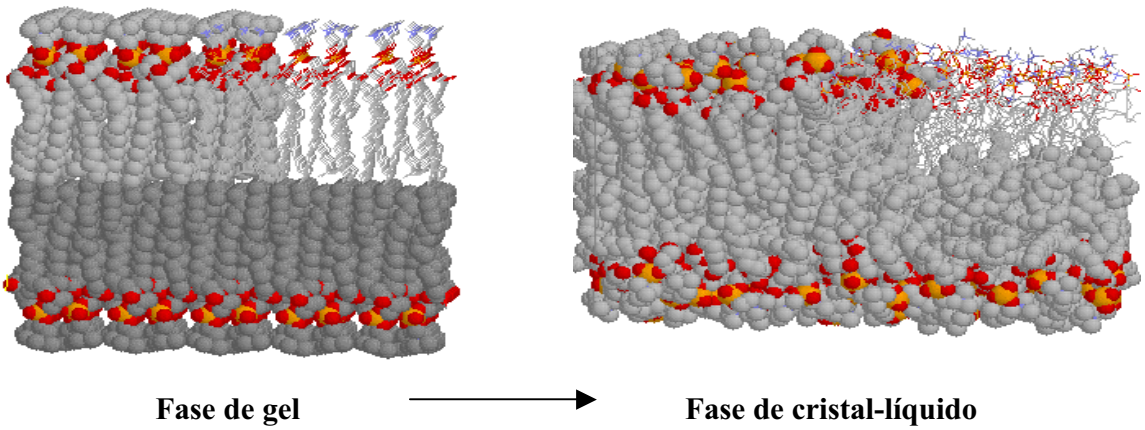

Figura 9. Esquema de la transición de fase de los fosfolípidos.

La calorimetría diferencial de barrido (differential scanning calorimetry, DSC) es una herramienta fundamental para investigar la transición de fase de los fosfolípidos en modelos de membrana. El comportamiento termotrópico de los fosfolípidos se ha estudiado ampliamente, y éste determina propiedades tales como la permeabilidad, la fusión, la agregación e, incluso, la unión a proteínas, que afectan a la estabilidad de los liposomas y a su comportamiento en sistemas biológicos [93-95].

La T_m para un fosfolípido puro tiene un valor característico que aumenta al incrementar la longitud de la cadena hidrocarbonada, dado que las interacciones hidrofóbicas que se producen son mayores. Si la bicapa está formada por fosfolípidos insaturados la temperatura de transición es menor, ya que los enlaces de tipo cis evitan un gran empaquetamiento siendo las interacciones de tipo Van der Waals menores. En las membranas biológicas esta transición de fase es mucho más amplia ya que es más compleja por estar formada por muchos componentes.

En el presente trabajo se estudian modelos de membrana constituidos por fosfolípidos y el efecto producido por los péptidos al interaccionar con éstos. Además, se analizan los parámetros típicos de los termogramas a distintas proporciones de péptido añadidos a los liposomas, como son: la temperatura a la cual se produce la transición principal (T_m), el cambio de entalpía asociado (ΔH) y la amplitud del pico asociado a la transición principal en el punto medio ($\Delta T_{1/2}$)

6.4 Espectroscopia de fluorescencia

La espectroscopia de fluorescencia es una técnica que nos ayuda a caracterizar una molécula con propiedades fluorescentes y a conocer las interacciones de ésta con los disolventes del medio, con otras moléculas o con modelos de membrana. Los péptidos son moléculas que pueden contener grupos cromóforos en su estructura, como el anillo aromático del triptófano, de la fenilalanina o de la tirosina. Así, al incidir una radiación electromagnética con una longitud de onda adecuada, la energía es absorbida por la molécula y ésta pasa de un estado electrónico fundamental a un estado excitado. Finalmente, cuando la molécula vuelve al estado fundamental la energía puede transformarse en fluorescencia al emitirse un fotón, o bien, puede haber una desactivación no radiante (colisiones entre las moléculas, disipación en forma de calor...) [96].

En la presente tesis doctoral, se analiza la fluorescencia intrínseca de los péptidos, ya que éstos contienen aminoácidos con grupos cromóforos y los cambios producidos en el entorno del grupo cromóforo (el triptófano) cuando interacciona con modelos de membrana como los liposomas. Asimismo, se mide la capacidad de los péptidos de permeabilizar las vesículas que contienen fluoróforos en su interior, la capacidad de fusionar membranas, o bien la situación de los péptidos en la membrana fosfolipídica.

6.4.1 Fluorescencia intrínseca

La fluorescencia intrínseca de los péptidos cambia según el entorno del grupo cromóforo, en nuestro caso el triptófano. El péptido en solución acuosa tiene un espectro definido por la longitud de onda en el máximo del espectro de emisión (λ) y por la intensidad de fluorescencia [97]. El estudio de los péptidos en presencia de liposomas, nos aporta información acerca del cambio en el entorno del triptófano en cada péptido, de forma que si el péptido interacciona con las vesículas fosfolipídicas, el triptófano se encuentra en un entorno más apolar. Este cambio se traduce en un desplazamiento del máximo de emisión a longitudes de onda menores (blue shift) [98].

6.4.2 Liberación de contenidos vesiculares

La capacidad de los péptidos de desestabilizar las membranas fosfolipídicas se puede observar mediante el ensayo de liberación de marcadores fluorescentes. Cuando en el interior de los liposomas se encapsula una sonda fluorescente (ANTS) y un apantallador de ésta (DPX), no se produce emisión de fluorescencia. Si el péptido es capaz de desestabilizar la membrana y liberar las sondas, el efecto de la dilución produce que el apantallador no sea efectivo y, por tanto, incrementa la intensidad de emisión de fluorescencia del ANTS. Existen otros marcadores fluorescentes (calceína) que cuando están encapsulados dentro de los liposomas y se encuentran en elevada concentración no emiten fluorescencia (autoapantallamiento). Si se produce rotura de los liposomas, la dilución de la sonda produce la emisión de fluorescencia [99-101].

6.4.3 Fusión de membranas

La capacidad de un péptido para fusionar membranas se puede medir realizando el ensayo de transferencia de energía por resonancia (resonace energy transfer, RET) de Struck [102]. En este ensayo existen dos sondas fluorescentes; un donador (NBD-PE) y un aceptor de energía (rodamina, Rho-PE), que forman parte de la composición de la bicapa lipídica (Figura 10). La sonda donadora es excitada y la energía producida de la emisión de fluorescencia sirve para excitar a la sonda aceptora. La eficacia de la transferencia de energía es mayor cuando las sondas se encuentran cercanas y es menor al aumentar la distancia. En el ensayo que se realiza se trabaja con dos poblaciones distintas de liposomas; unos liposomas sin marcar y otros marcados con las sondas fluorescentes. Si el péptido es capaz de fusionar las membranas de las distintas poblaciones, la transferencia de energía es menor y, por lo tanto, se observa un aumento en la emisión de fluorescencia de la sonda donadora.

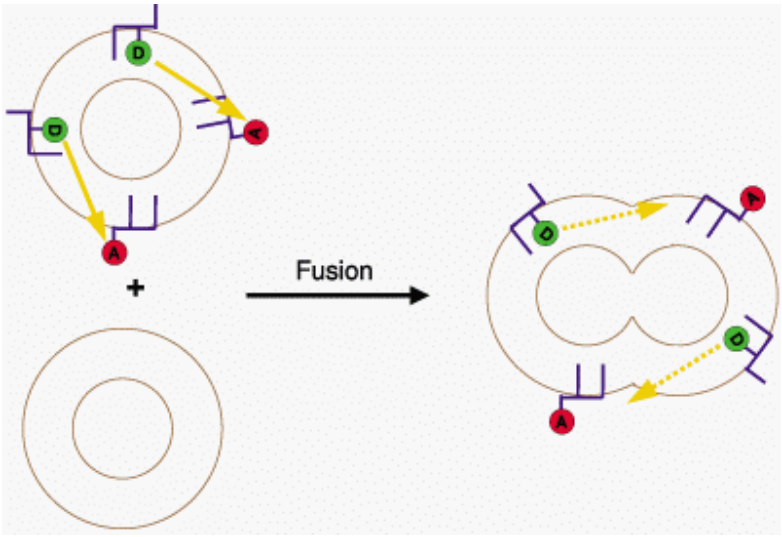

Figura 10. Esquema del ensayo de transferencia de energía por resonancia.
A: aceptor de energía, D: donador de energía.

6.4.4 Apantallamiento de sondas fluorescentes

La realización de este ensayo nos permite averiguar el cambio en la accesibilidad de un péptido cuando se encuentra en presencia de apantalladores acuosos (acrilamida) [103] o de fase orgánica (lípidos bromados) [104] y de liposomas. El efecto de los péptidos en las sondas viene dado por la interacción de éstos con los fosfolípidos. Por un lado, la sonda acuosa acrilamida esta menos apantallada en presencia de liposomas, si los péptidos interaccionan con éstos. Por otro lado, el apantallamiento en los lípidos bromados nos informa a qué nivel se encuentran los péptidos en la bicapa fosfolipídica.

6.5 Microscopía electrónica de transmisión (MET)

La MET es un tipo de microscopía que nos permite observar estructuras de un tamaño de entre 5 y 10 nm. Las muestras se depositan sobre una rejilla metálica que está recubierta de un polímero (formvar). Como las muestras biológicas son transparentes al paso de electrones se tiñen con una sustancia (uranilo) que absorbe los electrones y así se puede visualizar (tinción negativa). Una parte de los electrones rebotan o son absorbidos por el objeto y otros lo atraviesan posibilitando la observación de la imagen. La visualización de liposomas en el microscopio en ausencia o en presencia de péptido nos permite evaluar el efecto producido en la morfología de los liposomas. Esta técnica se ha utilizado para visualizar el efecto de péptidos con modelos de membrana [105;106].

6.6 Espectroscopia UV-Visible

Cuando un haz de luz monocromática atraviesa una disolución parte de la radiación puede ser absorbida. El proceso de absorción viene dado por la ley de Lambert-Beer:

$$A = \log \frac{I_0}{I} = \varepsilon \cdot b \cdot c \qquad (12)$$

donde A es la absorbancia, I_0 e I son las intensidades de radiación electromagnética incidente y transmitida, ε es el coeficiente de extinción molar o coeficiente de extinción, b el espesor de cubeta y c la concentración.

La interacción de los péptidos con células o liposomas se puede evaluar a partir de la variación en la absorbancia mediante ensayos de hemólisis o agregación, respectivamente.

6.6.1 Ensayo de agregación

En este ensayo se estudia la capacidad de los péptidos de agregar liposomas. El efecto de agregación se manifiesta como un aumento en la absorbancia de la solución. Si un péptido tiene la capacidad de producir agregados, al añadirse en una dispersión lipídica se produce un aumento de la absorbancia a una longitud de onda de 436nm [107].

6.6.2 Ensayo de hemólisis

El efecto de una sustancia hemolítica en contacto con glóbulos rojos produce un aumento en la absorbancia debido a la liberación de la hemoglobina [108-110]. Dado que se ha descrito que los péptidos fusogénicos tienen la capacidad de producir hemólisis [61], mediante este ensayo se puede medir la capacidad hemolítica de las secuencias sintetizadas.

6.7 Estudios conformacionales

El estudio de la conformación de los péptidos es importante para conocer mejor las características intrínsecas de éstos. Los péptidos de secuencia aminoacídica corta, normalmente no presentan una conformación definida. Sin embargo, si éstos son capaces de unirse a los modelos de membrana en estudio pueden adoptar una conformación más ordenada, probablemente similar a la que se encuentra en la proteína nativa. En los péptidos de fusión se ha descrito que, la conformación adoptada por éstos durante la unión a la membrana celular es muy importante para su actividad fusogénica [111;112].

La estructura secundaria, está relacionada con el ordenamiento espacial de los aminoácidos próximos entre si en la secuencia lineal. Cuando las relaciones estéricas son de naturaleza regular originan una estructura periódica. La hélice α, el giro β y la lámina β son elementos de estructura secundaria. Por el contrario, cuando una proteína o un péptido no tienen una estructura definida se dice que presentan una estructura desordenada o al azar.

Estructura de hélice α

En la estructura de hélice α la secuencia aminoacídica gira alrededor de un eje y las cadenas laterales quedan en la superficie de la hélice. Cada giro tiene una unidad repetitiva de 3.6 aminoácidos. La hélice se encuentra estabilizada por enlaces de hidrógeno de los grupos amida, entre el hidrógeno unido al nitrógeno (electropositivo) del residuo (i) y el átomo de oxígeno (electronegativo) del residuo (i+4).

Las hélices son anfipáticas; tienen una zona polar en la superficie y una zona hidrofóbica en la cara interna.

En las secuencias peptídicas las interacciones entre las cadenas laterales de los aminoácidos pueden estabilizar o desestabilizar la α-hélice. Residuos como Asn, Ser, Thr, y Leu desestabilizan la hélice. La Pro, al ser un aminoácido en el que el nitrógeno se encuentra en un anillo, le confiere mucha rigidez y no tiene hidrógeno con el que poder formar el puente de hidrógeno. Por todo ello, es el principal disruptor de α-hélices [113]. Por otro lado, aunque la Pro sea el principal agente desestabilizador, en algunos casos puede contribuir a que los residuos posteriores tengan una conformación helicoidal, ya que no necesita ningún aceptor de hidrógeno y esto es beneficioso para la estabilidad de la hélice.

Estructura de giro β

Los giros β se producen cuando la cadena peptídica cambia bruscamente y, generalmente se encuentran en zonas superficiales de las proteínas. En el giro β están involucrados cuatro residuos que están formando un ángulo de 180 grados. El giro se estabiliza por el enlace de hidrógeno que se produce entre el grupo C=O del residuo (i) y el grupo NH del residuo (i+3). En los giros es muy frecuente la presencia de Gly y Pro en posiciones (i+1) y (i+2).

Hoja plegada β

La cadena polipeptídica está prácticamente extendida en forma de lámina. La distancia axial entre los aminoácidos es de 3.5 Å y está estabilizada por puentes de hidrógeno entre grupos NH y CO de las diferentes cadenas polipeptídicas. Las cadenas adyacentes en la hoja β pueden estar dirigidas en la misma dirección (hojas β paralelas) o en direcciones opuestas (hojas β antiparalelas).

Por todo ello, se realiza el estudio de la conformación de los péptidos en solución y en presencia de modelos de membrana, lo que nos aporta información sobre la estructura de los péptidos cuando se producen las interacciones con los lípidos.

6.7.1 Espectroscopia de dicroísmo circular (CD)

La técnica de dicroísmo circular nos permite conocer la estructura secundaria de los péptidos sintetizados midiendo la actividad óptica de la molécula.

La luz plano polarizada está compuesta por dos componentes, uno circularmente a la derecha (D) y otro circularmente a la izquierda (I). Cuando dicho haz de luz atraviesa un medio ópticamente activo, podemos obtener las medidas de dicroísmo circular calculando la diferencia entre la luz absorbida por un componente respecto a otro.

$$\Delta A = Ai - Ad \qquad (13)$$

donde ΔA es la diferencia entre las absorbancias de la luz polarizada circularmente a la izquierda (Ai) y la luz polarizada circularmente a la derecha (Ad). ΔA sigue la ley de Lambert-Beer, por tanto los valores están relacionados con la diferencia entre los respectivos coeficientes de extinción ($\Delta A = \Delta\varepsilon \cdot b \cdot c$).

El grupo cromóforo mayoritario presente en los péptidos es el grupo amida que se encuentra en el enlace peptídico, así como el grupo aromático presente en las cadenas laterales de algunos aminoácidos (Trp, Tyr, Phe) [114]. En los espectros de los péptidos aparecen bandas características que dependen de los tipos de enlaces y del grado de ordenación adoptado. La polarización de la luz que sale al interaccionar con las moléculas quirales, en este caso los péptidos, es elíptica porque está formada por la combinación de dos ondas circulares de sentidos opuestos y con distinta amplitud. Los resultados se determinan en valores de elipticidad molar por residuo ($mdeg \cdot cm^2 \cdot dmol \cdot residuo^{-1}$), y éstos se obtienen a partir de la elipticidad molar dividido por el número de residuos que componen el péptido o proteína. En una proteína o péptido nos podemos encontrar con estructuras desordenadas o “random coil”, α-hélice, lámina β o giroβ (Figura 11).

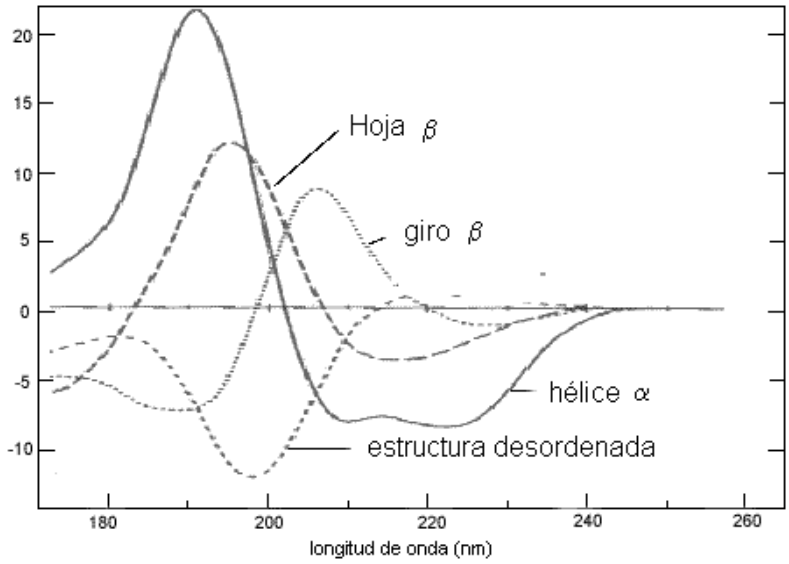

Figura 11. Espectros de dicroísmo circular de las estructuras que se encuentran en proteínas y péptidos.

Las bandas características de cada estructura aparecen a distintas longitudes de onda y con distinta intensidad. Una estructura desordenada o "random coil" presenta un mínimo intenso a 198 nm. La estructura de hélice α presenta dos bandas negativas a 222 y 208nm y una banda positiva a 191-193 nm. La lámina β presenta una banda negativa entre 210-225 nm y una banda positiva entre 190-200 nm, mientras que el giro β presenta la banda negativa a 200 nm y la banda positiva a 210 nm.

Los datos obtenidos de dicroísmo circular se pueden tratar mediante programas informáticos (por ejemplo, K2D, Contin, Lincomb-Brahms) que permiten una determinación cuantitativa de la estructura secundaria de los péptidos [115-117]. El porcentaje de α-hélice también se puede determinar utilizando el formalismo de Chen (Ecuación 14) [118], donde se asume que la máxima elipticidad teórica de un péptido o proteína a 222 nm depende del número de residuos y de la elipticidad a 222 nm de una hélice de infinita longitud.

$$\%\alpha - hélice = [\theta] \Big/ \{-39.500[1-(2.757n)]\} \qquad (14)$$

6.7.2 Espectroscopia de infrarrojo por transformada de Fourier (FT-IR)

El estudio de la conformación de los péptidos por espectroscopia de infrarrojo, se realiza mediante el estudio de las bandas de absorción producidas por la vibración de los enlaces del grupo amida en el enlace peptídico. Para las proteínas existen siete bandas amida, pero las más importantes y sensibles son la I, II y III. La mayoría de estudios utilizan la banda amida I, que aparece entre 1600 y 1700 cm^{-1} y que corresponde a la vibración del enlace C=O, C-N y N-H [119]. Como ocurre en la técnica de dicroísmo circular, dependiendo de

la posición de la banda que contiene varios componentes solapados, obtendremos una estructura secundaria distinta. La deconvolución de la banda I es más sencilla que en la técnica de dicroísmo circular porque se pueden aproximar a curvas de tipo Lorentziano o Gaussiano [120]. El análisis permite la obtención de distintas bandas con la posibilidad de calcular la proporción de cada conformación obtenida. Las longitudes de onda en las que aparecen las distintas conformaciones son las siguientes: la estructura desordenada o random coil aparece entre 1640-1650 cm^{-1}; cuando la banda se desplaza a mayor longitud de onda, aparece la hélice α hasta 1660 cm^{-1}; la lámina β se presenta entre 1615-1640 cm^{-1} con una banda secundaria en 1670-1680 cm^{-1} y la lámina β antiparalela está centrada aproximadamente en 1630 cm^{-1}; por último el giro β se localiza sobre 1660 cm^{-1}.

OBJETIVOS

El objetivo principal de esta tesis se basa en la definición del péptido de fusión del virus de la hepatitis G. Con ese fin, se pretende realizar experimentos biofísicos con diversas regiones peptídicas previamente seleccionadas y sintetizadas utilizando modelos de membrana. Los objetivos concretos encaminados a la consecución del objetivo anterior son los siguientes:

- Selección de secuencias peptídicas de la proteína estructural E2 del virus de la hepatitis G que puedan constituir el péptido de fusión del virus. La selección se realizará siguiendo dos criterios distintos: selección de la zona N-terminal y de alguna zona interna de la proteína que cumpla criterios de fusogenicidad según las escalas semiempíricas (Wimley & White, Kyte & Doolitle entre otros).

- Síntesis manual de los péptidos escogidos siguiendo protocolos en fase sólida. Purificación de las secuencias peptídicas por cromatografía de alta resolución a escala preparativa (HPLC) y caracterización mediante análisis de aminoácidos, espectrometría de masas y HPLC a escala analítica.

- Caracterización fisicoquímica de los péptidos. Estudio de la actividad superficial de los péptidos y de la capacidad de formar monocapas estables mediante la realización de isotermas de compresión.

- Estudios de la interacción de los péptidos con modelos de membrana monomoleculares. Cinéticas de penetración de los péptidos con monocapas fosfolípidicas. Isotermas de compresión de los fosfolípidos extendidos solos, de fosfolípidos con péptidos en la subfase, o de monocapas mixtas péptido/fosfolípido.

- Estudio de la morfología de las películas de los componentes estudiados (péptidos, fosfolípidos o péptido/fosfolípido) por microscopía del ángulo de Brewster (BAM).

- Estudio de la interacción de los péptidos con bicapas lipídicas (liposomas) mediante técnicas biofísicas (calorimetría diferencial de barrido, espectroscopia de fluorescencia, microscopía de transmisión electrónica y espectrometría visible). Realización de experimentos para determinar específicamente si los péptidos tienen propiedades fusogénicas (ensayos de liberación de contenidos vesiculares, de fusión, de agregación y de hemólisis).

- Estudio de la conformación adoptada por los péptidos en distintos medios (acuoso, mimético de membrana y distintos modelos de membrana) mediante las técnicas de dicroísmo circular y espectroscopia de infrarrojo por transformada de Fourier, para tratar de establecer una relación entre la estructura de los péptidos y su capacidad de interacción con los modelos de membrana utilizados.

La realización de estos objetivos se encuentran descritos en los artículos que forman la parte central de la tesis.

Artículo 1	Larios, C., Busquets, M.A., Carilla, J., Alsina, M.A., Haro, I. (2004) Effects of overlapping GBV-C/HGV synthetic peptides on biomembrane models. *Langmuir*, **20**, 11149-11160
Artículo 2	Larios C., Christiaens B., Gómara, M.J., Alsina, M.A. and Haro, I. (2005) Interaction of synthetic peptides corresponding to hepatitis G virus (HGV/GBV-C) E2 structural protein with phospholipid vesicles, *FEBS Journal,* **272**, 2456-2466.
Artículo 3	Larios, C., Casas, J., Alsina, M.A., Mestres, C., Gómara, M.J., and Haro, I., (2005) Characterization of a putative fusogenic sequence in the E2 hepatitis G virus protein, *Arch. Biochem. Biophys*., 442 (2): 149-159.
Artículo 4	Larios, C., Miñones, J.Jr., Haro, I., Alsina, M.A. and Busquets, M.A., (2005) Study of adsorption, langmuir and penetration into phospholipid monolayers of E2(279-298) peptide, J. Phys. Chem. B, enviado.

En el anexo de la presente tesis se incluyen trabajos que directa o indirectamente han ayudado a conocer las técnicas biofísicas utilizadas. Los trabajos mostrados tienen como objetivo el estudio de las interacciones entre péptidos sintéticos y modelos de membrana. Aunque el estudio que se describe en el artículo del anexo I, no forma parte del tema que se trata en esta tesis, ha tenido utilidad para entrar en contacto con los péptidos sintéticos y sus interacciones con lípidos. El trabajo descrito en el anexo IV, aunque forma parte de la sección de resultados, se ha querido incluir en el anexo debido a que el artículo en cuestión está todavía realizándose.

Anexo 1	Larios, C., Espina, M., Alsina, M.A., and Haro, I. (2004) Interaction of three beta-interferon domains with liposomes and monolayers as model membranes, *Biophys. Chem.*, **11**, 123-133
Anexo 2	Larios C., Carilla, J., Busquests, M.A., Alsina, M.A. and Haro, I., (2004) Perturbations induced by synthetic peptides belonging to the E2 structural protein of Hepatitis G virus (GBV-C/HGV) in lipid membranes: a differential scanning calorimetry study, *J. Phys. IV*, **113**, 31-34 .
Anexo 3	Larios, C., Casas, J., Alsina, M.A., Mestres, C., and Haro, I., (2005), *Interaction with membrane model systems of synthetic putative fusion peptides derived from hepatitis G virus E2 Protein*, Luminiscence, **20**, 279-281.
Anexo 4	Larios, C., Miñones J. Jr., Haro, I, Busquets, M.A, Alsina M.A, (2005), *Miscibility and Langmuir studies of the interaction of the E2(279-298) peptide sequence of GBV-C/ HGV with DPPC and DMPC phospholipids,* en preparación

Artículo 1: Efectos de tres péptidos sintéticos solapantes de GBV-C/HGV en modelos de biomembrana

Cristina Larios, María A. Busquets, Josep Carilla, María A. Alsina e Isabel Haro

Departamento de Química de Péptidos y Proteínas, Instituto de Investigaciones Químicas y Ambientales de Barcelona, IIQAB-CSIC
Departamento de Fisicoquímica, Facultad de Farmacia, Universidad de Barcelona.

Cristina Larios, María A. Busquets, Josep Carilla, María A. Alsina, Isabel Haro (2004)
Effects of overlapping GBV-C/HGV synthetic peptides on biomembrane models.
Langmuir, **20**, 11149-11160

Resumen

El presente estudio ha sido llevado a cabo para examinar las propiedades fisicoquímicas de tres péptidos solapantes pertenecientes a la proteína de la envoltura E2 del virus de la hepatitis G (GBV-C/HGV): E2(17-26), E2(12-26) y E2(7-26), y sus interacciones con modelos de membrana fosfolipídica utilizando técnicas biofísicas. Se describen los resultados relativos a la actividad superficial y a la interacción de los péptidos con monocapas y liposomas compuestos de dos fosfolípidos zwitteriónicos: dipalmitoilfosfatidilcolina (DPPC), dimiristoilfosfatidilcolina (DMPC) y una mezcla de DMPC con el fosfolípido aniónico dimiristoilfosfatidilglicerol (DMPG). Los resultados informan sobre el efecto de la longitud de cadena aminoacídica en sus interacciones con los modelos de biomembranas. El péptido de mayor longitud de cadena interacciona en mayor medida con todos los fosfolípidos estudiados como resultado de una combinación de fuerzas electrostáticas e hidrofóbicas.

Effects of Overlapping GB Virus C/Hepatitis G Virus Synthetic Peptides on Biomembrane Models

Cristina Larios,[†,‡] María A. Busquets,[‡] Josep Carilla,[§] María A. Alsina,[‡] and Isabel Haro*[,†]

Department of Peptide Protein Chemistry and Laboratory of Thermal Analysis, IIQAB-CSIC, Jordi Girona 18-26, 08034 Barcelona, Spain, and Associated Unit CSIC, Department of Physical Chemistry, Faculty of Pharmacy, University of Barcelona, Avda. Joan XXIII s/n, 08028 Barcelona, Spain

Received June 11, 2004. In Final Form: September 15, 2004

The present study was undertaken to examine the physicochemical properties of three overlapping peptides belonging to the E2 envelope protein of Hepatitis G virus (GBV-C/HGV) and its interaction with phospholipid biomembrane models using biophysical techniques. We describe our findings concerning the surface activity and the interaction of the peptides with monolayers and liposomes composed of the zwitterionic phospholipids dipalmitoylphosphatidylcholine and dimyristoylphosphatidylcholine (DMPC) and a mixture of DMPC with the anionic phospholipid dimyristoylphosphatidylglycerol. The results inform about the effect of the chain length on their interaction with biomembrane models. The longest chain peptide interacts in a higher extent with all the phospholipid studied as a result of a combination of hydrophobic and electrostatic forces.

1. Introduction

Model studies using lipid membrane systems consisting of one or few lipid components have been carried out because of the difficult accessibility of living cells. These experimental models have been performed to understand the complex interplay between the membrane structure and the activity of membrane-binding peptides, enzymes, and proteins.[1,2]

GB virus C (GBV-C) and Hepatitis G virus (HGV) are two isolates of the same virus that were independently but simultaneously identified in 1996.[3,4] GBV-C/HGV that belongs to the Flaviviridae family is an enveloped RNA virus with a single-stranded positive-sense genome of approximately 9400 nucleotides.[5] The putative structural proteins comprising the core and the two structural envelope glycoproteins, E1 and E2, are located within the N terminus of the polyprotein, while the nonstructural proteins reside within the C-terminal part.[6] GBV-C/HGV is spread worldwide, and infections with the virus have been found in healthy people and in different patient groups.[7−10] GBV-C/HGV may be transmitted via blood, via intravenous drug users, vertically/perinatally from mother to child, and by sexual contact, and it has also been found in saliva. The diagnosis of GBV-C/HGV infection is currently done by two methods: reverse transcription polymerase chain reaction that diagnoses an ongoing infection and enzyme linked immunosorbent assay that detects specific antibodies against E2 glycoprotein, indicating a past infection.[11,12]

As a result of the fact that specific interactions between peptides and membranes containing phospholipids are involved in important processes such as antigen presenting, we have studied the interaction of three putative antigenic overlapping peptides belonging to the E2 structural protein of GBV-C/HGV, namely, E2(17-26), E2-(12-26), and E2(7-26), with biomembrane models. The methods used to locate these antigenic peptide sequences have been mainly based on physicochemical structural properties such as hydrophobicity and surface accessibility.[13] In the present work we have studied the peptides in aqueous solution and in the presence of different membrane model systems composed of zwitterionic phospholipids (dipalmitoylphosphatidylcholine, DPPC, and dimyristoylphosphatidylcholine, DMPC) or mixtures of DMPC with a negatively charged phospholipid (dimyristoylphosphatidylglycerol, DMPG), to examine the influence of the electrostatic and hydrophobic components in the interaction of the synthetic peptides with lipids. To evaluate its incorporation and location in the model membrane and to study its effect on the integrity and phase behavior of the phospholipid model membrane, we have used a wide variety combination of biophysical techniques such as Langmuir−Blodgett films, differential

* Corresponding author: Dr. Isabel Haro. E-mail: ihvqpp@iiqab.csic.es. Tel.: 34 934006109. Fax: 34 932045904.
† Department of Peptide Protein Chemistry, IIQAB-CSIC.
‡ University of Barcelona.
§ Laboratory of Thermal Analysis, IIQAB-CSIC.

(1) Haro, I.; Mestres, C.; Reig, F.; Alsina, M. A. *Curr. Top. Pept. Protein Res.* **1999**, *3*, 111−121.
(2) Muñoz, M.; García, M.; Reig, F.; Alsina, M. A.; Haro, I. *Analyst* **1998**, *123*, 2223−2228.
(3) Linnen, J.; Wages, J., Jr.; Zhang-Keck, Z. Y.; Fry, K. E.; Krawczynski, K. Z.; Alter, H.; Koonin, E.; Gallagher, M.; Alter, M.; Hadziyannis, S.; Karayiannis, P.; Fung, K.; Nakatsuji, Y.; Shih, J. W.; Young, L.; Piatak, M., Jr.; Hoover, C.; Fernandez, J.; Chen, S.; Zou, J. C.; Morris, T.; Hyams, K. C.; Ismay, S.; Lifson, J. D.; Kim, J. P. *Science* **1996**, *271*, 505−508.
(4) Simons, J. N.; Pilot-Matias, T. J.; Leary, T. P.; Dawson, G. J.; Desai, S. M.; Schlauder, G. G.; Muerhoff, A. S.; Erker, J. C.; Buijk, S. L.; Chalmers, M. L. *Proc. Natl. Acad. Sci. U.S.A.* **1995**, *92*, 3401−3405.
(5) Leary, T. P. *J. Med. Virol.* **1996**, *48*, 60−67.
(6) Kim, J. P.; Fry, E. *J. Virol. Hep.* **1997**, *4*, 77−79.
(7) Saitoh, H.; Moriyama, M.; Matsumura, H.; Goto, I.; Tanaka, N.; Aarakawa, Y. *Hepatol. Res.* **2002**, *22*, 288−296.
(8) Huang, J. J.; Lee, W. C.; Ruaan, M. K.; Wang, M. C.; Chang, T. T.; Young, K. C. *Eur. J. Clin. Microbiol. Infect. Dis.* **2001**, *20*, 374−379.
(9) Tillmann, H. L.; Manns, M. P. *Antiviral Res.* **2001**, *52*, 83−90.
(10) Rey, D.; Vidinic-Moularde, J.; Meyer, P.; Schmitt, C.; Fritsch, S.; Lang, J. M.; Stoll-Keller, F. *Eur. J. Clin. Microbiol. Infect. Dis.* **2000**, *19*, 721−724.
(11) Lara, C.; Halasz, R.; Sonnerborg, A.; Sallberg, M. *J. Clin. Microbiol.* **1998**, *36*, 255−257.
(12) Dille, B. J.; Surowy, T. K.; Gutierrez, R. A.; Coleman, P. F.; Knigge, M. F.; Carrick, R. J.; Aach, R. D.; Hollinger, F. B.; Stevens, C. E.; Barbosa, L. H.; Nemo, G. J.; Mosley, J. W.; Dawson, G. J.; Mushahwar, I. K. *J. Infect. Dis.* **1997**, *175*, 458−461.
(13) Van Regenmortel, M. H. V.; Briand, J. P.; Muller, S.; Plaué, S. *Synthetic polypeptides as antigens*; Elsevier: Amsterdam, 1988; pp 1−39.

10.1021/la048551g CCC: $27.50
Published on Web 11/06/2004

scanning calorimetry (DSC), fluorescence spectroscopy, and electron microscopy. Furthermore, circular dichroism (CD) measurements were used to try to understand the structural features that may be important to explain the physicochemical properties E2 GBV-C/HGV synthetic peptides.

2. Materials and Methods

2.1. Chemicals. DPPC, DMPC, and DMPG were purchased from Avanti Polar-Lipids, Inc. Their purity was higher than 99%, and they were used without further purification. Chloroform and methanol pro-analysis used as spreading solvents for the lipids were from Merck. The water was purified by deionization and then by passing it through a Millipore Milli-Q purification system (Milli-Q system, Millipore Corp.; 18.2 MΩ cm and pH 5.8). Dimethylformamide (DMF) was purchased from Sharlau. Rink Amide MBHA resin and amino acid derivatives were obtained from Novabiochem. Coupling reagents were obtained from Fluka and Novabiochem. Trifluoroacetic acid (TFA) was supplied by Merck, and scavengers such as 1,2-ethanedithiol (EDT) or triisopropylsilane (TIS) were from Sigma-Aldrich. Phosphate buffered saline (PBS), pH 7.4 (17 mM NaH_2PO_4, 81 mM Na_2HPO_4, 50 mM NaCl), and 5 mM *N*-2-hydroxyethylpiperazine-*N*′-2-ethanesulfonic acid (Hepes) buffer, pH 7.4, were used.

2.2. Peptide Syntheses. The syntheses of E2(17-26), E2(12-26), and E2(7-26) were carried out in the solid phase following a Fmoc/tBut strategy. The peptides were obtained manually on a Rink Amide MBHA resin (0.65 mequiv/g) by means of a *N*,*N*′-diisopropylcarbodiimide/1-hydroxybenzotriazole activation. For difficult couplings 2-(1*H*-benzotriazole-1-yl)-1-3-3-tetramethyluronium tetrafluoroborate and *N*,*N*′-diisopropylethylamine agents were used. Threefold molar excesses of Fmoc-amino acids were used throughout the synthesis. The stepwise addition of each residue was assessed by the Kaiser test.[14] During the synthetic processes carried out to obtain the peptides, repeated couplings for the incorporation of Trp^{17}, Glu^{12}, Pro^{10}, Arg^{9}, and Gly^{7} were needed. Peptide resins were removed from the reaction column and washed with DMF, isopropyl alcohol, and ether and dried in a vacuum. Final deprotection of the side-chain functional groups and cleavage of peptides from the resin were simultaneously achieved by a mixture of TFA and scavengers (H_2O, TIS, and EDT), at room temperature for about 3 h with occasional agitation. The crude peptides were precipitated with diethyl ether. Then, the samples were washed to remove the scavengers, dissolved in water, and lyophilized. Crude peptides were purified by semipreparative high performance liquid chromatography (HPLC) in a C-18 silica column. The peptides were eluted with a linear acetonitrile gradient from 10 to 40%, containing 0.05% TFA in water at a flow rate of 2 mL/min and detected at 215 nm. Purified peptides were characterized by analytical HPLC, amino acid analysis, and electrospray mass spectrometry (ES-MS).

2.3. Monolayer Studies. The experiments were performed on a Langmuir film balance KSV5000 (Helsinki, Finland) equipped with a Wilhelmy platinum plate.

2.3.1. Surface Activity. Surface activity measurements were carried out in a cylindrical trough (volume 70 mL, 30 cm^2) with mechanical stirring. The trough was filled with PBS, and increasing volumes of concentrated peptide solutions (mg/mL) were injected directly into the subphase through a lateral hole. Pressure increases were recorded continuously for 60 min.[15]

2.3.2. Insertion of Peptides into Monolayers. The same methodology was used in the presence of phospholipid monolayers. Monolayers were formed by spreading the phospholipids from a 1 mg/mL stock solution in chloroform/methanol (2:1; v/v), directly to the air−water interface, to reach the required initial surface pressure (5, 10, or 20 mN/m). After pressure stabilization, the peptide solution was injected directly underneath the monolayer and pressure increases were recorded as previously described.[16]

2.3.3. Compression Isotherms. Compression isotherms were carried out in a Teflon trough (surface area 17 000 mm^2, volume 1000 mL). The surface pressure of the monolayers was measured by a Wilhelmy plate pressure sensor, and the system was periodically calibrated with stearic acid. The uncertainty in the area per molecule obtained from the isotherms was about ±5%. Phospholipid or peptide films were spread from 1 or 2 mg/mL chloroform/methanol (2:1; v/v) solutions, respectively, and at least 10 min were allowed for solvent evaporation. The monolayer was compressed with an area reduction rate of 20 mm^2/min up to its collapse pressure. All experiments were performed at 21 ± 1 °C. Each run was repeated three times, and the reproducibility was ±0.01 nm^2/molecule.[17]

2.4. Vesicles Preparation. Lipid vesicles of different lipid compositions were prepared for DSC and fluorescence measurements. Pure DPPC, DMPC, or DMPC/DMPG (2:1) were separately dissolved in a chloroform/methanol (2:1, v/v) mixture, and the lipid solutions were dried under a nitrogen stream. The samples were stored overnight in a vacuum oven at room temperature to eliminate the residual solvent. Then, the lipid films were hydrated with Hepes buffer (5 mM, pH 7.4). Multilamellar vesicles (MLVs) for DSC were obtained by vortexing the mixtures at a temperature above the highest gel to liquid-crystalline phase transition of the sample. For fluorescence purposes, large unilamellar vesicles (LUVs) of DPPC, DMPC, and DMPC/DMPG (2:1) were prepared by hydration of the lipid film with Hepes buffer followed by 10 freeze−thaw cycles. LUVs were made by standard extrusion techniques using two 100-nm polycarbonate filters (Nucleopore, Pleasanton, CA) in a high-pressure extruder (Lipex, Biomembranes, Vancouver, Canada) above the transition temperature of the phospholipids.[18] Phospholipid concentration was determined by phosphorus quantification as previously described.[19] The liposome's size was measured by the sample diffusion coefficient by photon correlation spectroscopy (Coulter N4 MB, Luton, U.K.) and was of 90 ± 9 nm with a polydispersity index lower than 0.15.

2.5. DSC Measurements. A total of 30 μL of MLVs were sealed in standard aluminum calorimetric pans (40 μL) and submitted to three heating/cooling cycles. The final lipid concentration was 0.6 μmol of DPPC or 3 μmol of DMPC and DMPC/DMPG (2:1). MLVs were prepared as described in section 2.4 and analyzed alone or with peptides at different lipid/peptide molar ratios.

Data from the first scan was always discarded to avoid mixing artifacts. The endothermic peak from the second scan of the control sample was used as a reference template. Scans were carried out in a DSC 821e Mettler Toledo (Greifensee, Switzerland) calorimeter, at heating and cooling rates of 5 °C min^{-1} over the sample from 0 to 60 °C for DPPC MLVs and from 0 to 40 °C for DMPC and DMPC/DMPG (2:1) MLVs. The calorimeter was calibrated using indium.[20] Molar enthalpies of transition (ΔH) were calculated from peak areas by means of START Mettler Toledo system software.

2.6. Fluorescence Measurements. Fluorescence experiments were performed on a Perkin-Elmer (Beaconsfield Bucks, U.K.) spectrofluorimeter LS 50, using 1-cm path length quartz cuvettes. The excitation and emission bandwidths were set at 6 nm each, the wavelength used being 280 and 340, respectively. Emission fluorescence spectra were recorded for each peptide at a 1 μM concentration in 5 mM Hepes, pH 7.4, at room temperature by the incremental addition of 4−16 μL aliquots of a 7 mM phospholipid solution. The lipid to peptide molar ratios were 25:1, 50:1, 100:1, 200:1, 300:1, 400:1, and 500:1. Suspensions were continuously stirred, and they were left to equilibrate for 3 min before recording the spectrum. Fluorescence intensities were corrected for a light scattering contribution by subtraction

(14) Kaiser, E.; Colescott, R. L.; Bossinger, C. D.; Cook, P. I. *Anal. Biochem.* **1970**, *34*, 595−598.
(15) Gómara, M. J.; Girona, V.; Reig, F.; Alsina, M. A.; Haro, I. *Mater. Sci. Eng., C* **1999**, *8*−*9*, 487−493.
(16) Mestres, C.; Ortiz, A.; Haro, I.; Reig, F.; Alsina, M. A. *Langmuir* **1997**, *13*, 5669−5673.
(17) Alsina, M. A.; Pérez, J. A.; García, M.; Reig, F.; Haro, I. *Supramol. Sci.* **1997**, *4*, 195−199.
(18) Elorza, B.; Elorza, M. A.; Sainz, M. C.; Chantres, J. R. *J. Microencapsulation* **1993**, *10*, 237−248.
(19) Böttcher, C. S. F.; Van Gent, C. M.; Fries, C. *Anal. Chim. Acta* **1961**, *24*, 203−204.
(20) Rojo, N.; Gómara, M. J.; Alsina, M. A.; Haro, I. *J. Pept. Res.* **2003**, *61*, 318−330.

of the appropriate vesicle blank and a parallel lipid titration of *N*-acetyltriptophanamide, which does not interact with lipids.[21] The absorbance of peptide samples was measured by using a LKB-Biochrom Ultrospec II Spectrophotometer at 280 and 340 nm.

Assuming a two-state equilibrium between water-soluble aggregates and membrane-bound peptides, the apparent mole fraction partition coefficients were determined by fitting the binding curves, obtained after representing the quotient between fluorescence intensity of titrated samples and that corresponding to peptide solutions at the same solution (F/F_0) versus the lipid/peptide relationship, to the equation $I = f_{bound}I_{max} + (1 - f_{bound})I_0$, for which I is the relative fluorescence intensity, I_0 is the intensity in the absence of lipid, and $f_{bound} = K_xL/(W + K_xL)$, where K_x is the mole-fraction partition coefficient, L is the lipid concentration, and W is the molar concentration of water (55.3 M at 25 °C).

2.7. Electron Microscopy. The peptide−vesicle complexes were obtained by incubating phospholipid vesicles (0.14 mM) with the peptide (40 μM) at 37 °C for 1 h. Carbon-coated grids were hydrophilized by glow discharge, and a drop of MLVs with or without peptide was placed on the grid. The samples were stained with 2% uranyl acetate solution[22] and examined in an electron microscope (Hitachi H-600 AB Electron Microscope).

2.8. CD Measurements. Far-UV CD spectroscopy was performed on a Jasco J720 spectropolarimeter (Hachioji, Tokyo, Japan). A quartz cell with a 1.0-mm path length was used with low peptide concentrations (15−100 μM) to avoid peptide complex formation. All measurements were performed at 5 °C flushed with nitrogen (20 L min^{-1}), and the results were plotted as the mean residue ellipticity $[\theta]_{mrw}$ (deg·cm^2·$dmol^{-1}$) against the wavelength λ (nm).

Peptide conformation experiments were recorded in aqueous buffer and in the presence of structure-promoting solvents, such as trifluoroethanol (TFE) and hexafluoroisopropanol (HFIP) or in a mimetic membrane environment of sodium dodecyl sulfate (SDS). Data from five consecutive scans were averaged and processed to improve the signal-to-noise ratio. Before reading the peptide spectra, a blank spectrum of the buffer solution (5 mM Hepes, pH 7.4) was subtracted. The spectra were measured between 190 and 260 nm using a spectral bandwidth of 1 nm and a scan speed 10 nm/min. The percentage of α-helix conformation in the peptides was estimated using the formalism of Chen et al.[23] This approach assumes that the maximum theoretical ellipticity for a given peptide or protein at 222 nm may be derived from the number of amino acid residues n and the ellipticity at 222 nm of a helix of infinite length is described by eq 1.

$$\% \text{ α-helix} = [\theta]/\{-39.500[1 - (2.75/n)]\} \quad \text{deg·cm}^2\text{·dmol}^{-1} \tag{1}$$

Another method for estimating secondary structure and for quantification of the experimental CD results was deconvolution of the spectra using K2D, Lincomb-Brahms, and Contin programs[24] in a compatible computer.

3. Results and Discussion

3.1. Selection of GBV-C/HGV Domains and Peptide Synthesis. The selection of GBV-C/HGV peptides from structural E2 protein was performed by alignment of 31 published sequences of virus isolates from the Genbank database (Table 1). The consensus sequences obtained by means of a comparative study of the GBV-C/HGV isolates using the Clustalw program (www.ebi.ac.uk/clustalw) were defined by analyzing the accessibility profile of the protein according to Janin[25] and the hydrophobicity at interface of E2 protein as determined by the Wimley and White scale.[26] The selected peptide sequences belong to the amino terminal portion of E2 that is most likely exposed on the virion surface and could be recognized by neutralizing antibodies.[27] Figure 1 illustrates the accessibility and hydrophaty plots that correspond to the structural E2 protein. The location of the selected peptide fragments is indicated.

Table 1. Alignment of a Fraction of the N Terminus (1-26) of the E2 Protein from 31 Published Sequences of the HGV Virus, from the Genbank Database

HGV/GBV-C	E2(1-26)
U36380_Africa	APASVLGSRPFEAGLTWQSCSCRSNG 26
AF006500_China_	APASVLGSRPFEAGLTWQSCSCEANG 26
AB003292_Japan_	APASVLGSRPFEPGLTWDSCSCRANG 26
U75356_China_	APASVLGSRPFEPGLTWQSCSCRANG 26
D87714_Japan_	APASVLGSRPFEPGLTWQSCSCRANG 26
D87709_Japan_	APASVLGSRPFEPGLTWQSCSCRANG 26
AB003288_Japan_	APASVLGSRPFEPGLTWQSCSCRANG 26
D87262_Japan_	APASVLGSRPFEPGLTWQSCSCRANG 26
D87263_Japan_	APASVLGSRPFEPGLTWQSCSCRANG 26
D87715_Japan_	APASVMGSRPFEPGLTWQSCSCRANG 26
D87711_Japan_	APAAVMGSRPFEPGLTWQSCSCRANG 26
D87712_Japan_	APAAVLGSRPFEPGLTWQSCSCKSNG 26
D90601_Japan_	APASVMGSRPFEPGLTWQSCSCKSNG 26
AB008335_Japan_	APAAVLGSRPFEPGLTWQSCSCXANG 26
AB013500_Ghana_	VPVSVLGSRPFEPGLTWQSCSCRSNG 26
D87708_Japan_	APASVLGSRPFEPGLTWQSCSCRSNG 26
AB003293_Japan_	APASVLGSRPFEPGLTWQSCSCRSNG 26
U94695_USA_	APASVLGSRPLQPGLTWQSCSCRSNG 26
D90600_Japan_	APASVLGSRPFDYGLTWQSCSCRANG 26
AF104403_Europe_	APASVLGSRPFDYGLTWQSCSCRANG 26
U45966_USA_	APASVLGSRPFDYGLTWQSCSCRANG 26
AB003289_Japan_	APASVMGSRPFDFGLTWQTCSCRANG 26
AB003290_China_	APASVMGSRPFDFGLTWQTCSCRANG 26
U44402_USA_	APASVLGSRPFDYGLTWQTCSCRANG 26
AF031827_USA_	APASVMGSRPFDYGLTWQSCSCRANG 26
AF031828_USA_	APASVMGSRPFDYGLTWQSCSCRANG 26
AF031829_USA_	APASVMGSRPFDYGLTWQSCSCRANG 26
AB013501_Bolivia_	APASVMGSRPFDYGLTWQSCSCRSNG 26
D87255_Japan_	APASVLGSRPFDRGLTWQSCSCRANG 26
D87710_Japan_	APASVLGSRPFDRGLTWQSCTCRANG 26
U63715_Africa	APASVLGSRPFDRGLTWQSCSCRANG 26

The selected peptide sequences were successfully synthesized following the strategy described in the experimental section. Yields based on peptidyl−resin weight increase were almost quantitative. Crude peptides were purified by semipreparative HPLC using acetonitrile gradients in aqueous 0.05% TFA. Purified synthetic products were characterized by HPLC, amino acid analyses, and ES-MS (Table 2). Aliquots of lyophilized peptides were quantified by absorbance measurements at 280 nm and stored at −20 °C until their use.

3.2. Lipid Monolayers as a Membrane Model.

3.2.1. Surface Activity. While E2(17-26) did not show surface activity as a result of its high hydrophilicity, when E2(12-26) and E2(7-26) were injected into an aqueous subphase, the surface tension at the air/water interface was lowered, thus, indicating an accumulation of the peptides into the interface. The E2(12-26) and E2(7-26) incorporation in the surface increased with concentration up to saturation. To evaluate the surface activity, the excess and area/molecule at the interface were calculated by applying eqs 2 and 3 and the results are shown in Table 3.

$$\Gamma = \Delta\pi/RT\,\Delta \ln c \tag{2}$$

$$A = 1/\Gamma N \tag{3}$$

where R is 8.31 J/(K mol), T is the temperature (294 K),

(21) De Kroon, A. I.; Soekarjo, M. W.; De Gier, J.; Oekruisff, B. *Biochemistry* **1990**, *29*, 8229−8240.
(22) Grau, A.; Ortiz, A.; de Godos, A.; Gómez Fernández, J. C.; *Arch. Biochem. Biophys.* **2000**, *377*, 315−323.
(23) Chen, Y. H.; Yang, J. T.; Chau, K. H. *Biochemistry* **1974**, *13*, 3350−3359.
(24) Greenfield, N. S. *Anal. Biochem.* **1996**, *235*, 1−10.
(25) Janin, J. *Nature* **1979**, *277*, 491−493.
(26) Wimley, W. C.; White, S. H. *Nat. Struct. Biol.* **1996**, *3*, 842−848.
(27) Takahashi, K.; Hijikata, M.; Aoyama, K.; Hoshino, H.; Hino, K.; Mishiro, S. *Int. Hepatol. Com.* **1997**, *6*, 253−263.

Table 2. Peptide Characterization

peptide	amino acid analysis[a]	HPLC[b]	ES-MS[c]
E2(17-26): WQSCSCRANG	N = 1.53(1); S = 1.15(2); Q = 1.09(1); A = 1.07(1); G = 1.09 (1); R = 0.88 (1)	$k' = 2.8$	$[M^+]$: 1110.7
E2(12-26): EPGLTWQSCSCRANG	N = 1.62(1); T = 0.88(1); S = 1.29(2); Q = 2.20(2); P = 1.39(1); G = 1.94(2); A = 1.14(1); L = 0.91(1); R = 0.93(1)	$k' = 3.6$	$[M^+]$: 1608.0
E2(7-26): GSRPFEPGLTWQSCSCRANG	N = 1.96(1); T = 1.08(1); Q = 2.63(2); P = 2.53(2); G = 3.30(3); A = 1.40(1); L = 1.11(1); F = 0.92(1); R = 0.93(1); S = 2.62 (3)	$k' = 5.2$	$[M^+]$: 2152.8

[a] Amino acid analysis (theoretical values in parentheses). [b] Eluents, (A) H_2O (0.05% TFA) and (B) CH_3CN (0.05% TFA); gradient, 85% A to 65% A in 30 min; detection, $\lambda = 215$ nm; flow, 1 mL/min. [c] Matrix-assisted laser desorption ionization time-of-flight mass spectrometry.

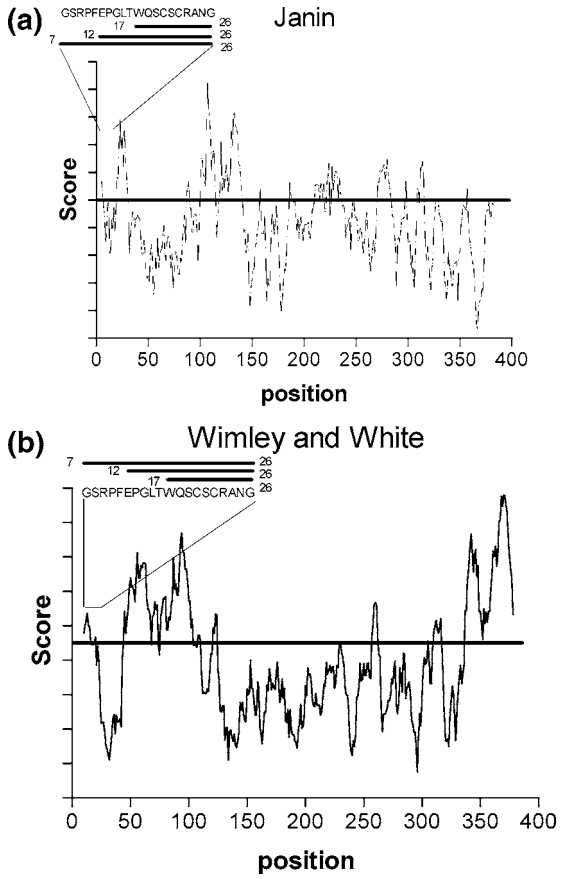

Figure 1. (a) Protein profile (mean value for a window of nine amino acids) elaborated using the Janin accessibility scale and (b) hydrophaty plot (mean value window of 19 amino acids) elaborated using the Wimley and White scale. The locations of E2(17-26), E2(12-26), and E2(7-26) sequences are indicated.

$\Delta\pi$ is the pressure increase achieved after 120 min, c is the peptide concentration, and N is the Avogadro number.

The pressure increases for E2(12-26) and E2(7-26) were 10 ± 0.2 and 11 ± 0.4 mN/m at the highest peptide concentration, respectively. The surface excess and area/molecule calculated[28] were very similar, being approximately 7.0×10^{-7} mol/m^2 and 2.2 nm^2/molecule, respectively. $\Delta\pi$ versus concentration for the peptides showing surface activity, E2(12-26) and E2(7-26), had a linear increase at low concentrations, which is a typical behavior of surface-active peptides (figure not shown).

Table 3. Pressure Increase, $\Delta\pi$; Surface Excess Concentration, Γ; and Molecular Area, A, for the E2(12-26) and E2(7-26) as a Function of the Peptide Concentration (c) in the Subphase

peptide	c (μM)	Γ (mol/m^2)	$\Delta\pi$ (mN/m)	A (nm^2/molecule)
E2(12-26)	0.99	3.9×10^{-7}	6.60	4.26
	1.65	5.2×10^{-7}	8.10	3.19
	2.66	4.9×10^{-7}	8.50	3.39
	3.29	6.9×10^{-7}	10.0	2.40
E2(7-26)	0.66	3.6×10^{-7}	6.50	4.61
	0.99	4.7×10^{-7}	7.90	3.53
	1.83	7.5×10^{-7}	11.1	2.21
	2.32	7.5×10^{-7}	11.1	2.21
	3.22	7.9×10^{-7}	11.1	2.10

3.2.2. Insertion of Peptides into Monolayers. The lipid monolayers assayed were composed of zwitterionic lipids such as DPPC and DMPC or mixtures of DMPC with the anionic lipid DMPG. Two different concentrations of peptides were injected into the subphase at a slightly lower peptide saturation concentration found in the previous experiments to assess that the peptide behavior with lipids does not depend on the concentration.

Peptide injection beneath the lipid monolayer resulted in an increase in surface pressure indicating peptide interaction with the lipid. $\Delta\pi$ was highly dependent on the initial surface pressure and lipid composition. Figure 2a−c shows the end point pressure difference or maximum pressure increases at 5, 10, and 20 mN/m of initial surface pressure for each peptide with the three lipid compositions used. The general trend observed from these plots indicates that the interaction with lipids increases in the order E2-

(28) Sospedra, P.; Haro, I.; Alsina, M. A.; Reig, F.; Mestres, C. *Langmuir* **1999**, *15*, 5303−5308.

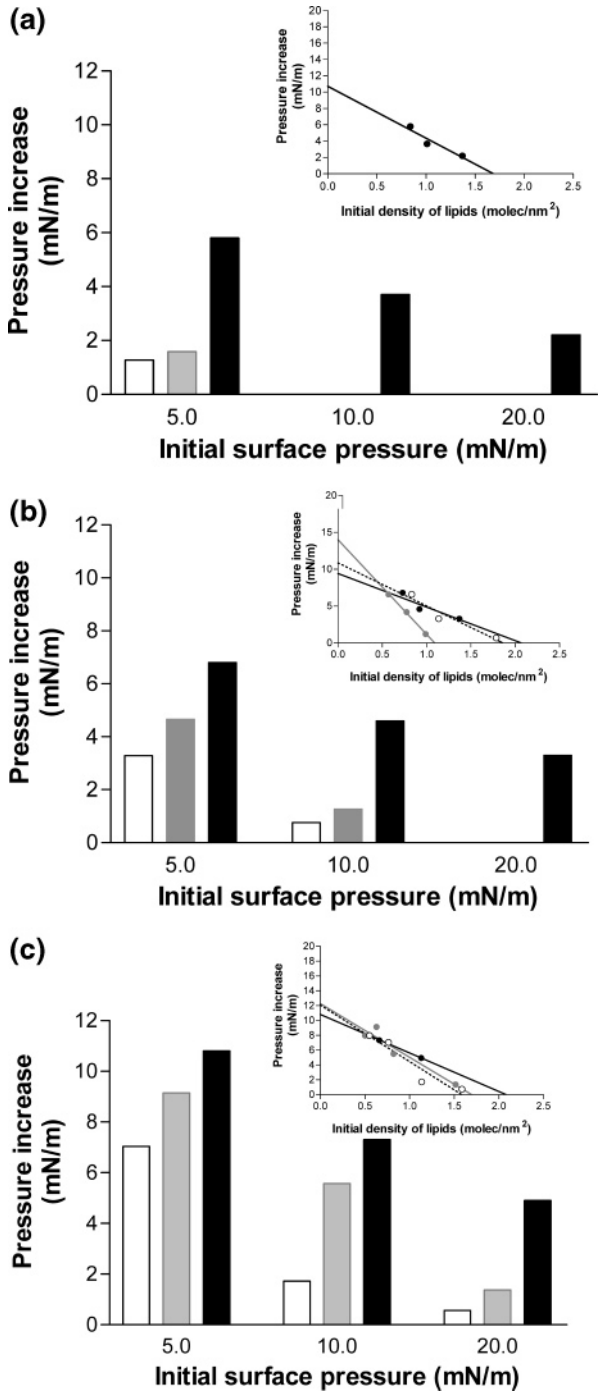

Figure 2. Pressure increases versus the initial surface pressure (5, 10, or 20 mN/m) of DPPC (empty bars), DMPC (grey bars), or DMPC/DMPG (2:1; black bars) in the presence of (a) E2(17-26), (b) E2(12-26), and (c) E2(7-26). Peptides were injected into the subphase beneath the monolayer spread at an air/water interface. The peptide concentrations were 1.83 μM for E2(17-26) and E2(7-26) and 1.65 μM for E2(12-26). The inset plots the $\Delta\pi$ values as a function of the initial density of lipids (molecule/nm^2). DPPC (open circle); DMPC (grey circle); and DMPC/DMPG (2:1; black circle). Symbols represent triplicate measurements, and lines were generated by the linear regression of the data points.

(17-26) < E2(12-26) < E2(7-26). Thus, the longer the peptide, the higher $\Delta\pi$. The charge of the lipid monolayer also plays a role on surface pressure increase. The interaction increases in the order DPPC < DMPC < DMPC/DMPG. E2(17-26) and E2(7-26) are positively charged peptides whereas E2(12-26) is neutral. A higher interaction of the positive peptide E2(17-26) with the negative lipid DMPG was expected than that observed with the neutral E2(12-26); however, the hydrophobic contribution seems to be more relevant than the electrostatic one.

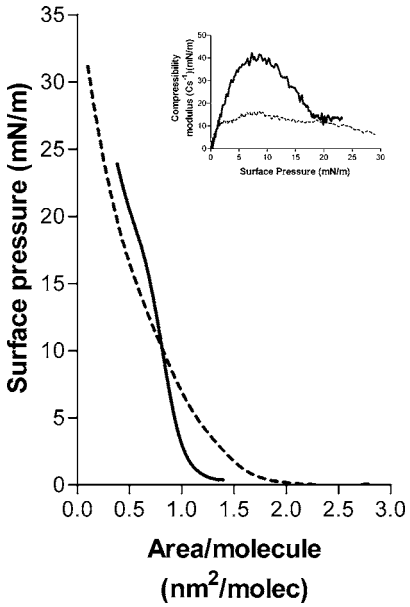

Figure 3. $\pi-A$ isotherms of E2(12-26) (continuous line) and E2(7-26) (dotted line) at the air/water interface at 21 ± 1 °C. Peptides were spread from chloroform/methanol (2:1; v/v) solutions onto a PBS at pH 7.4. [5.59 10^{16} molecules for E2-(12-26) and 2.79 × 10^{16} molecules for E2(7-26)]. The inset shows the elastic compressibility modulus versus surface pressure ($C_s^{-1}-\pi$).

To get more insight about the interaction between peptides and monolayers, exclusion density (σ_{ex}), which gives information about the capacity of penetration of the peptides in the monolayer, was calculated.[29] Insets of Figure 2 (a−c) illustrate the lipid density versus pressure increases, for the three peptides and the three lipid compositions. As expected from previous results, the highest value of σ_{ex} corresponds to the anionic mixture DMPC/DMPG (2:1), being 2.1 molecule/nm^2 for the longest and intermediate peptide and 1.7 molecule/nm^2 for the shortest. As far as the zwitterionic compositions are concerned, the last peptide does not show any interaction neither with DPPC nor with DMPC. E2(12-26) shows a higher affinity for the rigid DPPC than for the fluid DMPC, σ_{ex} being 1.8 ± 0.3 and 1.1 ± 0.1 molecule/nm^2, respectively. Finally, for E2(7-26) no significant differences are observed for DMPC and DPPC with a σ_{ex} of about 1.7 ± 0.2 molecule/nm^2.

3.2.3. Compression Isotherms of Peptides. Several peptide concentrations were spread on a PBS surface but only the longer and intermediate sequences were able to form monolayers because of the large solubility of the polypeptides as stated by the hysteresis cycles (figure not shown), as well as by the value of the area per residue calculated from the isotherm (see below). Figure 3 shows for these peptides the typical dynamic isotherms characterized by an S shape and with an inflection point corresponding to two-dimensional closed packed residues.[30] The apparent area per residue calculated at the inflection point is for both peptides around 0.05 nm^2 instead of the characteristic value of 0.15 nm^2 when no solubilization occurs. Although the E2(12-26) isotherm

(29) Maget-Dana, R. *Biochim. Biophys. Acta* **1999**, *1462*, 109−140.
(30) MacRitchie, F. *Chemistry at Interfaces*; Academic Press: San Diego, 1990.

looks more condensed than that corresponding to the longer peptide (the last one reaches smaller areas), both peptides showed smooth $\pi-A$ curves. To get clearer information about these monolayer states, the elastic compressibility modulus [$C_s^{-1} = -A(d\pi/dA)$, where $d\pi/dA$ is the slope of the πA curve] was calculated and plotted versus surface pressure ($C_s^{-1}-\pi$; inset Figure 3). The higher the value for C_s^{-1}, the lower was the interfacial elasticity and, thus, the tighter is the monolayer. At low surface pressures (high areas) C_s^{-1} is very low, characteristic of a two-dimensional state. Upon compression, we observe significant differences in C_s^{-1} for the two peptides. Values for E2(7-26) are low (the maximum value about 15 mN/m) and very similar in all the surface pressures. For E2(12-26) the shape of the plot shows a gradual increase of C_s^{-1} that reaches its maximum at 43 mN/m and decreases to 15 mN/m as the surface pressure increases, indicating a more condensed state than the longer peptide. Despite these differences, according to the literature[30] typical pressures for a two-dimensional state of polypeptides before the formation of three-dimensional loops are comprised between 12.5 and 50 mN/m.

Because the main aim of this experiment was to assess the peptide ability to form stable monolayers, peptide molecules spread onto the surface were different for E2-(12-26) and E2(7-26) being 5.59×10^{16} and 2.79×10^{16} molecules, respectively.

Although conclusions about peptide conformation based solely on dynamic $\pi-A$ isotherms are subject to uncertainty because of factors such as peptide dissolution into the subphase and deviations from ideal packing geometry, several authors have predicted peptide conformation from the isotherm shape.[31−33] In our case, the limiting area of the isotherms is concerned, and it is very similar for both peptides, about 1 ± 0.03 and 0.8 ± 0.05 nm^2/molecule for E2(12-26) and E2(7-26), respectively. These areas are considerably smaller than that expected for a helical peptide monolayer with the molecules lying flat on the water.[34] Also, it should be mentioned that the rather small chain length of these peptides (15 and 20 amino acids) should not favor intramolecular cross-β folding of the peptide chains.[31] From these results we are not able to predict a preferential peptide orientation by this system.

3.2.4. Interaction of the Peptides with Lipid Monolayers. The effect of the peptide contained in the subphase on the lipid compression isotherms shape and area/molecule was evaluated. The same lipids used in the insertion experiments were selected for these types of measurements. The $\pi-A$ isotherm of DPPC shows a phase transition at about 5 mN/m as described in the literature.[35] In the presence of the peptides, it becomes broader and appears at higher areas. E2(17-26) has a slight expanding effect on the DPPC monolayer at pressures below 40 mN/m (Figure 4a). Above this value, the shape of the isotherm in the presence and absence of this peptide is identical, indicating that the peptide has been squeezed out from the interface. The expanding effect on the isotherm that represents an increase in molecular area induced by the insertion of the peptides into the lipid monolayer is more evident in the longer peptides. The neutral peptide, E2(12-26), shifted

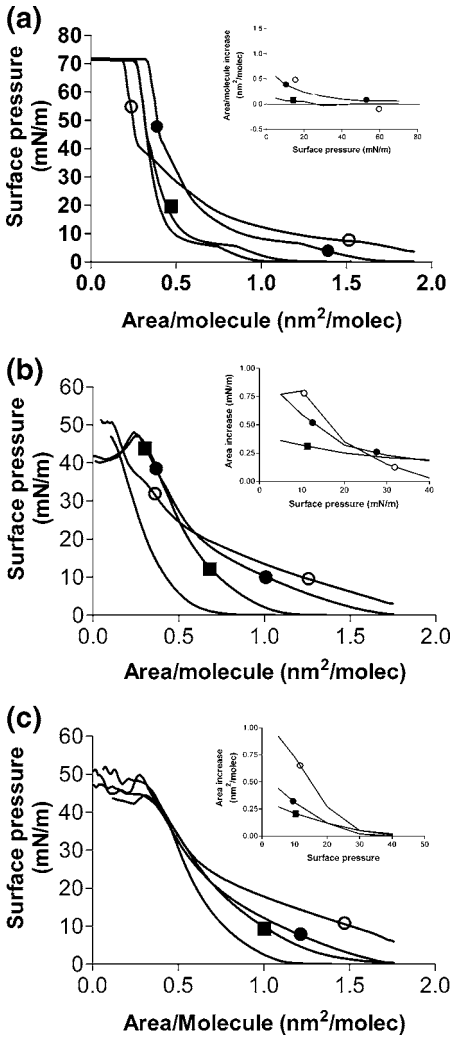

Figure 4. Compression isotherms of (a) DPPC, (b) DMPC, and (c) DMPC/DMPG (2:1) in the presence of 0.99 μM E2(17-26) (■); E2(12-26) (●); or E2(7-26) (○) into the PBS suphase at pH 7.4. The inset shows for each lipid composition the area increase calculated by subtracting the area/molecule in the presence of peptide into the subphase from the area/molecule of the isotherm of the pure lipid(s).

the $\pi-A$ isotherm toward higher areas during all the compression cycles. This indicates the incorporation of the peptide into the monolayer as a consequence of hydrophobic forces because both components lack charge. The longest peptide sequence, E2(7-26), shows an expanding effect up to a pressure of 35 mN/m. At higher values an unexpected monolayer contraction was observed. Such a decrease in the area occupied per molecule suggests the formation of peptide/phospholipid domains as observed with other peptides. For all the peptides, the collapse pressure was reached at the same value, 71 mN/m. Similar are the results observed with the fluid DMPC, where the remarkable shift of the $\pi-A$ isotherms toward higher areas increases with peptide length regardless of the peptide charge, indicating lipid−peptide miscibility (Figure 4b). However, as observed with DPPC for the longer peptide, area/molecule decreases from 20 to 38 mN/m, quicker than for the other two peptides and area/molecule values, and approaches that of the pure lipid. At 38 mN/m there is a change in the isotherm slope, suggesting the collapse point and multilayer formation.[36] DMPC isotherms in the presence of E2(17-26) or E2(12-26) collapse at the same pressure.

(31) Maget-Dana, R.; Lelièvre, D.; Brack, A. *Biopolymers* **1999**, *49*, 415−423.
(32) Bi, X.; Flach, C. R.; Pérez-Gil, J.; Andreu, D.; Oliveira, E.; Mendelshon, R. *Biochemistry* **2002**, *41*, 8385−8395.
(33) Fullagar, W. K.; Aberdeen, K. A.; Bucknall, D. G.; Kroon, P. A.; Gentle, I. R. *Biophys. J.* **2003**, *85*, 2624−2632.
(34) Dieudonné, D.; Gericke, A.; Flach, C. R.; Jaing, X.; Farid, R. S.; Mendelsohn, R. *J. Am. Chem. Soc.* **1998**, *120*, 792−799.
(35) Trommeshausser, D.; Silke, K.; Bergelson, L. D.; Galla, H.; *Chem. Phys. Lipids* **2000**, *107*, 83−92.

Table 4. Limiting Area for E2(17-26), E2(12-26), and E2(7-26) Obtained from $\pi-A$ Isotherms of DPPC, DMPC, or DMPC/DMPG (2:1)

	limiting area (nm^2/molecule)		
	DPPC	DMPC	DMPC/DMPC (2:1)
pure lipid	0.42	0.32	0.72
Peptide			
E2(17-26)	0.40	0.66	0.82
E2(12-26)	0.50	0.79	0.90
E2(7-26)	0.35	0.55	0.90

On the other hand, the charge and length seem to influence peptide incorporation into DMPC/DMPG (2:1) monolayers (Figure 4c). The highest expansion is observed with the largest and most positive peptide, thus, indicating an electrostatic and hydrophobic contribution. The neutral E2(12-26) and the shortest and positive E2(17-26) show a similar isotherm being identical above the surface pressure of 20 mN/m. For E2(17-26) and E2(12-26), the $\pi-A$ isotherm coincides with that corresponding to the pure lipid mixture at pressures higher than 35 mN/m and for E2(7-26) at values higher than 42 mN/m.

To clarify the extent of peptide interaction with lipid monolayers we have calculated the area increase by subtracting the area/molecule of the isotherm of the pure lipid(s) from the area/molecule of the same isotherm in the presence of peptide into the subphase (inset of Figure 4).

Table 4 shows the limiting area, A_0, for the different lipid compositions. For DPPC and the mixture DMPC/DMPG, the A_0 values are very similar. More significant are the differences observed with DMPC. For all the lipid compositions, the highest A_0 value corresponds to the intermediate peptide while the longest one has the smaller values, except for the lipid mixture DMPC/DMPG with a value equal to that of E2(12-26). If comparing with the pure lipid, peptide presence in the subphase results in an increase in A_0, except for the system E2(17-26)−DPPC.

Fluidity of the monolayer has a clear influence on peptide interaction as observed if comparing DPPC and DMPC isotherms. The ability of the peptides to shift the $\pi-A$ isotherm toward higher areas is greater for DMPC than for DPPC.

For all lipids, the presence of the longest peptide results in a pressure increase of approximately 5 mN/m before compression, as a consequence of peptide insertion into the lipid monolayers regardless of its charge or rigidity of the lipid acyl chains.

3.3. Lipid Vesicles as the Membrane Model.

3.3.1. DSC Studies. DSC was used to study the effect of the three synthetic peptides on MLVs of different lipid compositions. Lipid membranes are characterized by a thermotropic phase transition between an ordered gel state and a disordered liquid-crystalline phase. The parameters studied in the phase transition are the phase transition temperature (T_m), which is the gel−liquid to crystal transition; the width at half-height of the endothermic peak ($\Delta T_{1/2}$), which measures the cooperatively of the transition; and the enthalpy of the transition (ΔH) obtained by integrating the peak areas in the thermograms.

Interactions of the peptides with a bilayer ordered structure could influence vesicle transition thermotropic parameters. Table 5 shows the effect in the thermotropic parameters of MLVs of zwitterionic DPPC and DMPC and a mixture of DMPC with the anionic phospholipid DMPG after the addition of 0, 2, 5, 10, 20, and 30 mol % of the three overlapping peptides. Experiments were performed in triplicate, and the obtained standard deviation values for T_m, ΔH, and $\Delta T_{1/2}$ were lower than 0.3, 3.5, and 0.4, respectively.

The chain melting transition (T_m) of DPPC and DMPC was not significantly affected by the addition of GBV-C/

Table 5. Thermotropic Parameters of the Gel to Liquid-Crystalline Phase Transition of DPPC, DMPC, and DMPC/DMPG (2:1) MLVs Prepared in the Presence of Peptides E2(17-26), E2(12-26), and E2(7-26) at 0, 2, 5, 10, 20, and 30 mol %

	T_m[a] (°C)	ΔH (kJ/mol)	$\Delta T_{1/2}$[b]
DPPC	41.5	34.9	0.7
	E2(17-26)		
2%	41.5	31.0	0.8
5%	41.5	26.5	0.8
10%	41.6	30.1	0.8
20%	41.7	27.9	1.1
30%	41.7	28.4	1.0
	E2(12-26)		
2%	42.2	20.3	1.2
5%	41.5	23.6	0.7
10%	41.5	42.1	0.7
20%	41.6	25.5	0.9
30%	41.7	25.0	1.0
	E2(7-26)		
2%	41.5	26.2	0.7
5%	41.3	35.4	0.6
10%	41.3	20.6	0.7
20%	41.3	25.2	0.7
30%	41.4	27.0	0.9
DMPC	23.4	18.6	0.7
	E2(17-26)		
2%	23.4	18.0	0.9
5%	23.4	18.0	1.1
10%	23.6	17.8	1.2
20%	23.6	17.2	1.3
30%	23.7	16.6	1.5
	E2(12-26)		
2%	23.2	17.1	0.8
5%	23.1	15.2	1.0
10%	23.1	11.7	1.2
20%	23.2	11.2	1.8
30%	23.1	6.7	2.7
	E2(7-26)		
2%	23.9	17.8	1.4
5%	23.7	15.7	1.1
10%	23.6	15.5	1.1
20%	23.7	10.9	2.0
30%	25.3	10.8	4.9
DMPC/DMPG (2:1)	23.9	20.5	2.2
	E2(17-26)		
	24.2	19.7	2.6
2%	24.3	20.4	3.1
5%	23.4	20.4	3.2
10%	24.4	16.7	2.6
20%	24.5	11.7	3.0
30%			
	E2(12-26)		
2%	24.4	18.4	3.2
5%	24.5	19.5	3.7
10%	24.8	19.1	3.4
20%	25.8	13.0	4.3
30%			
	E2(7-26)		
2%	23.9	22.1	2.5
5%	24.0	22.1	2.6
10%	24.3	19.8	4.1
20%	27.6	9.4	5.9
30%			

[a] Main transition peak temperature. [b] Temperature width at half-height of the heat absorption peak.

(36) Leonard, M. R.; Bogle, M. A.; Carey, M. C.; Donovan, J. M. *Biochemistry* **2000**, *39*, 16064−16074.

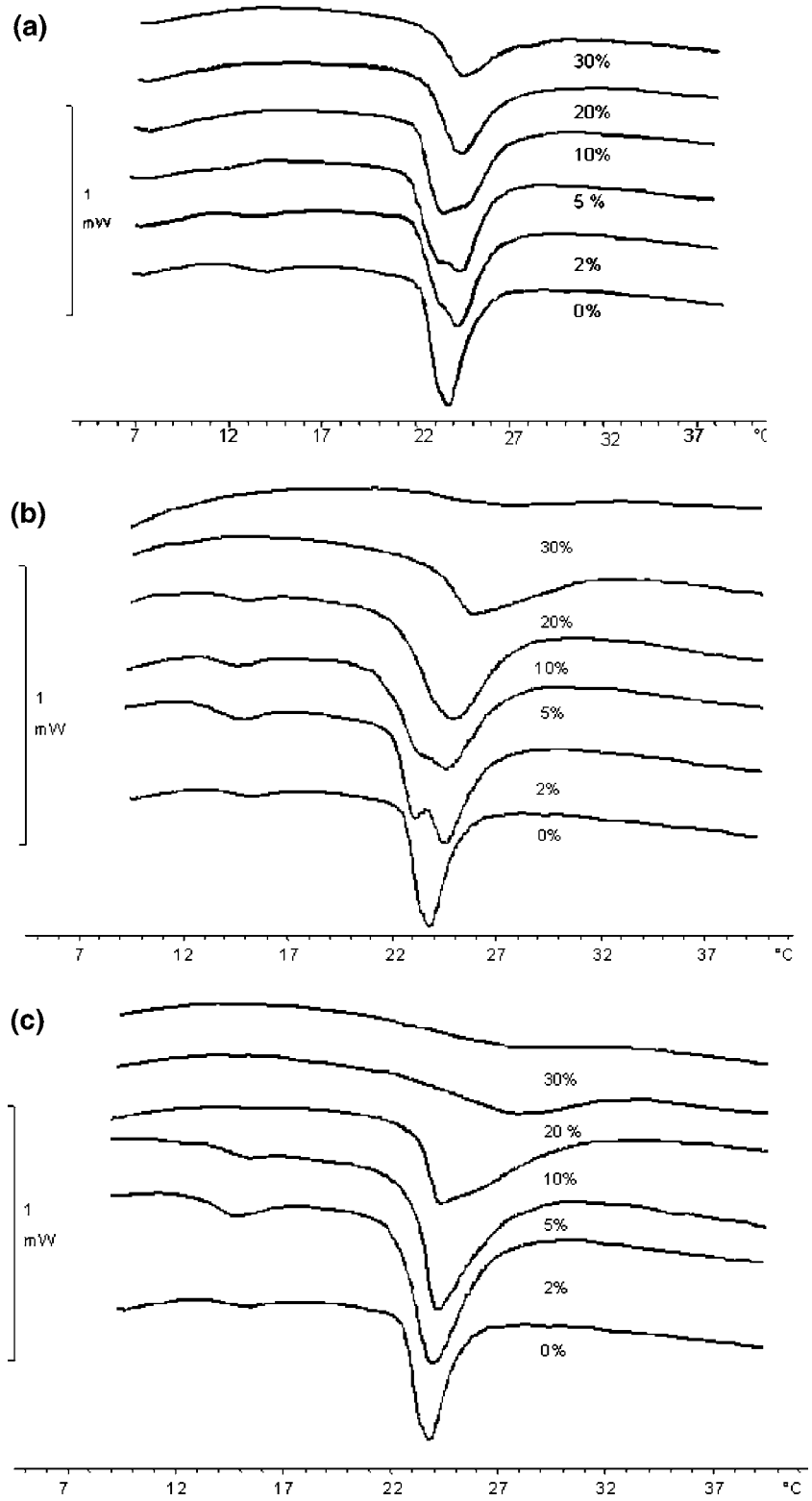

Figure 5. DSC heating endotherms of DMPC/DMPG (2:1) MLVs were obtained in the presence of 0, 2, 5, 10, 20, and 30 mol % E2(17-26) (a), E2(12-26) (b), and E2(7-26) (c). The curves refer to the second scan in the heating mode at a temperature scanning rate of 5 °C/min.

HGV peptides. This observation indicates that the interactions of the peptides with these phospholipids does not alter significantly the packing of hydrocarbon chains in the gel and liquid-crystalline states.[37,38] However, the melting profile for the 2:1 binary mixture of DMPC/DMPG vesicles shifted to higher temperatures for the three peptides (Figure 5). Furthermore, at 30 mol % of E2(12-26) and E2(7-26) the transition disappeared (Figure 5b,c), ΔH being significantly lower after the addition of E2(7-26) and E2(12-26) compared to E2(17-26). The observed decrease in ΔH could be the result of the diminished hydrophobic interactions between the phospholipid acyl

(37) Poklar, N.; Fritz, J.; Macek, P.; Vesnaver, G.; Chalikian, T. V.; *Biochemistry* **1999**, *38*, 14999−15008.

(38) Rojo, N.; Gómara, M. J.; Busquets, M. A.; Alsina, M. A.; Haro, I. *Talanta* **2003**, *60*, 395−404.

chains themselves due to intercalation and, therefore, the interaction with GBV-C/HGV peptides. In the DPPC thermotropic profile the transition enthalpy increased at 5 mol % with E2(7-26) and at 10 mol % in E2(12-26) but decreased at higher percentages. The decrease of ΔH in DMPC MLVs was higher in the presence of E2(7-26) (≈75%) followed by the decrease in the presence of E2-(12-26) (≈50%). In the DMPC/DMPG melting profile the effect of the addition of GBV-C/HGV peptides in the enthalpy value was similar to that observed for pure DMPC MLVs. For E2(17-26) and E2(12-26) there was a little increase in the ΔH until 10%. Finally, the decrease obtained for all peptides at high concentrations was higher than for DMPC.

On the other hand, while the width of the transitions, measured as $\Delta T_{1/2}$, did not change significantly in DPPC MLVs, the transition of DMPC and DMPC/DMPG samples broadened after the incorporation of the peptides, showing a greater effect the E2(7-26) peptide sequence. The broadening of the endothermic peak indicates that the peptides incorporate into the MLVs, disrupting the correlation between lipidic molecules.

With DMPC/DMPG (2:1) being the composition that showed the stronger interaction with the peptides, DSC profiles of mixtures containing increasing amounts the GBV-C/HGV peptides are shown in Figure 5.

Figure 5a shows the endothermic phase transitions for DMPC/DMPG in the presence of E2(17-26). The thermogram of the pure phospholipid mixture showed a pretransition from a tilted to a rippled chain gel phase ($L\beta'-P\beta'$) at 14 °C and a main phase transition (T_m) from the gel to liquid-crystalline phase ($P\beta'-L\alpha$) at 24 °C. Our results indicate that in the presence of 2 mol % of the 10-mer peptide the pretransition did not disappear at all. The main transition was slightly displaced to a higher temperature and presents a little shoulder at a lower temperature. At 5 mol %, the pretransition disappeared and the main transition broadened increasing the shoulder at low temperature. At 10 mol % peptide the main transition was shifted to a low temperature and the shoulder appeared at a high temperature. The appearance of a shoulder indicates that there may be inhomogeneous mixing of E2(17-26) with the phospholipids or that the presence of different lipid−peptide populations are induced. At 20 mol % peptide, the endotherm presents a symmetrical peak without a shoulder. With increasing the peptide to 30 mol %, the peak broadened and became smaller.

Figure 5b shows the DSC profile for DMPC/DMPG and E2(12-26). In general, like E2(17-26), this peptide caused a broadening and a shift of phase transition to higher temperatures. Addition of 2 mol % of the 15-mer peptide did not abolish the pretransition and the main transition splits into two peaks, one at 23,0 °C and the other at 24,4 °C, indicative of the initiation of inhomogeneous mixing. Increasing the peptide content to 5 mol %, still did not abolish the pretransition, and the main transition resulted in a coalescence of the peaks into a broad peak with a low temperature shoulder. At concentrations of 10 to 20 mol % the peak was symmetrical with a significant broadening of the gel to liquid-crystalline lamellar phase transition. Finally, at 30 mol % of peptide the peak disappeared.

Figure 5c shows the endotherms for DMPC/DMPG in the presence of increasing amounts of E2(7-26). Addition of the 20-mer peptide until 5 mol % did not caused the disappearance of the pretransition and the main transition was broadened and remained symmetric. At 10 mol % of peptide the peak became asymmetric, with a high temperature shoulder that suggests the presence of two different phospholipid populations. At 20 mol % the peak practically disappeared and at 30% there was no phase transition.

The different behavior between the three peptides could be attributed to the length of the chain as well as the different net charge that would favor a combination of hydrophobic and electrostatic interactions.[39] If electrostatic forces were responsible, the positively charged peptides E2(17-26) and E2(7-26), would decrease ΔH in a larger extent that the neutral E2(12-26). However, in agreement with the monolayer experimental results, the E2(12-26) sequence decreases ΔH in a higher extent than the E2(17-26) peptide, thus, indicating that electrostatic interactions seem to play only a minor role for the mixing of DMPC/DMPG with peptides. It must be expected that the binding of the positively charged peptides to the bilayer is stabilized by the presence of DMPG and probably through DMPG domain formation.

3.3.2. Peptides Binding to Lipid Vesicles: Intrinsic Emission Fluorescence Measurements. The interaction of overlapping peptides E2(17-26), E2(12-26), and E2(7-26) with DPPC, DMPC, and DMPC/DMPG (2:1) lipids was also studied by monitoring the changes in the Trp fluorescence emission spectra of the peptides upon addition of LUVs. The emission maximum of a buried Trp within globular proteins is located between 320 and 330 nm, a Trp partially buried has a maximum between 330 and 345 nm, and the emission of a fully exposed Trp is in the range of 345−355 nm.[40]

Consequently, to know about these lipid/peptide interactions we have evaluated the change in the wavelength of the Trp emission maximum (λ_{em}) after the addition of increasing percentages of LUVs. The corresponding λ_{em} was plotted as a function of lipid/peptide relationship (Figure 6).

As shown, fluorescence spectra at room temperature with DPPC and DMPC did not show any shift at the assayed lipid/peptide ratios, thus, indicating the lack of binding. On the other hand, in the presence of DMPC/DMPG liposomes the binding with the peptides took place. E2(17-26), E2(12-26), and E2(7-26) in buffer medium had λ_{em} values of 357, 356, and 354 nm, respectively, indicating a polar environment for the Trp residues that was lower the larger the peptide sequence was. Trp location into the peptide sequence could also influence its ability to interact with liposomes. In presence of DMPC/DMPG (2:1) liposomes at a peptide/lipid molar ratio of 1:500, the peptides charged positively, which are E2(17-26) and E2(7-26), showed blue shifts of 13 and 11 nm, respectively. However, a blue shift of around 7 nm was observed for the neutral peptide, E2(12-26). These values are indicative of the Trp residue located in a less polar environment indicating an interaction and a partial penetration of the peptides into the hydrophobic tail of the bilayer without being completely buried.

To measure peptides partitioning quantitatively, the fluorescence intensity at the λ_{em} of the lipid-bound state was analyzed by titrating lipid vesicles into an aqueous solution of the peptides. Because the three peptides are monomeric in aqueous solutions at the studied concentrations, as revealed by the unchanged intrinsic fluorescence of soluble GBV-C/HGV peptides (data not shown), we were able to analyze their binding isotherms as a partition equilibrium. The partition coefficients obtained from the binding curves were $K_x = 6.6 \times 10^6$ and $K_x = 7.4 \times 10^6$ for

(39) Sospedra, P.; Mestres, C.; Haro, I.; Muñoz, M.; Busquets, M. A. *Langmuir* **2002**, *18*, 1231−1237

(40) Wimley, W. C.; White, S. H. *Biochemistry* **2000**, *39*, 4432−4442.

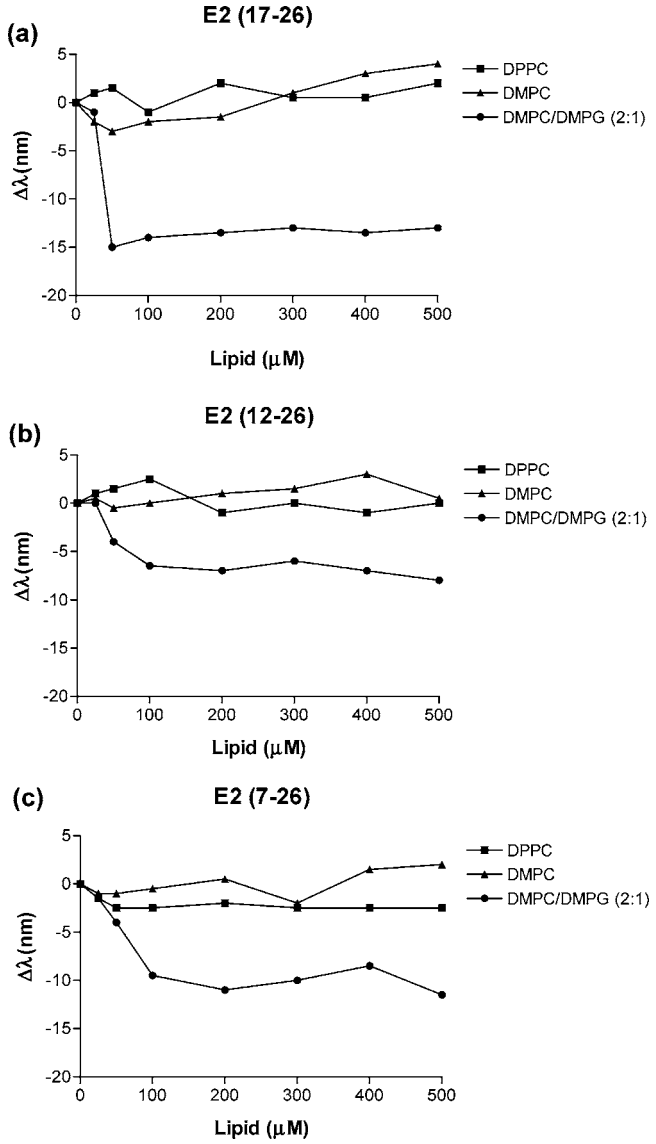

Figure 6. Fluorescence properties of the tryptophan residues of the peptides. λ_{em} is the blue shift in the wavelength of maximum emission, in the presence of DPPC, DMPC, and DMPC/DMPG (2:1) vesicles as a function of lipid/peptide. Peptide concentration in the cuvette was 1 μM.

the positively charged peptides, which are E2(17-26) and E2(7-26), respectively, this value being 1 order of magnitude lower for the neutral peptide [$K_x = 5.0 \times 10^5$ for E2(12-26)]. Our results suggest then that the affinity and the extent of the interaction are considerably greater for anionic than for zwitterionic membranes. Also the peptide charge of the N-terminal E2 peptides seems to play an important role on the biophysical activity of the protein, the two positively charged peptides showing quite comparable behaviors in terms of lipid−peptide interaction.

3.3.3. Interaction of the Larger Peptide with MLVs Monitored by Negative Stain Electron Microscopy. To investigate how the peptide interaction with phospholipids was, suspensions of MLVs were directly visualized by negative staining under electron microscopy, before and after the treatment with the peptide. DMPC or DMPC/DMPG (2:1) MLVs of approximately 200 nm (0.114 mM) were incubated for 1 h alone or with 35 mol % of E2(7-26) in Hepes.

Figure 7 shows micrographs of MLV without peptide DMPC (a), DMPC/DMPG (2:1) (c), or with E2(7-26) (b and d) negatively stained with 2% uranil acetate solution. It can be observed that the incubation of the peptide with liposomes had an effect on the morphology of the vesicles. The liposomes appeared mainly aggregated, thus, confirming the interaction of the peptide with the phospholipids. Otherwise, the control liposomes (Figure 7a,c) had a regular shape. However, at a peptide concentration of 40 μM, the 20-mer peptide induced low aggregation but some wrinkled in the membrane structure of both DMPC and DMPC/DMPG (2:1) liposomes. The liposomes have become wrinkled probably due to the presence of the peptide in its surface. There is in the literature a great diversity of electron microscopy studies with fusion peptides.[41−43] These peptides have the ability to induce vesicle aggregation or even fragmentation of previous fused liposomes. Our results clearly show that the GBV-C/HGV E2 peptide studied induced vesicle aggregation, these results being confirmed by an increase in optical density at 436 nm (data not shown).

3.3.4. Secondary Structure of GBV-C/HGV Peptides: CD Studies. The conformation of the three synthetic overlapping peptides has been analyzed by CD in the far-UV region. Spectral changes were not observed up to 100 μM peptide concentrations, thus, indicating the absence of intramolecular aggregation, in agreement with the results obtained from the unchanged intrinsic fluorescence at this concentration.

The CD spectra of E2(17-26), E2(12-26), and E2(7-26) in 5 mM Hepes buffer showed predominantly unordered conformations with a clear negative band around 198 nm characteristic of random coil structures, the percentages of α-helix in all cases being lower than 10%.

To investigate the conformational behavior of the peptides in a quasi-membrane medium, we used organic solvents such as TFE and HFIP with dielectric constants between pure water and the hydrocarbon chains of biological membranes. Another medium that we used was SDS. SDS forms micelles at a concentration above 4 mM, so it can be used as a mimic of negatively charged bilayers and can provide an anisotropic environment similar to that of lipid vesicles.[44]

Our results show that the helical content in the presence of TFE or HFIP increased up to 20%; however, we observed that fluorated alcohols mainly induced β-type structures (Table 6). As an example, Figure 8 shows the effect of 50% HFIP in the CD spectra of the three E2 peptides studied. The minimum at 200 nm characteristic of an aperiodic structure was shifted to larger wavelengths, suggesting more ordered structures, and the bands characteristic of α-helix, located at 208 and 222 nm, appeared. After quantifying the helical content by Yang parameters, values around 15 and 20% were respectively obtained for the 20- and 15-mer peptides, the shortest E2 sequence giving a lower α-helix content (around 5%).

Regarding the experiments carried out in the membrane mimetic medium of SDS and at concentrations above the critical micelle concentration, micellar SDS has been reported to stabilize α-helix,[45] and our results show that SDS contributes to stabilize β-sheet structures as seen in Table 6. The CD spectra measured in the presence of SDS micelles had a negative band, around 215 nm, and no

(41) Rodríguez-Crespo, I.; Yélamos, B.; Albar, J. P.; Peterson, D. L.; Gavilanes, F. *Biochim. Biophys. Acta* **2000**, *1463*, 419−428.
(42) Peisajovich, S. G.; Epand, R. F.; Epand, R. M.; Shai, Y. *Eur. J. Biochem.* **2002**, *269*, 4342−50.
(43) Ulrich, A. S.; Tichlaar, W.; Förster, G.; Zschörnig, O.; Weinkauf, S.; Meyer, H. *Biophys. J.* **1999**, *77*, 829−41.
(44) Blondelle, S. E.; Forood, B.; Houghten, R. A.; Pérez-Payá, E. *Biopolymers* **1997**, *42*, 489−498.
(45) Waterhous, D. V.; Johnson, W. C., Jr. *Biochemistry* **1994**, *33*, 2121−2128.

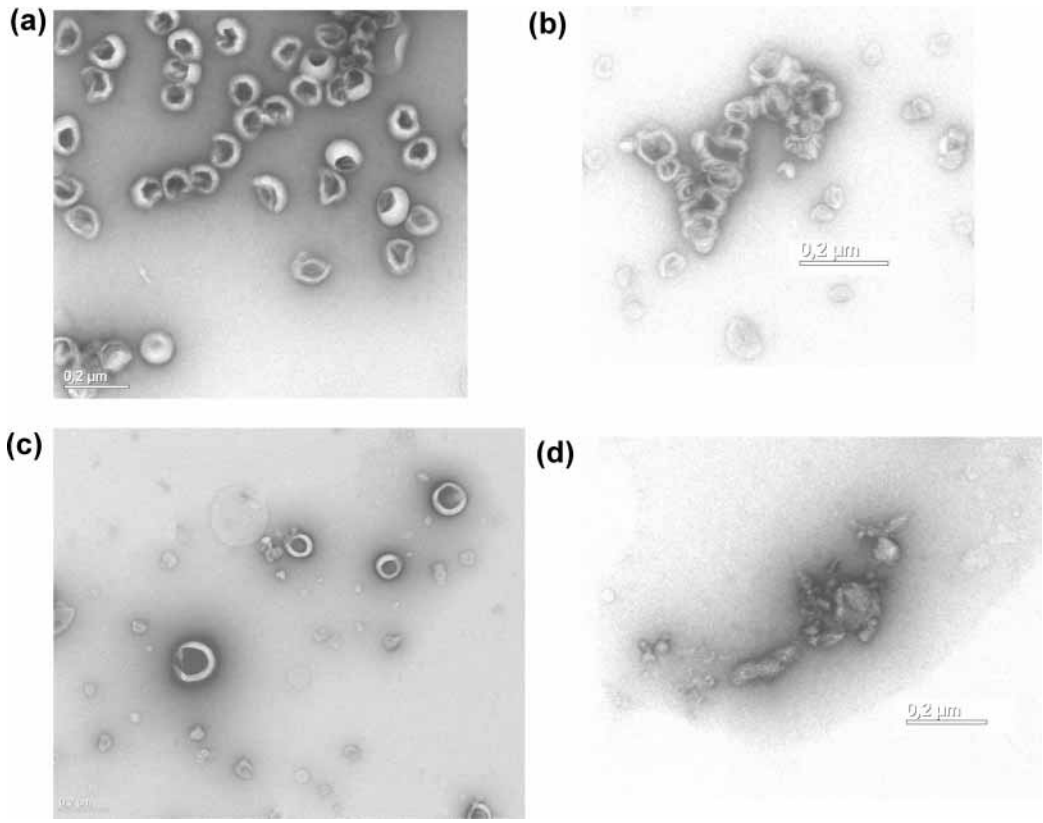

Figure 7. Electron micrographs of liposomes and liposome−E2(7-26) peptide complexes. The complexes were obtained by incubating the vesicles with the peptide (39 μM) in buffer medium at pH 7.4 for 1 h at 37 °C. DMPC and DMPC/DMPG (2:1) vesicles in the absence (a, c) or presence (b, d) of E2(7-26), respectively.

Table 6. Estimation, from the CD Spectra, of the Content of α-Helix, β-Sheet, β-Turn, and Random Coil of the Peptides According to the Different Deconvolution Computer Programs

	E2(17-26)				E2(12-26)				E2(7-26)			
	Hepes	HIFP	TFE	SDS	Hepes	HIFP	TFE	SDS	Hepes	HFIP	TFE	SDS
						K2D						
α-helix	7	8	7	8	7	14	10	8	7	13	9	9
β-sheet	50	45	51	45	51	31	41	41	49	32	44	44
random coil	43	47	42	47	42	55	48	51	44	55	48	47
						Lincomb−Brahms						
α-helix	3.6	7	4	2.3	1	15		13	7	14	1	
β-sheet	40	38	43	41	42	33	42	28	28	34	46	47
β-turn					6	9	18	11	12	8	6	7
random coil	56	54	52	56	51	43	40	47	53	44	47	46
						Contin						
α-helix	9	21	12	8	1	18	12	12	13	16	10	7
β-sheet	42	35	52	38	43	35	52	45	42	32	39	43
β-turn	31	28	35	32	34	27	35	33	31	32	31	30
random coil	18	16	1	22	22	20	1	10	14	20	20	20

band at 208 nm, suggesting the presence of mainly β-sheet structures. As described and quantified in Table 6, GBV-C/HGV peptides were best fitted with a combination of β-sheet, β-turn, and aperiodic structures.

Even though it was difficult to clearly define the secondary structure of GBV-C/HGV peptides in the presence of SDS micelles, according to Lincomb−Brahms and K2D CD-deconvolution programs (Table 6), the quantification of β-type structures adopted by the positively charged peptides, which are the 10- and 20-mer peptides, gives higher values than those obtained for the zwitterionic peptide sequence (15-mer peptide). Thus, the β-structure of GBV-C/HGV peptides must be an important requirement for lipid perturbation activity. As reported in recent studies on fusion peptides,[46] most of them favored

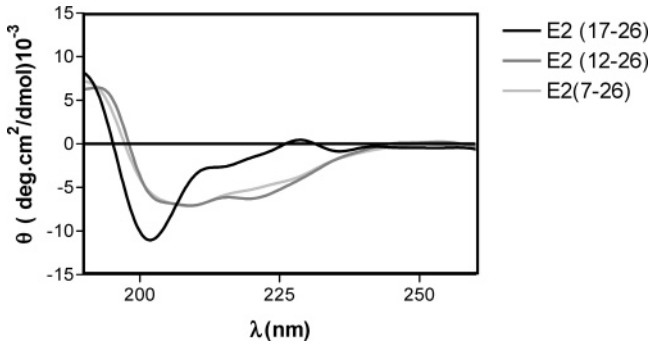

Figure 8. CD spectra of E2(17-26), E2(12-26), and E2(7-26) in the presence of 50% HIFP.

β-sheet structure as the putative fusogenic conformation in vesicular systems.

(46) Lee, A. G. *Biochim. Biophys. Acta* **2003**, *1612*, 1−40.

While information derived from the isotherms does not fulfill any of the requirements described in the literature to assign a preferential peptide secondary structure,[30] the presence of structural agents such as TFE or SDS changes notably the peptide's conformation. Therefore, the differences in the results could be explained in terms of conformation differences depending on the surrounding media of the peptides.

4. Conclusions

In this paper, the interaction of three overlapping peptides of the E2 structural protein of GBV-C/HGV was examined to determine whether the differences in their interactions with lipid model membranes could explain their role in the processes involved in the virus activity. As a general trend, the larger the peptide sequence the stronger the interaction with mono- and bilayers regardless of their charge [10-mer peptide (+) < 15-mer peptide (n) < 20-mer peptide (+)].

Phospholipid composition also has significant effects, the interaction of the peptides being higher with the anionic mixture DMPC/DMPG (2:1; mol/mol) than with the zwitterionic DMPC or DPPC as shown by the kinetics of penetration in monolayers, intrinsic fluorescence, and DSC measurements. The fluorescence emission spectra collected with the overlapping peptides at varying peptide concentrations revealed a blue shift in the wavelength of maximum emission for Trp containing peptides indicating an embedding of these peptides into the hydrophobic core of the bilayer. On the other hand, the reduction of the enthalpy corresponding to the main transition while have virtually no effect on the enthalpy of pure DPPC or DMPC is remarkable. The relevance of the preferential interaction with anionic membranes could be of importance because of the fact that although the bulk of the lipids in a membrane are zwitterionic some membrane proteins require small amounts of anionic lipids or other hydrophobic molecules such as cholesterol for activity. Furthermore, the affinity for the anionic model membranes measured as partition coefficients gave values 1 order of magnitude lower for the neutral peptide, thus, reinforcing the idea that the peptide charge seems also to play a role in the lipid−peptide binding, and this fact could also be related with the different structural propensities of the three overlapping peptides as revealed by the CD studies. To sum up, the negatively charged surface of model lipid membranes and the β-type structure were required for peptide's action.

The peptide's capacity for modifying the biophysical properties of phospholipid mono- and bilayers could provide an additional driving force for the merging of the viral and target cell membranes. For instance, these results could indicate their direct role in membrane fusion and, therefore, might be essential for the assistance and enhancement of the viral and cell fusion process.

Acknowledgment. This work was funded by Grants BQU2003-05070-CO2-01/02 from the Ministerio de Ciencia y Tecnología (Spain) and a predoctoral grant awarded to C.L. The excellent technical assistance of Ms. Amelia López (Laboratory of Thermal Analysis, IIQAB-CSIC) and Dr. Carmen López (Electron Microscopy and In situ Molecular Identification Unit of Barcelona, Science Park) is greatly acknowledged. We thank Professor I. Panaiotov for the interesting discussions on the monolayer section.

LA048551G

Artículo 2: Interacción de péptidos sintéticos correspondientes a la proteína estructural del virus de la hepatitis G (HGV/GBV-C) con vesículas fosfolipídicas

Cristina Larios, Bart Christiaens, M. José Gómara, M. Asunción Alsina e Isabel Haro

Departamento de Química de Péptidos y Proteínas, Instituto de Investigaciones Químicas y Ambientales de Barcelona, IIQAB-CSIC.
Departamento de Fisicoquímica, Facultad de Farmacia, Universidad de Barcelona.
Laboratorio de Química de Lipoproteínas, Departamento de Bioquímica, Universidad de Gante, Bélgica.

Cristina Larios, Bart Christiaens, M. José Gómara, M. Asunción Alsina and Isabel Haro (2005) Interaction of synthetic peptides corresponding to hepatitis G virus (HGV/GBV-C) E2 structural protein with phospholipid vesicles, *FEBS Journal,* **272**, 2456-2466.

Resumen

La interacción con bicapas lipídicas de dos péptidos sintéticos con secuencias pertenecientes al segmento cercano a la región N-terminal y una región interna de la proteína estructural E2 del virus de la hepatitis G (HGV/GBV-C), [E2(7-26) y E2(279-298)] respectivamente, se caracteriza en este trabajo. Ambos péptidos son solubles en agua, pero se asocian espontáneamente a bicapas, mostrando una mayor afinidad por membranas aniónicas que zwiteriónicas. Sin embargo, mientras E2(7-26) es difilmente transferible desde el agua a la interfase de la membrana, E2(279-298) si que es capaz de penetrar en bicapas cargadas negativamente permaneciendo en la interfase lípido/agua. El ambiente no polar claramente induce a una transición estructural en el péptido E2(279-298) desde una conformación desordenada hacia una hélice α, la cual es responsable de las perturbaciones producidas en las bicapas, conduciendo a una permeabilización de las vesículas. Los resultados indican que este péptido del segmento interno podría intervenir en el proceso de fusión de la membrana del HGV/GBV-C.

the FEBS Journal

Interaction of synthetic peptides corresponding to hepatitis G virus (HGV/GBV-C) E2 structural protein with phospholipid vesicles

Cristina Larios[1,2], Bart Christiaens[3], M. José Gómara[1], M. Asunción Alsina[2] and Isabel Haro[1]

1 Department of Peptide and Protein Chemistry, IIQAB-CSIC, Barcelona, Spain
2 Associated Unit CSIC, Department of Physical Chemistry, Faculty of Pharmacy, University of Barcelona, Spain
3 Laboratory of Lipoprotein Chemistry, Department of Biochemistry, Ghent University, Belgium

Keywords
circular dichroism; fluorescence assays; hepatitis G virus (HGV/GBV-C); lipid vesicles; synthetic peptides

Correspondence
I. Haro, Department of Peptide and Protein Chemistry, IIQAB-CSIC, Jordi Girona 18-26 08034, Barcelona, Spain
Fax: +34 9320 45904
Tel: +34 9340 06109
E-mail: ihvqpp@iiqab.csic.es

(Received 25 February 2005, revised 8 March 2005, accepted 17 March 2005)

doi:10.1111/j.1742-4658.2005.04666.x

The interaction with phospholipid bilayers of two synthetic peptides with sequences corresponding to a segment next to the native N-terminus and an internal region of the E2 structural hepatitis G virus (HGV/GBV-C) protein [E2(7–26) and E2(279–298), respectively] has been characterized. Both peptides are water soluble but associate spontaneously with bilayers, showing higher affinity for anionic than zwitterionic membranes. However, whereas the E2(7–26) peptide is hardly transferred at all from water to the membrane interface, the E2(279–298) peptide is able to penetrate into negatively charged bilayers remaining close to the lipid/water interface. The nonpolar environment clearly induces a structural transition in the E2(279–298) peptide from random coil to α-helix, which causes bilayer perturbations leading to vesicle permeabilization. The results indicate that this internal segment peptide sequence is involved in the fusion of HGV/GBV-C to membrane.

The hepatitis G virus (HGV) and the GB virus C (GBV-C) are strain variants of a recently discovered enveloped RNA virus belonging to the Flaviviridae family, which is transmitted by contaminated blood and/or blood products, intravenous drug use, from mother to child and by sexual intercourse. The natural history of HGV/GBV-C infection is not fully understood, and its potential to cause hepatitis in humans is questionable [1]. Moreover, the mode of entry of HGV/GBV-C into target cells is not known.

Elucidation of the mechanism of the fusion of enveloped viruses with target membranes has attracted considerable attention because of its relative simplicity and potential clinical importance. Apart from the functions of viral binding to target membranes and the activation of viral fusion proteins, usually only one viral protein is responsible for the actual membrane fusion step. However, the nature of the interaction of viral fusion proteins with membranes and the mechanism by which these proteins accelerate the formation of membrane fusion intermediates are poorly understood [2]. In this sense, specialized hydrophobic conserved domains ('fusion peptides') have been postulated to be absolutely required for the fusogenic activity [3,4].

The envelope proteins (E) of flaviviruses have been described as class II fusion proteins that have structural features that set them apart from the well-known rod-like 'spikes' of influenza virus or HIV. They are predominantly nonhelical, having instead a β-sheet-type

Abbreviations
E, envelope proteins; HCV, hepatitis C virus; HGV/GBV-C, hepatitis G virus; LUV, large unilamellar vesicle; PamOlePtdCho, 1-palmitoyl-2-oleoylphosphatidylcholine; PamOlePtdGro, 1-palmitoyl-2-oleoylphosphatidylglycerol; SUV, small unilamellar vesicle; TBEV, tick-borne encephalitis virus.

structure; they are not cleaved during biosynthesis and appear to have fusion peptides within internal loop structures, distant from the N-terminus [5]. The only protein of this class for which a high-resolution structure is available is the envelope glycoprotein E of the flavivirus tick-borne encephalitis virus (TBEV) [6]. It has been proposed that a highly conserved loop at the tip of each subunit of the flavivirus E protein (sequence element containing amino acids 98–110 of the flavivirus E protein) may serve as an internal fusion peptide, as it is directly involved in interactions with target membranes during the initial stages of membrane fusion [7]. Because of the structural homology, extrapolating knowledge from the TBEV structure to hepatitis C virus (HCV) leads to the idea that E2 may be the fusion protein. Although very little is known about the HCV cell fusion process, sequence alignment between the TBEV E protein and the HCV E2 protein suggests that residues 476–494 in E2 may play a role in viral fusion [8]. As HGV/GBV-C is the most closely related human virus to HCV [9], it can be expected that E2 sequences of these related viruses are functionally equivalent, and therefore conserve some structural similarity. However, owing to the low pairwise sequence identity with HCV E2 (< 20%), attempts to align these sequences using sequence information and/or through their predicted secondary structure have been unsuccessful and have given ambiguous results [8].

Besides, experimental information on the type of interactions established by internal fusion peptides with membranes is at present limited. Predictive structural analyses indicate that internal fusion peptides are segmented into two regions separated by a putative turn or loop, which usually contains one or more Pro residues. This organization seems to be fundamental to the fusogenic function [10]. It has been shown that Pro residues display the highest propensity for turn induction at the membrane interface in poly(Leu) stretches [11,12] and therefore play important structural roles in membrane-inserted peptide chains [13].

The direct involvement of fusion peptides in virus–cell fusion is supported by studies using model membranes, membrane mimetic systems, and synthetic peptide fragments representing functional and nonfunctional fusion peptide sequences, which demonstrate that, after insertion, only functional sequences generate target-membrane perturbations [4].

In this study, we report on the interaction of an N-terminal (E2(7–26)) and an internal (E2(279–298)) synthetic peptide sequence of the E2 structural protein of HGV/GBV-C with phospholipid membranes of different composition. To select these peptides, the profiles of Kite and Doolittle (hydropathicity index) and Chou and Fasman (secondary-structure prediction) were used to determine E2 regions sharing both partition into membranes and β-turn structure tendencies. In this sense, the two selected E2 regions, in spite of having Pro within their primary sequences, showed different features. Thus, whereas E2(7–26) has a high β-turn content but no membrane affinity, the region of E2 located between residues 279 and 298 has both predictive features.

The secondary structure of both peptides was measured by CD. We monitored several parameters that determine peptide–membrane interaction, and combined analysis of the data obtained provides insights into HGV/GBV-C–membrane interaction.

Results

The E2 peptides synthesized are amphiphilic because of the presence of hydrophobic and hydrophilic amino acids in their composition which make them water soluble and able to associate with model membranes. E2(7–26) (GSRPFEPGLTWQSCSCRANG) contains two positively charged Arg residues (Arg9 and Arg23), which could be important for the interaction with negatively charged phospholipid membranes [14]. E2(279–298) (AGLTGGFYEPLVRRCSELAG) is a neutral peptide containing two positive arginines (Arg285, Arg286) and two negatively charged amino acids (Glu282, Glu290); it has an isoelectric point (pI) of 6.18 and a mean hydrophobicity (H_0) of 0.13.

A Trp residue was incorporated at the N-terminus of the wild E2(279–298) sequence to provide a suitable chromophore for monitoring lipid–peptide interaction. The presence of this Trp residue in W-E2(279–298) modified neither the hydrophobicity (0.16) nor the pI (6.14) of the parent E2(279–298) peptide.

Binding of E2 peptides to model membranes

Lipid interaction of the E2 peptides was studied by monitoring Trp fluorescence changes on titration of peptide solutions with small unilamellar vesicles (SUVs).

In Tris/HCl buffer containing 150 mM NaCl, the maximal Trp fluorescence emission wavelength (λ_{max}) of the peptides was 347 and 350 nm for E2(7–26) and W-E2(279–298), respectively. Our results show that, in lipid-free peptides, Trp residues are highly exposed to water.

To investigate the contribution of electrostatic interactions, the peptides were titrated with both neutral and negatively charged vesicles. Titration of the

peptides with neutral 1-palmitoyl-2-oleoylphosphatidylcholine (PamOlePtdCho) SUVs resulted in no shift for E2(7–26) and a shift of only 1 nm for W-E2(279–298).

Incubation of E2(7–26) peptide with negatively charged vesicles, PamOlePtdCho/1-palmitoyl-2-oleoylphosphatidylglycerol (PamOlePtdGro) (75/25) and egg PtdCho/brain PtdSer (65/35), had little effect on the Trp fluorescence intensity of the peptide and did not affect the shape of the Trp fluorescence spectrum. Blue shifts of 3 nm and 1 nm were found for this peptide upon titration with 200 μM PamOlePtdCho/PamOlePtdGro (75/25) and 200 μM PtdCho/PtdSer (65/35). In contrast, addition of the negatively charged vesicles to the E2(279–298) peptide shifted the maximal Trp fluorescence emission to lower wavelengths. The larger blue shift of 11 nm was measured for the peptide titration with egg PtdCho/brain PtdSer (65/35). Blue shifts of this magnitude have been observed when surface-active Trp-containing peptides interact with lipid membranes and are consistent with the Trp residue partition into a more hydrophobic environment [15–19]. This also indicates that the Trp residues are only partially buried in the vesicles, as a moiety that is fully protected from water is expected to have emission at $\approx$320 nm.

As a general rule, on titration with negatively charged vesicles, Trp fluorescence decreased and the wavelength of maximal Trp fluorescence shifted to lower wavelengths. As an example, Fig. 1 shows the curves of the peptides in buffer and in the presence of PamOlePtdCho/PamOlePtdGro SUVs.

The electrostatic interactions were further studied by titration of the peptides with egg PtdCho/brain PtdSer (65/35) SUVs in Tris/HCl buffer without salt. For both peptides, the blue shift increased up to 14 and 15 nm for E2(7–26) and W-E2(279–298), respectively.

After titration with egg PtdCho/brain PtdSer (65/35) SUVs without salt, the blue shift was also accompanied by a decrease in the Trp fluorescence intensity. Plotting the percentage of initial fluorescence as a function of the lipid concentration (Fig. 2) enabled calculation of K_d values. For both peptides, the titration curves show saturable binding. The affinity for egg PtdCho/brain PtdSer (65/35) SUVs was higher for W-E2(279–298) than for E2(7–26) [K_d was 67 ± 10 μM for E2(7–26) and 31 ± 2.5 μM for W-E2(279–298)] (Table 1).

Finally, the effect of membrane rigidity was studied using PamOlePtdCho/PamOlePtdGro/cholesterol (45/30/25) SUVs. The presence of cholesterol in the lipid bilayer had a minor effect, as there was a shift in λ_{max} of 3 nm for E2(7–26) and 6 nm for W-E2(279–298).

Peptide conformation

In buffer, the CD spectra for the E2 peptides showed the characteristics of a random-coil conformation, as indicated by the presence of a negative band at

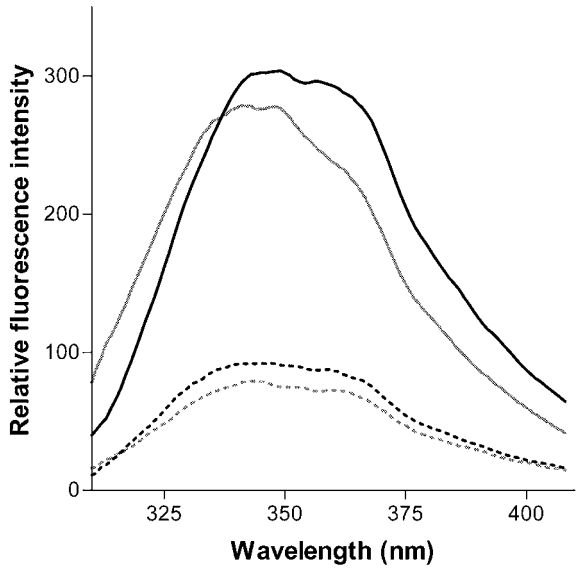

Fig. 1. Fluorescence emission spectra of the E2(7–26) (black broken line) and W-E2(279–298) (black solid line) peptides (2 μM) in Tris/HCl buffer (pH 8)/0.15 mM NaCl (black) and in the presence of 0.2 mM PamOlePtdCho/PamOlePtdGro (75/25) SUVs (grey).

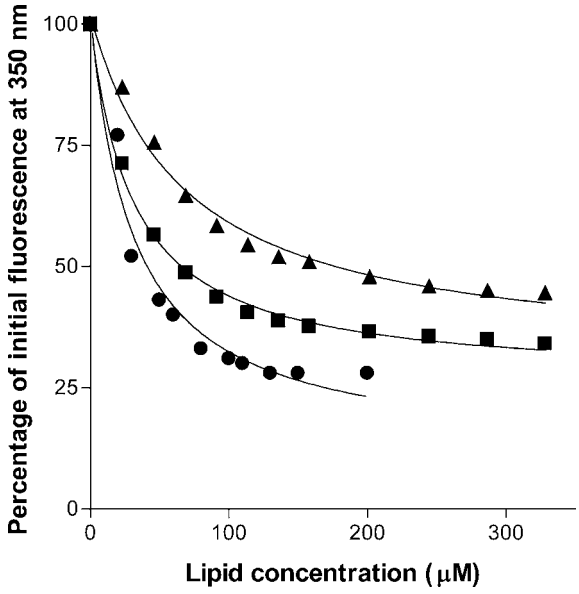

Fig. 2. Fluorescence titration curves of E2(7–26) (▲), W-E2(279–298) (■) and penetratine(43–58) (●) with egg PtdCho/brain PtdSer (65/35) SUVs without salt. Curve-fitting of the experimental data is represented by solid lines.

Table 1. Maximal Trp emission wavelength (λ max) for lipid-free and lipid-bound E2(7–26), W-E2(279–298) and P(48–53) peptides, apparent dissociation constants (K_d) for titration of the peptides with egg PtdCho/brain PtdSer (65/35) SUVs, and Stern–Volmer constants (K_{sv}) for acrylamide quenching of Trp fluorescence of the peptides before and after incubation with egg PtdCho/brain PtdSer (60/40) SUVs. P(43–58), Penetratine(43–58).

	E2(7–26)	W-E2(279–298)	P(43–58)
λ_{max} (nm)			
Buffer	347	350	347
PamOlePtdCho	347	349	347
PamOlePtdCho/PamOlePtdGro (75/25)	344	342	337
PamOlePtdCho/PamOlePtdGro/Chol (45/30/25)	344	344	339
Egg PtdCho/brain PtdSer (65/35)	346	339	338
Egg PtdCho/brainPS buffer no salt (65/35)	332	336	339
K_d (μM)			
Egg PtdCho/brain PtdSer (65/35)	67 ± 10	31 ± 2.5	5.5 ± 0.1
K_{sv} (M^{-1})			
Buffer	13.6 ± 0.6	26.6 ± 0.2	18.6 ± 1.1
Egg PtdCho/brain PtdSer (60/40)	6.8 ± 0.2	7.2 ± 0.2	2.7 ± 0.1

198 nm. In aqueous 2,2,2-trifluoroethanol solutions, the percentage of α-helix in W-E2(279–298) increased, whereas this was not the case for E2(7–26). In Fig. 3, as an example, the CD spectra of E2 (279–298) in buffer, in 50% (v/v) trifluoroethanol, and in PamOlePtdCho/PamOlePtdGro (2 : 1) SUVs are shown. We can observe the change to a more structured conformation when the mimetic membrane solvent trifluoroethanol or SUVs are added.

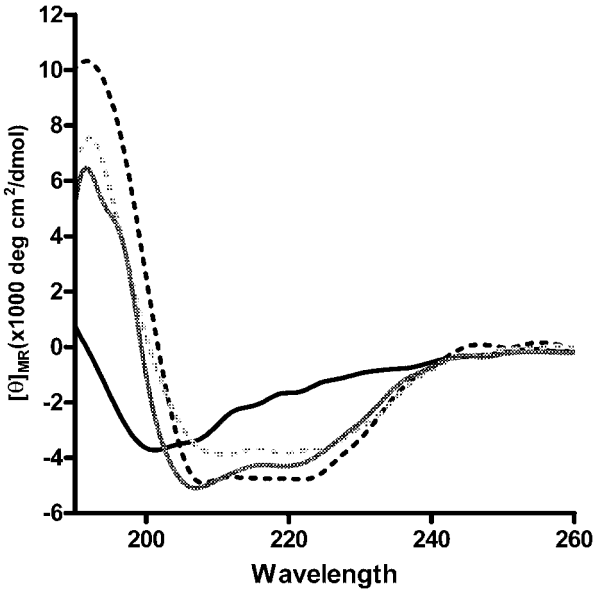

Fig. 3. CD spectra of W-E2(279–298) (22 μM) in phosphate buffer, pH 7.4 (black solid line), 50% trifluoroethanol (black broken line) and PamOlePtdCho/PamOlePtdGro (80/20) SUVs (grey broken line). CD spectrum of penetratine(43–58) in PamOlePtdCho/PamOlePtdGro (80/20) SUVs (grey solid line).

Incubation with mixed PamOlePtdCho/PamOlePtdGro (80/20) or PamOlePtdCho/PamOlePtdGro/cholesterol (50/25/25) SUVs increased the α-helix content of W-E2(279–298) (Table 2). In contrast, the percentage of β-type structure decreased. In all cases, E2(7–26) remained mainly unstructured, even when bound to phospholipid vesicles.

Acrylamide quenching

The accessibility of the Trp residues of the E2 peptides to the neutral, water-soluble acrylamide quencher was examined in the absence and presence of phospholipid vesicles. Fluorescence of Trp decreased in a concentration-dependent manner after the addition of acrylamide to the peptide solution in the presence or absence of liposomes (data not shown). Figure 4 shows the Stern-Volmer plots for acrylamide quenching of E2 peptides in buffer, and in the presence of egg PtdCho/brain PtdSer (60/40) SUV vesicles. The Stern-Volmer quenching constants (K_{sv}) of the lipid-free peptides were 13.6 ± 0.6 M^{-1} for E2(7–26) and 26.6 ± 0.2 M^{-1} for W-E2(279–298) (Table 1), indicating that the Trp residue of the peptides was readily quenched by acrylamide. Incubation with egg PtdCho/brain PtdSer (60/40) SUVs decreased the K_{sv} values twofold for E2(7–26) and 3.7-fold for W-E2(279–298), showing in the latter case that the Trp residues are more protected from the quencher.

Quenching by brominated lipids

The depth of insertion of the Trp residues of E2 peptides into lipid bilayers was estimated by dibromo-PtdCho

Table 2. α-Helical, β-structure and random coil content of the E2 peptides, as calculated using the K2D and CONTIN programs, and based on the mean residue ellipiticity at 222 nm [33]. TFE, trifluoroethanol.

	% α-Helix			% β-Structure			% Random oil	
	θ_{222}	K2D	CONTIN	β-Sheet (K2D)	β-Sheet (K2D)	β-Turn (CONTIN)	K2D	CONTIN
E2(7–26)								
Buffer	13	8	12	41	27	24	50	37
25% TFE	15	9	12	36	32	22	55	34
50% TFE	18	14	16	30	29	23	42	33
PamOlePtdCho	11	7	9	51	34	23	50	36
PamOlePtdCho/PG (80/20)	15	8	11	41	31	22	50	36
PamOlePtdCho/PG/Chol (50/25/25)	15	8	4	41	44	18	56	32
E2(279–298)								
Buffer	15	10	13	34	16	16	56	55
25% TFE	33	10	14	36	17	14	55	55
50% TFE	34	28	37	15	14	16	58	33
PamOlePtdCho	20	33	37	16	20	14	50	28
PamOlePtdCho/PG (80/20)	28	46	42	20	15	16	33	27
PamOlePtdCho/PG/Chol (50/25/25)	29	57	47	10	17	16	33	19

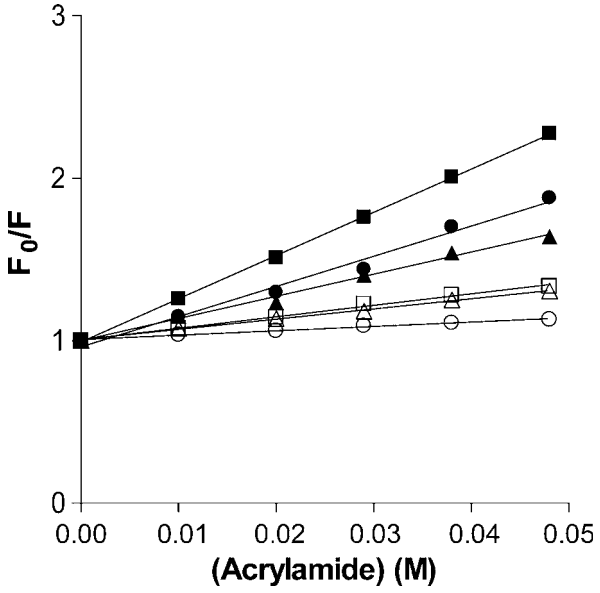

Fig. 4. Stern–Volmer plots for acrylamide quenching of E2(7–26) (triangles), W-E2(279–298) (squares) and penetratine(43–58) (circles). Filled symbols represent the peptides in aqueous buffer; open symbols represent the peptides in the presence of 0.2 mM egg PtdCho/brain PtdSer (60/40) SUVs.

quenching. Both peptides were quenched more efficiently by $Br_{6,7}$-PtdCho than by $Br_{11,12}$-PtdCho (Fig. 5), suggesting that they remain close to the lipid/water interface. For both lipid quenchers, Trp quenching efficiency was higher for W-E2(279–298) than for E2(7–26), indicating deeper insertion of W-E2(279–298) into the membrane.

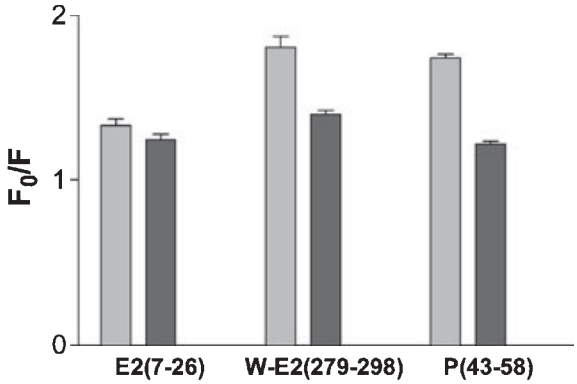

Fig. 5. Trp quenching efficiency (F_0/F) of E2(7–26), W-E2(279–298) and penetratine(43–58) peptides (2 μM) bound to egg PtdCho/brain PtdSer (65/35) SUVs (lipid to peptide molar ratio 0.01) by $Br_{6,7}$-PtdCho (grey bars) and $Br_{11,12}$-PtdCho (black bars).

Membrane permeabilization

Figure 6 shows the calcein leakage out of egg PtdCho/brain PtdSer (70 : 30) large unilamellar vesicles (LUVs) induced by the E2 peptides. Leakage of 70% was reached for E2(7–26) at a peptide to lipid ratio of 2 : 1. For W-E2(279–298), complete lysis of the LUVs was reached at a peptide to lipid ratio of 1 : 1. For the E2(7–26) peptide, a sigmoidal dose–response curve was obtained, indicating peptide co-operativity, whereas this was not the case for W-E2(279–298) (Fig. 6A). Calcein leakage kinetics were faster for the W-E2(279–298) peptide, which induced complete vesicle lysis after 15 min compared with 1 h for the E2(7–26) peptide (Fig. 6B).

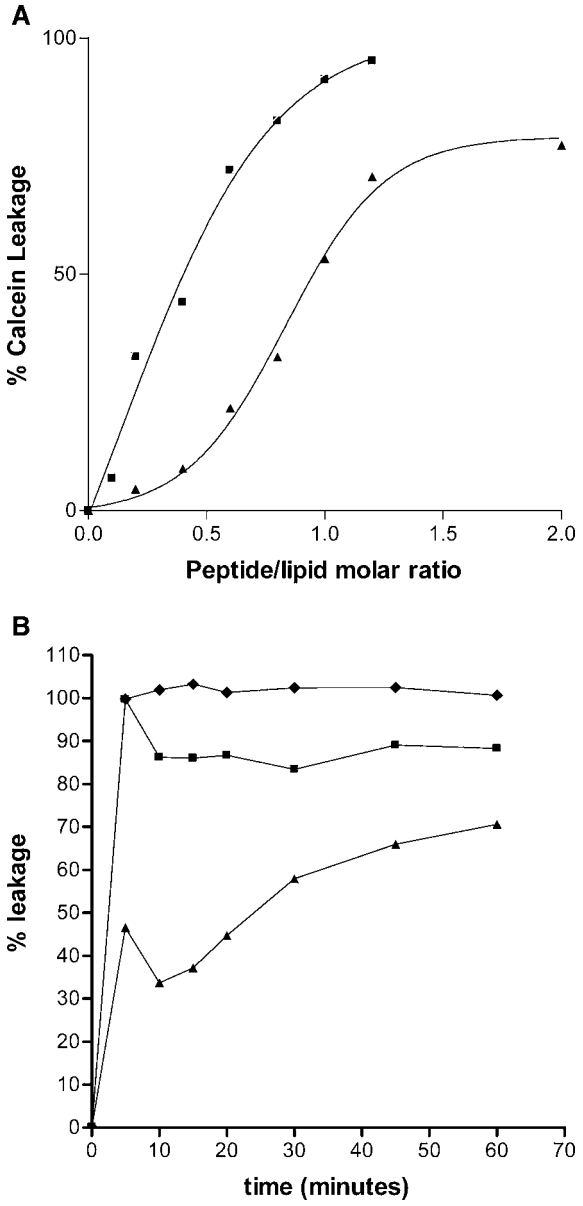

Fig. 6. (A) Calcein leakage induced by E2(7–26) (▲) and W-E2(279–298) (■) from egg PtdCho/brain PtdSer (70/30) LUVs as a function of peptide to lipid molar ratio. (B) Percentage of leakage vs. time for E2(7–26) (▲), W-E2(279–298) (■), and melittin (●). Peptide to lipid molar ratio 1 : 1 (E2 peptides) and 1 : 25 (melittin).

Vesicle aggregation

Incubation of egg PtdCho/brain PtdSer (60/40) SUVs with E2(7–26) peptide induced vesicle aggregation at a 0.2 peptide to lipid ratio, as indicated by the increase in A_{436} (Fig. 7). In contrast, the W-E2(279–298) peptide did not show any increase in A_{436}.

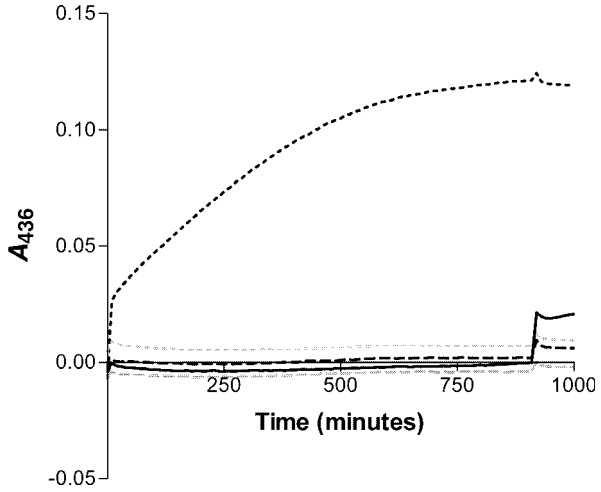

Fig. 7. Turbidity (A_{436}) of dispersion of egg PtdCho/brain PtdSer SUVs in the absence (solid line) and presence of the E2(7–26) (black) and W-E2(279–298) (grey) peptides at 0.04 (broken line) and 0.2 (dotted line) peptide to lipid molar ratio.

Discussion

HGV/GBV-C is the most closely related human virus to HCV, both of them belonging to the small enveloped viruses of the Flaviviridae family. A stretch of conserved, hydrophobic amino acids within the E2 envelope glycoprotein of HCV has been proposed as the virus fusion peptide [8]. However, because of the low pairwise sequence identity with HCV E2 (< 20%), it has not been feasible to select a stretch of residues in the HGV/GBV-C E2 protein, with sequence homology to the highly conserved loop of the flavivirus E protein described as an internal fusion peptide.

In this study we have analysed the interactions of an N-terminal and an internal peptide sequence of the E2 structural protein of HGV/GBV-C with model membranes, in order to understand the possible mode of penetration of HGV/GBV-C into the membrane cells. These synthetic peptides are characterized by the presence of Pro residues, which have been reported to play important roles in membrane-inserted peptide chains, specifically promoting kinks at the level of the membrane interface. Moreover, they have a high content of aliphatic hydrophobic residues, such as Val and Leu, and aromatic hydrophobic residues (Tyr, Phe, Trp), as well as the three small amino acids Gly, Ala, Thr. It has been suggested that these particular amino-acid contents may confer structural plasticity on these peptides, which seems to be crucial for the fusion process [20].

Although fusion peptides have been widely described as short hydrophobic segments of viral envelope glycoproteins with a very low content of hydrophilic amino acids, the presence of acidic residues in the fusion peptides of some low-pH-activated viral fusion proteins has been observed [21]. Moreover, it has been reported that the putative internal fusion peptide of TBEV is highly constrained by multiple interactions, including several internal hydrogen bonds and salt bridges [22]. The analogue fusion peptide proposed for HCV is characterized by a positively charged region, which has been shown experimentally to be important for heteromeric association between envelope proteins E1 and E2 [8]. Therefore, the presence of hydrophilic amino acids in the fusion peptides of flaviviruses seems to be crucial for the fusion process.

We have investigated the fluorescence properties of the Trp residues of E2(7–26) and W-E2(279–298) peptides in buffer as well as in the presence of neutral and negatively charged vesicles. In lipid-free peptides, both Trp residues are highly exposed to the aqueous phase, suggesting a monomeric rather than aggregated structure. This was confirmed by the extent of acrylamide quenching. Moreover, CD measurements showed that both peptides are randomly structured in buffer.

The addition of neutral lipid vesicles to the peptides induced no blue shift of λ_{max}, suggesting that the peptides hardly interacted at all with PamOlePtdCho SUVs. The E2(7–26) peptide titration with negatively charged vesicles [PamOlePtdCho/PamOlePtdGro (75/25) and PtdCho/PtdSer (65/35)] showed a slight blue shift in Trp fluorescence, suggesting a weak interaction between this sequence and negatively charged SUVs. In contrast, W-E2(279–298) strongly interacted with PtdCho/PtdSer (65/35) vesicles, as the blue shift of Trp was 11 nm.

To study the contribution of electrostatic interactions to the binding of both peptides with negatively charged SUVs, titration of the peptides with PtdCho/PtdSer vesicles was carried out in the absence of salt. The E2(7–26) peptide showed a significantly higher blue shift of Trp fluorescence in buffer without salt, whereas W-E(279–298) showed a similar fluorescence spectrum to that obtained in 10 mM Tris/HCl buffer containing 0.15 M NaCl. These results suggest that electrostatic interactions play a principal role in the binding of E2(7–26) to negatively charged residues. In contrast, a higher contribution of hydrophobic compared with electrostatic interactions is expected to control the binding of W-E2(279–298) to PtdCho/PtdSer vesicles. This is supported by the vesicle aggregation results induced on the addition of peptides to PtdCho/PtdSer (60/40) SUVs. Thus, in contrast with W-E2(279–298) peptide, the E2(7–26) sequence promoted vesicle aggregation, confirming that the binding of this peptide to PtdCho/PtdSer vesicles is mainly due to electrostatic interactions.

Acrylamide and dibromo-PtdCho quenching experiments were performed to estimate the depth of insertion of the Trp residues of E2 peptides into lipid bilayers. The Stern-Volmer quenching constants for the PtdCho/PtdSer-incubated peptides, as well as the Trp quenching efficiency by brominated lipids, indicated a deeper insertion of W-E2(279–298) into the membrane than E2(7–26) peptide. Moreover, $Br_{6,7}$-PtdCho quenched the Trp residue in W-E2(279–298) more efficiently than $Br_{11,12}$-PtdCho, suggesting that this peptide remains close to the lipid/water interface.

Cell membranes have an asymmetric distribution of zwitterionic and negatively charged phospholipids characterized by localization in the inner leaflet of the bilayer of the second one. In a previous study [14], it has been suggested that the preferential interaction of the synthetic peptides with anionic membranes may be related to the fact that some membrane proteins, having clusters of basic amino acids, require small amounts of anionic lipids to interact with the cell membrane.

Induction of vesicle permeability on addition of peptide fragments representing fusion peptide sequences has been shown to correlate well with fusion peptide functionality, in most instances. In this study, we compared the ability of E2(7–26) and W-E2(279–298) to induce leakage from PtdCho/PtdSer (70 : 30) vesicles. The calcein release induced by the peptides was dependent on the concentration, so when a sufficient high concentration of the peptides is reached, a larger aggregated form could induce the membrane permeability. The W-E2(279–298) peptide showed significantly higher leakage activity than E2(7–26), as the former was able to induce extensive efflux of aqueous contents into the medium at a peptide to lipid molar ratio two times lower. This vesicle permeabilization process appears to be mediated by the peptide conformation adopted in membranes. CD experiments showed that the addition of 50% trifluoroethanol or negatively charged vesicles induced α-helical conformation in the W-E2(279–298) peptide. However, the E2(7–26) peptide conformation in a membraneous environment remained random coil like.

The data together suggest that the E2(7–26) peptide is hardly transferred at all from water to the membrane interface, as it mainly interacts electrostatically with the vesicle surface. In contrast, the W-E2(279–298) peptide is able to penetrate into negatively charged bilayers remaining close to the lipid/water interface. This nonpolar environment induces a peptide structural transi-

tion from random coil to α-helix, causing bilayer perturbations that lead to vesicle permeabilization.

In summary, our data suggest that the internal region (279–298) of the E2 structural protein may be involved in the fusion process of HGV/GBV-C.

Experimental procedures

Materials

Egg yolk PtdCho, brain PtdSer, PamOlePtdCho, PamOlePtdGro, 1-palmitoyl-2-stearoyl-(6–7)dibromo-*sn*-glycero-3-phosphocholine ($Br_{6,7}$-PtdCho) and 1-palmitoyl-2-stearoyl-(11–12)dibromo-*sn*-glycero-3-phosphocholine ($Br_{11,12}$-PtdCho) were from Avanti Polar Lipids (Alabaster, AL, USA). Calcein was from Fluka (Bucks, Switzerland). Rink amide MBHA and Novasyn TGR resins, amino-acid derivatives and coupling reagents were obtained from Fluka and Novabiochem (Nottingham, UK). Dimethylformamide was purchased from Sharlau (Barcelona, Spain). Trifluoroacetic acid was supplied by Merck (Poole, Dorset, UK) and scavengers such as ethanedithiol and tri-isopropylsilane were from Sigma-Aldrich (Steinheim, Germany).

Peptide synthesis

The peptides were synthesized manually following procedures described previously [23,24]. The syntheses were carried out by solid-phase methodology following an Fmoc/tBu strategy with a *N,N′*-di-isopropylcarbodiimide/1-hydroxybenzotriazole activation. For the incorporation of Cys293 into the E2(279–298) and W-E2(279–298) peptides, repeated coupling using 2-(1*H*-benzotriazol-1-yl)-1,1,3,3-tetramethyluronium tetrafluoroborate and *N,N′*-di-isopropylethylamine as activators was needed.

Threefold molar excesses of Fmoc-amino acids were used throughout the synthesis. The stepwise addition of each residue was determined by Kaiser's test [25]. Peptides were cleaved from the resin with a trifluoroacetic acid solution containing appropriate scavengers (either water and 1,2-ethanedithiol or water, tri-isopropylsilane ethanedithiol), and purified by HPLC on a semipreparative C_{18} kromasil column. The samples were eluted with a linear gradient of acetonitrile in an aqueous solution of 0.05% trifluoroacetic acid. Purified peptides were checked by analytical HPLC in an analytical C_{18} kromasil column, MALDI-TOF MS, and amino-acid analysis. Peptides were lyophilized and stored at 4 °C.

Positive control peptides

Penetratine(43–58) [26] and melittin [27] were used as positive control peptides throughout all the experimentation carried out. Penetratine(43–58) was used as a control in binding to SUVs, acrylamide quenching, brominated phospholipid quenching, and CD experiments. Melittin was used as a control in the leakage experiments.

Vesicle preparation

Lipid films were prepared by dissolving the phospholipids in a chloroform/methanol (2/1, v/v) solution, followed by solvent evaporation under a flow of nitrogen and overnight vacuum. Multilamellar vesicles were obtained by vortex mixing of the lipid films in 10 mM Tris/HCl buffer, pH 8.0, containing 0.15 M NaCl for 10 min above the phase transition temperature. On the one hand, SUVs were then obtained by sonication of the multilamellar vesicles at 4 °C using a Sonics Material Vibra-Cell™ sonicator. Titanium debris was removed by centrifugation. SUVs were separated from multilamellar vesicles by gel filtration on a Sepharose CL 4B column. The top fractions of the SUVs peak were pooled, concentrated and stored at 4 °C. On the other hand, LUVs were prepared by freeze-thawing the multilamellar vesicles in liquid nitrogen (15 times) [28], and extrusion through two stacked 100-nm polycarbonate filters (15 times; Nucleopore, Pleasanton, CA, USA) in a high-pressure extruder (Lipex Biomembranes, Vancouver, Canada) and stored at 4 °C.

PtdCho concentration was determined by an enzymatic colorimetric assay (bioMérieux), and total phospholipid concentration was determined by phosphorus analysis [29].

Trp fluorescence titrations

Fluorescence titrations were performed on an Aminco Bowman series 2 spectrofluorimeter, equipped with a thermostatically controlled cuvette holder (22 °C). Fluorescence emission spectra of 2 μM peptide solutions in 10 mM Tris/HCl containing 0.15 M NaCl, pH 8.0, in either the absence or presence of lipids, were recorded between 310 nm and 450 nm, with an excitation wavelength of 290 nm, at a slit width of 4 nm. The fluorescence spectra were instrument corrected for light scattering, by subtracting the corresponding spectra of the SUVs.

Changes in Trp fluorescence were used to evaluate peptide-lipid binding. The apparent dissociation constants were calculated from plots of the fluorescence intensity at 350 nm, expressed as the percentage of the fluorescence of the lipid-free peptides vs. the added lipid concentration. The data were analysed using Graphpad software, by means of the following equation:

$$F = \{F_0 + F_1(1/K_d)[L_{tot}]\}/\{1 + (1/K_d)[L_{tot}]\} \quad (1)$$

where F is the fluorescence intensity at a given added lipid concentration, F_0 the fluorescence intensity at the beginning of the titration, F_1 the fluorescence at the end of the titration, K_d the dissociation constant, and $[L_{tot}]$ the total lipid concentration [30].

CD measurements

CD was measured on a Jasco 710 spectropolarimeter (Hachioji, Tokyo, Japan) between 184 and 260 nm in a quartz cell with a path length of 0.1 cm. Nine spectra were recorded and averaged. The spectra of the lipid-free peptides were measured in sodium phosphate buffer (50 mg·mL^{-1}) or in the presence of increasing percentages of trifluoroethanol (25%, 50%, 75%). CD spectra of lipid-bound peptides at peptide to lipid molar ratios of 1 : 20 or 1 : 40 were recorded after 1 h incubation at room temperature. The spectra were corrected by subtraction of the spectrum of the SUVs alone {results are expressed as mean residue ellipticities $[\theta]_{MR}$ (degree.cm^2·dmol^{-1})}. The secondary structure of the peptides was obtained by curve-fitting, using the K2D and Contin programs by the Dichroweb® server at http://www.cryst.bbk.ac.uk7cdweb [31,32]. The helical content of the peptides was also calculated from the mean residue ellipticity at 222 nm [33].

Acrylamide quenching experiments

For acrylamide quenching experiments, an excitation wavelength of 290 nm was used. Aliquots of the water–soluble acrylamide (10 M stock solution) were added to 2 μM peptide in 10 mM Tris/HCl buffer, pH 8.0, in the absence or presence of SUVs. The lipid/peptide mixtures (molar ratio 50 : 1) were incubated for 30 min at room temperature before the measurements. Fluorescence intensities at 350 nm were monitored after each acrylamide addition at 25 °C. The values obtained were corrected for dilution, and the scatter contribution was derived from acrylamide titration of a vesicle blank. K_{sv}, which is a measure of the accessibility of Trp to acrylamide, was obtained from the slope of the plots of F_0/F vs. [quencher], where F_0 and F are the fluorescence intensities in the absence and presence of quencher, respectively [18,34]. As acrylamide does not partition significantly into membrane bilayers, the value of K_{sv} can be considered the fraction of the peptide residing in the surface of the bilayer as well as the amount of nonvesicle-associated free peptide.

Brominated lipid quenching experiments

Quenching of Trp by brominated phospholipids was performed to find the localization of this residue in bilayers [35,36]. Peptides (2 μM) were incubated for 30 min at 22 °C with a 50-fold molar excess of lipids in 10 mM Tris/HCl buffer, pH 8. Emission spectra were recorded between 310 and 450 nm with an excitation wavelength of 290 (± 4 nm). The quenching efficiency (F_0/F) was calculated by dividing the Trp fluorescence intensity of the peptide in the presence of egg PtdCho/brain PtdSer (60/40) SUVs (F_0), by the Trp fluorescence intensity of the peptide in the presence of dibromo-PtdCho/brain PtdSer (70/30) SUVs (F). F_0/F was compared for quenching by $Br_{6,7}$-PtdCho and $Br_{11,12}$-PtdCho lipid-phase quenchers.

Assay of calcein leakage

Dequenching of encapsulated calcein fluorescence resulting from the leakage of aqueous content out of LUVs was used to assess the vesicle leakage activity of the peptides. LUVs containing calcein were obtained by hydration of the dried film in 10 mM Tris/HCl buffer, pH 8.0, containing 70 mM calcein. LUVs were prepared as described above, and non-encapsulated calcein was removed by gel filtration on a Sephadex G-100 column. Calcein leakage out of LUVs (50 μM lipids) was measured after 15 min incubation at 22 °C in the same buffer as was used for the fluorescence titrations. Calcein fluorescence was measured at 520 nm, with an excitation of 490 nm and slit widths of 4 nm, of a 50-fold diluted 20 μL sample of the peptide/lipid incubation mixture containing 50 μM lipids. Leakage (%) was calculated using the following equation:

$$\%\,\text{Leakage} = ([F - F_0]/[F_{100} - F_0]) \times 100 \qquad (2)$$

where F_0 is the fluorescence intensity of LUVs alone, F, the fluorescence intensity after incubation with the peptide, and F_{100}, the fluorescence intensity after the addition of 10 μL 5% (v/v) Triton X-100.

Assay of vesicle aggregation

The ability of the peptides to induce vesicle aggregation was studied by monitoring the turbidity of a SUV suspension of egg PtdCho/brain PtdSer (60/40) (50 μM) at 436 nm over 1 h (22 °C) on an Uvikon 941 spectrophotometer (peptide lipid to molar ratios of 0.2 and 0.04).

Acknowledgements

This work was funded by grants BQU2003-05070-CO2-01/02 from the Ministerio de Ciencia y Tecnología (Spain) and a predoctoral grant awarded to C. L. We are very grateful to Dr B. Vanloo for helpful discussions.

References

1 Stapleton JT (2003) GB virus type C/hepatitis G virus. *Semin Liver Dis* **23**, 137–148.
2 Martin II, Ruysschaert J & Epand RM (1999) Role of the N-terminal peptides of viral envelope proteins in membrane fusion. *Adv Drug Deliv Rev* **38**, 233–255.
3 White JM (1990) Viral and cellular membrane fusion proteins. *Annu Rev Physiol* **52**, 675–697.

4 Nieva JL & Agirre A (2003) Are fusion peptides a good model to study viral cell fusion? *Biochim Biophys Acta* **1614**, 104–115.
5 Voisset C & Dubuisson J (2004) Functional hepatitis C virus envelope glycoproteins. *Biol Cell* **96**, 413–420.
6 Rey FA, Heinz FX, Mandl C, Kunz C & Harrison SC (1995) The envelope glycoprotein from tick-borne encephalitis virus at 2 Å resolution. *Nature* **375**, 291–298.
7 Allison SL, Schalich J, Stiasny K, Mandl CW & Heinz FX (2001) Mutational evidence for an internal fusion peptide in flavivirus envelope protein E. *J Virol* **75**, 4268–4275.
8 Yagnik AT, Lahm A, Meola A, Roccasecca RM, Ercole BB, Nicosia A & Tramontano A (2000) A model for the hepatitis C virus envelope glycoprotein E2. *Proteins* **40**, 355–366.
9 Robertson B, Myers G, Howard C, Brettin T, Bukh J, Gaschen B, Gojobori T, Maertens G, Mizokami M, Nainan O, Netesov S, Nishioka K, Shini T, Simmonds P, Smith D, Stuyver L & Weiner A (1998) Classification, nomenclature, and database development for hepatitis C virus (HCV) and related viruses: proposals for standardization. International committee on virus taxonomy. *Arch Virol* **143**, 2493–2503.
10 Delos SE, Gilbert JM & White JM (2000) The central proline of an internal viral fusion peptide serves two important roles. *J Virol* **74**, 1686–1693.
11 Monne M, Hermansson M & von Heijne G (1999) A turn propensity scale for transmembrane helices. *J Mol Biol* **288**, 141–145.
12 Monne M, Nilsson I, Elofsson A & von Heijne G (1999) Turns in transmembrane helices: determination of the minimal length of a 'helical hairpin' and derivation of a fine-grained turn propensity scale. *J Mol Biol* **293**, 807–814.
13 Orzaez M, Salgado J, Gimenez-Giner A, Perez-Paya E & Mingarro I (2004) Influence of proline residues in transmembrane helix packing. *J Mol Biol* **335**, 631–640.
14 Larios C, Busquets MA, Carilla J, Alsina MA & Haro I (2004) Effects of overlapping GB virus C/hepatitis G virus synthetic peptides on biomembrane models. *Langmuir* **20**, 11149–11160.
15 Contreras LM, Aranda FJ, Gavilanes F, Gonzalez-Ros JM & Villalain J (2001) Structure and interaction with membrane model systems of a peptide derived from the major epitope region of HIV protein gp41: implications on viral fusion mechanism. *Biochemistry* **40**, 3196–3207.
16 Oren Z, Ramesh J, Avrahami D, Suryaprakash N, Shai Y & Jelinek R (2002) Structures and mode of membrane interaction of a short alpha helical lytic peptide and its diastereomer determined by NMR, FTIR, and fluorescence spectroscopy. *Eur J Biochem* **269**, 3869–3880.
17 Surewicz WK & Epand RM (1984) Role of peptide structure in lipid–peptide interactions: a fluorescence study of the binding of pentagastrin-related pentapeptides to phospholipid vesicles. *Biochemistry* **23**, 6072–6077.
18 Lakowicz JR (1983) Principles of fluorescence spectroscopy. In *Principles of Fluorescence Spectroscopy*, pp. 257–301. Plenum Press, New York.
19 Plasencia I, Rivas L, Keough KM, Marsh D & Perez-Gil J (2004) The N-terminal segment of pulmonary surfactant lipopeptide SP-C has intrinsic propensity to interact with and perturb phospholipid bilayers. *Biochem J* **377**, 183–193.
20 Del Angel VD, Dupuis F, Mornon JP & Callebaut I (2002) Viral fusion peptides and identification of membrane-interacting segments. *Biochem Biophys Res Commun* **293**, 1153–1160.
21 Zhang L & Ghosh HP (1994) Characterization of the putative fusogenic domain in vesicular stomatitis virus glycoprotein G. *J Virol* **68**, 2186–2193.
22 Allison SL, Schalich J, Stiasny K, Mandl CW & Heinz FX (2001) Mutational evidence for an internal fusion peptide in flavivirus envelope protein E. *J Virol* **75**, 4268–4275.
23 Rojo N, Gomara MJ, Haro I & Alsina MA (2003) Lipophilic derivatization of synthetic peptides belonging to NS3 and E2 proteins of GB virus-C (hepatitis G virus) and its effect on the interaction with model lipid membranes. *J Peptide Res* **61**, 318–330.
24 Larios C, Espina M, Alsina MA & Haro I (2004) Interaction of three beta-interferon domains with liposomes and monolayers as model membranes. *Biophys Chem* **111**, 123–133.
25 Kaiser E, Colescott RL, Bossinger CD & Cook PI (1970) Color test for detection of free terminal amino groups in the solid-phase synthesis of peptides. *Anal Biochem* **34**, 595–598.
26 Thoren PE, Persson D, Esbjorner EK, Goksor M, Lincoln P & Norden B (2004) Membrane binding and translocation of cell-penetrating peptides. *Biochemistry* **43**, 3471–3489.
27 Benachir T & Lafleur M (1995) Study of vesicle leakage induced by melittin. *Biochim Biophys Acta* **1235**, 452–460.
28 Mayer LD, Hope MJ & Cullis PR (1986) Vesicles of variable sizes produced by a rapid extrusion procedure. *Biochim Biophys Acta* **858**, 161–168.
29 Bartlett GR (1958) Phosphorous assay in column chromatography. *J Biol Chem* **234**, 466–468.
30 Christiaens B, Symoens S, Verheyden S, Engelborghs Y, Joliot A, Prochiantz A, Vandekerckhove J, Rosseneu M, Vanloo B & Vanderheyden S (2002) Tryptophan fluorescence study of the interaction of penetratin peptides with model membranes. *Eur J Biochem* **269**, 2918–2926.
31 Lobley A, Whitmore L & Wallace BA (2002) DICHROWEB: an interactive website for the analysis of protein secondary structure from circular dichroism spectra. *Bioinformatics* **18**, 211–212.

32 Whitmore L & Wallace BA (2004) DICHROWEB, an online server for protein secondary structure analyses from circular dichroism spectroscopic data. *Nucleic Acids Res* **32**, W668–W673.
33 Chen YH, Yang JT & Martinez HM (1972) Determination of the secondary structures of proteins by circular dichroism and optical rotatory dispersion. *Biochemistry* **11**, 4120–4131.
34 Eftink MR & Ghiron CA (1976) Exposure of tryptophanyl residues in proteins. Quantitative determination by fluorescence quenching studies. *Biochemistry* **15**, 672–680.
35 De Kroon AI, Soekarjo MW, De Gier J & De Kruijff B (1990) The role of charge and hydrophobicity in peptide–lipid interaction: a comparative study based on tryptophan fluorescence measurements combined with the use of aqueous and hydrophobic quenchers. *Biochemistry* **29**, 8229–8240.
36 Bolen EJ & Holloway PW (1990) Quenching of tryptophan fluorescence by brominated phospholipid. *Biochemistry* **29**, 9638–9643.

Artículo 3: Caracterización de una posible secuencia fusogénica en la proteína E2 del virus de la hepatitis G

Cristina Larios, Jordi Casas, María A. Alsina, Concepción Mestres, María J. Gómara e Isabel Haro

Departamento de Química de Péptidos y Proteínas, Instituto de Investigaciones Químicas y Ambientales de Barcelona, IIQAB-CSIC.
Departamento de Fisicoquímica, Facultad de Farmacia, Universidad de Barcelona.

Cristina Larios, Jordi Casas, María A. Alsina, Concepción Mestres, María J. Gómara and Isabel Haro (2005) Characterization of a putative fusogenic sequence in the E2 hepatitis G virus protein, *Arch. Biochem. Biophys*., 442 (2) 149-159.

Resumen

Con el propósito de comprender mejor el proceso de fusión mediado por proteínas de la envoltura del virus de la hepatitis G (HGV/GBV-C) iniciado en el trabajo 2 (FEBS Journal, **272**, 2005, 2456-2466), en el presente artículo se investiga la interacción con membranas de dos péptidos solapantes pertenecientes a la proteína estructural E2, E2(267-284) y E2(279-298) utilizando modelos de membrana. Los péptidos son comparados según su capacidad de perturbar bicapas lipídicas mediante diferentes técnicas como la calorimetría diferencial de barrido y la espectroscopia de fluorescencia. Además, el comportamiento conformacional de los péptidos en diferentes medios se estudia por espectroscopia de infrarrojo por transformada de Fourier y por dicroísmo circular. Los resultados muestran que sólo el péptido E2(279-298) es capaz de unirse con elevada afinidad a membranas cargadas negativamente, permeabilizar bicapas lipídicas eficientemente, inducir hemólisis y promover la fusión inter-vesicular. Esta capacidad fusogénica puede estar relacionada con la conformación inducida en el péptido cuando éste interacciona con las membranas diana.

Available online at www.sciencedirect.com
SCIENCE DIRECT®
Archives of Biochemistry and Biophysics 442 (2005) 149–159
ABB
www.elsevier.com/locate/yabbi

Characterization of a putative fusogenic sequence in the E2 hepatitis G virus protein

Cristina Larios [a,b], Jordi Casas [a,b], María A. Alsina [b], Concepción Mestres [b], María J. Gómara [a], Isabel Haro [a,*]

[a] *Department of Peptide and Protein Chemistry, IIQAB-CSIC, Jordi Girona, Salgado 18-26, 08034 Barcelona, Spain*
[b] *Physicochemistry Department (CSIC Associated Unit), Faculty of Pharmacy, University of Barcelona, Av.Joan XXIII s.n., 08028 Barcelona, Spain*

Received 11 May 2005, and in revised form 28 June 2005
Available online 1 August 2005

Abstract

With the aim of better understanding the fusion process mediated by the envelope proteins of the hepatitis G virus (HGV/GBV-C), we have investigated the interaction with model membranes of two overlapping peptides [(267–284) and (279–298)] belonging to the E2 structural protein. The peptides were compared for their ability to perturb lipid bilayers by means of different techniques such as differential scanning calorimetry and fluorescence spectroscopy. Furthermore, the conformational behaviour of the peptides in different membrane environments was studied by Fourier-transform infrared spectroscopy and circular dichroism. The results showed that only the E2(279–298) peptide sequence was able to bind with high affinity to negatively charged membranes, to permeabilize efficiently negative lipid bilayers, to induce haemolysis, and to promote inter-vesicle fusion. This fusogenic activity could be related to the induced peptide conformation upon interaction with the target membrane.

Keywords: Hepatitis G virus; E2 structural protein; Fusogenic peptide; Solid-phase peptide synthesis; Liposomes; Model membranes; Fluorescence spectroscopy; Differential scanning calorimetry; Circular dichroism; Fourier-transform infrared spectroscopy

The hepatitis G virus (HGV/GBV-C)[1] is the most closely related human virus to the hepatitis C virus (HCV) both belonging to the small enveloped viruses of the *flaviviridae* family. The envelope proteins (E) of flaviviruses have been described as class II fusion proteins which have structural features that set them apart from the class I fusion proteins represented by orthomyxo-, retro-, paramyxo-, and filoviruses. They are predominantly non-helical, having instead a β-sheet type structure; they are not cleaved during biosynthesis and appear to have fusion peptides within internal loop structures, distant from the N terminus [1]. The only protein of this class for which a high-resolution structure is currently available is the envelope glycoprotein E of the flavivirus tick-borne encephalitis virus (TBEV) [2]. It has been proposed that a highly conserved loop at the tip of each subunit of the flavivirus E protein (sequence element containing amino acids 98–110 of the flavivirus E protein) may serve as an internal fusion peptide since it is directly involved in interactions with target membranes during the initial stages of membrane fusion [3].

* Corresponding author. Fax: +34932045904.
E-mail address: ihvqpp@iiqab.csic.es (I. Haro).

[1] *Abbreviations used:* HGV/GBV-C, hepatitis G virus; HCV, hepatitis C virus; TBEV, tick-borne encephalitis virus; DSC, differential scanning calorimetry; DMPC, dimiristoylphosphatidylcholine; DMPG, dimiristoylphosphatidylglycerol; DMTAP, dimyristoyltrimethylammonium propane; PC, L-α-phosphatidylcholine; PG, L-α-phosphatidylglycerol; DMF, dimethylformamide; TFA, trifluoroacetic acid; DIPCD, *N*,*N*′-diisopropylcarbodiimide; HOBt, 1-hydroxybenzotriazole; TBTU, 2-(1*H*-benzotriazole-1-il)-1-3-3-tetramethyluronium-tetrafluoroborate; DEIA, *N*,*N*-diisopropylethylenamine; TIS, triisopropylsilane; EDT, ethanedithiol; HPLC, high-performance liquid chromatography; MLVs, multilamellar vesicles; FTIR, Fourier-transform infrared spectroscopy; LUVs, large unilamellar vesicles; SUVs, small unilamellar vesicles; ANTS, 8-aminonaphthalene-1,3,6-trisulphonic acid sodium salt; DPX, *p*-xylenebis(pyridinium)bromide; rRBC, rabbit red blood cells.

0003-9861/$ - see front matter © 2005 Elsevier Inc. All rights reserved.
doi:10.1016/j.abb.2005.06.027

Although very little is known about the HCV cell fusion process, the sequence alignment between the TBEV E protein and the HCV E2 protein suggests that residues 476–494 in E2 may play a role in viral fusion [4]. Since HGV/GBV-C is the most closely related human virus to the HCV [5], it can be expected that E2 sequences of these related viruses are functionally equivalent, and therefore preserve some structural similarity. Nevertheless, due to the low pairwise sequence identity to HCV E2 (<20%), it has not been feasible to select a stretch of residues in the HGV/GBV-C E2 protein, with the sequence homology of the highly conserved loop of the flavivirus E protein described as an internal fusion peptide.

To simulate protein-mediated fusion, many studies on peptide-induced membrane fusion have been conducted on model membranes such as liposomes and have employed synthetic peptides corresponding to the putative fusion sequences of viral proteins [6]. In this sense, in a previous work we synthesized the HGV/GBV-C E2(279–298) peptide sequence to study its interaction with model membranes and we suggested that this internal region of the E2 structural protein could be involved in the fusion process of the HGV/GBV-C [7]. In the present study, in an attempt to further characterize the fusion peptide of the HGV/GBV-C envelope protein we have selected and synthesized the overlapped region (267–284) of the E2 structural protein. This peptide also accomplishes the particular amino acid composition criteria established for fusion peptides since it has an elevated frequency in the small amino acids Gly and Ala (39%), and in some aliphatic hydrophobic residues (33%). It has been suggested that these particular amino acid contents could confer to the fusion peptides' structural plasticity that seem to be crucial for the fusion process [8]. Moreover, it has been described the presence of acidic residues in the fusion peptides of some low-pH-activated viral fusion proteins [9]. In this sense the E2 (267–284) peptide sequence is also characterized by the presence of two Glu residues that could be involved in the low-pH-triggered fusion process.

Since the lipid requirements for flavivirus fusion have not been studied in the same detail as those of alphaviruses [10–12], we have investigated the model membrane binding of the two putative fusion peptides (E2(279–298) and E2(267–284)) to assess the influence of specific lipids in the target membrane. Thus, we have analysed lipid–peptide interactions depending on the electrostatic properties of the lipids. The peptides were compared for their ability to interact and perturb membranes by means of different techniques such as differential scanning calorimetry (DSC) and fluorescence spectroscopy. In addition, they were also tested for their capacity to induce both leakage of vesicular contents and vesicle fusion as well as to lyse erythrocytes. Furthermore, we have studied the conformational behaviour of the peptides in water and in different membrane environments by Fourier-transform infrared spectroscopy (FTIR) and circular dichroism (CD).

Materials and methods

Chemicals

Dimiristoylphosphatidylcholine (DMPC), dimiristoylphosphatidylglycerol (DMPG), dimyristoyltrimethylammonium propane (DMTAP), egg L-α-phosphatidylcholine (PC), and egg L-α-phosphatidylglycerol (PG) were purchased from Avanti Polar-Lipids, Inc. Chloroform and methanol pro-analysis, used as spreading solvents for the lipids, were from Merck. Ultra pure water produced by deionization and nanopure purification coupled to a Milli-Q purification system (Milli-Q system, Millipore Corp.) up to a resistivity of 18.2 MΩ cm was used. The buffers used in the experiments were *N*-(2-hydroxyethyl)piperazine-*N*′-ethanesulphonic acid (Hepes buffer, 5 mM, pH 7.4) and (hydroxymethyl)aminomethane (Tris buffer, 10 mM, pH 7.4).

Pre-loaded Wang resin, Novasyn TGR resin, and the *N*-α-Fmoc-amino acids were obtained from Novabiochem (Nottingham, UK). Dimethylformamide (DMF) and 2-propanol were purchased from Scharlau Chemie, S.A. (Barcelona, Spain). Washing solvents such as acetic acid and diethyl ether were obtained from Merck (Poole, Dorset, UK). Trifluoroacetic acid (TFA) and synthesis reagents used were of analytical grade and were supplied by Sigma–Aldrich–Fluka (Bucks, Switzerland).

Peptide synthesis

Peptides were synthesized manually by a solid phase methodology following an Fmoc/tBu strategy by means of an *N*,*N*′-diisopropylcarbodiimide (DIPCD)/1-hydroxybenzotriazole (HOBt) activation [13]. The synthesis of E2(267–284): (LLGTEVSEVLGGAGLTGG) was carried out on a pre-loaded Wang resin (0.44 mEq/g) and the synthesis of E2(279–298): (AGLTGGF YEPLVRRCSELAG) was performed on a Novasyn TGR resin (0.29 mEq/g). For difficult couplings 2-(1*H*-benzotriazole-1-il)-1-3-3-tetramethyluroniumtetrafluoroborate (TBTU) and *N*,*N*-diisopropylethylenamine (DEIA) agents were used. Side-chain protection was effected by the following: tBu for Ser, Thr, and Tyr, Pmc for Arg, and Trt for Cys.

A threefold molar excess of Fmoc-amino acids was used throughout the synthesis. The stepwise addition of each residue was assessed by the Kaiser's (ninhydrin) test [14] and repeated couplings were carried out when a

positive ninhydrin test was obtained. In addition, mass spectra of intermediate products, especially after difficult couplings, were obtained to better follow the synthesis.

The synthesized peptides were deprotected from the side-chain groups and cleaved from the resin with a treatment of trifluoroacetic acid (TFA) containing appropriate proportions of scavengers such as H_2O, triisopropylsilane (TIS), and ethanedithiol (EDT).

The crude peptides were purified by preparative high-performance liquid chromatography (HPLC) on a chromatograph equipped with a C18-silica column. The purified peptides were characterized by analytical HPLC, amino acid analysis, and electrospray mass spectrometry (see Table 1 of supplementary material).

Preparation of lipid vesicles: SUVs, LUVs, and MLVs

Multilamellar vesicles (MLVs) of phospholipids were prepared for Fourier-transform infrared spectroscopy (FTIR) and differential scanning calorimetry (DSC) studies. Briefly, dry lipid was dissolved in a chloroform/methanol (2:1) mixture and the lipid solution was dried by slow evaporation under a constant flow of nitrogen. The last traces of solvents were removed under vacuum at 50 °C. Afterwards, the lipid films were suspended in Hepes buffer (5 mM, pH 7.4) and MLVs were obtained by vortexing the mixtures above the gel to liquid–crystalline phase transition of the lipid.

Large unilamellar vesicles (LUVs) were prepared according to the extrusion method of Hope et al. [15] in 5 mM Hepes, pH 7.4.

Phospholipid concentration was determined by phosphorus quantification as previously described [16]. The size of vesicles was measured by the sample diffusion coefficient by photon correlation spectroscopy (Coulter N4 MB, Luton, England, UK).

For CD and lipid mixing experiments, small unilamellar vesicles (SUVs) of the different phospholipids tested were prepared as follows. MLVs were sonicated (Vibracell, Sonics & Materials, Connecticut, USA) and afterwards the titanium traces were eliminated by ultracentrifugation. Phospholipid concentration was determined as described for LUVs.

Trp fluorescence titrations

Fluorescence experiments were performed on a Perkin-Elmer (Beaconsfield Bucks, UK) spectrofluorimeter LS 50 using a 1 cm path length quartz cuvette. Emission fluorescence spectra were recorded for each peptide at 1 μM in Hepes 5 mM, pH 7.4, at room temperature using an excitation wavelength of 285 nm and slits of 5 nm. Peptide–phospholipid interactions were assessed by monitoring the changes in the fluorescence spectra when LUVs were incubated with 1 μM peptide concentrations (lipid to peptide molar ratios of 25:1, 50:1, 100:1, 200:1, 300:1, 400:1, and 500:1). Suspensions were continuously stirred and they were left to equilibrate for 3 min before recording the spectrum. Fluorescence intensities were corrected for light scattering contribution by subtraction of the appropriate vesicle blank and a parallel lipid titration with *N*-acetyltryptophanamide [17]. The apparent dissociation constants (K_d) were calculated from plots of the fluorescence intensity at 350 nm, expressed as the percentage of the fluorescence of the lipid-free peptides vs. the added lipid concentration. The data were analysed using Graphpad software, by means of the following equation:

$$F = (F_0 + F_1 * (1/K_d)[L_{tot}])/(1 + (1/K_d)[L_{tot}]), \quad (1)$$

where F is the fluorescence intensity at a given added lipid concentration, F_0 the fluorescence intensity at the beginning of the titration, F_1 the fluorescence at the end of the titration, K_d the dissociation constant, and $[L_{tot}]$ the total lipid concentration [18].

Differential scanning calorimetry

Differential scanning calorimetry experiments of MLVs were performed using a DSC 821E Mettler Toledo calorimeter, following the methodology previously described [19]. Briefly, hermetically sealed aluminium pans containing buffer (reference cell) and sample were used. Sample pans were loaded by adding 30 μL of lipid vesicle suspension corresponding to approximately 0.3 mg phospholipid with and without peptide. Differences in the heat capacity between the sample and the reference cell were obtained by raising the temperature at a constant rate of 5 °C/min in the range of 0–40 °C for DMPC and DMPC/DMPG and 0–60 °C for DMPC/DMTAP. All samples were submitted to three heating/cooling cycles. Data from the first scan were always discarded to avoid false results coming from the possible lipid–peptide mixing in the sample under heating and the endothermic peak from the second scan of the control sample was used as a reference template. To ensure scan-to-scan reproducibility three consecutive scans of the sample were performed. DSC runs were carried out within the same day of liposome preparation.

High-resolution Micro DSC III Setaram microcalorimeter was used to better visualize the thermograms of DMPC/DMPG-E2(279–298) mixtures at small concentrations of peptide. Differences between the sample and the reference cell were obtained by raising the temperature at a constant rate of 0.5 °C/minute over a temperature range of 5–40 °C. Mathematical analyses were performed using Microcal Origin Software (version 6.0), which allowed multiple peak curve fitting.

Infrared spectroscopy

The infrared measurements were performed on a Nicolet Avatar 360 Fourier-transform infrared spectrometer equipped with a deuterated triglyceride sulphate detector. Each spectrum was obtained by collecting 50 interferograms with a nominal resolution of 4 cm^{-1}. A Ca_2F flow cell with a window of 100 μm pathlength spacer was used. Spectra of lipid–peptide mixtures were performed and reference spectra of solvents were recorded in the same micro-cells and under identical instrument conditions as samples, which contain a peptide concentration of 2 mg/mL. Difference spectra were obtained by digitally subtracting the solvent spectrum from the sample spectra.

To resolve overlapping bands, the spectra were processed using Peakfit software. Second derivative spectra were calculated to identify the positions of the component bands in the spectra. The deconvoluted spectrum was fitted with Gaussian band shapes by an iterative curve fitting procedure until good agreements were achieved between experimental and simulated spectra.

Circular dichroism

CD spectra were recorded on a Jasco J810 spectropolarimeter (Hachioji, Tokyo, Japan) equipped with a Peltier type temperature controller at 5 °C flushed with a nitrogen flux of 10 L min^{-1} in a quartz cell with 0.1 mm path length. CD spectra were acquired between 190 and 260 nm using a spectral bandwidth of 0.2 mm at a scan speed of 10 nm/min. Three scans were averaged for each sample and the respective buffer baselines were subtracted from the sample. CD data and the curves were smoothed using the program supplied by Jasco.

Peptide conformation experiments were performed at 30 μM in aqueous buffer (Hepes 5 mM, pH 7.4) and in the presence of structure-promoting solvents such as trifluoroethanol (TFE) at different percentages. CD spectra of lipid–peptide mixtures at a peptide to lipid molar ratios of 1:1 were recorded and corrected by subtraction of the SUVs alone. The results were expressed as mean residue ellipticities $[\theta]_{MR}$ (degree cm^2 $dmol^{-1}$). The secondary structure of the peptides was quantified by curve-fitting, using the K2D and Contin programs by the Dichroweb server at www.cryst.bbk.ac.uk7cdweb [20,21]. The percentage of α-helix in the peptides was also estimated using the formalism of Chen et al. [22].

Leakage of vesicular contents: ANTS/DPX assay

Dequenching of co-encapsulated 8-aminonaphthalene-1,3,6-trisulphonic acid sodium salt (ANTS) and *p*-xylenebis(pyridinium)bromide (DPX) fluorescence resulting from dilution was measured to assess the leakage of aqueous contents from vesicles [23]. ANTS/DPX were encapsulated in LUVs of PC or PC/PG mixtures when dried lipid films were hydrated in Hepes buffer, pH 7.4, containing 20 mM NaCl, 12.5 mM ANTS, and 45 mM DPX. To avoid spontaneous leakage, the osmolarity of both buffers was adjusted to 190 mosM using a cryoscopic osmometer (Fiske one-ten). Afterwards, non-encapsulated ANTS/DPX was removed by gel filtration on a Sephadex G-75 (Amersham Pharmacia Biotech, Upsala, Sweden) column eluted with 5 mM Hepes with 100 mM NaCl (pH 7.4). ANTS/DPX leakage out of the LUVs (100 μM lipids) was measured after 45 min incubation at room temperature or above the transition temperature in the case of PC. Leakage was monitored by measuring the increase in ANTS/DPX fluorescence intensity at 520 nm, with an excitation of 355 nm and slits of 5 nm. Peptide–lipid molar ratios were ranging from 1/1 to 1/100. The percentage of leakage was calculated as

$$\%\ \text{leakage} = [(F - F_0)/(F_{100} - F_0)] \times 100, \quad (2)$$

where F_0 is the initial fluorescence of LUVs; F the fluorescence intensity after incubation with the peptide; F_{100}, fluorescence intensity after addition of 10 μL of a 10% (v/v) Triton 100 solution (complete lysis of the LUV).

Lipid mixing assay

Lipid mixing of LUVs of PC/PG was measured using the resonance energy transfer assay of Struck et al. [24]. Lipid vesicles containing 0.6 mol% each of NBD-PE (energy donor) and Rho-PE (energy acceptor) and unlabelled vesicles were prepared at a 1:5 mixture of labelled and unlabelled vesicles (140 μM total phospholipid concentration) and were suspended in 1500 μL of 10 mM Tris buffer, pH 7.4, and a small volume of peptide was added. The increase at 540 nm was monitored the excitation being at 467 nm. The fluorescence intensity of the lipid vesicles without peptide was the zero percent of lipid mixing and the fluorescence upon the addition of Triton X-100 (0.1% v/v) was referred to a 100% of lipid mixing.

Haemolysis of rabbit red blood cells

The peptides were tested for their haemolytic activities against rabbit red blood cells (rRBC). rRBC were prepared from fresh venous blood collected in 6 mM EDTA and washed twice (centrifugation for 10 min at 700*g*, room temperature) in 30 mM Tris–HCl, 100 mM NaCl, 1 mM EDTA, pH 7.4, and then suspended in the same buffer. Peptides were incubated with 0.13% rRBC (v/v) in 1 mL of Tris buffer for 45 min at 37 °C. Thereafter intact cells were pelleted (15,800*g*, 3 min) and the released haemoglobin was measured by the absorbance at 415 nm as described in [25]. The extent of haemolysis was calculated as follows

$$\% \text{ haemolysis} = [(A_{pep} - A_0)/(A_w - A_0)] \times 100, \quad (3)$$

where A_{pep} and A_0 are the absorbances of the samples incubated with and without peptide, and A_w is the absorbance observed after hypotonic lysis with pure water.

Results and discussion

Experimental information on the type of interactions established by the internal fusion peptides of class II fusion proteins with membranes is at present limited. The only protein of this class for which a high-resolution structure is available is the E protein of TBE virus and thus provides the first example of the native structure of an internal fusion peptide. The X-ray crystal structure of the TBE virus E protein showed that the putative internal fusion peptide is constituted by a loop between two anti-parallel strands. This region is highly constrained by multiple interactions including several internal hydrogen bonds, one salt bridge, and one disulphide bond [3].

Although there is not available structural data about the envelope proteins of other flaviviruses, predictive structural analyses support the notion that the internal fusion peptides are segmented into two regions separated by a putative turn or loop.

Consequently, to identify putative internal fusion peptides within the E2 envelope protein of HGV/GBV-C, we have studied the profiles of Kite and Doolittle (hydropathicity index) and Chou and Fasman (secondary structure prediction) to select E2 regions sharing both partition into membranes and β-turn structure tendencies (Fig. 1). In a previous work, the E2(279–298) peptide region was synthesized and biophysically characterized [7]. In this work, the E2(267–284) peptide, which should be expected to be a better candidate as an internal fusion peptide according to these predictive profiles, has been selected and synthesized. Furthermore, this peptide also accomplishes the particular amino acid composition criteria established for fusion peptides that have been mentioned in the Introduction section.

Interaction of E2 peptides with model membranes

It has been described that spontaneous fusion peptide assembly into model membranes may also reflect the early events that mediate fusion peptide integration into target membranes. In this sense, we have studied the lipid interactions of the two E2 peptides using large unilamellar liposomes of different composition.

Peptide binding to lipid vesicles was investigated by intrinsic Trp fluorescence emission experiments, measuring the fluorescence quantum yield, and the wavelength of the emission maximum in the absence and in the presence of different lipid/peptide ratios of LUVs. To this end, peptide analogues that contain a N-terminal Trp residue were synthesized.

The maximal Trp fluorescence emission wavelength (λ_{max}) of E2(267–284)W and E2(279–298)W was 350 nm in buffer thus indicating that the Trp is highly exposed to the aqueous medium.

To investigate the contribution of electrostatic interactions, the peptides were titrated with neutral, negatively, and positively charged vesicles. Titration of the

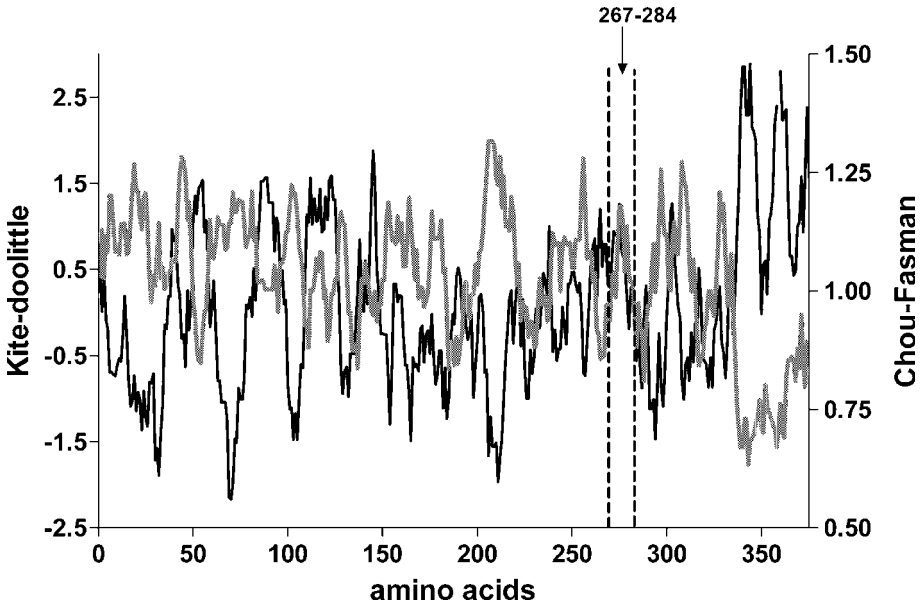

Fig. 1. Primary structure analysis of the HGV/GBV-C E2 protein. The plots (mean value for a window of 18 amino acids) were made using the Kyte–Doolittle hydrophobicity index (grey), and Chou and Fasman secondary structure prediction (black) scale for individual residues.

E2(267–284)W with DMPC and DMPC/DMPG (2/1) LUVs had no significant effect on the Trp fluorescence emission spectra. However, a blue shift of 5 nm was found for this peptide upon addition of DMPC/DMTAP (2/1) as a consequence of the electrostatic interactions between the positively charged phospholipid and the glutamic residues ($Glu^{271,274}$) of the peptide.

Incubation of E2(279–298)W peptide with DMPC only decreased the fluorescence intensity, but had no effect on the λ_{max}. Contrarily, the addition of mixed DMPC/DMPG and DMPC/DMTAP shifted the λ_{max} to lower wavelengths (blue shifts of 18 and 13 nm, respectively) (see Fig. 1 of supplementary material) as well as decreased the fluorescence intensity. These values are indicative that the Trp residue is located in a less polar environment when there is a charged phospholipid in the lipid vesicles, showing an interaction and a partial penetration of the peptide into the hydrophobic tail of the bilayer [26]. Plotting the percentage of initial fluorescence as a function of the lipid concentration (Fig. 2) enabled the calculation of K_d values. The titration curves for E2(279–298)W peptide show saturable binding. The peptide affinity for negatively charged vesicles (K_d was 110.3 ± 15.6 μM for DMPC/DMPG) was higher than those for positively charged and neutral liposomes (K_d was 166.9 ± 33.1 and 359.8 ± 23.4 μM for DMPC/DMTAP and DMPC, respectively). These results are in agreement with those previously obtained when titrated the peptide with PC/PS (65/35) vesicles [7] thus indicating that the E2(279–298)W peptide strongly interacts with negatively charged vesicles.

The effects of E2 peptides on the thermotropic properties of the phospholipid bilayers were measured using differential scanning calorimetry (DSC). Multilamellar vesicles of pure DMPC and mixtures of DMPC/DMPG 2:1, DMPC/DMTAP 2:1, and those containing different concentrations of the two peptides were studied to get more information about the peptide interaction with model membranes.

DMPC exhibits two phase transitions, a pre-transition at approximately $T_p \simeq 14$ °C and the main transition at $T_m \simeq 23$ °C [27]. Both E2 peptides did not show a significant displacement of the phase transition midpoint of DMPC-MLVs (Fig. 3A), although the broadening of the main transition peak, described as peak width at half height, was considerable at the highest peptide percentage

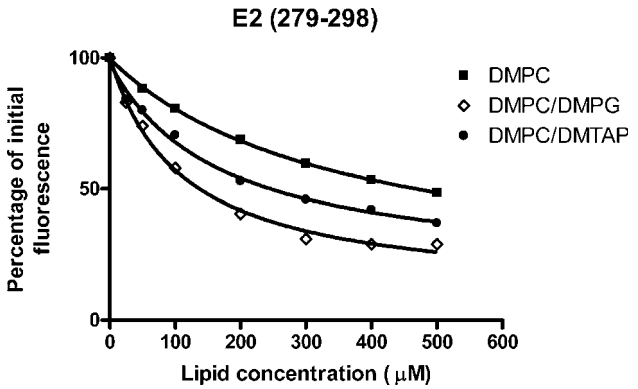

Fig. 2. Fluorescence titration curves of E2(279–298)W with different lipid compositions: DMPC (■), DMPC/DMPG (◊) and DMPC/DMTAP (●). Curve-fitting of the experimental data is represented with solid lines.

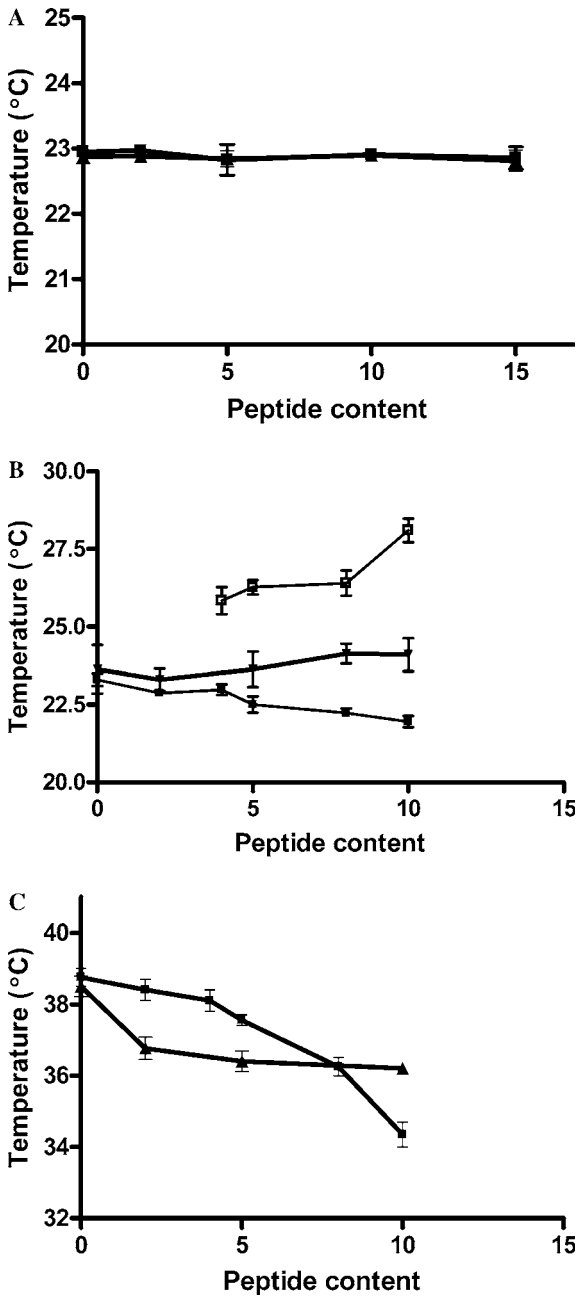

Fig. 3. Temperature variation of the main transition peak as a function of peptide content, E2(267–284) (▲) and E2(279–298) (■,□) at the three studied phospholipid compositions, DMPC (A), DMPC/DMPG (B), and DMPC/DMTAP (C).

(data not shown). These results indicate that there is a non-cooperative mixing of the peptides with DMPC bilayers, the peptides probably being localized in the outer part of the bilayer without penetrating as we have also assessed with the fluorescence experiments.

The thermograms of DMPC/DMPG vesicles were highly different in the presence of E2(267–284) or E2(279–298) (Fig. 3B). As shown in this figure, while E2(267–284) did not significantly modify the T_m, the main transition profile split into two almost separate peaks at E2(279–298) peptide contents higher than 0.02 of peptide/lipid molar ratio. The distance between the transition temperatures of the higher- and lower-melting components increased when rising peptide/lipid relationships. Furthermore, there was a broadening of the peak, accompanied with a little decrease in enthalpy (data not shown). The early disappearance (around 0.01 peptide/lipid molar ratio) of the main transition peak clearly indicates a high perturbation of the DMPC/DMPG bilayer after its interaction with E2(279–298). According to the fluorescence studies performed, this peptide strongly interacts with negatively charged phospholipids probably due to the presence of positive charged amino acids ($Arg^{291,292}$) within its primary sequence.

On the other hand, the interaction of E2(267–284) with DMPC/DMTAP 2:1 (Fig. 3C) involves a decrease of 2 °C in T_m that can be interpreted as a fluidification of the bilayer, induced by partial penetration and consequent deformation of the packing of the phospholipid chains [28]. Similarly, E2(279–298) in the presence of DMPC/DMTAP vesicles was also able to induce a shift (around 4 °C) of the main transition peak.

To sum up, as expected from the results of the fluorescence experiments, the perturbations exerted by the two differently charged peptides were strongly dependent on the electrical charge of the polar group of the phospholipids.

With the aim to better analyse the effect produced by E2(279–298) in DMPC/DMPG MLVs, the thermotropic behaviour of the peptide/lipid mixtures was analysed in a microDSC III calorimeter. Likewise, the thermograms presented a phase separation in the main transition peak. This effect was noticed at smaller concentrations of the peptide (0.02 peptide/lipid molar ratio) than those observed in the conventional calorimetric analysis. The thermograms consisted of two overlapped components which were fitted with a Gaussian function. Several examples of such fittings are shown in Fig. 4. It can be observed that the peak located at the higher temperature increased when the content of the E2(279–298) peptide was higher. When achieved a peptide:lipid molar ratio of 0.04 (Fig. 4C) the main transition peak was split into two almost separate peaks, one located near 24 °C and the other around 27 °C. From these results and according to others [29,30], we suggest that the peptide could form specific domains after interacting with the negatively charged DMPG. The presence of phase separations and the appearance of a new peak at higher temperatures than the transition temperature

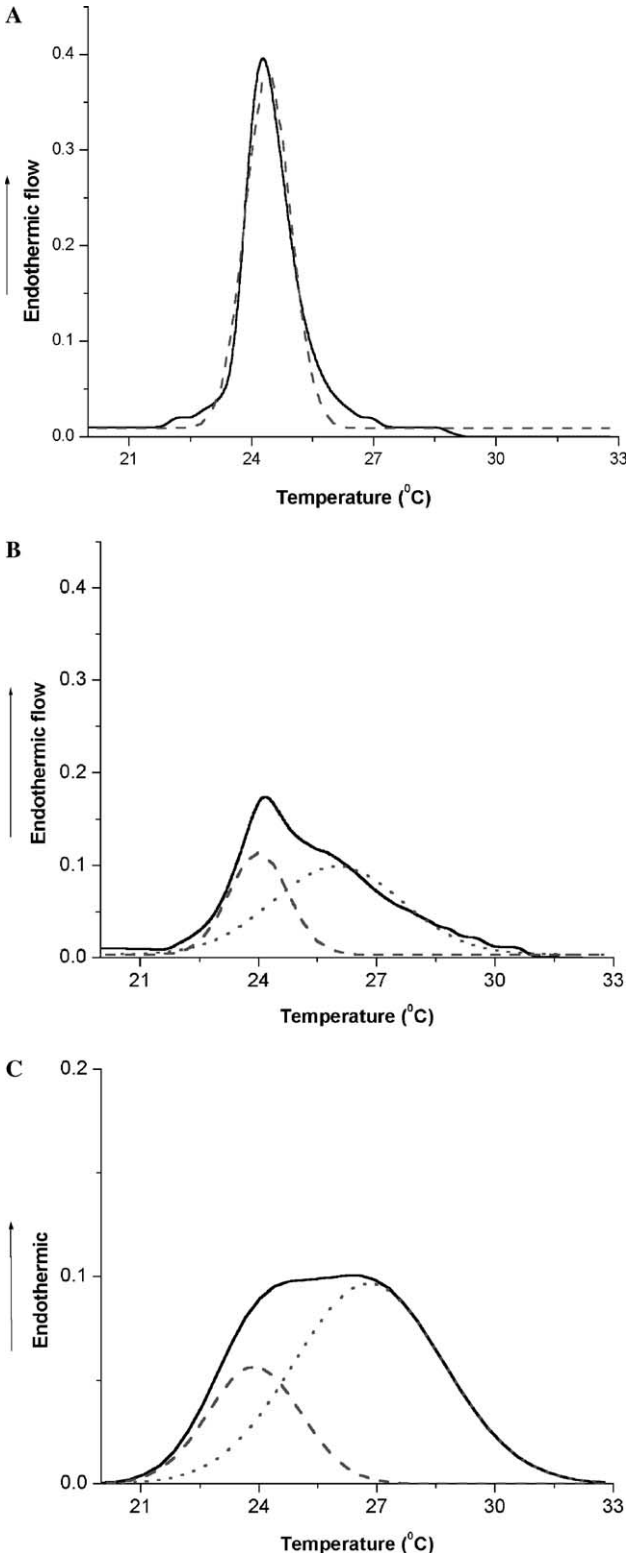

Fig. 4. Deconvolution thermograms of DMPC/DMPG mixtures alone (A) or with 0.02 (B), 0.04 (C) E2(279–298) peptide/phospholipid molar ratio.

of the pure lipids would suggest that the peptide is likely to be located in the surface with a shallow penetration of the peptide into the lipid bilayer.

Conformational study

It has been described that the conformational behaviour of fusion peptides is greatly important for their fusogenic activity [31,32]. To investigate whether the different behaviour of the peptides in their interaction with model membranes could be related to their structures, we determined the conformation of the membrane-bound peptides by means of infrared spectroscopy (FTIR) and circular dichroism (CD).

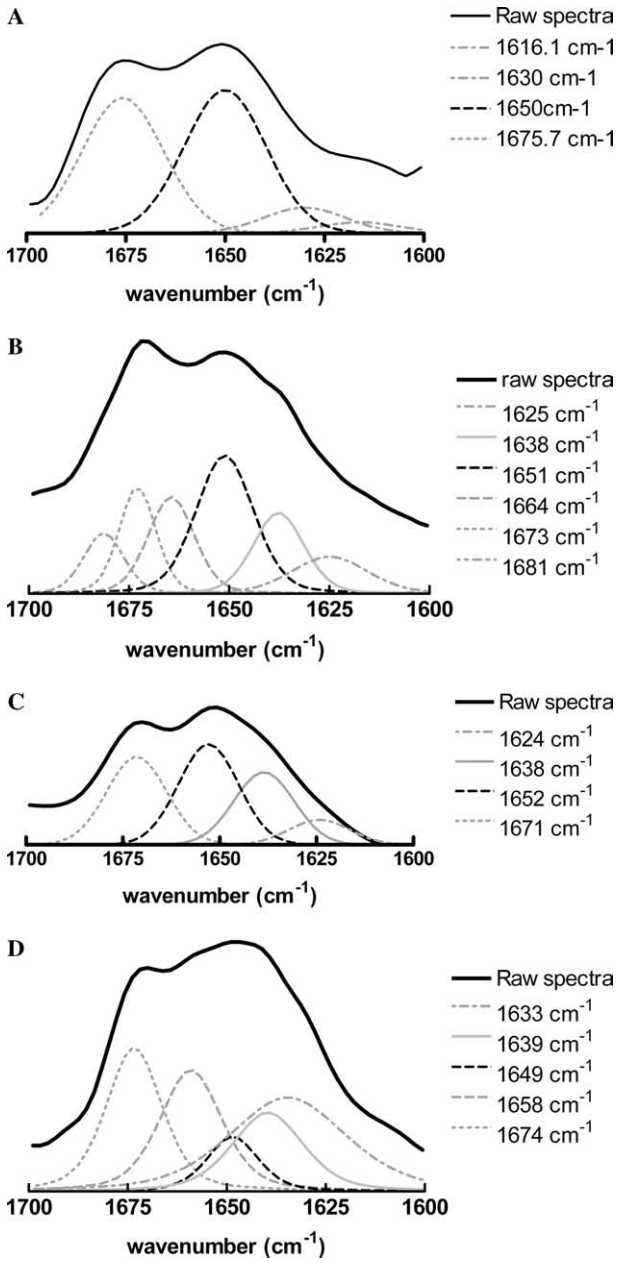

Fig. 5. FTIR conformational analysis of E2(267–284) (A and C) and E2(279–298) (B and D) in D_2O (A and B) and in the presence of DMPC/DMPG MLVs (C and D).

Figs. 5A and B show the amide I band of the infrared spectra as well as the deconvoluted spectra in D_2O for E2(267–284) and E2(279–298) peptides, respectively. The amide I band has its maximum at 1650 cm^{-1} for E2(267–284) and 1651 cm^{-1} for E2(279–298) peptides which can be related with unstructured conformations including open loops [33]. The amide I peak located at 1672 cm^{-1} arises from the counterion trifluoroacetate (TFA).

The infrared spectrum of the E2(267–284) peptide in the presence of multilamellar vesicles of DMPC/DMPG 2/1 shows the major deconvoluted component centered at 1652 cm^{-1} which can be correlated to unordered conformations (Fig. 5C). The component at 1638 cm^{-1} can be attributed to intramolecular C=O vibrations of β-sheets and that at 1624 cm^{-1} is probably due to aggregated extended structures. Therefore, the addition of negatively charged vesicles to the E2(267–284) did not affect the peptide conformation significantly. In contrast, the infrared spectrum of the E2(279–298) peptide in the presence of DMPC/DMPG 2/1 liposomes was quite different (Fig. 5D). In this sense, the major component band centered at 1650 cm^{-1} in D_2O decreased in the presence of negatively charged vesicles and a component band appeared at 1658 cm^{-1} which could be assigned to α-helical structures. Moreover, the bands located around 1635 cm^{-1} could be attributed to β-sheet conformations.

These results are supported by the experimental data obtained by circular dichroism. The experimental CD spectra of the free peptides in buffer showed unordered conformations. When trifluoroethanol (TFE) was added, the peptides adopted helical conformations increasing when the TFE content was higher (see Figs. 2 and 3 of supplementary material). The minimum around 200 nm characteristic of an aperiodic structure was maintained upon addition of neutral or negatively charged liposomes to the E2(267–284) peptide. When analyzing this peptide in the presence of DMPC/DMTAP a slightly different peptide secondary structure was induced with a bias toward more ordered conformations (Fig. 6a and Table 2 of supplementary material).

On the other hand, the addition of liposomes of different lipid composition to the E2(279–298) peptide clearly contributed to the stabilization of more ordered secondary structures. As shown in Fig. 6B, a maximum at 195 nm and two minima near 208 and 222 nm, characteristic of α-helix structure, were observed, the largest contribution of the helical conformation being observed upon addition of DMPC/DMPG liposomes (quantitative CD data are given in Table 2 of supplementary material).

As illustrated in Fig. 7, two-dimensional projections of both E2 peptide sequences could be a suitable

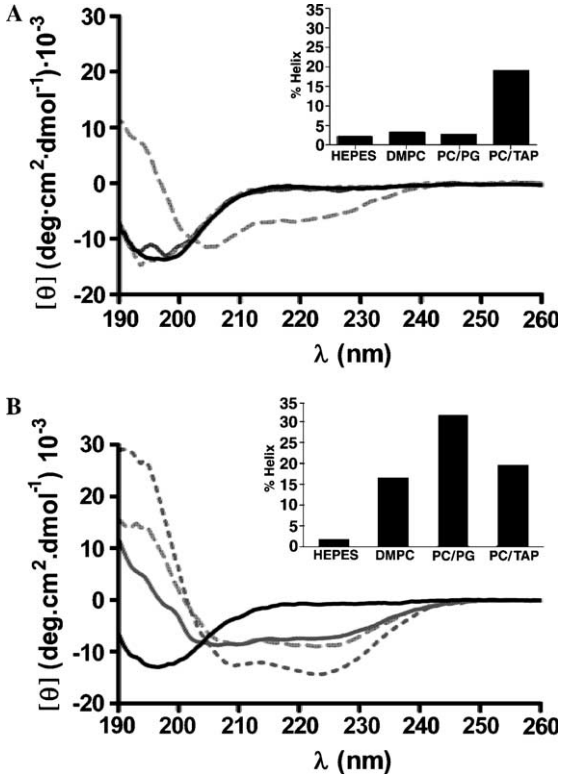

Fig. 6. CD spectra of E2(267–284) (A) and E2(279–298) (B) in buffer and SUVs of DMPC, DMPC/DMPG, and DMPC/DMTAP. Inset: estimation from the CD spectra of the content in α-helix in different media.

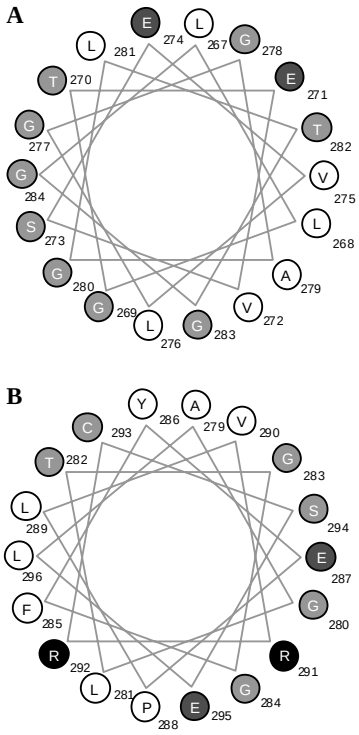

Fig. 7. Helical wheel projection of E2 peptides: (A) E2(276–284); (B) E2(279–298). Annotated numbers represent the relative locations of amino acid residues (white, hydrophobic; light grey, polar; dark grey, acid; black, basic) within protein primary structure.

approximation of the 3D disposition of the amino acids. It can be observed that each helix possesses a glycine-rich polar face and a wide hydrophobic domain rich in bulky aliphatic amino acids. The presence of charged amino acids located within the apolar domain plays a crucial role in the peptide binding to lipid vesicles via electrostatic interactions. Thus, the addition of negatively charged vesicles to E2(279–298) induces an α-helix conformation which is stabilized by the electrostatic interaction of the positively charged residue ^{292}Arg and the negatively charged lipid heads. In contrast, only the addition of DMPC/DMTAP vesicles to the E2(267–284) promotes the structuration of this peptide which could be based on the electrostatic interaction of the ^{271}Glu and ^{274}Glu residues with positively charged lipids.

Membrane destabilization

It has been described that viral fusion peptides show lytic effects after binding to liposomes. In addition, vesicle suspensions treated with these sequences may undergo mixing of lipid components, an activity that may be correlated with virus-induced membrane fusion.

To further explore the possible distortion of the bilayer organization induced by the E2 synthetic peptides, the effect of these peptides on the release of the encapsulated fluorophores ANTS/DPX was monitored by dequenching of the ANTS.

Fig. 8A shows the dependence of PC vesicle leakage on the lipid to peptide molar ratio. Leakage of 50% was reached for E2(279–298) peptide at a lipid to peptide ratio of 2:1, while the E2(267–284) peptide was clearly less efficient permeabilizing neutral vesicles.

Significant differences were obtained when assayed negatively charged vesicles leakage. Thus, the addition of the E2(279–298) peptide to PC/PG LUVs induced complete lysis of liposomes at a lipid to peptide ratio of 1:1 (Fig. 8B) whereas the E2(267–284) peptide hardly exerted any effect on PC/PG vesicles (data not shown). Percentage of ANTS/DPX leakage induced by E2(279–298) in PC and PC/PG vesicles at a function of time is shown in Figs. 4 and 5 of Supplementary material. Intervesicular lipid mixing assay was performed on negatively charged vesicles to get more insights into the fusion activity of the E2(279–298) peptide. As depicted in Fig. 8B, E2(279–298) produced lipid mixing of PC/PG liposomes in a dose-dependent manner. Fig. 6 of supplementary material shows the experimental changes in fluorescence intensity of PC/PG lipid vesicles induced by this peptide.

Besides, since a good correlation has been observed between the ability of a particular sequence to support fusion in the intact protein and its ability to induce

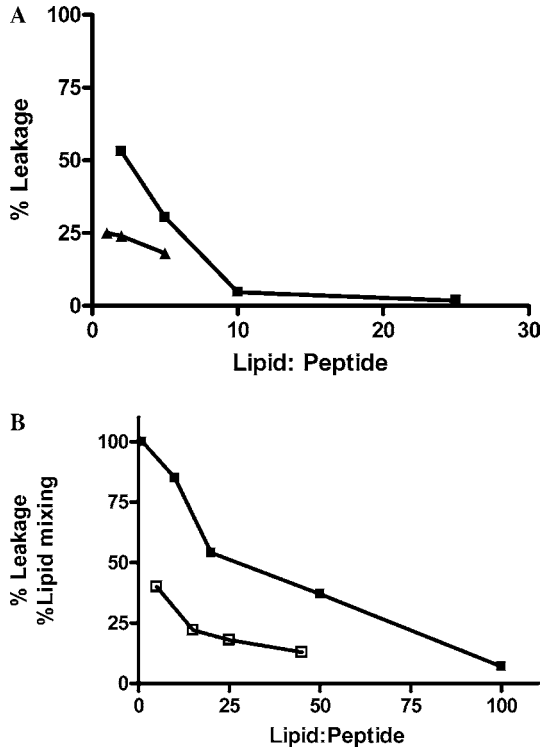

Fig. 8. (A) ANTS/DPX leakage induced by E2(267–284) (▲) and E2(279–298) (■) in PC vesicles. (B) ANTS/DPX leakage (■) and lipid mixing (□) induced by E2(279–298) in PC/PG vesicles.

haemolysis [34–36], haemolysis experiments had been performed to further analyse the fusion properties of both E2 peptides. The haemolytic activity of the two peptides was assayed on rabbit RBC, in terms of percentage of haemolysis. While a concentration of 200 μM of the E2(279–298) peptide induced 100% haemolysis of RBC, the haemolytic activity of the E2(267–284) was quite lower since it was necessary a peptide concentration of 400 μM to reach a 50% of haemolysis (see Fig. 7 of supplementary material). The remaining activity observed for E2(267–284) could be explained by the shared region between both overlapping E2 peptides (279–284: AGLTGG).

Conclusions

Altogether, the experimental data obtained in this work reinforce the hypothesis that the E2(279–298) peptide could be an internal fusion peptide of HGV/GBV-C. In our hands, the E2(279–298) sequence was able, on the one hand, to bind with high affinity to negatively charged membranes modifying the biophysical properties of phospholipid model membranes and, on the other hand, to permeabilize efficiently negatively charged vesicles. Furthermore, in the present study lipid mixing and haemolysis clearly indicate the ability of this particular sequence to support HGV-GBV-C-induced membrane fusion.

In contrast to the expectation by the prediction algorithms, E2(267–284) hardly interacts with negative lipid membranes and neither permeabilizes vesicles nor induces efficient haemolysis.

The conformational studies performed led us also to conclude that the E2(279–298) fusogenic activity could be related to the spatial disposition of charged amino acids, which seems to be suitable for the interaction with the target membrane. Peptide–lipid interaction (critical for bilayer destabilization) stabilizes the α-helical conformation of lipid-bound peptide, being modulated by the hydrophobic environment of Arg residues and the membrane composition.

Acknowledgments

This work was supported by Project BQU2003-0507-C02-01/02 from the *Ministerio de Ciencia y Tecnología* (Spain). C. Larios is the recipient of a pre-doctoral grant also from the MCyT.

Appendix A. Supplementary data

Supplementary data associated with this article can be found, in the online version, at doi:10.1016/j.abb.2005.06.027.

References

[1] C. Voisset, J. Dubuisson, Biol. Cell 96 (2004) 413–420.
[2] F.A. Rey, F.X. Heinz, C. Mandl, C. Kunz, S.C. Harrison, Nature 375 (1995) 291–298.
[3] S.L. Allison, J. Schalich, K. Stiasny, C.W. Mandl, F.X. Heinz, J. Virol. 75 (2001) 4268–4275.
[4] A.T. Yagnik, A. Lahm, A. Meola, R.M. Roccasecca, B.B. Ercole, A. Nicosia, A. Tramontano, Proteins 40 (2000) 355–366.
[5] B. Robertson, G. Myers, C. Howard, T. Brettin, J. Bukh, B. Gaschen, T. Gojobori, G. Maertens, M. Mizokami, O. Nainan, S. Netesov, K. Nishioka, T. Shini, P. Simmonds, D. Smith, L. Stuyver, A. Weiner, Arch. Virol. 143 (1998) 2493–2503.
[6] E.I. Pecheur, J. Sainte-Marie, A. Bienvene, D. Hoekstra, J. Membr. Biol. 167 (1999) 1–17.
[7] C. Larios, B. Christiaens, M.J. Gomara, M.A. Alsina, I. Haro, FEBS J. 272 (2005) 2456–2466.
[8] V.D. Del Angel, F. Dupuis, J.P. Mornon, I. Callebaut, Biochem. Biophys. Res. Commun. 293 (2002) 1153–1160.
[9] L. Zhang, H.P. Ghosh, J. Virol. 68 (1994) 2186–2193.
[10] J. Corver, A. Ortiz, S.L. Allison, J. Schalich, F.X. Heinz, J. Wilschut, Virology 269 (2000) 37–46.
[11] S.W. Gollins, J.S. Porterfield, J. Gen. Virol. Pt. 67 (1) (1986) 157–166.
[12] K. Stiasny, C. Koessl, F.X. Heinz, J. Virol. 77 (2003) 7856–7862.
[13] W.C. Chan, P.D. White, Fmoc Solid Phase Peptide Synthesis, Oxford University Press, New York, 2000.
[14] E. Kaiser, R.L. Colescott, C.D. Bossinger, P.I. Cook, Anal. Biochem. 34 (1970) 595–598.

[15] M.J. Hope, M.B. Bally, G. Webb, P.R. Cullis, Biochim. Biophys. Acta 812 (1985) 55–65.
[16] G.R. Bartlett, J. Biol. Chem. 234 (1958) 466–468.
[17] R.B. Weinberg, M.K. Jordan, J. Biol. Chem. 265 (1990) 8081–8086.
[18] B. Christiaens, S. Symoens, S. Verheyden, Y. Engelborghs, A. Joliot, A. Prochiantz, J. Vandekerckhove, M. Rosseneu, B. Vanloo, S. Vanderheyden, Eur. J. Biochem. 269 (2002) 2918–2926.
[19] N. Rojo, M.J. Gomara, M.A. Busquets, M.A. Alsina, I. Haro, Talanta 60 (2003) 395–404.
[20] A. Lobley, L. Whitmore, B.A. Wallace, DICHROWEB: an interactive website for the analysis of protein secondary structure from circular dichroism spectra, Bioinformatics 18 (2002) 211–212.
[21] L. Whitmore, B.A. Wallace, DICHROWEB, an online server for protein secondary structure analyses from circular dichroism spectroscopic data, Nucleic Acids Res. 32 (2004) W668–W673.
[22] Y.H. Chen, J.T. Yang, H.M. Martinez, Biochemistry 11 (1972) 4120–4131.
[23] H. Ellens, J. Bentz, F.C. Szoka, Biochemistry 23 (1984) 1532–1538.
[24] D.K. Struck, D. Hoekstra, R.E. Pagano, Biochemistry 20 (1981) 4093–4099.
[25] M. Ferreras, F. Hoper, S.M. Dalla, D.A. Colin, G. Prevost, G. Menestrina, Biochim. Biophys. Acta 1414 (1998) 108–126.
[26] P.E. Thoren, D. Persson, E.K. Esbjorner, M. Goksor, P. Lincoln, B. Norden, Biochemistry 43 (2004) 3471–3489.
[27] J.R. Silvius, in: P.C. Jost, O.H. Griffith (Eds.), Lipid–Protein Interactions, John Wiley, New York, 1982, pp. 239–281.
[28] D. Papahadjopoulos, M. Moscarello, E.H. Eylar, T. Isac, Biochim. Biophys. Acta 401 (1975) 317–335.
[29] K. Lohner, E.J. Prenner, Biochim. Biophys. Acta 1462 (1999) 141–156.
[30] S.G. Peisajovich, R.F. Epand, R.M. Epand, Y. Shai, Eur. J. Biochem. 269 (2002) 4342–4350.
[31] D. Rapaport, Y. Shai, J. Biol. Chem. 269 (1994) 15124–15131.
[32] S. Lee, R. Aoki, O. Oishi, H. Aoyagi, N. Yamasaki, Biochim. Biophys. Acta 1103 (1992) 157–162.
[33] M. Mar Martinez-Senac, S. Corbalan-Garcia, J.C. Gomez-Fernandez, Biochemistry 39 (2000) 7744–7752.
[34] J.L. Nieva, A. Agirre, Biochim. Biophys. Acta 1614 (2003) 104–115.
[35] X. Han, D.A. Steinhauer, S.A. Wharton, L.K. Tamm, Biochemistry 38 (1999) 15052–15059.
[36] K.J. Cross, S.A. Wharton, J.J. Skehel, D.C. Wiley, D.A. Steinhauer, EMBO J. 20 (2001) 4432–4442.

Artículo 4: Estudio de absorción, langmuir y penetración en monocapas fosfolipídicas del péptido E2(279-298)

Cristina Larios, José Jr. Miñones, Isabel Haro, María A. Alsina y María A. Busquets

Departamento de Química de Péptidos y Proteínas, Instituto de Investigaciones Químicas y Ambientales de Barcelona, IIQAB-CSIC.
Departamento de Fisicoquímica, Facultad de Farmacia, Universidad de Barcelona.
Departamento de Química Física, Facultad de Farmacia, Universidad de Santiago de Compostela

Cristina Larios, José Jr. Miñones, Isabel Haro, María A. Alsina and María A. Busquets (2005) Study of adsorption, langmuir and penetration into phospholipid monolayers of E2(279-298) peptide, J. Phys. Chem. B, enviado.

Resumen

En este trabajo se investigan las propiedades fisicoquímicas del péptido sintético perteneciente a la secuencia (279-298) de la proteína E2 del virus de la hepatitis G (GBV-C/HGV) realizando monocapas de adsorción junto con monocapas de extensión. Las medidas de actividad superficial y las isotermas de compresión de E2(279-298) se realizan sobre subfases de distinta fuerza iónica para evaluar sus efectos en el péptido. Los resultados obtenidos indican que las monocapas de E2(279-298) en presencia de un elevado contenido de sales exhiben un mayor área que las obtenidas en agua como subfase. Con tal de conocer la topografía de la monocapa, imágenes de monocapas del péptido puro se obtienen en el microscopio del ángulo de Brewster (BAM). La capacidad de interacción del péptido con modelos de membrana monomolecular se mide realizando cinéticas de penetración de DPPC, DMPC y mezclas de DMPC/DMPG a área constante con el péptido en la subfase. Se realizan también las isotermas de extensión de estos fosfolípidos y sus mezclas sobre subfase PBS y subfase PBS con péptido adicionado. El objetivo de estos experimentos es conocer la influencia del péptido cuando está presente en la subfase y los estados de ordenación de las moléculas en las isotermas. Los resultados obtenidos muestran que se produce interacción del péptido con este modelo de membrana y que la longitud de cadena es un parámetro importante a tener en cuenta al estudiar interacciones péptido-lípido. Además se discute el papel del grupo voluminoso polar de la DMPG en la interacción.

Study of adsorption and penetration of E2 (279-298) peptide into phospholipid monolayers.

Larios, C[1,2].; Miñones, J. Jr[3]; Haro, I.[2]; Alsina, M.A.[1]; Busquets, M.A.[1*]

[1]Associated Unit CSIC, Department of Physical Chemistry, Faculty of Pharmacy, University of Barcelona, Av. Joan XXIII s/n 08028 Barcelona, Spain.

[2] Department of Peptide & Protein Chemistry, IIQAB-CSIC, Jordi Girona 18-26 08034 Barcelona, Spain;

[3] Department of Physical Chemistry, Faculty of Pharmacy, University of Santiago de Compostela, Santiago de Compostela, Spain.

Keywords: GBV-C/HGV, Langmuir monolayers, ionic strength, phospholipids, Brewster angle microscopy.

Title running head: E2(279-298) peptide physicochemical characterization.

Abstract

The physicochemical properties of a synthetic peptide corresponding to the sequence (279-298) of the hepatitis G virus (GBV-C/HGV) E2 protein were investigated using adsorption together with Langmuir film monolayers. Surface activity and compression isotherms of E2(279-298) were carried out at different subphase ionic strength to evaluate their effects on peptide. The results obtained indicated that the monolayers of E2(279-298) in the presence of high content of salts exhibited a greater area than those obtained on water as subphase. In order to better know the topography of the monolayer, Brewster angle microscopy (BAM) images of pure peptide monolayers were realized. Penetration kinetics of the peptide into the pure lipid monolayers of dipalmitoylphosphatidylcholine (DPPC), dimyristoylphosphatidylcholine (DMPC) and mixtures of dimyristoylphosphatidylcholine/ dimyristoylphosphatidylglicerol (DMPC/ DMPG) were performed to know their ability to insert in a model membrane system. Furthermore, these phospholipid monolayers were compressed on PBS substrates with peptide to know the interaction between both components. The results show that lipid acyl chain length is an important parameter to be taken into account in studying peptide-lipid interactions, although the paper of the voluminous polar group of DMPG on the interaction is also discussed.
.

* To whom the correspondence should be sent.
Department of Physical Chemistry, Faculty of Pharmacy, University of Barcelona.
Av. Joan XXIII s/n 08028 Barcelona, Spain
Tel: +34934024556
Fax: +34934035987
mabusquetsvinas@ub.edu

1. Introduction

One important step in virus infection is the fusion process initiated by envelope proteins. Although it is clear that the envelope proteins (E) of the virus are responsible for the contact of the virus with the target cell, the entry of GBV-C/HGV into the cells is at present unknown. However, the genome organization of GBV-C/HGV is similar to that of the hepatitis C virus (HCV) for which the entry into the cells is believed to be mediated by the envelope protein E2[1]. This protein contains a fragment near the C-terminal, named fusion peptide that belongs to the class II of the internal fusion peptides described for other viruses [2].

The fusion peptides of several viruses have been studied by biophysical techniques in order to better understand the entry mechanism. In a previous work, we selected a peptide from the E2 envelope protein E2(279-298) with the sequence AGLTGGFYEPLVRRCSELAG and performed biophysical studies with liposomes as model membranes[3]. This peptide sequence interacted in a higher extent with negatively charged lipids probably by the stabilization of the positive residues present in the peptide, effect concomitant with a conformation change from a random coil to an amphipathic alpha helix. Furthermore, the peptide perturbed the lipid bilayer and caused carboxyfluorescein leakage, without deeper penetration of the peptide into the hydrophobic core of the bilayer. This apparent surface behaviour raises the importance of analyzing the physicochemical properties of the peptide as well as its interaction with lipids at the surface level.

Taking into consideration the above premises, the aim of the present work is to study the physicochemical properties of the E2(279-298) with special emphasis on the influence of ionic strength on peptide surface properties, by using adsorption and Langmuir-monolayer techniques at the air-water interface [4,5] together with Brewster angle microscopy (BAM) to visualize the structure and morphology of the monolayers. The results obtained suggest that the increase of subphase ionic strength stabilizes the monolayer. On another hand, we have examined the lipid-peptide interactions in different monolayer systems by means of penetration kinetics and pressure-area isotherms. The obtained information from these experiments, at different subphase compositions, is useful to understand the mechanism of interaction between peptide and membrane lipids. The higher penetration of peptide into phospholipids is attained when the monolayers are in the liquid expanded state and the bigger interaction was observed with DMPC.

2.- **Materials and methods**

2.1.Chemicals

Amino acids and TGR Novasyn resin were obtained from Novabiochem. Dimethylformamide (DMF) was purchased from Sharlau. Washing solvents such as acetic acid, diethylether, and trifluoroacetic acid (TFA) were obtained from Merck. 2- (1H-Benzotriazol-1-yl)- 1,1,3,3- tetramethylamonium tetrafluoroborate (TBTU), N,N'- diisopropylcarbodiimide (DIPCDI) and N- hydroxybenzotriazole (HOBt) coupling reagents were obtained from Fluka and Novabiochem. Scavengers such as ethanedithiol (EDT) or triisopropilsilane (TIS) were from Sigma-Aldrich. Dipalmitoylphosphatidylcholine (DPPC), dimyristoylphosphatidylcholine (DMPC), and dimyristoylphosphatidylglicerol (DMPG) were from Avanti Polar Lipids Inc. and were used without further purification. Chloroform and methanol were purchased from Merck. Water was double distilled and deionised (MilliQ system, Millipore) (18.2 MΩcm, pH 5.8). Phosphate buffered saline used for the subphase was PBS (A) (16 mM $NaH_2PO_4 \cdot 12\ H_2O$, 81 mM Na_2HPO_4, 48 mM NaCl) (A) and PBS (B) (10 mM phosphate buffer, 2.7 mM KCl, 137 mM NaCl) (B) was purchased from Sigma-Aldrich.

2.2. *Peptide Synthesis*

The synthesis of E2(279-298) in a TGR Novasyn resin (0.29 $meq.g^{-1}$) as a C-terminal carboxamide was achieved by following a Fmoc/tbut strategy. Couplings were realized with diisopropylcarbodiimide / hydroxybenzotriazole (DIPCDI/HOBt). Threefold molar excess of amino acids were used during the synthesis, and the coupling was evaluated by the ninhydrin test[6]. Repeated coupling was needed for Cys 293. Deprotection of the lateral chains of the peptide and cleavage from the resin was carried out with a mixture of trifluoroacetic acid (TFA)/ethaneditiol (EDT) /Water/triisopropylsilane (TIS)

(94/2.5/1/2.5). Peptide was finally isolated by precipitation with ethyl ether, centrifuged and lyophilized. Crude peptide was purified by semi preparative HPLC on a C_{18} silica column. Samples were eluted with acetonitrile (A)/ Water (W) (0.05% TFA) in a linear gradient of 90%W/40%W at a flow rate of 2 mL·min^{-1} and detected at 215 nm. Purified peptide was characterized by analytical HPLC, amino acid analysis and Maldi Toff mass spectrometry[3].

2.3. Monolayer studies

Measurements were performed on a Langmuir film balance KSV 5000 (Helsinki, Finland) equipped with a Wilhelmy platinum plate and a Teflon trough that was rinsed with ethanol and with distilled water before use. All experiments were performed at 21±1 °C [7,8].

2.3.1.Surface activity of the peptide

Surface activity measurements were performed in a cylindrical Teflon trough (volume 70 mL, surface area 30 cm^2). The subphases used were water, phosphate-buffered saline PBS (A) and PBS (B). Increasing volumes of concentrated peptide solutions were injected below the surface through a lateral hole. Changes in surface tension were measured as a function of time for 90 min.

2.3.2 Penetration of the peptide into monolayers

The same trough described above was used in this study. Stock solutions of DPPC, DMPC and DMPC/DMPG (2/1) in chloroform/methanol (3:1) were spread at the air/water interface using a Hamilton syringe, to obtain 5, 10, 20 or 32 mN·m^{-1} of initial surface pressure. After 15 min of stabilization, a peptide solution at a lower peptide concentration than that corresponding to the saturation was injected into the subphase of PBS (A) and the increase in surface pressure was recorded during 90 min.

2.3.3 Compression isotherms

Compression isotherms of E2 (279-298) peptide were carried out in a Teflon trough (volume 1000 mL, surface area 170 cm^2) containing 850 mL of water, PBS (A) or PBS (B). Compression isotherms of DPPC, DMPC or DMPC/DMPG (2/1) monolayers spread on aqueous subphase containing PBS (A) (control) or peptides at 0.25 μM concentration were performed. After 15 min for evaporation of the solvents and to attain the equilibrium, compression of peptide or lipid monolayers was performed at a rate of 25 and 17 Å^2/molec. min, respectively. Each run was repeated three times and the accuracy of the measurements was 1 x 10^{14} Å^2/molecule.

2.4 Brewster angle microscopy

Brewster angle microscopy images and ellipsometric measurements were performed with BAM 2 Plus (NFT, Göttingen, Germany) equipped with a 30 mW laser emitting *p*-polarized light at 532 nm wavelength which was reflected off the air/water interface at approximately 53.1º (Brewster angle), as described by Rodriguez Patino et al.[9]. The shutter speed used was 1/50s. In measuring the relative reflectivity of the film, a camera calibration was necessary. The intensity at each point of the BAM image depends on the local thickness and film optical properties. The expected signal at a certain angle is given by the Fresnel equation. A comparison of this theoretical intensity (Ip), with the measured grey value (G) should allow generating a calibration curve Ip(G), relating any measured G value to its corresponding Ip value. Provided that the camera and digitizer response is linear, this is a straight line:

$$I = |Rp|^2 = Cd^2 \qquad [1]$$

Where C is a constant, d is the film thickness, and Rp is the *p*-component of the light. The reflected light intensity may be calculated from a single layer optical model as a function of the film thickness *d* and the refractive index *n.* This is the concept:

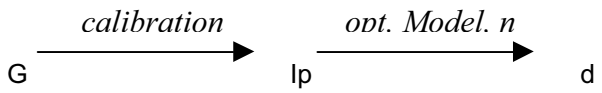

The lateral resolution of the microscope was 2 μm, and the images were digitalized and processed to optimize image quality; those shown below correspond to 768 x 572 pixels.

3. Results and discussion

3.1. Peptide adsorption monolayers.

3.1.1.- Adsorption of peptide onto the air-water interface.

The surface activity of E2 (279-298) peptide was measured by injecting increasing volumes of a concentrated peptide solution (1mg/mL) into water, PBS (A) and PBS (B) subphases and recording the surface pressure achieved in function of time. Figure 1A shows the plot of the change in surface pressure as a function of time upon injection of E2 peptide into water. A small gradual adsorption of peptide was observed at low peptide concentration (0.25 μM) and, due to its hydrophilic character, the maximum surface pressure (around 0.4 mN/m) was not achieved until 40 minutes. The higher the peptide concentration in the subphase the faster was its incorporation in the interface and the higher was the maximum surface pressure attained. For the maximum peptide concentration of 1.97 μM, the equilibrium surface pressure was around 7 mN/m.

Increasing saline concentration of the buffered subphase, PBS (A), increased peptide surface activity, resulting in a π of 12 mN/m at peptide concentration of 1.97 μM (Figure 1B). Similar results were obtained for PBS (B) (Figure not shown), thus indicating that the surface activity of the peptide increased with the ionic strength of the subphase.

These experimental curves provided information on the suitable concentration of the peptide that should be used in the bulk subphase for the experiments of penetration kinetics. Because of the maximum pressure attained for the peptide concentration of 0.25 μM into PBS(A) is slightly lower than the equilibrium spreading pressure of the peptide on this subphase[10], this peptide concentration was used in further penetration studies.

The analysis of the peptide adsorption process from the subphase to the air/water interface allows the calculation of the peptide surface excess concentration (Γ) by applying the Gibbs adsorption equation in its simpler form:$\Gamma = (\Delta\pi/RT\Delta \ln c)$. Where R is the gas constant (8.31 J/Kmol), T the temperature (294 K), $\Delta\pi$ is the pressure increase achieved after 90 min. and c the concentration. The surface molecular area (A) is given by the expression: $A=1/\Gamma N$, where N is the Avogadro´s number. These values, corresponding to the maximum adsorption, are shown in Table 1. It can be deduced that the surface excess concentration increased with the content of the peptide into the different subphases studied and with their ionic strength, whereas the surface molecular area at the maximum adsorption decreased, being this value lower at higher saline substrate concentration. Increasing ionic strength seems to enhance the hydrophobicity of the peptide, as it has been observed for other amphipatic peptides[11] due to the salting out provoked by the salts.

3.2.- Peptide Langmuir monolayers.

3.2.1.- π-A isotherms and Cs^{-1}-π curves.

The compression isotherms of E2(279-298) monolayers spread at the air/water interface on different subphases (Figure 2) showed the ability of the peptide to form monolayers although without reaching the collapse. Spreading larger volumes of the peptide solution did not produce important changes in the shape of the isotherm and the collapse was neither reached. Monolayer stability was assessed by stopping the barriers for 30 min at half compression cycle. No modification of the pressure was observed indicating a lack of peptide desorption and consequently confirming the monolayer stability.

The π–A curve for E2 monolayer spread on water exhibits three regions of different slope. At low surface pressures, the monolayer is in the liquid expanded state with a value of the compressional modulus (defined as $Cs^{-1} = - A\, d\pi/dA$) relatively low, below 13 mN/m (see inset of Fig. 2), characteristic of this state[12]. Upon compression, the monolayer undergoes a phase transition at $\pi \approx 5$ mN/m, which is seen as a pseudo-plateau in the course of the compression isotherm and as minimum in the C_s^{-1}-π curve. This phase transition LE-LC spans over the areas of approximately 196 $Å^2$/molecule to 124 $Å^2$/molecule. Beyond this transition, at low molecular areas, the surface pressure rises due to the increase of molecular packing. The monolayer reaches the liquid condensed state, but without a net collapse as a consequence of the film instability resulting from its dissolution into the aqueous subphase.

The above–mentioned phase transition can be more clearly seen in the plot of the compressional modulus as a function of the surface pressure (inset of Figure 2). The points A and B correspond to the beginning and to the end of the LE-LC transition. The values of surface pressure relative to these points A and B were 4.9 mN/m and 7.2 mN/m, respectively.

This plateau in the π-A isotherms of polymers and polypeptides monolayers has been explained in different ways. Malcom[13-15] has suggested that the plateau is due to the formation of a bilayer.This was first observed by Takenaka et al.[16] and Takeda et al.[17,18], who by means of polarized infrared and transmission techniques, found that when films were transferred on germanium plates at surface pressures above the plateau, they were almost twice in thickness comparing to those transferred below the plateau surface pressure. Nevertheless, other authors have suggested that the plateau is due to molecular segments being partially lifted from the water surface[19] or forced from the air-water interface to a subsurface region[20,21]. For the E2 peptide the results obtained with BAM seems to confirm the last interpretation (see later).

The presence of phosphate buffered subphases, PBS (A) and PBS (B), induces changes in the shape of the isotherms. The plateaux corresponding to the LE-LC transition start at higher surface pressures and are more bended. This can be more clearly observed in the plots of the compressional modulus as a function of the surface pressure (inset of Figure 2). Increasing the ionic strength, the points A corresponding to the beginning of the transition appear at higher surface pressure: 9.2 and 10.5 mN/m for PBS(A) and PBS(B) substrates, respectively. Also, the increasing values of C_s^{-1} indicate the decrease of film compressibility and, thus, the progressive disappearance of the phase transition.

The limiting area obtained by extrapolating the linear region of the π-A curve below the plateau to π=0 was 291 $Å^2$/molecule on water subphase. Increasing ionic strength results in a higher limiting area, this can be taken as evidence for enhanced monolayer stability on saline subphases. Similar results, regarding the influence of electrolytes on π-A isotherms, were described by Phillips et al.[22] for poly-L-glutamic acid monolayers at the air-water interface. Growth of the monolayer molecular area with increasing ionic strength might be due presumably to the “salting out” effect provoked by the salts.

Table 2 compiles the results of the molecular areas at two different pressures. One at 5 mN/m that corresponds to the beginning of the transition and the other at 20 mN/m after the transition in the liquid condensate state for peptide monolayers spread on water and on buffered subphases of different ionic strength. Furthermore, the pressures at the beginning and at the end of the transition (π_i and π_{end}) are indicated for each peptide isotherm.

3.2.2. BAM images.

BAM images taken along the full monolayer compression at 20 ºC on water are shown in Figure 3. In the liquid expanded (LE) state, at surface pressures below 5 mN/m, the pictures are completely homogeneous (see figure 3A, taken at 0.9 mN/m). Once the plateau surface pressure is attained, circular holes start to appear (image B), thus demonstrating that the film is less homogeneous. When the LE–LC transition region is exceeded, bright circular spots can be observed (image C), which increase in number and size as the compression proceeds (image D). These spots may be considered to be the evidence of the nucleation of 3D structures. As the nucleation proceeds, the nuclei arrange themselves in lines (image E) leading to a kind of the monolayer collapse. When the monolayer is

expanded to its initial area, some holes remain dispersed in the expanded phase (image F), proving that the peptide film does not return to its initial state when compressed up to the maximum pressure observed, within the experimental time.

The images of Figure 4 were recorded on phosphate buffered substrate, PBS (A), at pH 7.4. At low surface pressure region, the image is homogeneous (image A) and does not change upon film compression during the transition region (image B). At π=16.2 mN/m, in the post-transition region, small circular spots can be observed (image C). At higher surface pressures (22.9 mN/m), irregular domains of condensed phase appear (image D), which increase in number upon monolayer compression and fuse together, forming compact agglomerates, at the surface pressure of 27 mN/m (image E). Upon decompression to the maximum molecular area, the monolayer does not recuperate the homogeneous structure, remaining small circular domains of condensed monolayer dispersed in the liquid expanded phase (image F). This lack of reversibility could be due to the high intramolecular attraction forces among peptide molecules that result in a condensed monolayer structure upon compression that is not reverted during decompression.

3.2.3.-Curves of monolayer thickness (d) and surface pressure (π) versus time (t).

On water subphase, the monolayer thickness versus time curve, together with the π-t curve, are shown in Figure 5A. Upon film compression, along the liquid-expanded phase, the thickness increases monotonically (similarly to surface pressure), from 0.5 nm at the start of film compression ($\pi \tilde{}$ 0 mN/m) until 1.54 nm at the beginning of the transition phase (5 mN/m). This corresponds to an increase in the film thickness of 3 times. In the LE-LC transition region, the thickness remains practically constant at 1.6 nm, without noise peaks, which is to be expected taking into account the BAM images observed in this region (Figure 3-B). As soon as the liquid condensed state is reached, the film thickness and the noise peaks increase significantly due to the formation of round-shaped domains (image D, Figure 3).

On PBS (A) substrate, the behaviour is similar (Figure 5B). Thus, in the liquid-expanded phase, the thickness is practically the same than that recorded on pure water, and only at the beginning of LE-LC transition the thickness increases markedly until 2.4 nm. Along the transition state, the film thickness is maintained practically constant (2.4-2.6 nm), indicating that the monolayer thickness is not longer changing in the plateau.

The fact that the film thickness remains constant along the LE-LC transition region seems to reject the theory of the formation of a bilayer during the transition. In our opinion, in this region the compression would force out the peptide molecular segments from the air-water interface into a subsurface region, termed the “transition layer” by Nitsch and Maksymiw[21] in their studies of catalase monolayer. The visualization of this behaviour can be observed in Scheme 1, in which when the peptide is compressed adopts an “accordion” conformation of loops and tails with the polar groups immersed into the subphase. Under this hypothesis, the surface pressure should not have changed at all on the plateau under ideal compression conditions, since the decrease in area should be completely account for the immersion of molecular segments into the subphase, with no change in the film pressure and thickness. The slight increase in both magnitudes, observed in practice, can be attributed to a continuous compression without reaching the equilibrium.

Beyond the end of the plateau, further compression of the monolayer provokes the dissolution of some molecular segments (Scheme 1) and, for this reason, the collapse is not completely achieved.

The formation of loops and tails partially immersed into the water subphase, could result in a film heterogeneity as reflected in the holes observed in BAM images when the monolayer is in the LE-LC transition region (Figure 3B). On PBS(A) substrate, most of the peptide segments remain at the interface, due to the “salting out” effect. Consequently BAM images are homogeneous in the LE-LC transition, without holes (Figure 4B) and the monolayer is thicker than the obtained with water.

3.3.- Peptide penetration into phospholipid monolayers at constant surface pressures.

The ability of E2(279-298) peptide to penetrate into phospholipid monolayers was studied injecting 18 μL of 0.95 mM peptide solution in water (the concentration into the trough was 0.25 μM) beneath phospholipid monolayers spread on PBS(A) subphases at initial surface pressures (π_0) of 5, 10, 20 and 32 mN/m. Penetration experiments were carried out using phospholipids with different head groups (DMPC and DMPG) and with different acyl chain length (DPPC and DMPC).

Figure 6 shows the increase of surface pressure induced for the peptide incorporation after 90 minutes in different phospholipid monolayers. The higher the initial pressure the lower the effect of the peptide, because of the increasing packing of the lipid molecules. As a general trend, peptide penetration is higher and very similar for DMPC and DMPC/DMPG (2:1) mixed monolayers, which exhibit a liquid expanded state (LE) (see later Figures 8 and 9), than for DPPC monolayer, which is in the liquid condensed state (LC) above the pressure of 10 mN/m, and in the liquid expanded state (LE) below π = 5 mN/m (see later, Figure 7). Therefore, at π_0 = 5 mN/m, where the three phospholipids are in the same LE surface state, $\Delta\pi$ is slightly lower for DPPC than for DMPC or DMPC/DMPG. However, at 10 mN/m, the values of $\Delta\pi$ for DPPC become the half comparing to those obtained for DMPC or DMPC/ DMPG films, and one third at 20 mN/m. From these results we can conclude that the nature of the headgroups has no significant influence on penetration. However, the surface state of the monolayer (LE or LC), which is predicted by the acyl chain length of the phospholipid, is an important parameter for peptide penetration.

The monolayer exclusion pressure[23], π_{ex}, i.e. the maximum initial surface pressure at which the peptide does not penetrates into the monolayer, obtained by extrapolating the plot of $\Delta\pi$ versus π at $\Delta\pi$ = 0 (figure not shown), was 27 mN/m for DPPC and 33 mN/m for DMPC and DMPC/DMPG systems. These values confirm the above results about the better peptide uptake by lipids in the LE state than in the LC state regardless of the nature of the lipid headgroup.

3.4- Interaction of peptide molecules with Langmuir phospholipid monolayers.

The interaction of E2(279-298) with Langmuir phospholipid monolayers was also studied by analysing the changes in the compression isotherms of pure phospholipids due to the presence of the peptide into the subphase. This analysis can explain the nature and the extent of the interaction. If the peptide is desorbed completely as the film is compressed, the resulting isotherm corresponding to the mixed film would be similar to the pure phospholipid, and no interaction would be observed. On the contrary, if there is any deviation from the pure isotherm of the phospholipid it could be attributed to the incomplete desorption of the peptide and thus to interaction between both components.

Figures 7, 8 and 9 show the π- A isotherms of DPPC, DMPC and DMPC/DMPG (2:1) spread on a PBS (A) subphase with and without peptide at a concentration of 0.25 μM. The presence of peptide molecules in the substrate induces an initial surface pressure, due to its intrinsic adsorption at the air-water interface[23]. Moreover, it is observed a decrease in the compressional modulus (inset of figures) and an increase of the molecular areas of phospholipid monolayers. For example, at surface pressure of 10 mN/m, ΔA calculated by subtracting the area (A) of the pure lipid monolayer from the A of the lipid film in presence of peptide was 52.7, 67.2 and 50.5 $Å^2$/molecule for DPPC, DMPC and DMPC/DMPG, respectively. For the three systems studied, ΔA values decreased when the trough area was reduced during the monolayer compression. For DPPC and DMPC (Figures 7 and 8), ΔA remains positive until the collapse pressure, being higher for DMPC, thus proving a greater interaction between this phospholipid and the peptide. For DMPC/DMPG mixed film, ΔA becomes zero at surface pressure of 27 mN/m, corresponding to an area of 55 $Å^2$/molecule (Figure 9). A null value of ΔA indicates that the peptide is ejected of the monolayer.

For pure DPPC (Figure 7), we observed the existence of a plateau at 6 mN/m in the isotherm, which corresponds to the LE-LC phase transition in agreement with literature[24-27]. In presence of the peptide, such a phase transition becomes broader at 8-10 mN/m, coexisting both LE and LC states in a bigger area range. Pure DMPC monolayer (Figure 8) does not show the LE-LC transition as described

elsewhere[28], but in presence of the peptide a broad plateau in the π-A curve is observed, which could be attributed to the presence of the peptide in the monolayer. A similar effect was observed for the mixture DMPC/DMPG (2/1) (Figure 9). The plateau showed in the π-A curves of phospholipid/peptide mixed films corresponds to the LE-LC phase transition observed in the pure peptide monolayers as was shown in Figure 2. This behaviour is a clear evidence of the peptide penetration into lipid monolayers. All phase transitions can be more clearly seen as a minimum in the C_s^{-1}-π curves (inset of figures 7, 8 and 9).

The effects produced by the peptide on the different phospholipid monolayers studied show the existence of an interaction with all lipids tested. However, a more obvious interaction was observed with DMPC phospholipid. The higher changes in surface pressure, molecular area and compressibility induced for the peptide on the DMPC monolayer confirm this affirmation. On the other hand, although the penetration of peptide molecules into the more condensed monolayer of DPPC is lower than into the expanded mixed film DMPC/DMPG, as was shown in Figure 6, the interaction of peptide with DPPC is higher than in the mixed DMPC/DMPG system in the π-A experiments, since ΔA remains positive until the film collapse, without rejection of peptide from the DPPC monolayer (Figure 7), whereas ΔA becomes zero for the mixed phospholipid system at high surface pressures (Figure 9). These results can be interpreted by supposing the existence of two types of interaction: for DPPC or DMPC a main hydrophobic interaction between phospholipid hydrocarbon chains and peptide molecular segments is established, being stronger for DMPC because of the greater penetration of peptide in this film, as was shown in Figure 6. Nevertheless, for the DMPC/ DMPG system, there is a contribution of both, hydrophobic and electrostatic interactions, being the last one repulsive when the peptide and the lipid molecules are very closed. This could explain the rejection of peptide from the mixed monolayer when is compressed.

As a summary, the most relevant insights derived from the present work can be addressed to two aspects concerning to i) peptide stability at the air water interface, and ii) its interactions with phospholipids, both helpful in the physicochemical characterization the E2 (279-298) sequence. The peptide forms stable monolayers as shown by the surface activity studies and compression isotherms. Results obtained by both assays are strongly dependent on the ionic strength of the media. The higher the ionic strength, the higher the stability of the monolayer. This dependence is also evidenced with the monolayer topography determined by the BAM technique. On another hand, the peptide modifies the surface behaviour of phospholipid monolayers thus assessing its capacity to interact with lipids.

In conclusion, our findings argue in favour of considering the E2 (279-298) sequence a candidate for further experiments to determine its potential role in the fusion mechanism that regulates the entry of the Hepatitis G virus (GBV-C/ HGV) into the host cell.

Acknowledgement

This work was supported by Grants BQU2003-05070-CO2-01/02 from the Ministerio de Ciencia y Tecnología (Spain) and a predoctoral grant awarded to C. Larios.

Figure captions

Scheme 1.- Representation of peptide conformation at the air-water interface (A) at the liquid expanded state, (B) at the LE-LC phase transition and (C) at the liquid condensed state.

Figure 1 – Adsorption of E2 (279-298) into the water-air interface: (A) in water subphase; (B) in PBS (A) subphase.

Figure 2.- Surface pressure (π) versus mean area per molecule (A) for peptide monolayers spread on water (?-?), PBS (A) (¦-¦) and PBS (B) (X-X) substrates. Inset: Compressional modulus plot (C_s^{-1}) versus surface pressure (π).

Figure 3.-. BAM images corresponding to peptide monolayers spread on water at different surface pressures: (A) at 0.9 mN/m; (B) at 6.4 mN/m; (C) at 12 mN/m; (D) at 20 mN/m; (E) at 24 mN/m; (F) after the expansion at 0.1 mN/m.

Figure 4. BAM images corresponding to peptide monolayers spread on PBS(A) substrates at different surface pressures: (A) at 0.5 mN/m; (B) at 12.7 mN/m; (C) at 16.2 mN/m; (D) at 22.9 mN/m; (E) at 27 mN/m; (F) after the expansion at 0 mN/m;

Figure 5. Time evolution of surface pressure (black symbols) and thickness (white symbols) during the compression of the peptide monolayer spread: (A) water subphase. (B) PBS (A) subphase.

Figure 6.- Increasing pressure ($\Delta\pi$) recorded after injection of peptide under DPPC (empty bars), DMPC (grey bars) and DMPC/DMPG (2:1) (black bars) monolayers spread at initial surface pressures of 5, 10, 20 and 32 mN/m.

Figure 7.- Compression isotherms of pure DPPC monolayers spread on PBS (A) subphase (1) or PBS (A) with E2(279-298) (2). Inset: plots of compressional modulus vs. surface pressure.

Figure 8.- Compression isotherms of pure DMPC monolayers spread on PBS (A) subphase (1) or PBS (A) with E2(279-298) (2). Inset: plots of compressional modulus vs. surface pressure.

Figure 9.- Compression isotherms of pure DMPC/DMPG (2:1) mixed monolayers spread on PBS (A) subphase (1) or PBS (A) with E2(279-298) (2). Inset: plots of compressional modulus vs. surface pressure.

Table 1. Adsorption of peptide from the water and from the PBS(A) subphases into the air-water interface. Maximum surface excess concentration (Γ) and surface molecular area (A) values.

Concentration (μM)	(Γ) (mol m^{-2})		Area/molecule ($Å^2$/molec)	
	water	PBS (A)	water	PBS (A)
0.16	-------	$4.19 \cdot 10^{-8}$	----	3960
0.22	----	$1.20 \cdot 10^{-7}$	----	1380
0.25	$1.9 \cdot 10^{-8}$	$2.4 \cdot 10^{-7}$	8740	690
0.33	$1.1 \cdot 10^{-7}$	$2.5 \cdot 10^{-7}$	1520	650
0.54	$1.6 \cdot 10^{-7}$	$3.2 \cdot 10^{-7}$	1040	510
0.68	$1.5 \cdot 10^{-7}$	$3.7 \cdot 10^{-7}$	1080	450
1.32	$2.1 \cdot 10^{-7}$	$3.7 \cdot 10^{-7}$	790	450
1.97	$2.3 \cdot 10^{-7}$	$4.1 \cdot 10^{-7}$	720	400

Table 2.- Characteristic parameters for E2(279-298) peptide monolayers spread on water and on buffered substrates of different ionic strength. $A_{\pi=5\ mN/m}$: area corresponding at the beginning of the LE-LC transition. $A_{\pi=20\ mN/m}$: area corresponding to the liquid condensed region. π_i : surface pressure at the beginning of the phase transition. π_{end} : surface pressure at the end of transition region.

Subphase	$A_{\pi=5\ mN/m}$ ($Å^2$/molec.)	$A_{\pi=20\ mN/m}$ ($Å^2$/molec.)	π_i (mN/m)	π_{end} (mN/m)
Water	193	33	5	7
PBS (A)	231	41	9	13
PBS (B)	250	57	11	14

References

(1) Yagnik, A.T., Lahm, A., Meola, A., Roccasecca R.M., Ercole, B.B., Nicosia, A., Tramontano, A., *Proteins* **2000,** *40*, 355-366.

(2) Lescar, J., Rousell, A., Wien, M.W., Navaza, J., Tramontano, A., Fuller, S.D., Wengler, G., Wengler, G., Rey, F.A., *Cell* **2001,** *105*, 137-148.

(3) Larios, C., Christiaens, B., Gómara, M.J. Alsina M.A., Haro, I., FEBS J., 2005, *272*, 2456-2466.

(4) Pitcher, W.H., III, Keller, S. L., Huestis, W. H. *Biochim.Biophys.Acta* **2002,** *1564*, 107-113.

(5) Sospedra, P., Mestres, C., Haro, I., Muñoz, M., Busquets, M.A., *Langmuir* **2002,** *18*, 1231-1237.

(6) Kaiser, E., Colescott, R.L., Bossinger, C.D., Cook, P.I., *Anal.Biochem.* **1970,** *34*, 595-598.

(7) Sospedra, P., Muñoz, M., García, M., Alsina, M.A., Mestres, C., Haro, I., *Biopolymers* **2000,** *54*, 477-488.

(8) Clausell, A., Busquets, M.A., Pujol, M., Alsina, M.A., Cajal, Y., *Biopolymers* **2004,** *75*, 480-490.

(9) Rodriguez Patino, J., Sanchez, C. C., Rodriguez Niño, M. R. *Langmuir* **1999,** *15*, 2484-2492.

(10) Rafalski, M., Lear, J. D., DeGrado, W. F. *Biochemistry* **1990***, 29,* 7917-7922.

(11) Ege, C., Lee, K. Y. C. *Biophysical Journal* **2004,** *87*, 1732-1740.

(12) Davies, J.T and Rideal, E.K. In *Interfacial Phenomena*, 2nd ed.; Academic Press: New York. **1963**; p.265.

(13) Malcolm, B.R. *Proc. R. Soc. London* **1968**, *305*, 363.

(14) Malcolm, B.R. *Progr. Surface Membrane Sci*. **1973**, *7*, 183.

(15) Malcolm, B.R. *J. Colloid Interface Sci*. **1985**, *104*, 520-529.

(16) Takenaka,T., Harada, K., Matsumoto, M. *J. Colloid Interface Sci*. **1980**, *73*, 569-577.

(17) Takeda, F., Matsumoto, M., Takenaka, T. and Fujiyoshi, Y. *J. Colloid Interface Sci*. **1981**, *84*, 220-227.

(18) Takeda, F., Matsumoto, M., Takenaka, T., Fujiyoshi, Y., Uyeda, N. *J. Colloid Interface Sci*. **1983**, *91*, 267-271.

(19) Kaku,M., Hsiung, H., Sogah, D.Y., Levy, M., Rodríguez Parada, J.M. *Langmuir* **1992**, *8*, 1239-1242.

(20) Shuler, R.L., Zisman, W.A. *Macromolecules* **1972**, *5*, 487-492.

(21) Nitsch, W. and Maksymiw, R. *Colloid Polym. Sci*. **1990**, *268*, 452.

(22) Phillips,M.C., Jones, M.N., Patrick, C.P., Jones, N.B. and Rodgers, M. *J. Colloid Interface Sci* **1979**, *72*, 98-105.

(23) Bougis, P., Rochat, H., Pieron, G., Verger, R., *Biochemistry* **1981,** *20*, 4915-4920.

(24) Zhao, L. and Feng, S. S. *J Colloid Interface Sci.* **2004,** *274*, 55-68.

(25) Miñones Jr, J., Miñones, J., Conde,O., Rodríguez Patino, J.M., Dynarowick-Latka, P. *Langmuir* **2002**, *18*, 2817-2827.

(26) Miñones Jr, J., Dynarowick-Latka, P., Conde, O., Miñones, J., Iribarnegaray, I., Casas, M. *Colloids Surf. B.* **2003**, *29*, 205-215.

(27) Miñones Jr, J., Conde, O. In "*Recent Res. Devel.Surface & Colloids"* **2004,** *1*, 375**.**

(28) Larios, C., Busquets, M.A., Carilla, J., Alsina, M.A., Haro, I. *Langmuir* **2004,** *20*, 11149-11160.

Figure 1 A

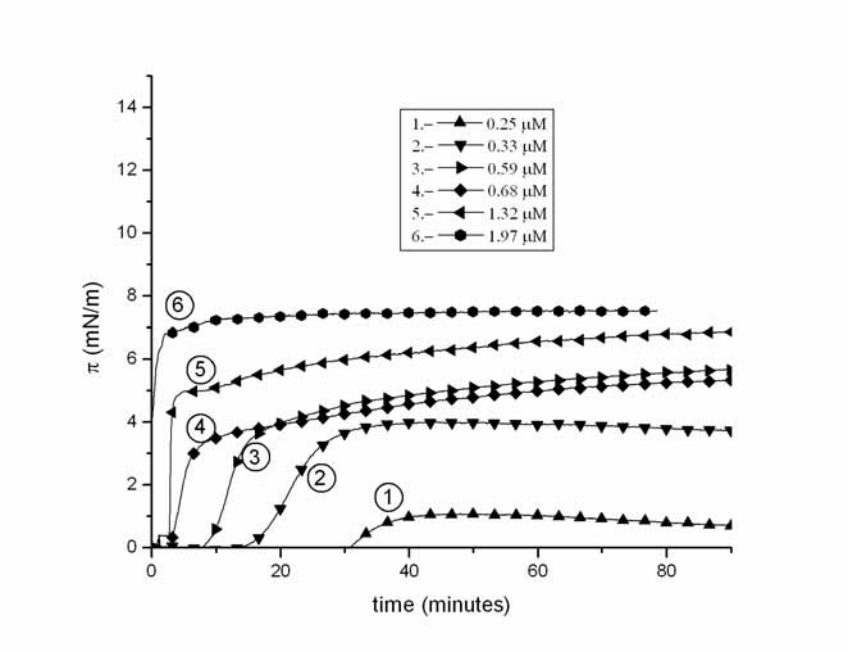

Figure 1B

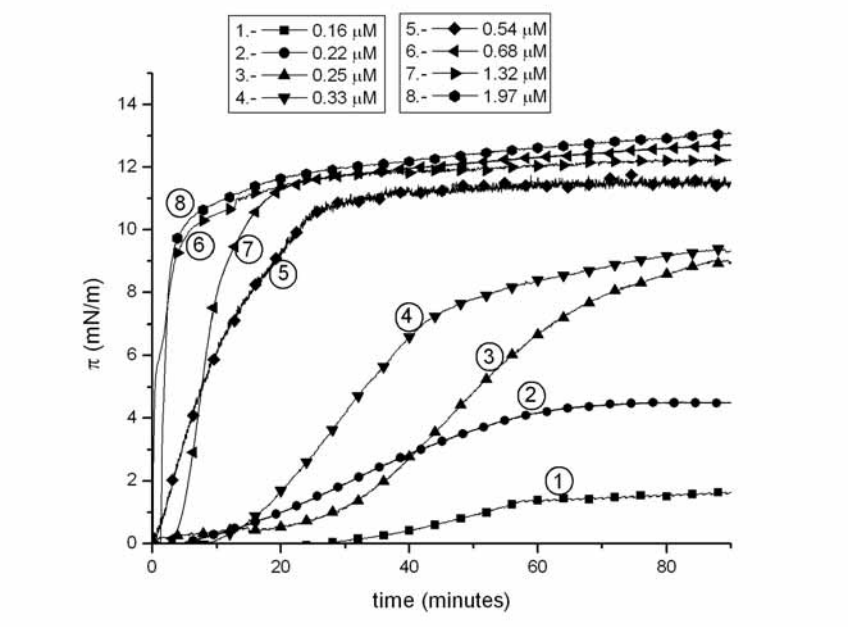

Figure 2.

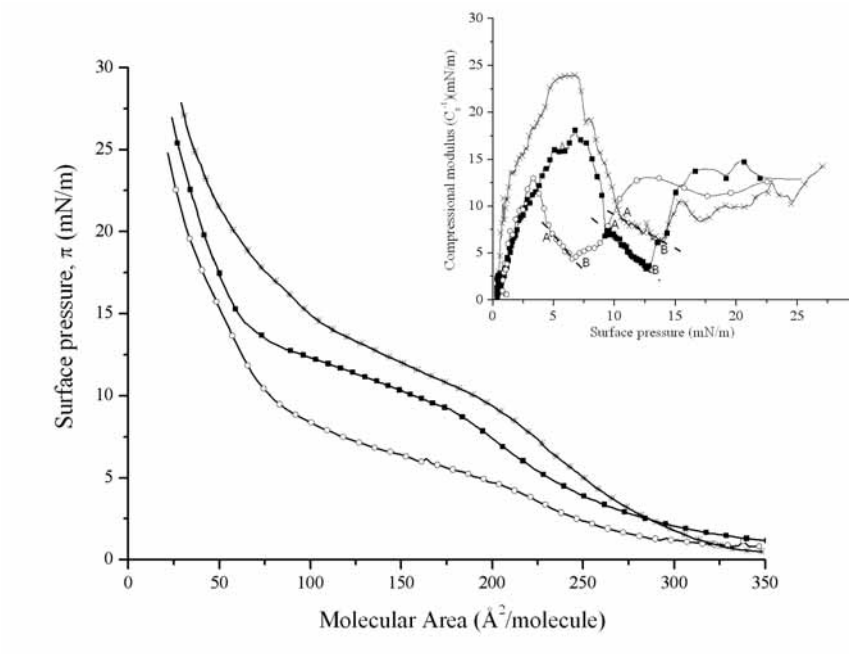
Surface pressure, π (mN/m)
Molecular Area (Å²/molecule)
Compressional modulus (C_s⁻¹),mN/m)
Surface pressure (mN/m)
A
B

Figure 3.

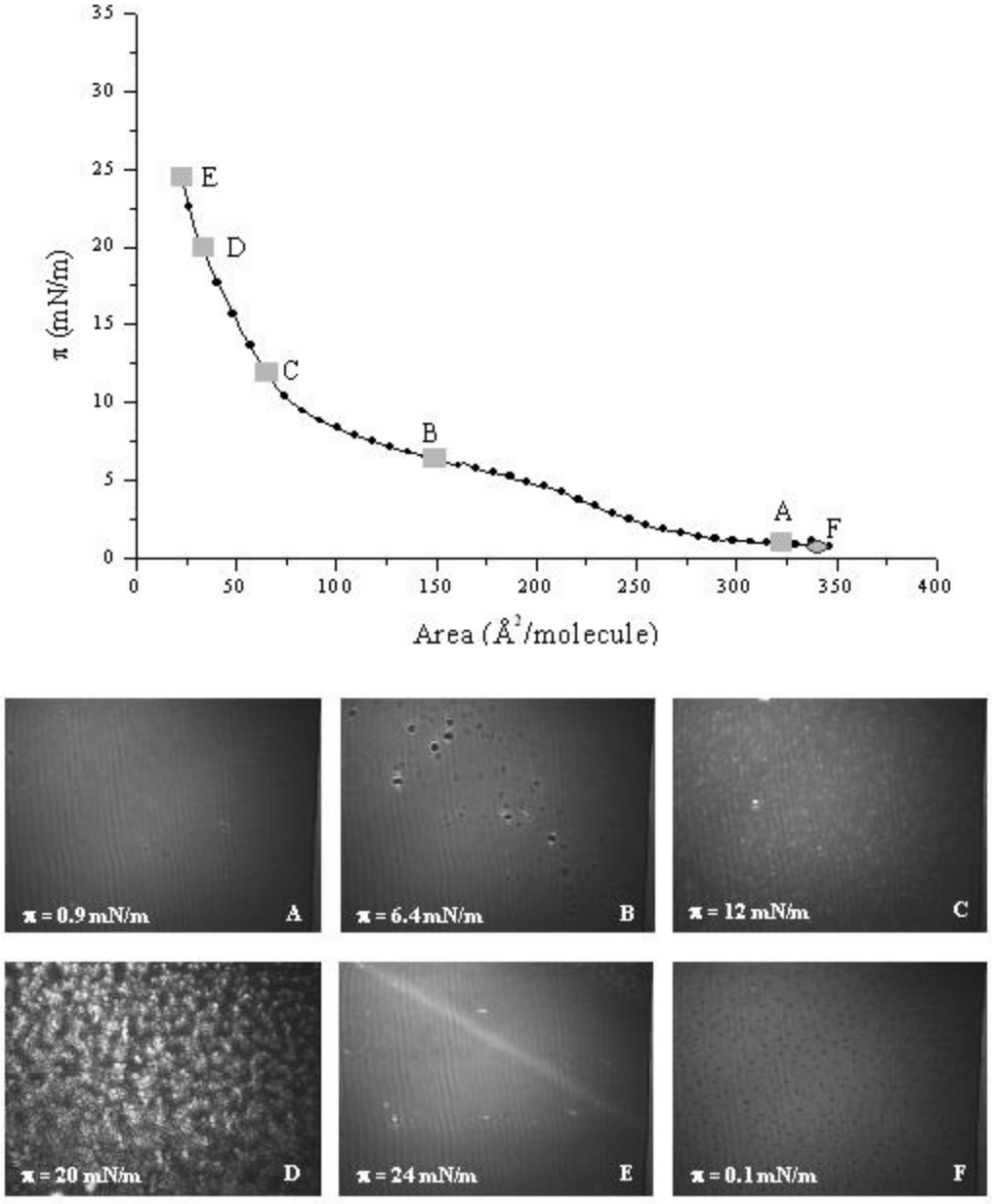
π (mN/m)
Area (Å²/molecule)
E
D
C
B
A
F
π = 0.9 mN/m
A
π = 6.4 mN/m
B
π = 12 mN/m
C
π = 20 mN/m
D
π = 24 mN/m
E
π = 0.1 mN/m
F

Figure 4

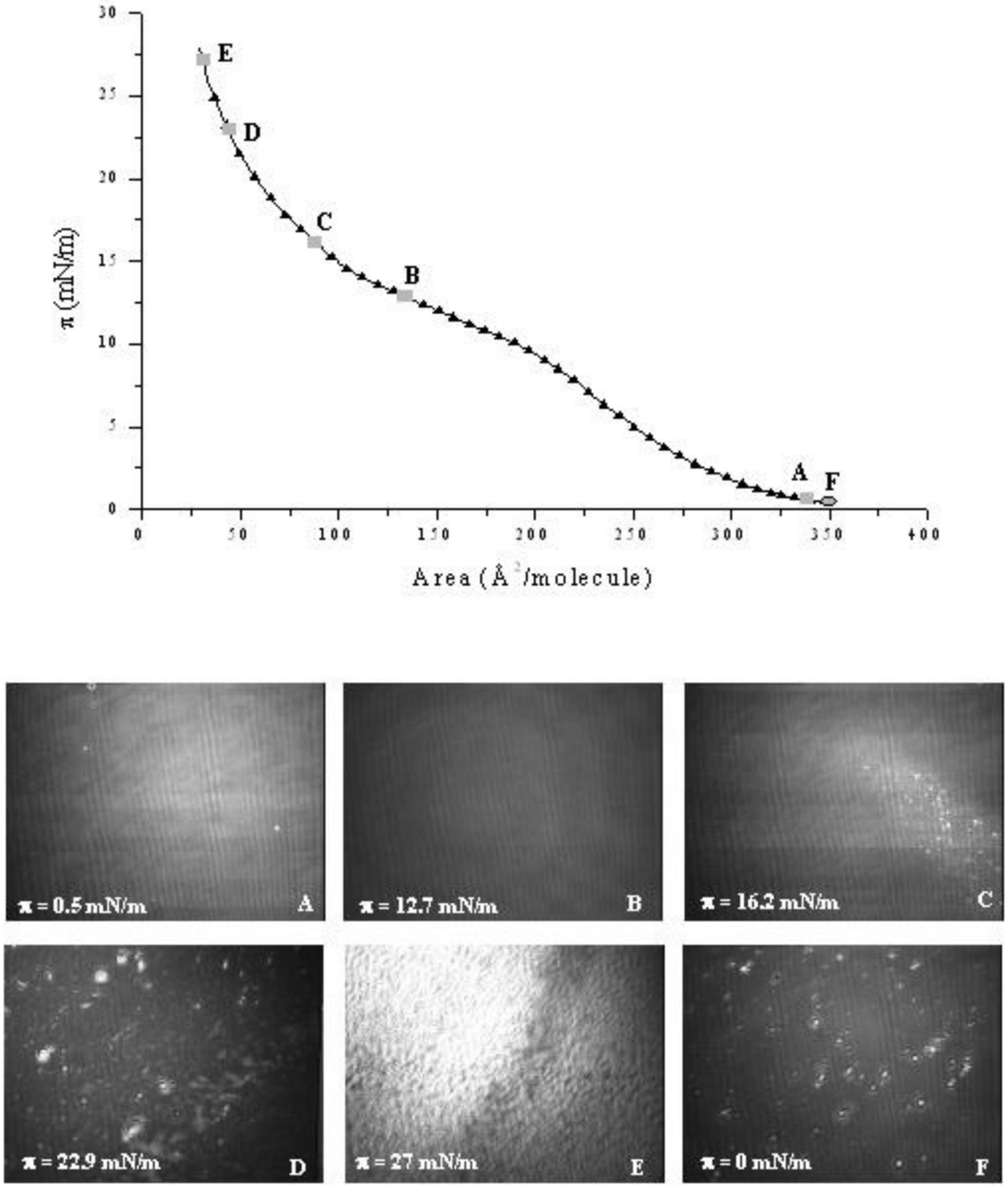
π (mN/m)
Area (Å²/molecule)
E
D
C
B
A
F
π = 0.5 mN/m
A
π = 12.7 mN/m
B
π = 16.2 mN/m
C
π = 22.9 mN/m
D
π = 27 mN/m
E
π = 0 mN/m
F

Figure 5A.

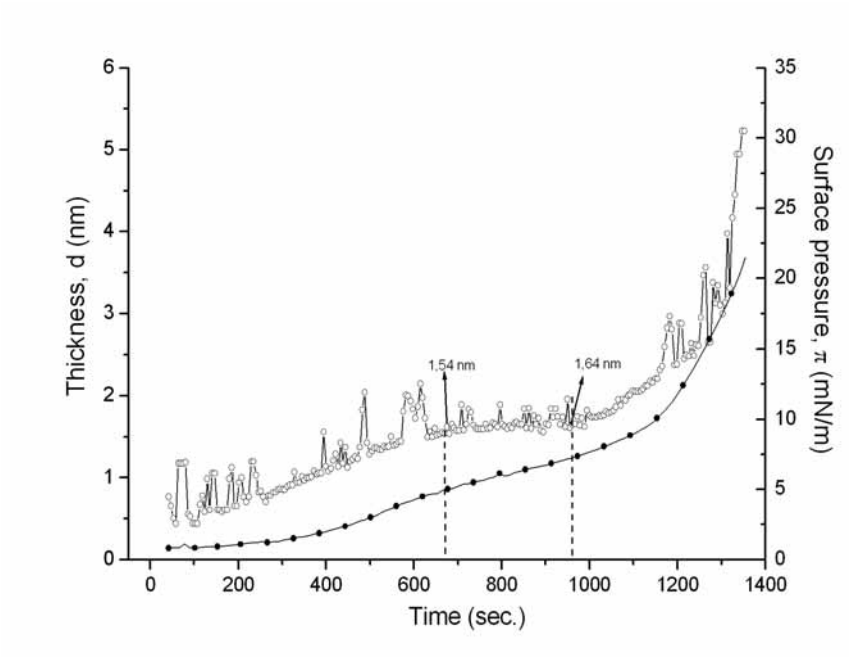

Figure 5B

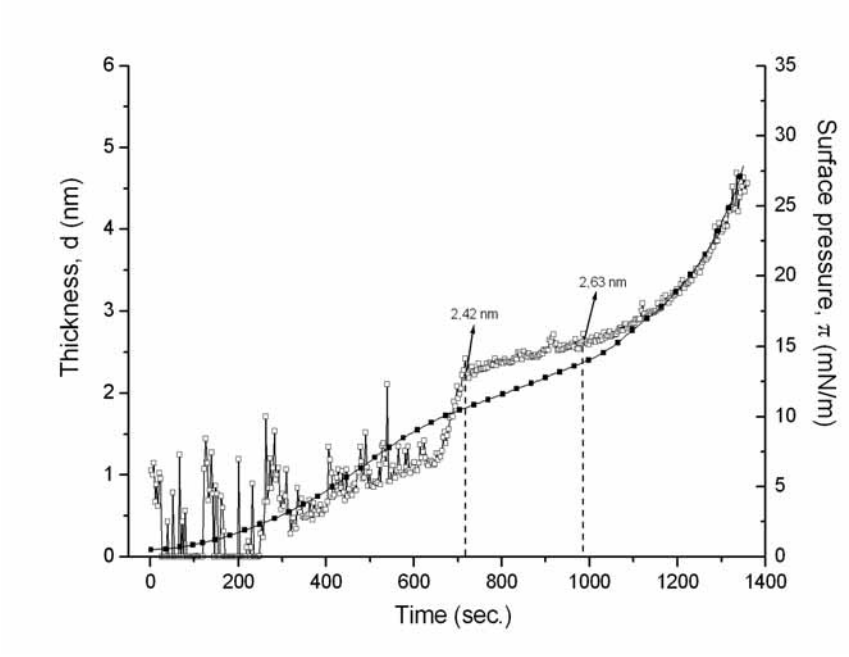

Figure 6.

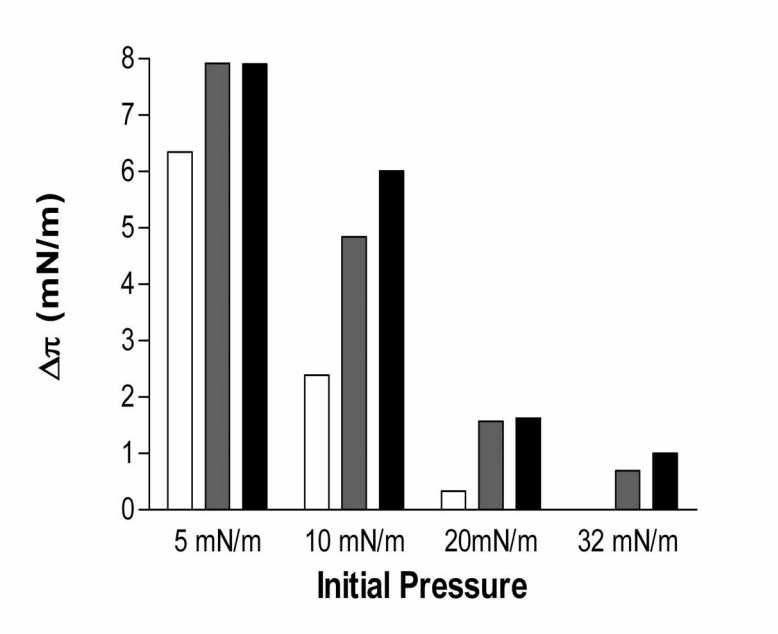

Figure 7

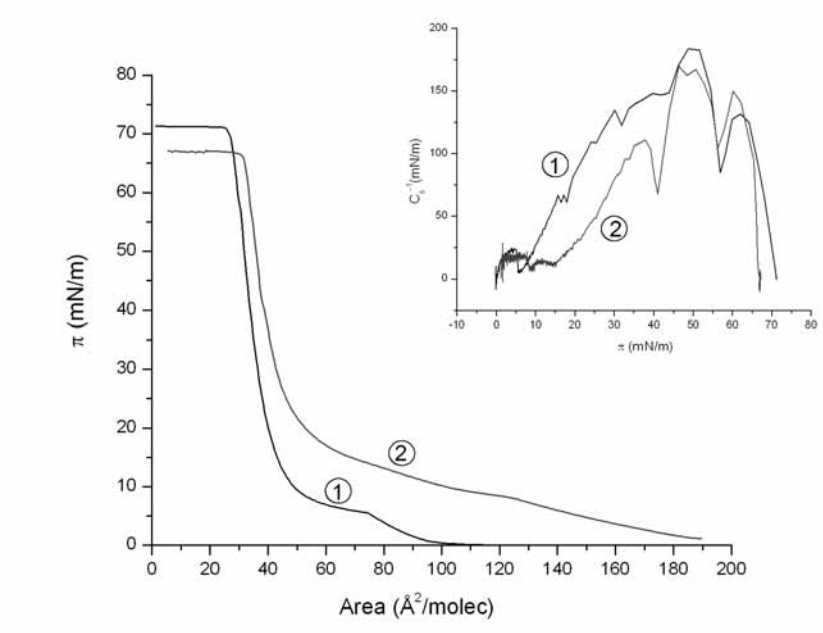

Figure 8

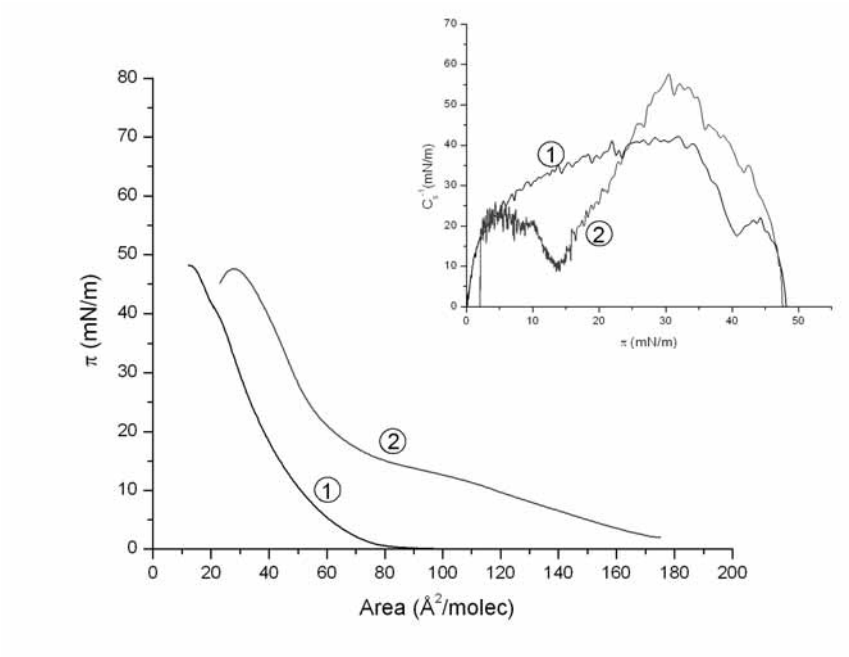

Figure 9

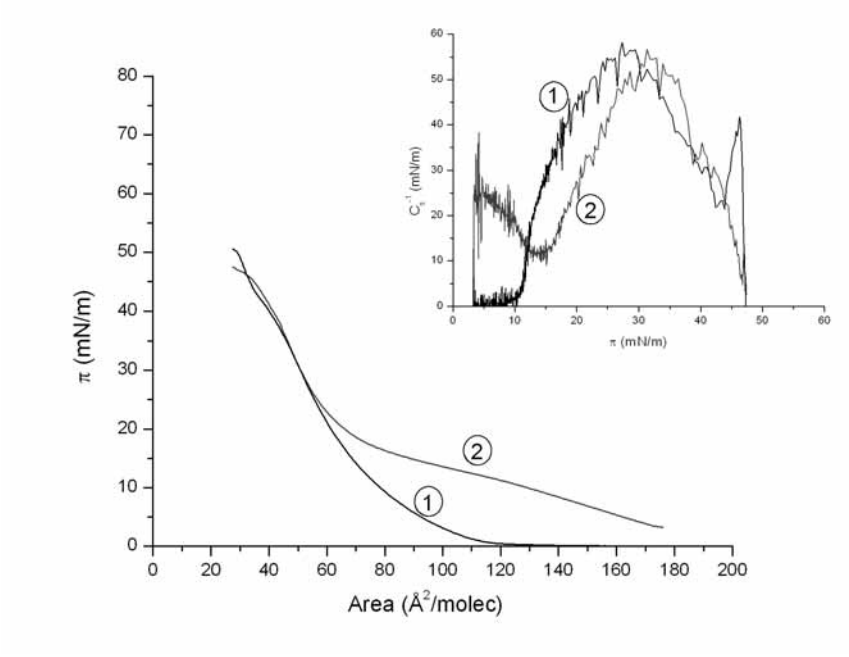

TOC image (Scheme 1)

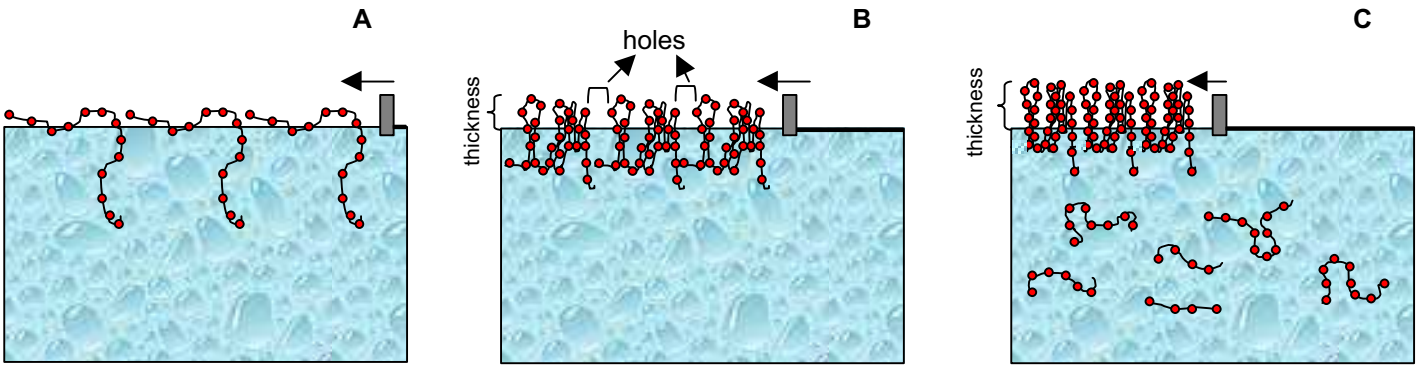

RESULTADOS

Se han realizado muchos estudios sobre las interacciones que se producen entre los virus y las células, pero aún quedan muchas cuestiones por resolver. Aunque el virus de la hepatitis G (GBV-C/HGV) es asintomático, se ha demostrado recientemente que puede tener gran importancia clínica ya que parece interferir en la replicación del virus causante del SIDA [33-35].

En el proceso de entrada de los virus con envuelta proteica a las células huésped son de suma importancia unas proteínas denominadas "de fusión" presentes en la membrana vírica. Este proceso de desestabilización y entrada en la célula requiere energía, la cual se obtiene por el cambio conformacional y por las interacciones específicas entre las proteínas estructurales del virus y la membrana celular. Así, estas proteínas promueven la adhesión y la fusión de ambas membranas, con la consecuente entrada del virus en la célula. Las proteínas de la envoltura suelen tener en su estructura una secuencia de unos 20 aminoácidos que se denomina "péptido de fusión" y que es la que se encarga propiamente de la fusión.

El trabajo de la presente tesis doctoral, se ha basado en la búsqueda y en el estudio del péptido de fusión del virus GBV-C/ HGV que por analogía con otros virus de la misma familia podría encontrarse en la proteína estructural E2 [63]. Antes de realizar la síntesis de los péptidos candidatos a ser secuencias de fusión, se alinearon 31 secuencias publicadas del virus de la hepatitis G en la base de datos Genbank (www.ncbi.nlm.nih.gov). Se compararon mediante el programa Clustalw (www.ebi.ac.uk/clustalw) y la secuencia consenso se estudió con las escalas de predicción semiempíricas descritas en la Introducción (sección 4). Se escogieron dos regiones distantes dentro de la proteína estructural E2 que cumplieran los requisitos de ser péptidos de fusión del GBV-C/ HGV.

- Una secuencia situada en la zona amino terminal ya que se han descrito muchos péptidos de fusión N-terminales (glicoproteínas de clase I). Éstos están presentes en virus tan importantes como el virus de la gripe o el virus del SIDA. La región seleccionada N-terminal de la proteína E2 se encuentra expuesta en la membrana viral, por tanto, puede interaccionar con la membrana celular y puede ser reconocida por anticuerpos. La región escogida E2(7-26) (*GSRPFEPGLTWQSCSCRANG)* es una zona altamente conservada entre las diferentes cepas del virus **(Tabla 1, trabajo 1)** y además forma un bucle (loop) que indica que esta zona está expuesta en el virión [121]. Esta secuencia se analizó mediante las escalas de accesibilidad (escala de Janin) y de hidrofobicidad (escala de Wimley & White) **(Figura 1, trabajo 1)**. Se sintetizaron tres péptidos solapantes correspondientes a esta región N-terminal, E2(17-26), E2(12-26) y E2(7-26), con la finalidad de estudiar el efecto de la longitud de la cadena aminoacídica en la interacción con los modelos de membrana estudiados.

- Una secuencia situada en la zona interna ya que los péptidos de fusión internos (glicoproteínas de clase II) se encuentran en virus de la familia *Flaviviridae*, a la cual pertenece el virus de la hepatitis G. Esta zona es también interesante estudiarla porque, algunas proteínas fusogénicas presentan secuencias internas que, aunque no son propiamente péptidos de fusión si que están implicados en el proceso de fusión

[122]. La región escogida, E2(279-298) *(AGLTGGFYEPLVRRCSELAG)*, está localizada en la parte interna de la secuencia aminoacídica de la proteína. Se observó mediante diferentes escalas que este péptido también era capaz de formar giros β (escala de Chou & Fasman) e insertarse en membranas (escala de Kyte & Doolittle) **(Figura 1, trabajo 3)**.

Además de las características ya descritas para ambas regiones, éstas se seleccionaron por presentar en su secuencia aminoácidos importantes para la acción fusogénica. La presencia de aminoácidos alifáticos (valina y leucina) y aromáticos (tirosina, fenilalanina y triptófano) es importante para la interacción de la secuencia en las membranas lipídicas. Aminoácidos de pequeño tamaño como la alanina, la glicina y la treonina son muy importantes en los péptidos fusogénicos ya que éstos confieren la plasticidad estructural necesaria [58]. Las prolinas inducen la formación de giros β. Se ha descrito que las zonas antigénicas se caracterizan por la presencia de giros β. Por otro lado, las prolinas también se encuentran formando parte de los péptidos de fusión internos, ya que al formar giros β a este nivel se encuentran en la superficie de la membrana viral y pueden interaccionar e insertarse en la bicapa [52].

Una vez seleccionados los péptidos se procedió a la síntesis en fase sólida siguiendo la estrategia Fmoc/tBu. Los crudos peptídicos se purificaron mediante cromatografía de alta resolución (HPLC) y posteriormente se caracterizaron mediante análisis por HPLC analítico, análisis de aminoácidos y espectrometría de masas confirmando la presencia de los péptidos esperados **(Tabla 2, trabajo1; Tabla 1 material suplementario, trabajo 3).**

Una vez obtenidos los péptidos sintéticos se procedió a la caracterización de las propiedades fisicoquímicas de los péptidos y a la realización de estudios biofísicos utilizando modelos de membrana. Para ello, se emplearon fosfolípidos de distinta longitud de cadena hidrocarbonada y carga de la cabeza polar. Asimismo, se emplearon modelos de membrana de distinto grado de complejidad utilizando desde el modelo más sencillo, las monocapas lipídicas, a las bicapas lipídicas (MLVs, LUVs y SUVs), y finalmente el sistema más complejo como son las membranas celulares (eritrocitos).

7 Propiedades fisicoquímicas de los péptidos

Región E2(7-26)

El péptido más corto, E2(17-26) no presentó actividad superficial debido a su elevada hidrofilia. Los péptidos E2(12-26) y E2(7-26) si presentaron actividad superficial, que fue mayor al incrementar la concentración de los mismos **(Tabla 3, trabajo1)**. Como era de esperar, el péptido E2(17-26) no formó monocapas estables, pero sí que las formaron los péptidos E2(12-26) y E2(7-26). Para definir mejor los estados de ordenación de las moléculas en las isotermas, se calculó el módulo de compresibilidad respecto al incremento de presión. El péptido E2(12-26) alcanzó un valor de compresibilidad mayor, encontrándose en un estado menos expandido. E2(7-26) obtuvo un máximo prácticamente

constante a todas las presiones estudiadas. Según la literatura, los valores obtenidos para ambos péptidos indicaban un estado de líquido expandido [88].

Región E2(279-298):

Se estudió la actividad superficial del péptido en medio acuoso con distintas concentraciones de sales en la subfase (agua y PBS). Al aumentar la concentración de iones, el péptido se incorporó más rápidamente a la interfase y se produjo un aumento de su actividad superficial **(Figura 1, trabajo 4)**. Dicho aumento también se vio reflejado en el cálculo del exceso superficial **(Tabla1, trabajo 4)**.

E2(279-298) formó una isoterma de compresión estable aunque no se alcanzara el colapso. El estado de ordenación de las moléculas en la isoterma del péptido a bajas presiones era de líquido expandido, luego aparecía una transición de fase de líquido expandido a líquido condensado (LE-LC) y, a presiones superficiales más elevadas se encontraba en estado de líquido condensado, no alcanzándose la presión de colapso. Cuando la subfase tenía una concentración superior de sales, la isoterma fue menos compresible y, por tanto, estaba más expandida **(Figura 2, trabajo 4)**. El cálculo del módulo de compresibilidad mostró un mínimo que indicaba el cambio de fase de LE a LC. Este mínimo apareció a presiones superiores al aumentar la concentración de sales en la subfase. El máximo del módulo de compresibilidad se encontró por debajo de 50 mN/m, indicando que el péptido se encontraba en forma de líquido expandido durante la compresión. El valor del área límite (A_0), calculado al trazar una recta tangente en la isoterma (en la fase de LE ($A_{0(LE)}$) y LC ($A_{0(LC)}$) y su intersección en el eje de las abcisas, se incrementó al aumentar la fuerza iónica de la subfase, evidenciando una vez más una expansión de la isoterma por una ionización de la monocapa. La presencia de sales sustituye los contraiones H^+ del agua (H_30^+) situados alrededor de los grupos cargados negativamente por cationes de mayor diámetro (por ejemplo, Na^+) y esto le confiere una mayor estabilidad a la monocapa, probablemente por el efecto de "salting out" descrito por Philips et al. [123]. Este efecto indica que la presencia de sales favorece las interacciones de tipo electrostático e impide la disolución del péptido en la subfase.

Las isotermas se visualizaron mediante la técnica del microscopio del ángulo de Brewster (BAM). La isoterma del péptido con agua en la subfase fue homogénea a bajas presiones (estado de líquido expandido). Al alcanzarse la transición de fase (LE-LC) aparecieron unos dominios circulares indicando que la monocapa estaba más empaquetada pero que existían espacios entre las moléculas. Al sobrepasar la transición de fase, aparecieron unas manchas brillantes que fueron aumentando a medida que se iba comprimiendo más la monocapa. Estas manchas podrían indicar la presencia de estructuras tridimensionales. Finalmente, las imágenes mostraron una raya brillante que indicaba el colapso de la monocapa (este colapso no se había visualizado en la isoterma). Cuando la monocapa se expandió de nuevo, la imagen no fue del todo homogénea indicando que no volvía a su estado inicial **(Figura 3, trabajo 4)**. La isoterma con PBS en la subfase fue homogénea hasta después de la transición de fase. A partir de este momento, aparecieron manchas que fueron en aumento hasta formar aglomerados. Como sucedía en la subfase de agua pura, la expansión de la isoterma a las condiciones iniciales de área, mostró una prevalencia de

dominios circulares característicos de la monocapa del estado condensado en la fase de líquido expandido **(Figura 4, trabajo 4)**.

Se estudiaron las isotermas respecto al espesor de la monocapa en agua y en PBS (A). Al comprimir la monocapa el espesor fue aumentando progresivamente. El aumento alcanzado hasta la transición de fase fue tres veces superior respecto al inicial. En el intervalo de fase de LE-LC el grosor permaneció constante y, de nuevo, aumentó al comprimir más la isoterma hasta alcanzar la presión de colapso, debido a la formación de los dominios visualizados mediante la técnica del BAM. Cuando se utilizó PBS como sustrato, el espesor fue similar al del agua hasta el inicio de la transición LE-LC que aumentó bruscamente. Durante el estado de transición se mantuvo constante y una vez sobrepasada la transición, aumentó de nuevo apareciendo picos de ruido característicos de la formación de dominios. El hecho de que en la transición de fase no se aumentara el grosor podría ser debido a la disposición adoptada por el péptido. Al inicio de la compresión, el péptido estaría más extendido ya que tendría más movilidad. En la fase de LE-LC aumentaría el grosor porque las moléculas de péptido se encuentran más cercanas adoptando una forma de acordeón, donde las partes polares estarían hacia el agua y las partes apolares hacia el aire. Al llegar al colapso el grosor sería el máximo y algunas moléculas pasarían a la subfase (Figura 12).**(Figura 5, trabajo 4)**.

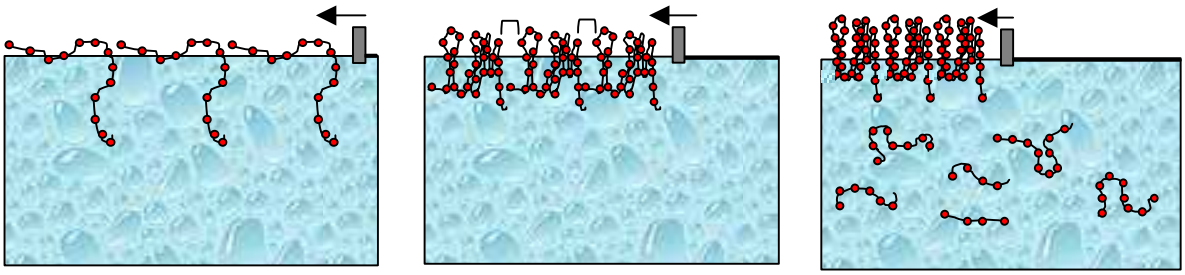

Figura 12. Disposición adoptada por E2(279-298) en la interfase aire-agua al ir comprimiendo la isoterma.

8 Interacción con modelos de membrana

Los estudios con modelos de membranas han sido ampliamente referenciados, ya que mimetizan la membrana celular. Éstos nos pueden proporcionar información que puede ser extrapolada a nivel celular. En el estudio de los péptidos de fusión, la utilización de modelos de membrana es imprescindible para conocer la interacción péptido-membrana celular [124-126].

8.1 Estudio con membranas monomoleculares

8.1.1 Cinéticas de penetración

Cuando se estudiaron los diferentes fosfolípidos (DPPC, DMPC, DMPC/DMPG) como modelos de membrana monomoleculares, se observó que el incremento de presión obtenido fue mayor al aumentar la longitud de cadena de los péptidos solapantes (E2(7-26)>E2(12-26)>E2(17-26)) **(Figura 2, trabajo 1)**. Asimismo, la interacción fue mayor con la mezcla que contenía el fosfolípido cargado negativamente. En el caso del péptido E2(279-298) la interacción fue más elevada para los fosfolípidos en estado de líquido expandido (DMPC y DMPC/DMPG) y a presiones superficiales iniciales menores **(Figura 6, trabajo 4)**.

8.1.2 Isotermas de compresión

Otro estudio destinado al análisis de la interacción péptido-fosfolípido consistió en la realización de isotermas de compresión de los fosfolípidos en presencia de péptidos en la subfase.

El péptido E2(17-26) produjo una expansión en todos los fosfolípidos estudiados, aunque ésta fue menor para la DPPC, la cual presentó una isoterma prácticamente idéntica a la registrada sobre subfase acuosa en ausencia de péptido. E2(12-26) también produjo expansión en todos los fosfolípidos, con un efecto más acusado en la isoterma de DMPC. El péptido de mayor longitud, E2(7-26), a bajas presiones produjo la mayor expansión en los fosfolípidos, siendo ésta más elevada para la mezcla DMPC/DMPG. En la isoterma de DPPC con E2(7-26) en la subfase, se produjo una contracción de la isoterma a elevadas presiones respecto al fosfolípido sin péptido en la subfase, que podría ser debida a la formación de aglomerados de fosfolípido/péptido **(Figura 4, trabajo 1)**. El área límite en la región más condensada de la isoterma previa al colapso ($A_{0(LC)}$) fue mayor para el péptido E2(12-26), excepto para la mezcla DMPC/DMPG que fue igual en E2(12-26) y E2(7-26) **(Tabla 4, trabajo 1)**.

E2(279-298) produjo expansión en todas las mezclas estudiadas. La mayor expansión fue para las isotermas de los fosfolípidos de menor empaquetamiento y en mayor grado para DMPC, indicando una mayor interacción con el péptido **(Figuras 7-9, trabajo 4)**. En las isotermas de DMPC y DMPC/DMPG se observó además la aparición de una transición de fase no presente en la isoterma del fosfolípido puro sobre subfase acuosa. Esta transición coincide con el cambio de LE-LC de la isoterma pura del péptido, por lo tanto, confirma la presencia de éste en las isotermas de dichos fosfolípidos.

8.1.3 Isotermas mixtas

El estudio con monocapas mixtas nos permitió conocer mejor la orientación, el empaquetamiento y las interacciones entre los componentes que las formaban.

Se realizaron isotermas mixtas de compresión de mezclas del péptido E2(279-298) con dos fosfolípidos zwitteriónicos (DPPC y DMPC) en agua **(Figura 1 y 2, Anexo 1)** y en subfase de PBS. Tal como ocurrió con el péptido puro, las isotermas mixtas realizadas sobre subfase con sales (PBS) presentaron un área molecular mayor que el obtenido sobre agua pura. La presión de colapso también fue más grande en PBS evidenciando un aumento en la estabilidad de la monocapa. La transición de fase de LE-LC también apareció a presiones superiores en la subfase PBS en todas las fracciones molares estudiadas.

Las isotermas con elevada proporción de fosfolípido se asemejaron a las isotermas de fosfolípido puro y viceversa, a medida que se iba aumentando la fracción molar de péptido, las isotermas se parecieron más a las del péptido puro. De los cálculos de la variación del área molecular y de la energía de Gibbs de exceso de mezcla se observó una desviación positiva respecto a la idealidad que fue mayor en el fosfolípido de menor longitud de cadena hidrocarbonada. El incremento en la energía de Gibbs indicó que la unión entre los componente era en forma de complejos, en los cuales el exceso de moléculas de fosfolípido o péptido, dependían de la fracción molar del péptido. Las isotermas se visualizaron con la utilización del microscopio del ángulo de Brewster (BAM). Las imágenes obtenidas por el BAM indicaron que el péptido se insertaba en la monocapa cambiando su morfología.

8.2 Estudio con bicapas fosfolipídicas

8.2.1 MLVs

El efecto de los péptidos en la transición de fase de los fosfolípidos (DPPC, DMPC, DMPC/DMPG y DMPC/DMTAP) se estudió mediante la técnica de calorimetría diferencial de barrido (Differential scanning calorimetry, DSC). La temperatura de transición desde un estado de gel a cristal líquido (T_m) no varió en la DPPC y la DMPC en presencia de los péptidos N-terminales, indicando o bien ausencia o bien una interacción débil péptido-lípido zwitteriónico [94;127]. Sin embargo, en la mezcla DMPC/DMPG se observó un desplazamiento de la T_m hacia temperaturas más elevadas al incrementar la proporción de los péptidos. Además, se produjo una disminución en la variación de la entalpía a medida que se aumentaba la concentración de péptido, siendo más acusada para E2(12-26) y E2(7-26), posiblemente debido a una disminución en las interacciones entre las cadenas carbonadas de los fosfolípidos a causa de la intercalación de los péptidos. El pico de la transición principal se fue ensanchando a medida que se iba incorporando péptido. Este efecto fue mayor para E2(7-26) y la mezcla DMPC/DMPG.

Además, los termogramas de la mezcla de DMPC/DMPG mostraron un desdoblamiento del pico de la transición principal, probablemente debido a mezclas no homogéneas de los

péptidos con los fosfolípidos, de tal modo que se forman poblaciones ricas en péptido y otras ricas en fosfolípidos **(Figura 5, trabajo1)**.

El efecto del péptido perteneciente a la región interna, E2(279-298) también fue más acusado para la mezcla DMPC/DMPG. En este caso, el termograma mostró la desaparición del pico correspondiente a la transición principal a porcentajes muy pequeños de péptido (Figura 13).

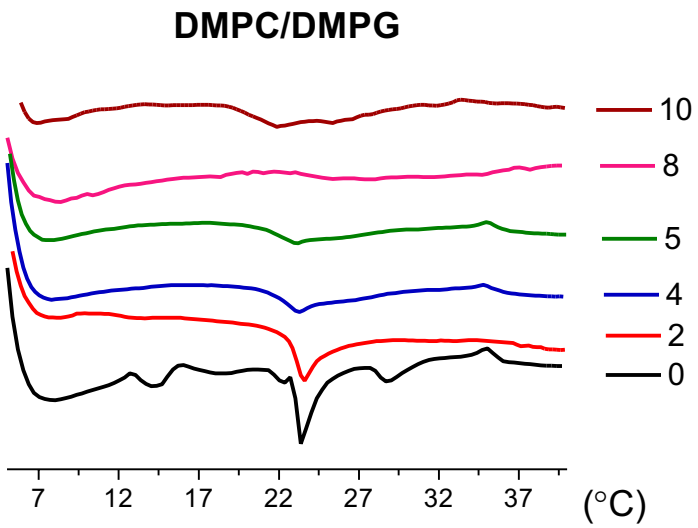

Figura 13. Termograma de DMPC/DMPG puro (0) y en presencia de concentraciones crecientes de E2 (279-298) (2, 4, 5, 8 y 10%).

Para el péptido interno de la proteína E2 también se estudió la mezcla DMPC/DMTAP (DMTAP cargado positivamente) siendo el efecto de E2(279-298) mayor que el observado en el fosfolípido zwitteriónico DMPC, pero menor que el efecto producido en la mezcla DMPC/DMPG **(Figura 3, trabajo 3)**. En un estudio más detallado de la mezcla fofolipídica que originó un mayor efecto (DMPC/DMPG) utilizando microcalorimetría se observó la formación de dos poblaciones, una enriquecida de fosfolípido y otra enriquecida de péptido, que podría conducir hacía la rápida desaparición del pico a bajas concentraciones **(Figura 4, trabajo 3)**.

Dado que E2(7-26) podría formar agregados al interaccionar con DMPC/DMPG (tal y como se observó en los estudios con membranas monomoleculares) se trató de visualizar la interacción con dos tipos de fosfolípidos, el zwitteriónico DMPC, y una mezcla con carga negativa, DMPC/DMPG. La técnica empleada fue la microscopía de transmisión electrónica, utilizada con otros péptidos para visualizar el efecto de la interacción de péptidos y fosfolípidos [128;129]. Tal y como se había previsto, se observó que el péptido producía agregación en los liposomas **(Figura 7, trabajo 1)**.

8.2.2 LUVs

La interacción de los péptidos con estos modelos de membrana se estudió mediante la observación de los cambios en la fluorescencia intrínseca del triptófano tras la interacción de los péptidos con LUVs (isotermas de unión). El Trp de los péptidos disueltos en tampón acuoso se considera expuesto en el medio y se caracteriza por presentar el máximo de emisión en un intervalo de longitudes de onda aproximadamente entre 345-355 nm. En los péptidos correspondientes a las secuencias amino terminales de la proteína E2, la adición de LUVs zwitteriónicos de DPPC y DMPC no produjo ningún cambio en el espectro de fluorescencia del triptófano, indicando poca interacción péptido-fosfolípido [130]. Sin embargo, para la mezcla DMPC/DMPG (65/35) se observó que el espectro de fluorescencia presentaba un desplazamiento hacia longitudes de onda menores debido a la unión del péptido con los liposomas [97]. Estos cambios fueron mayores para los péptidos con cargas positivas, es decir, E2(17-26) y E2(7-26) que para el péptido zwitteriónico E2(12-26) **(Figura 6, trabajo 1)**.

Tal como se muestra en la Figura 14, la secuencia peptídica E2(279-298), también produjo un mayor desplazamiento de la longitud de onda en el máximo de emisión al trabajar con la mezcla DMPC/DMPG. En este péptido se estudió también la interacción con la mezcla DMPC/DMTAP (65/35), que tal como ocurría en la técnica de DSC, ocasionaba una interacción mayor que la observada para los liposomas de DMPC pero menor que la obtenida al trabajar con la mezcla DMPC/DMPG. **(Figura 2, trabajo 3)**.

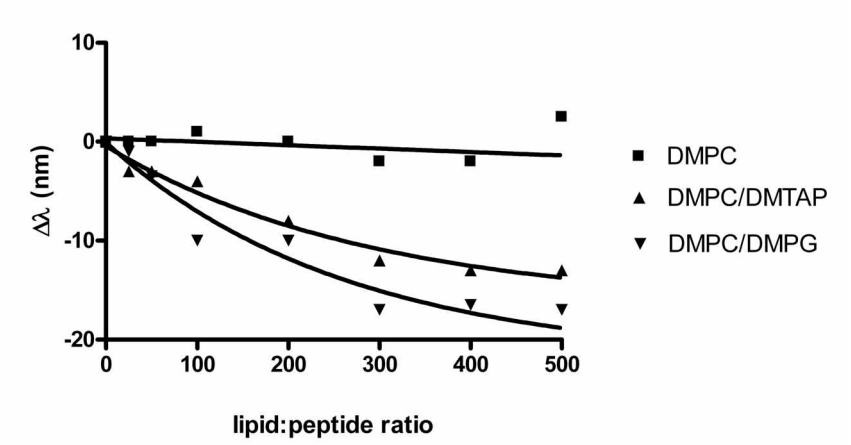

Figura 14. Desplazamiento de la longitud de onda en el máximo de emisión para el péptido E2(279-298) en presencia de LUVs de distinta composición.

Para los péptidos E2(7-26) y E2(279-298) se realizaron experimentos de liberación de contenidos vesiculares de LUVs de composición PC/PS (70/30) con la sonda calceína encapsulada en su interior. Se puso de manifiesto la capacidad de permeabilización de los péptidos, teniendo una mayor actividad el péptido E2(279-298) **(Figura 6, trabajo 2)**. Por ese motivo, se realizaron nuevos experimentos con E2(279-298) con liposomas neutros (PC) y con mezclas de PC/PG, pero con las sondas ANTS/DPX encapsuladas en su interior.

En la Figura 15 se puede observar la liberación del contenido acuoso causado por E2(279-298) con distintas proporciones de péptido. El efecto fue más acusado en la composición de PC/PG (65/35) y, en ésta, a la proporción mayor de péptido estudiada (1/1.2 L/P), se alcanzó el 100% de liberación casi instantáneamente.

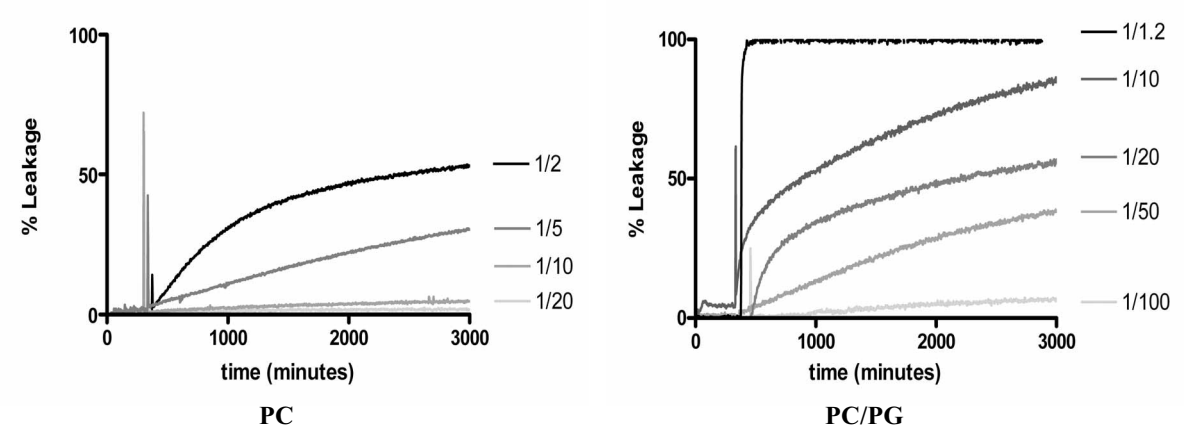

Figura 15. Experimento de liberación de contenidos vesiculares en liposomas de PC y PC/PG con el péptido E2(279-298) a distintas relaciones fosfolípido/péptido.

El ensayo de fusión de vesículas se realizó con el péptido E2(279-298) en contacto con PC/PG (65/35). En la Figura 16 se muestra el cambio producido en la intensidad de fluorescencia del espectro de emisión. Se produce un aumento en la emisión de la sonda donadora (λ=525nm) y una disminución en la intensidad de fluorescencia de sonda aceptora (λ=590nm). La mayor concentración de péptido estudiada (30 μM) dió lugar a un 40% de fusión, indicando la capacidad fusogénica del péptido.

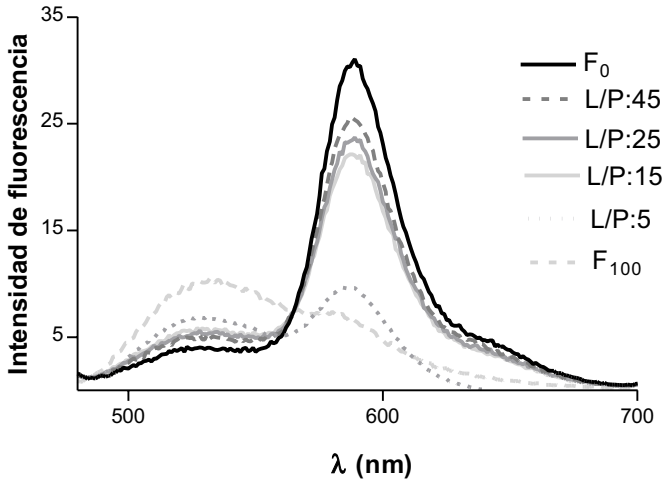

Figura 16. Cambios producidos por E2(279-298) en la intensidad de fluorescencia de liposomas de PC/PG marcados con NBD-PE y Rho-PE.

8.2.3 SUVs

En este modelo de membrana también se realizaron estudios de fluorescencia (isotermas de unión) con los péptidos E2(7-26) y E2(279-298). Se utilizaron diferentes composiciones de fosfolípidos para analizar el tipo de interacciones que se producían y en qué medida. En ambos péptidos el efecto producido era mínimo cuando los fosfolípidos eran neutros como se había visto en el estudio con LUVs. Sin embargo, cuando los liposomas tenían un fosfolípido con carga negativa si se producía una unión de los péptidos a los liposomas. Se puso de manifiesto un mayor desplazamiento de la longitud de onda del máximo de emisión hacia longitudes menores y un descenso en la intensidad de fluorescencia **(Figura 1, trabajo 2)**. Esto significaba que las interacciones de tipo electrostático eran importantes. Para profundizar en el tipo de interacciones de ambos péptidos, se realizó el experimento sin sales en el medio. La interacción fue similar en el caso del péptido E2(279-298) y mayor para el péptido E2(7-26). Esto nos llevó a concluir que el péptido amino terminal presentaba prácticamente interacciones de tipo electrostático, mientras que en el péptido de la región interna también se producían interacciones de tipo hidrofóbicas. La adición de colesterol a la composición lipídica, que confiere mayor rigidez a las vesículas, no produjo ningún aumento en la interacción con los liposomas **(Tabla 1, trabajo 2)**.

Los experimentos de apantallamiento del triptófano presente en los péptidos por la sonda acuosa acrilamida, determinaron que los péptidos se encontraban menos apantallados por la sonda cuando se añadieron SUVs, indicando una vez más la unión de los péptidos a los liposomas [131] **(Figura 4, trabajo 2)**. La disminución de apantallamiento del triptófano se analizó mediante la ecuación de Stern-Volmer. Las constantes obtenidas (Ksv), mostraron una mayor disminución para E2(279-298) en presencia de liposomas indicando una mayor protección del triptófano de la sonda acrilamida y por tanto, una mayor unión a los SUVs.

Para conocer el grado de inserción dentro de la membrana lipídica, se estudió la interacción con lípidos bromados de distinta longitud de cadena. La situación de los péptidos en la membrana era superficial, dado que el apantallamiento fue mayor con los lípidos bromados más cortos (Br-$_{6,7}$-PC) que con los de mayor longitud (Br-$_{11,12}$-PC) [132] **(Figura 5, trabajo 2)**. En los experimentos con sondas, tanto acuosas como lipídicas, la interacción con las membranas siempre fue mayor para E2(279-298) que para E2(7-26).

Finalmente, se realizó un ensayo de agregación de liposomas siguiendo el cambio en la absorbancia al añadir los péptidos. Tal como se había visto por microscopía electrónica, el péptido E2(7-26) produjo agregación en liposomas que contenían carga negativa, mientras que no lo hacía el péptido E2(279-298) **(Figura 7, trabajo 2)**. Esto confirmaba que el tipo de interacción entre E2(7-26) y los liposomas de carga negativa era básicamente de tipo electrostático [133].

8.2.4 Membranas celulares

Dado que E2(279-298) produjo una mayor desestabilización en los modelos de membrana testados, se estudió su efecto en un modelo más complejo de membrana celular (eritrocitos). El péptido produjo hemólisis cuando se puso en contacto con los eritrocitos, demostrando así su capacidad de interacción (Figura 17).

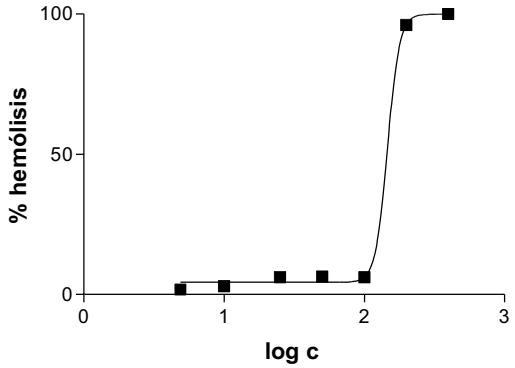

Figura 17. Hemólisis producida por E2(279-298) a las distintas concentraciones ensayadas.

De los resultados obtenidos tras trabajar con distintos modelos de biomembrana podemos afirmar que el péptido correspondiente a la secuencia interna de la proteína E2 (E2(279-298) presenta capacidad de interaccionar, penetrar y desestabilizar las membranas.

9 Estudios conformacionales

Se ha descrito que los péptidos de fusión cambian su conformación al unirse a las membranas lipídicas [134]. Por ello, en la presente tesis se llevó a cabo la determinación de la conformación de los péptidos tanto en solución como en presencia de modelos de membrana.

9.1 Dicroísmo circular (CD)

En primer lugar, la observación de la conformación adoptada por los péptidos, se realizó mediante la técnica de dicroísmo circular. Los péptidos en tampón acuoso no tenían ninguna conformación definida, presentaban una mezcla de estructuras con un mayor porcentaje de forma desordenada. Para los péptidos de la región amino terminal, la adición de disolventes fluorados como el trifluoroetanol (TFE) o el hexafluoroisopropanol (HFIP), con constantes dieléctricas entre el agua y las cadenas hidrocarbonadas de las membranas

biológicas, aumentó la proporción de estructuras ordenadas tipo lámina β y α-hélice, **(Figura 8, trabajo 1)**. Con estos péptidos se estudió también el efecto del docecilsulfato sódico (SDS) a concentraciones por encima de la concentración micelar crítica (mimético de membranas negativas). En este medio, aumentó la proporción en α-hélice en el péptido E2(12-26), mientras que en general se estabilizaba la estructura β **(Tabla 6, trabajo1)**. Por otro lado, el péptido de la zona interna, E2(279-298) mostró un aumento hacia una estructuración de tipo α-hélice cuando se estudió en presencia de TFE, siendo mayor al incrementar la proporción del disolvente trifluorado. En la Figura 18 se muestran los espectros del péptido en tampón acuoso y en diferentes porcentajes de TFE. Se puede observar un cambio en la elipticidad molar, el péptido en tampón acuoso tiene un mínimo característico de random coil a 198 nm que va cambiando a medida que se incorpora TFE, apareciendo dos mínimos a 208 y 222 nm característicos de la estructura en α-hélice.

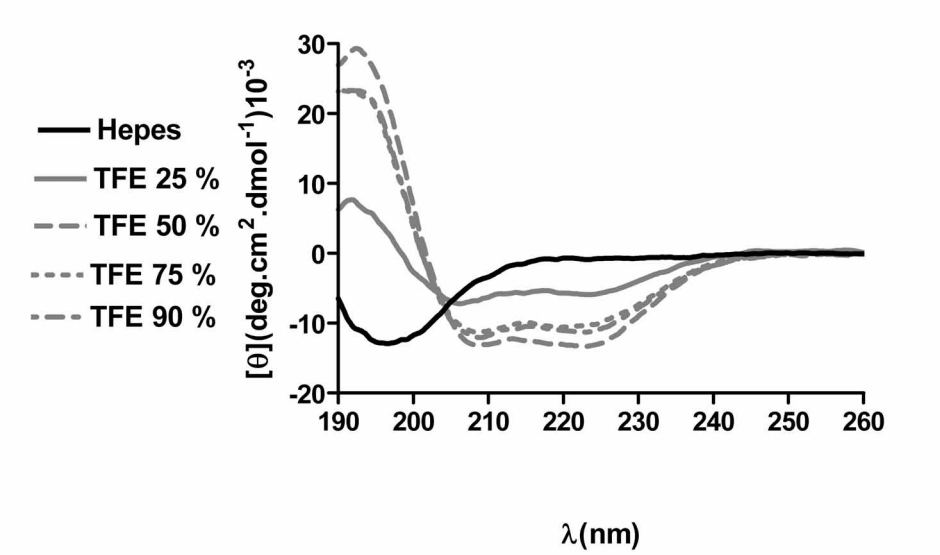

Figura 18. Espectros de dicroísmo circular de E2(279-298) en presencia de concentraciones crecientes de TFE.

Se estudió el cambio inducido en la estructura de E2(7-26) y E2(279-298) por la presencia de liposomas SUVs en el medio. Por un lado, el péptido de mayor longitud de la región N-terminal, no aumentó el porcentaje de estructuración de tipo α-hélice en contacto con SUVs de distinta composición. El péptido E2(279-298) mostró una estructuración similar a la observada en presencia de TFE **(Figura 3, trabajo 2)**. El cálculo del porcentaje de helicidad con el formalismo de Chen indicó que el péptido E2(7-26) presentaba un porcentaje de α-hélice prácticamente constante en los distintos medios probados, mientras que E2(279-298) aumentó casi al doble tanto en TFE como en liposomas con carga negativa **(Tabla 2, trabajo 2)**.

9.2 Espectroscopia de infrarrojo por transformada de Fourier (FTIR)

El estudio de FTIR se realizó con el péptido E2(279-298) en agua y en presencia de liposomas de DMPC/DMPG, para confirmar los resultados obtenidos por dicroísmo circular.

Los espectros obtenidos de la banda amida I fueron analizados mediante el programa de Peakfit®. Para identificar los distintos componentes se realizó la segunda derivada del espectro. El espectro deconvolucionado fue ajustado con una función Gaussiana. En agua, el péptido presentó una mezcla de componentes con un máximo a 1651 cm^{-1} atribuido a una conformación desordenada. Las otras bandas que aparecieron en el espectro eran indicativas de estructuras agregadas, de giro β y lámina β, así como la banda correspondiente al contraión del ácido trifluoroacético utilizado durante la síntesis peptídica. El espectro cambió cuando el péptido se puso en contacto con los liposomas. La banda centrada en 1649 cm^{-1} correspondiente a la conformación aperiódica disminuyó, y apareció un nuevo componente a 1658 cm^{-1} que se atribuye a la conformación de tipo α-hélice. Como ocurría en agua, también aparecieron bandas de estructuras tipo β, así como la banda característica de TFA **(Figura 5b y 5d, trabajo 3)**.

Se realizó un estudio de la disposición espacial del péptido E2(279-298) mediante la rueda de Edmunson, que analiza la posición de los aminoácidos cuando se distribuyen formando una hélice α **(Figura 7, trabajo 3)**. El péptido adoptaba una disposición con dos caras opuestas: una rica en aminoácidos polares y otra en aminoácidos hidrofóbicos. La cara hidrofóbica presentaba el aminoácido arginina que podría desestabilizar la α-hélice, por ello, la presencia de cargas negativas en los modelos de membrana utilizados en CD y FTIR estabilizaban esta conformación.

Con los resultados obtenidos del estudio conformacional (CD, FTIR) podemos afirmar que E2(279-298) se estructura, preferentemente en forma de α-hélice al unirse a los modelos de membrana estudiados.

DISCUSIÓN

El proceso de entrada de los virus con envuelta en una célula, que deriva en una posterior infección, requiere la fusión de la membrana viral y celular. El mecanismo por el cual el virus penetra en las células ha sido ampliamente estudiado, ya que su conocimiento permitiría encontrar la vía para frenar la infección a este nivel.

Los estudios realizados hasta el momento sobre las interacciones virus-célula, se han basado en el análisis del papel de las proteínas de membrana, y más concretamente, en una región de las mismas denominada péptido de fusión [135]. Cabe destacar que, aunque secuencialmente distintos, los péptidos de fusión hasta el momento identificados comparten características comunes en los distintos virus.

Una característica común de los péptidos de fusión es que se trata de una secuencia corta e hidrofóbica, capaz de interaccionar y desestabilizar membranas. Estos péptidos tienen una elevada afinidad por las membranas celulares, lo que hace posible su inserción en la bicapa lipídica. Existen dos tipos de péptidos de fusión, los que se encuentran en la región N-terminal correspondientes a las glicoproteínas de clase I [136] y los de la región interna, correspondientes a las glicoproteínas de clase II [137].

El mecanismo molecular por el cual se produce la fusión tiene todavía muchas lagunas por resolver. Lo que si se conoce es que, una vez que el péptido se ha unido a la membrana celular y ha adquirido la conformación activa, se produce un estadio intermedio de hemifusión. Finalmente, las dos membranas, la viral y la celular se fusionan, pudiendo el material genético pasar al interior de la célula [138]. Para intentar comprender mejor este mecanismo de acción, es necesario realizar estudios biofísicos con los péptidos de fusión empleando modelos de membrana.

En este sentido, en la presente tesis doctoral se ha escogido el virus de la hepatitis G (GBV-C/HGV) para estudiar el proceso de fusión del mismo. El virus de la hepatitis G, es un virus que aunque parece no ser patogénico, pertenece a una familia de virus, *Flaviviridae*, muy importante desde el punto de vista clínico. Dentro de ésta, se encuentran virus tan patogénicos como el virus del dengue, el virus de la fiebre amarilla o el virus de la hepatitis C [7]. El estudio del proceso de infección del virus de la hepatitis G, es además interesante ya que el GBV-C/HGV ha sido asociado con el virus del HIV. En este sentido, publicaciones recientes señalan que una infección conjunta de GBV-C/HGV con HIV ocasiona que el nivel de células inmunitarias no se vea disminuido, mejorando por tanto el curso de la enfermedad del SIDA. Se piensa que esto puede ser debido a una "lucha" entre ambos virus en la entrada de la célula. Por todos estos motivos, nos pareció muy interesante tratar de definir el péptido de fusión del GBV-C/HGV, para analizar el mecanismo de entrada de este virus en las células.

Un primer paso para conocer la entrada del virus de la hepatitis G en la célula es averiguar dónde se encuentra el péptido de fusión. En los inicios de este trabajo, no se había descrito todavía el péptido de fusión para este virus. Por esta razón, éste fue el principal objetivo de la presente tesis. Dentro de la familia F*laviviridae*, se conocen los péptidos de fusión del virus del dengue, del virus de la encefalitis asociada a ácaros o del virus de la hepatitis C [56;63;64;66]. En todos ellos, el péptido de fusión se encuentra en la zona interna de la

proteína estructural. Dado que el virus de la hepatitis G se asemeja estructuralmente al virus de la hepatitis C, la búsqueda del péptido de fusión se centró en la proteína estructural E2 también presente en el virus de la hepatitis C.

Se estudiaron dos regiones dentro de la proteína estructural: la región amino terminal, que aunque no es común para los virus de esta familia, es donde se encuentra el péptido de fusión de las glicoproteínas de clase I, como por ejemplo el virus del SIDA [47]. Por otro lado, se estudió también la zona interna de la proteína estructural E2, donde se tenía indicios de la localización de los péptidos de fusión de las glicoproteínas de clase II, presentes en la familia *Flaviviridae*.

La selección de los péptidos se basó tanto en los algoritmos de predicción descritos en la Introducción, como en la secuencia de aminoácidos. Los péptidos N-terminales escogidos presentaban giros β en su estructura; por lo tanto, teóricamente éstos estaban expuestos en la membrana viral. Además, contenían aminoácidos pequeños (Ala, Gly y Thr) y aminoácidos hidrofóbicos (Leu, Trp, Phe, Pro) comunes en los péptidos de fusión [139]. El péptido interno contenía una mayor proporción en estos aminoácidos, lo que le confería un carácter más hidrofóbico y una mejor capacidad de partición en las membranas (escala de Kyte & Doolittle). La presencia de un mayor número de aminoácidos pequeños, le podría conferir una mayor plasticidad para interaccionar con membranas. E2(279-298) contenía además un residuo de prolina en el centro de la secuencia. En los péptidos de fusión internos la presencia de este aminoácido se ha relacionado con la formación de un giro a éste nivel que parece ser el punto inicial de la interacción con la membrana celular [52]. Aunque las características fisicoquímicas de las secuencias de fusión contenidas en las proteínas estructurales del virus pueden ser distintas a las de los péptidos sintéticos con los cuales hemos trabajado, los estudios biofísicos realizados durante la tesis, permiten obtener información que puede ser extrapolada a la proteína de fusión de membrana.

Otra cuestión importante es la interacción de los péptidos de fusión con la membrana celular. Dado que el estudio de los péptidos sintéticos seleccionados con las membranas celulares es muchas veces dificultoso, se realizaron estudios biofísicos con distintos modelos de membrana, monocapas y bicapas fosfolipídicas. También se llevaron a cabo experimentos con eritrocitos, ya que se ha establecido una buena correlación entre la capacidad fusogénica de una secuencia y su capacidad de producir hemólisis [2]. De todos los estudios realizados, el péptido E2(279-298) es el que interaccionó en mayor medida con los modelos de membrana. Además, este péptido fue capaz de desestabilizar y penetrar en los sistemas en estudio, preferentemente en los sistemas que contenían cargas negativas.

El péptido de mayor longitud de la región N-terminal, E2(7-26), aunque también interaccionó con los distintos modelos de membrana, lo hizo preferentemente mediante interacciones electrostáticas.

Una vez seleccionado E2(279-298) como el mejor candidato para ser definido como péptido de fusión, se realizó un estudio comparativo con otro péptido cercano a esta región, para profundizar y descartar o corroborar a E2(279-298) como posible péptido de fusión. La región escogida (267-284), tiene 6 aminoácidos comunes con el péptido E2(279-298),

por tanto, comparte características de selección que le hacen ser favorable como péptido de fusión. Todos los estudios realizados de fluorescencia (unión a membranas lipídicas, liberación de contenidos vesiculares y fusión de membranas), los estudios de calorimetría diferencial de barrido y el experimento de hemólisis pusieron de manifiesto la capacidad de interacción, desestabilización y ruptura de los modelos de membranas y membranas celulares del péptido E2(279-298), teniendo siempre un efecto más acusado que E2(267-284).

Otro factor importante en el proceso de fusión, es el cambio conformacional que se produce en la proteína estructural cuando interacciona con la membrana celular, convirtiéndola en proteína activa, y por tanto, en proteína fusogénica [140]. Por ello, otro de los objetivos planteados en el inicio de la tesis doctoral, fue la realización de un estudio conformacional de los péptidos.

El péptido que experimentó un mayor cambio estructural hacia una conformación de tipo α-hélice al interaccionar con modelos de membrana fue E2(279-298). Este cambio fue mayor cuando el modelo de membrana contenía fosfolípidos cargados negativamente, indicando nuevamente que esta composición es importante para la acción del péptido. De esto puede deducirse, que la conformación adoptada por el péptido es importante para la unión y la desestabilización de las membranas.

Para entender mejor la relación estructura-actividad del péptido en el proceso de unión a las membranas, se realizó un estudio teórico de la disposición de los aminoácidos en la secuencia peptídica al situarse en forma de α-hélice (rueda de Edmunson). La disposición de E2(279-298) en forma de hélice α presenta dos caras, una donde se encuentran dispuestos los aminoácidos hidrofóbicos y otra con los aminoácidos polares. La región de los aminoácidos apolares, presenta el aminoácido arginina que "desestabiliza" la hélice-α. Cuando el péptido interacciona con fosfolípidos cargados negativamente, esta arginina se encuentra neutralizada, y por ello, el grado de helicidad y las interacciones con modelos de membrana que presentan cargas negativas son mayores.

Por tanto, con todos los estudios realizados podemos afirmar que E2(279-298) constituye un péptido de fusión interno del virus de la hepatitis G, el cual al interaccionar con los modelos de membrana estudiados, adopta una conformación activa en forma de α-hélice capaz de desestabilizar y fusionar los sistemas en estudio.

CONCLUSIONES

1. La selección de secuencias potencialmente fusogénicas pertenecientes a la proteína estructural E2 del virus de la hepatitis G (GBV-C/HGV), mediante escalas de predicción semiempíricas, y su síntesis en fase sólida, siguiendo una estrategia Fmoc/tBu, se han realizado satisfactoriamente.

2. La caracterización fisicoquímica de los péptidos se ha realizado mediante isotermas de adsorción y extensión. Los péptidos de la región amino terminal han mostrado un comportamiento distinto dependiendo del grado de hidrofobicidad. El péptido E2(17-26) no ha presentado actividad superficial ni isoterma estable debido a su elevada hidrofilia. Los péptidos E2(12-26) y E2(7-26) han mostrado actividad superficial, siendo más acusada en el péptido de mayor longitud. La actividad del péptido E2(279-298) se ha estudiado en distintos medios, incrementándose al aumentar la fuerza iónica de la subfase. E2(12-26), E2(7-26) y E2(279-298) han mostrado una isoterma de compresión estable.

3. La observación mediante el microscopio del ángulo de Brewster (BAM) ha permitido visualizar la monocapa de E2(279-298) in situ al comprimirse. El péptido se ha visualizado en forma de dominios que han incrementado con la presión. La formación de estructuras tridimensionales debido a un mayor empaquetamiento del péptido, se ha observado al final de la compresión.

4. La interacción de los péptidos con monocapas fosfolipídicas de DPPC, DMPC, y DMPC/DMPG (cinéticas de penetración e isotermas) ha sido mayor con los fosfolípidos más fluidos.

5. El estudio de monocapas mixtas de DPPC y DMPC con el péptido E2(279-298) ha producido desviaciones respecto a la idealidad. Esto es indicativo de una interacción entre los componentes y, dado que las desviaciones observadas son positivas, podemos decir que la interacción se produce en forma de complejos ricos en fosfolípidos (a bajas fracciones molares de péptido) o ricos en péptido (a elevadas fracciones molares de péptido).

6. Los estudios de calorimetría diferencial de barrido (DSC) indican que los parámetros termotrópicos (ΔH, $\Delta T_{1/2}$ y T_m) han sido modificados en presencia de los péptidos. La región N-terminal ha interaccionado en mayor medida con la composición DMPC/DMPG, siendo E2(7-26) el péptido que ha causado un mayor efecto sobre la bicapa lipídica. E2(279-298) ha producido un efecto más acusado, sobretodo en la composición negativa. Los experimentos por microcalorimetría han indicado que el péptido es capaz de interaccionar y cambiar los parámetros termodinámicos a muy bajas concentraciones.

7. Los estudios de microscopía electrónica de transmisión (MET) y de espectroscopia visible han servido para indicar la capacidad de agregación de liposomas del péptido E2(7-26) a diferencia de E2(279-298).

8. Los estudios de fluorescencia han indicado que los péptidos N-terminales se unen a las membranas fosfolipídicas en la superficie mediante interacciones de tipo electrostático, y son más marcadas en presencia de cargas negativas. El péptido E2(279-298) también interacciona en mayor medida con liposomas cargados negativamente, pero produce un efecto más acusado que los péptidos N-terminales. Éste péptido además tiene la capacidad de penetrar en la membrana fosfolipídica cerca de la interfase lípido/agua. Otra característica de E2(279-298) destacable respecto a E2(7-26) es que perturba, desestabiliza y fusiona los modelos de membrana testados (liberación de contenidos vesiculares, fusión de membranas). Estas características indican que puede tratarse de un péptido de fusión del virus de la hepatitis G.

9. El estudio de hemólisis con E2(279-298) pone de manifiesto que el péptido es capaz de perturbar membranas biológicas de forma similar a otros péptidos de fusión conocidos.

10. Los estudios conformacionales llevados a cabo mediante la técnica de dicroísmo circular han mostrado diferente conformación en medio fluorado o micelar (los péptidos N-terminales preferentemente en forma de estructura tipo β y la región interna con una conformación de tipo α-hélice). El estudio comparativo de E2(7-26) y E2(279-298) en presencia de liposomas, ha mostrado que E2(279-298) aumenta claramente su porcentaje de α-hélice a diferencia de E2(7-26). Esto nos indica que la estructura adoptada por E2(279-298) podría estar ligada a su interacción con los modelos de membrana estudiados.

    La realización del estudio de FTIR con el péptido E2(279-298) ha servido para confirmar el cambio desde una estructura mayoritaria desordenada en agua, hacia una estructuración de tipo α-hélice en presencia de TFE o SUVs.

BIBLIOGRAFÍA

[1] Martin,I., I, Ruysschaert,J., & Epand,R.M. (1999) Role of the N-terminal peptides of viral envelope proteins in membrane fusion. *Adv. Drug Deliv. Rev.*, **38,** 233-255.

[2] Cross,K.J., Burleigh,L.M., & Steinhauer,D.A. (2001) Mechanisms of cell entry by influenza virus. *Exp. Rev. Mol. Med.*, 1-18.

[3] Wahlberg,J.M. & Garoff,H. (1992) Membrane fusion process of Semliki Forest virus. I: Low pH-induced rearrangement in spike protein quaternary structure precedes virus penetration into cells. *J. Cell Biol.*, **116,** 339-348.

[4] Allison,S.L., Stiasny,K., Stadler,K., Mandl,C.W., & Heinz,F.X. (1999) Mapping of functional elements in the stem-anchor region of tick-borne encephalitis virus envelope protein E. *J. Virol.*, **73,** 5605-5612.

[5] Sattentau,Q.J. & Moore,J.P. (1991) Conformational changes induced in the human immunodeficiency virus envelope glycoprotein by soluble CD4 binding. *J. Exp. Med.*, **174,** 407-415.

[6] Hu,X.L., Ray,R., & Compans,R.W. (1992) Functional interactions between the fusion protein and hemagglutinin-neuraminidase of human parainfluenza viruses. *J. Virol.*, **66,** 1528-1534.

[7] Robertson,B., Myers,G., Howard,C., Brettin,T., Bukh,J., Gaschen,B., Gojobori,T., Maertens,G., Mizokami,M., Nainan,O., Netesov,S., Nishioka,K., Shin i T, Simmonds,P., Smith,D., Stuyver,L., & Weiner,A. (1998) Classification, nomenclature, and database development for hepatitis C virus (HCV) and related viruses: proposals for standardization. International Committee on Virus Taxonomy. *Arch. Virol.*, **143,** 2493-2503.

[8] Monath,T.P. (1994) Dengue: the risk to developed and developing countries. *Proc. Natl. Acad. Sci. U. S. A*, **91,** 2395-2400.

[9] Sathar,M., Soni,P., & York,D. (2000) GB virus C/hepatitis G virus (GBV-C/HGV): still looking for a disease. *Int. J. Exp. Pathol.*, **81,** 305-322.

[10] Major,M.E., Reherman,B., & Feinstone,S.M. (2001) *Hepatitis C viruses*. Lippincott, Philadelphia.

[11] Simons,J.N., Leary,T.P., Dawson,G.J., Pilot-Matias,T.J., Muerhoff,A.S., Schlauder,G.G., Desai,S.M., & Mushahwar,I.K. (1995) Isolation of novel virus-like sequences associated with human hepatitis. *Nat. Med.*, **1,** 564-569.

[12] Linnen,J., Wages,J., Jr., Zhang-Keck,Z.Y., Fry,K.E., Krawczynski,K.Z., Alter,H., Koonin,E., Gallagher,M., Alter,M., Hadziyannis,S., Karayiannis,P., Fung,K.,

Nakatsuji,Y., Shih,J.W., Young,L., Piatak,M., Jr., Hoover,C., Fernandez,J., Chen,S., Zou,J.C., Morris,T., Hyams,K.C., Ismay,S., Lifson,J.D., Kim,J.P., & . (1996) Molecular cloning and disease association of hepatitis G virus: a transfusion-transmissible agent. *Science*, **271,** 505-508.

[13] Stapleton,J.T. (2003) GB Virus Type C/Hepatitis G Virus. *Semin. Liver Dis.*, **23,** 137-148.

[14] Bukh,J., Kim,J.P., Govindarajan,S., Apgar,C.L., Foung,S.K., Wages,J., Jr., Yun,A.J., Shapiro,M., Emerson,S.U., & Purcell,R.H. (1998) Experimental infection of chimpanzees with hepatitis G virus and genetic analysis of the virus. *J. Infect. Dis.*, **177,** 855-862.

[15] Dawson,G.J., Schlauder,G.G., Pilot-Matias,T.J., Thiele,D., Leary,T.P., Murphy,P., Rosenblatt,J.E., Simons,J.N., Martinson,F.E., Gutierrez,R.A., Lentino,J.R., Pachucki,C., Muerhoff,A.S., Widell,A., Tegtmeier,G., Desai,S., & Mushahwar,I.K. (1996) Prevalence studies of GB virus-C infection using reverse transcriptase-polymerase chain reaction. *J. Med. Virol.*, **50,** 97-103.

[16] Lefrere,J.J., Ferec,C., Roudot-Thoraval,F., Loiseau,P., Cantaloube,J.F., Biagini,P., Mariotti,M., LeGac,G., & Mercier,B. (1999) GBV-C/hepatitis G virus (HGV) RNA load in immunodeficient individuals and in immunocompetent individuals. *J. Med. Virol.*, **59,** 32-37.

[17] Huang,J.J., Lee,W.C., Ruaan,M.K., Wang,M.C., Chang,T.T., & Young,K.C. (2001) Incidence, transmission, and clinical significance of hepatitis G virus infection in hemodialysis patients. *Eur. J Clin. Microbiol. Infect. Dis.*, **20,** 374-379.

[18] Berg,T., Naumann,U., Fukumoto,T., Bechstein,W.O., Neuhaus,P., Lobeck,H., Hohne,M., Schreier,E., & Hopf,U. (1996) GB virus C infection in patients with chronic hepatitis B and C before and after liver transplantation. *Transplantation*, **62,** 711-714.

[19] Rey,D., Vidinic-Moularde,J., Meyer,P., Schmitt,C., Fritsch,S., Lang,J.M., & Stoll-Keller,F. (2000) High prevalence of GB virus C/hepatitis G virus RNA and antibodies in patients infected with human immunodeficiency virus type 1. *Eur. J Clin. Microbiol. Infect. Dis.*, **19,** 721-724.

[20] Jarvis,L.M., Davidson,F., Hanley,J.P., Yap,P.L., Ludlam,C.A., & Simmonds,P. (1996) Infection with hepatitis G virus among recipients of plasma products. *Lancet*, **348,** 1352-1355.

[21] Simons,J.N., Desai,S.M., & Mushahwar,I.K. (2000) The GB viruses. *Curr. Top. Microbiol. Immunol.*, **242,** 341-375.

[22] Scallan,M.F., Clutterbuck,D., Jarvis,L.M., Scott,G.R., & Simmonds,P. (1998) Sexual transmission of GB virus C/hepatitis G virus. *J. Med. Virol.*, **55,** 203-208.

[23] Lefrere,J.J., Sender,A., Mercier,B., Mariotti,M., Pernot,F., Soulie,J.C., Malvoisin,A., Berry,M., Gabai,A., Lattes,F., Galiay,J.C., Pawlak,C., de,L., V, Chauveau,V., Hreiche,G., Larsen,M., Ferec,C., Parnet-Mathieu,F., Roudot-Thoraval,F., & Brossard,Y. (2000) High rate of GB virus type C/HGV transmission from mother to infant: possible implications for the prevalence of infection in blood donors. *Transfusion*, **40,** 602-607.

[24] Feucht,H.H., Zollner,B., Polywka,S., Knodler,B., Schroter,M., Nolte,H., & Laufs,R. (1997) Prevalence of hepatitis G viremia among healthy subjects, individuals with liver disease, and persons at risk for parenteral transmission. *J. Clin. Microbiol.*, **35,** 767-768.

[25] Brown,K.E., Wong,S., Buu,M., Binh,T.V., Be,T.V., & Young,N.S. (1997) High prevalence of GB virus C/hepatitis G virus in healthy persons in Ho Chi Minh City, Vietnam. *J. Infect. Dis.*, **175,** 450-453.

[26] Xiang,J., Daniels,K.J., Soll,D.R., Schmidt,W.N., LaBrecque,D.R., & Stapleton,J.T. (1999) Visualization and characterization of GB virus-C particles: evidence for a nucleocapsid. *J Viral Hepat.*, **6 Suppl 1,** 16-22.

[27] Gutierrez,R.A., Dawson,G.J., Knigge,M.F., Melvin,S.L., Heynen,C.A., Kyrk,C.R., Young,C.E., Carrick,R.J., Schlauder,G.G., Surowy,T.K., Dille,B.J., Coleman,P.F., Thiele,D.L., Lentino,J.R., Pachucki,C., & Mushahwar,I.K. (1997) Seroprevalence of GB virus C and persistence of RNA and antibody. *J. Med. Virol.*, **53,** 167-173.

[28] Thomas,D.L., Vlahov,D., Alter,H.J., Hunt,J.C., Marshall,R., Astemborski,J., & Nelson,K.E. (1998) Association of antibody to GB virus C (hepatitis G virus) with viral clearance and protection from reinfection. *J. Infect. Dis.*, **177,** 539-542.

[29] Tacke,M., Schmolke,S., Schlueter,V., Sauleda,S., Esteban,J.I., Tanaka,E., Kiyosawa,K., Alter,H.J., Schmitt,U., Hess,G., Ofenloch-Haehnle,B., & Engel,A.M. (1997) Humoral immune response to the E2 protein of hepatitis G virus is associated with long-term recovery from infection and reveals a high frequency of hepatitis G virus exposure among healthy blood donors. *Hepatology*, **26,** 1626-1633.

[30] Kanda,T., Yokosuka,O., Ehata,T., Maru,Y., Imazeki,F., Saisho,H., Shiratori,Y., & Omata,M. (1997) Detection of GBV-C RNA in patients with non-A-E fulminant hepatitis by reverse-transcription polymerase chain reaction. *Hepatology*, **25,** 1261-1265.

[31] Sallie,R., Shaw,J., & Mutimer,D. (1996) GBV-C virus and fulminant hepatic failure. *Lancet*, **347,** 1552.

[32] Alter,H.J. (1997) G-pers creepers, where'd you get those papers? A reassessment of the literature on the hepatitis G virus. *Transfusion*, **37,** 569-572.

[33] Xiang,J., Wunschmann,S., Diekema,D.J., Klinzman,D., Patrick,K.D., George,S.L., & Stapleton,J.T. (2001) Effect of coinfection with GB virus C on survival among patients with HIV infection. *N. Engl. J. Med.*, **345,** 707-714.

[34] Macalalad,A.R. & Snydman,D.R. (2002) GB virus C and mortality from HIV infection. *N. Engl. J. Med.*, **346,** 377-379.

[35] Polgreen,P.M., Xiang,J., Chang,Q., & Stapleton,J.T. (2003) GB virus type C/hepatitis G virus: a non-pathogenic flavivirus associated with prolonged survival in HIV-infected individuals. *Microbes. Infect.*, **5,** 1255-1261.

[36] Tanaka,Y., Mizokami,M., Orito,E., Ohba,K., Kato,T., Kondo,Y., Mboudjeka,I., Zekeng,L., Kaptue,L., Bikandou,B., M'Pele,P., Takehisa,J., Hayami,M., Suzuki,Y., & Gojobori,T. (1998) African origin of GB virus C/hepatitis G virus. *FEBS Lett.*, **423,** 143-148.

[37] Simmonds,P. (2001) The origin and evolution of hepatitis viruses in humans. *J Gen. Virol.*, **82,** 693-712.

[38] Smith,D.B., Basaras,M., Frost,S., Haydon,D., Cuceanu,N., Prescott,L., Kamenka,C., Millband,D., Sathar,M.A., & Simmonds,P. (2000) Phylogenetic analysis of GBV-C/hepatitis G virus. *J Gen. Virol.*, **81,** 769-780.

[39] Jahn,R. & Sudhof,T.C. (1999) Membrane fusion and exocytosis. *Annu. Rev. Biochem.*, **68,** 863-911.

[40] White,J.M. (1990) Viral and cellular membrane fusion proteins. *Annu. Rev. Physiol*, **52,** 675-697.

[41] Jardetzky,T.S. & Lamb,R.A. (2004) Virology: a class act. *Nature*, **427,** 307-308.

[42] Yu,Y.G., King,D.S., & Shin,Y.K. (1994) Insertion of a coiled-coil peptide from influenza virus hemagglutinin into membranes. *Science*, **266,** 274-276.

[43] Ghosh,J.K. & Shai,Y. (1999) Direct evidence that the N-terminal heptad repeat of Sendai virus fusion protein participates in membrane fusion. *J Mol. Biol.*, **292,** 531-546.

[44] Santos,N.C., Prieto,M., & Castanho,M.A. (1998) Interaction of the major epitope region of HIV protein gp41 with membrane model systems. A fluorescence spectroscopy study. *Biochemistry*, **37,** 8674-8682.

[45] Suarez,T., Gallaher,W.R., Agirre,A., Goni,F.M., & Nieva,J.L. (2000) Membrane interface-interacting sequences within the ectodomain of the human immunodeficiency virus type 1 envelope glycoprotein: putative role during viral fusion. *J Virol.*, **74,** 8038-8047.

[46] Skehel,J.J. & Wiley,D.C. (2000) Receptor binding and membrane fusion in virus entry: the influenza hemagglutinin. *Annu. Rev. Biochem.*, **69,** 531-569.

[47] Chan,D.C., Fass,D., Berger,J.M., & Kim,P.S. (1997) Core structure of gp41 from the HIV envelope glycoprotein. *Cell*, **89,** 263-273.

[48] Weissenhorn,W., Dessen,A., Calder,L.J., Harrison,S.C., Skehel,J.J., & Wiley,D.C. (1999) Structural basis for membrane fusion by enveloped viruses. *Mol. Membr. Biol.*, **16,** 3-9.

[49] Baker,K.A., Dutch,R.E., Lamb,R.A., & Jardetzky,T.S. (1999) Structural basis for paramyxovirus-mediated membrane fusion. *Mol. Cell*, **3,** 309-319.

[50] Weissenhorn,W., Carfi,A., Lee,K.H., Skehel,J.J., & Wiley,D.C. (1998) Crystal structure of the Ebola virus membrane fusion subunit, GP2, from the envelope glycoprotein ectodomain. *Mol. Cell*, **2,** 605-616.

[51] Heinz,F.X. & Allison,S.L. (2003) Flavivirus structure and membrane fusion. *Adv. Virus Res.*, **59,** 63-97.

[52] Delos,S.E., Gilbert,J.M., & White,J.M. (2000) The central proline of an internal viral fusion peptide serves two important roles. *J. Virol.*, **74,** 1686-1693.

[53] Gaudin,Y., Tuffereau,C., Durrer,P., Brunner,J., Flamand,A., & Ruigrok,R. (1999) Rabies virus-induced membrane fusion. *Mol. Membr. Biol.*, **16,** 21-31.

[54] Allison,S.L., Schalich,J., Stiasny,K., Mandl,C.W., & Heinz,F.X. (2001) Mutational evidence for an internal fusion peptide in flavivirus envelope protein E. *J. Virol.*, **75,** 4268-4275.

[55] Lescar,J., Roussel,A., Wien,M.W., Navaza,J., Fuller,S.D., Wengler,G., Wengler,G., & Rey,F.A. (2001) The Fusion glycoprotein shell of Semliki Forest virus: an icosahedral assembly primed for fusogenic activation at endosomal pH. *Cell*, **105,** 137-148.

[56] Bressanelli,S., Stiasny,K., Allison,S.L., Stura,E.A., Duquerroy,S., Lescar,J., Heinz,F.X., & Rey,F.A. (2004) Structure of a flavivirus envelope glycoprotein in its low-pH-induced membrane fusion conformation. *EMBO J.*, **23,** 728-738.

[57] Modis,Y., Ogata,S., Clements,D., & Harrison,S.C. (2004) Structure of the dengue virus envelope protein after membrane fusion. *Nature*, **427,** 313-319.

[58] Del Angel,V.D., Dupuis,F., Mornon,J.P., & Callebaut,I. (2002) Viral fusion peptides and identification of membrane-interacting segments. *Biochem. Biophys. Res. Commun.*, **293,** 1153-1160.

[59] White,J.M. (1992) Membrane fusion. *Science*, **258,** 917-924.

[60] Qureshi,N.M., Coy,D.H., Garry,R.F., & Henderson,L.A. (1990) Characterization of a putative cellular receptor for HIV-1 transmembrane glycoprotein using synthetic peptides. *AIDS*, **4,** 553-558.

[61] Nieva,J.L. & Agirre,A. (2003) Are fusion peptides a good model to study viral cell fusion? *Biochim. Biophys. Acta*, **1614,** 104-115.

[62] Voisset,C. & Dubuisson,J. (2004) Functional hepatitis C virus envelope glycoproteins. *Biol. Cell*, **96,** 413-420.

[63] Yagnik,A.T., Lahm,A., Meola,A., Roccasecca,R.M., Ercole,B.B., Nicosia,A., & Tramontano,A. (2000) A model for the hepatitis C virus envelope glycoprotein E2. *Proteins*, **40,** 355-366.

[64] Rey,F.A., Heinz,F.X., Mandl,C., Kunz,C., & Harrison,S.C. (1995) The Envelope Glycoprotein from Tick-Borne Encephalitis-Virus at 2 Angstrom Resolution. *Nature*, **375,** 291-298.

[65] Kuhn,R.J., Zhang,W., Rossmann,M.G., Pletnev,S.V., Corver,J., Lenches,E., Jones,C.T., Mukhopadhyay,S., Chipman,P.R., Strauss,E.G., Baker,T.S., & Strauss,J.H. (2002) Structure of dengue virus: implications for flavivirus organization, maturation, and fusion. *Cell*, **108,** 717-725.

[66] Modis,Y., Ogata,S., Clements,D., & Harrison,S.C. (2003) A ligand-binding pocket in the dengue virus envelope glycoprotein. *Proc. Natl. Acad. Sci. U. S. A*, **100,** 6986-6991.

[67] Laxton,C.D., McMillan,D., Sullivan,V., & Ackrill,A.M. (1998) Expression and characterization of the hepatitis G virus helicase. *J. Viral Hepat.*, **5,** 21-26.

[68] Flint,M., Thomas,J.M., Maidens,C.M., Shotton,C., Levy,S., Barclay,W.S., & McKeating,J.A. (1999) Functional analysis of cell surface-expressed hepatitis C virus E2 glycoprotein. *J. Virol.*, **73,** 6782-6790.

[69] Garry,R.F. & Dash,S. (2003) Proteomics computational analyses suggest that hepatitis C virus E1 and pestivirus E2 envelope glycoproteins are truncated class II fusion proteins. *Virology*, **307,** 255-265.

[70] Cevc,G. & Derek,M. (1987) In *Phospholipid bilayers: Physical principles and models* (Wiley,J., ed), pp. 2-28. New York.

[71] Buckland,A.G. & Wilton,D.C. (2000) Anionic phospholipids, interfacial binding and the regulation of cell functions. *Biochim. Biophys. Acta*, **1483,** 199-216.

[72] Smit,J.M., Waarts,B.L., Bittman,R., & Wilschut,J. (2003) Liposomes as target membranes in the study of virus receptor interaction and membrane fusion. *Methods Enzymol.*, **372,** 374-392.

[73] Nir,S. & Nieva,J.L. (2000) Interactions of peptides with liposomes: pore formation and fusion. *Prog. Lipid Res.*, **39,** 181-206.

[74] Verger,R. & Pattus,F. (1982) Lipid-Protein Interactions in Monolayers. *Chemistry and Physics of Lipids*, **30,** 189-227.

[75] Schwarz,G. & Taylor,S.E. (1999) Polymorphism and interactions of a viral fusion peptide in a compressed lipid monolayer. *Biophys. J*, **76,** 3167-3175.

[76] Maget-Dana,R. (1999) The monolayer technique: a potent tool for studying the interfacial properties of antimicrobial and membrane-lytic peptides and their interactions with lipid membranes. *Biochim. Biophys. Acta*, **1462,** 109-140.

[77] New,R.C.C. (1990) *Liposomes*. IRL Press at Oxford University Press, New York.

[78] Janin,J. (1979) Surface and inside volumes in globular proteins. *Nature*, **277,** 491-492.

[79] Kyte,J. & Doolittle,R.F. (1982) A simple method for displaying the hydropathic character of a protein. *J Mol. Biol.*, **157,** 105-132.

[80] Wimley,W.C. & White,S.H. (1996) Experimentally determined hydrophobicity scale for proteins at membrane interfaces. *Nat. Struct. Biol.*, **3,** 842-848.

[81] Chou,P.Y. & Fasman,G.D. (1979) Prediction of beta-turns. *Biophys. J*, **26,** 367-373.

[82] Merrifield,R.B. (1963) Solid-phase peptide synthesis. I. The synthesis of a tetrapeptide. *J. Am. Chem. Soc.*, **85,** 2149-2154.

[83] Carpino,L.A. & Han,G.A. (1972) The 9-fluorenylmethyloxycarbonyl amino-protecting group. *J. Org. Chem.*, **37,** 3404-3409.

[84] Kaiser,E., Colescott,R.L., Bossinger,C.D., & Cook,P.I. (1970) Color test for detection of free terminal amino groups in the solid-phase synthesis of peptides. *Anal. Biochem.*, **34,** 595-598.

[85] Sanz,P.P. (1992) *Fisicoquímica para Farmacia y Biología*. Ediciones científicas y técnicas Masson Salvat, Barcelona.

[86] Langmuir,I. (1917) The constitution and fundamental properties of solids and liquids. II. Liquids. *J. Am. Chem. Soc.*, **39,** 1848-1906.

[87] Lipp,M.M., Lee,K.Y., Zasadzinski,J.A., & Waring,A.J. (1996) Phase and morphology changes in lipid monolayers induced by SP-B protein and its amino-terminal peptide. *Science*, **273,** 1196-1199.

[88] Davies,J.T. & Rideal,E.K. (1963) *Interfacial phenomena*, Secon edition edn. Academic Press, New York.

[89] Gaines,G.L. (1966) *Insoluble monolayers at liquid-gas interfaces*. Interscience, New York.

[90] Goodrich,F.C. (1957) *Proceedings of the 11th International Congress on Surface Activity*, Bultorworths, London edn.

[91] Pagano,R.E. & Gershfeld,N.L. (1972) A millidyne film balance for measuring intermolecular energies in lipid films. *J. Colloid Interface Sci.*, **41,** 311-317.

[92] Lheveder,C., Meunier,J., & Hénon (2000) *Physical chemistry of biological interfaces*. Ed: Marcel Dekker.Inc., New York.

[93] Aranda,F.J. & Villalain,J. (1997) The interaction of abietic acid with phospholipid membranes. *Biochim. Biophys. Acta*, **1327,** 171-180.

[94] Poklar,N., Fritz,J., Macek,P., Vesnaver,G., & Chalikian,T.V. (1999) Interaction of the pore-forming protein equinatoxin II with model lipid membranes: A calorimetric and spectroscopic study. *Biochemistry*, **38,** 14999-15008.

[95] Koynova,R. & Caffrey,M. (1998) Phases and phase transitions of the phosphatidylcholines. *Biochim. Biophys. Acta*, **1376,** 91-145.

[96] Lakowicz,J.R. (1983) *Principles of fluorescence spectroscopy*. Plenum Press, New York.

[97] Wimley,W.C. & White,S.H. (2000) Designing transmembrane alpha-helices that insert spontaneously. *Biochemistry*, **39,** 4432-4442.

[98] Christiaens,B., Symoens,S., Verheyden,S., Engelborghs,Y., Joliot,A., Prochiantz,A., Vandekerckhove,J., Rosseneu,M., Vanloo,B., & Vanderheyden,S. (2002) Tryptophan fluorescence study of the interaction of penetratin peptides with model membranes. *Eur. J Biochem.*, **269,** 2918-2926.

[99] Ellens,H., Bentz,J., & Szoka,F.C. (1984) pH-induced destabilization of phosphatidylethanolamine-containing liposomes: role of bilayer contact. *Biochemistry*, **23,** 1532-1538.

[100] Christiaens,B., Grooten,J., Reusens,M., Joliot,A., Goethals,M., Vandekerckhove,J., Prochiantz,A., & Rosseneu,M. (2004) Membrane interaction and cellular internalization of penetratin peptides. *Eur. J Biochem.*, **271,** 1187-1197.

[101] Peisajovich,S.G., Epand,R.F., Pritsker,M., Shai,Y., & Epand,R.M. (2000) The polar region consecutive to the HIV fusion peptide participates in membrane fusion. *Biochemistry*, **39,** 1826-1833.

[102] Struck,D.K., Hoekstra,D., & Pagano,R.E. (1981) Use of Resonance Energy-Transfer to Monitor Membrane-Fusion. *Biochemistry*, **20,** 4093-4099.

[103] Eftink,M.R. & Ghiron,C.A. (1976) Exposure of tryptophanyl residues in proteins. Quantitative determination by fluorescence quenching studies. *Biochemistry*, **15,** 672-680.

[104] De Kroon,A.I., Soekarjo,M.W., De Gier,J., & De Kruijff,B. (1990) The role of charge and hydrophobicity in peptide-lipid interaction: a comparative study based on tryptophan fluorescence measurements combined with the use of aqueous and hydrophobic quenchers. *Biochemistry*, **29,** 8229-8240.

[105] Ulrich,A.S., Tichelaar,W., Forster,G., Zschornig,O., Weinkauf,S., & Meyer,H.W. (1999) Ultrastructural characterization of peptide-induced membrane fusion and peptide self-assembly in the lipid bilayer. *Biophys. J*, **77,** 829-841.

[106] Peisajovich,S.G., Epand,R.F., Epand,R.M., & Shai,Y. (2002) Sendai virus N-terminal fusion peptide consists of two similar repeats, both of which contribute to membrane fusion. *Eur. J Biochem.*, **269,** 4342-4350.

[107] Persson,D., Thoren,P.E., & Norden,B. (2001) Penetratin-induced aggregation and subsequent dissociation of negatively charged phospholipid vesicles. *FEBS Lett.*, **505,** 307-312.

[108] Oren,Z. & Shai,Y. (1997) Selective lysis of bacteria but not mammalian cells by diastereomers of melittin: structure-function study. *Biochemistry*, **36,** 1826-1835.

[109] Tejuca,M., Anderluh,G., Macek,P., Marcet,R., Torres,D., Sarracent,J., Alvarez,C., Lanio,M.E., Dalla,S.M., & Menestrina,G. (1999) Antiparasite activity of sea-anemone cytolysins on Giardia duodenalis and specific targeting with anti-Giardia antibodies. *Int. J. Parasitol.*, **29,** 489-498.

[110] Mangoni,M.L., Rinaldi,A.C., Di Giulio,A., Mignogna,G., Bozzi,A., Barra,D., & Simmaco,M. (2000) Structure-function relationships of temporins, small antimicrobial peptides from amphibian skin. *Eur. J. Biochem.*, **267,** 1447-1454.

[111] Lee,S., Aoki,R., Oishi,O., Aoyagi,H., & Yamasaki,N. (1992) Effect of amphipathic peptides with different alpha-helical contents on liposome-fusion. *Biochim. Biophys. Acta*, **1103,** 157-162.

[112] Rapaport,D. & Shai,Y. (1994) Interaction of fluorescently labeled analogues of the amino-terminal fusion peptide of Sendai virus with phospholipid membranes. *J Biol. Chem.*, **269,** 15124-15131.

[113] Richardson,J.S. & Richardson,D.C. (1988) Amino acid preferences for specific locations at the ends of alpha helices. *Science*, **240,** 1648-1652.

[114] Woody (1996) *Circular dichroism and the conformational analysis of biomolecules*. Plenum Press, New York.

[115] Lobley,A., Whitmore,L., & Wallace,B.A. (2002) DICHROWEB: an interactive website for the analysis of protein secondary structure from circular dichroism spectra. *Bioinformatics.*, **18,** 211-212.

[116] Whitmore,L. & Wallace,B.A. (2004) DICHROWEB, an online server for protein secondary structure analyses from circular dichroism spectroscopic data. *Nucleic Acids Res.*, **32,** W668-W673.

[117] Greenfield,N.J. (1996) Methods to estimate the conformation of proteins and polypeptides from circular dichroism data. *Anal. Biochem.*, **235,** 1-10.

[118] Chen,Y.H., Yang,J.T., & Martinez,H.M. (1972) Determination of the secondary structures of proteins by circular dichroism and optical rotatory dispersion. *Biochemistry*, **11,** 4120-4131.

[119] Bandekar,J. (1992) Amide modes and protein conformation. *Biochim. Biophys. Acta*, **1120,** 123-143.

[120] Susi,H. & Byler,D.M. (1986) Resolution-enhanced Fourier transform infrared spectroscopy of enzymes. *Methods Enzymol.*, **130,** 290-311.

[121] Takahashi,K., Hijikata,M., Aoyama,K., Hoshino,H., Hino,K., & Mishiro,S. (1997) Characterization of GBV-C/HGV viral genome:comparison among different isolates for a 2 Kb-sequence that covers entire E1 and most of 5' UTR and E2. *Int. Hepatol. Com.*, **6,** 253-263.

[122] Peisajovich,S.G. & Shai,Y. (2003) Viral fusion proteins: multiple regions contribute to membrane fusion. *Biochim. Biophys. Acta*, **1614,** 122-129.

[123] Phillips,M.C., Jones,N.B., Patrick,C.P., & Jones,N.B.a.R.M. (1979) Monolayers of block copolypeptides at the air-water interface. *J Colloid Interface Sci.*, **72,** 98-105.

[124] Wharton,S.A., Martin,S.R., Ruigrok,R.W., Skehel,J.J., & Wiley,D.C. (1988) Membrane fusion by peptide analogues of influenza virus haemagglutinin. *J. Gen. Virol.*, **69 (Pt 8),** 1847-1857.

[125] Gordon,L.M., Curtain,C.C., Zhong,Y.C., Kirkpatrick,A., Mobley,P.W., & Waring,A.J. (1992) The amino-terminal peptide of HIV-1 glycoprotein 41 interacts with human erythrocyte membranes: peptide conformation, orientation and aggregation. *Biochim. Biophys. Acta*, **1139,** 257-274.

[126] Epand,R.F., Martin,I., Ruysschaert,J.M., & Epand,R.M. (1994) Membrane orientation of the SIV fusion peptide determines its effect on bilayer stability and ability to promote membrane fusion. *Biochem. Biophys. Res. Commun.*, **205,** 1938-1943.

[127] Rojo,N., Gomara,M.J., Busquets,M.A., Alsina,M.A., & Haro,I. (2003) Interaction of E2 and NS3 synthetic peptides of GB virus C/Hepatitis G virus with model lipid membranes. *Talanta*, **60,** 395-404.

[128] Grau,A., Ortiz,A., de Godos,A., & Gomez-Fernandez,J.C. (2000) A biophysical study of the interaction of the lipopeptide antibiotic iturin A with aqueous phospholipid bilayers. *Arch. Biochem. Biophys.*, **377,** 315-323.

[129] Rodriguez-Crespo,I., Yelamos,B., Albar,J.P., Peterson,D.L., & Gavilanes,F. (2000) Selective destabilization of acidic phospholipid bilayers performed by the hepatitis B virus fusion peptide. *Biochim. Biophys. Acta*, **1463,** 419-428.

[130] Contreras,L.M., Aranda,F.J., Gavilanes,F., Gonzalez-Ros,J.M., & Villalain,J. (2001) Structure and interaction with membrane model systems of a peptide derived from the major epitope region of HIV protein gp41: implications on viral fusion mechanism. *Biochemistry*, **40,** 3196-3207.

[131] Thoren,P.E., Persson,D., Esbjorner,E.K., Goksor,M., Lincoln,P., & Norden,B. (2004) Membrane binding and translocation of cell-penetrating peptides. *Biochemistry*, **43,** 3471-3489.

[132] Oren,Z., Ramesh,J., Avrahami,D., Suryaprakash,N., Shai,Y., & Jelinek,R. (2002) Structures and mode of membrane interaction of a short alpha helical lytic peptide and its diastereomer determined by NMR, FTIR, and fluorescence spectroscopy. *Eur. J. Biochem.*, **269,** 3869-3880.

[133] Henriques,S.T. & Castanho,M.A. (2004) Consequences of nonlytic membrane perturbation to the translocation of the cell penetrating peptide pep-1 in lipidic vesicles. *Biochemistry*, **43,** 9716-9724.

[134] Kliger,Y., Peisajovich,S.G., Blumenthal,R., & Shai,Y. (2000) Membrane-induced conformational change during the activation of HIV-1 gp41. *J. Mol. Biol.*, **301,** 905-914.

[135] White,J., Kielian,M., & Helenius,A. (1983) Membrane fusion proteins of enveloped animal viruses. *Q. Rev. Biophys.*, **16,** 151-195.

[136] Gallaher,W.R. (1987) Detection of a fusion peptide sequence in the transmembrane protein of human immunodeficiency virus. *Cell*, **50,** 327-328.

[137] Whitt,M.A., Zagouras,P., Crise,B., & Rose,J.K. (1990) A fusion-defective mutant of the vesicular stomatitis virus glycoprotein. *J Virol.*, **64,** 4907-4913.

[138] Jahn,R., Lang,T., & Sudhof,T.C. (2003) Membrane fusion. *Cell*, **112,** 519-533.

[139] Tamm,L.K., Han,X., Li,Y., & Lai,A.L. (2002) Structure and function of membrane fusion peptides. *Biopolymers*, **66,** 249-260.

[140] Harter,C., James,P., Bachi,T., Semenza,G., & Brunner,J. (1989) Hydrophobic binding of the ectodomain of influenza hemagglutinin to membranes occurs through the "fusion peptide". *J Biol. Chem.*, **264,** 6459-6464.

ANEXO I: Interacciones de tres dominios de beta-interferón con liposomas y monocapas como modelos de membrana

Cristina Larios, Marta Espina, M.Asunción Alsina e Isabel Haro

Departamento de Química de Péptidos y Proteínas , Instituto de Investigaciones Químicas y Ambientales de Barcelona, IIQAB-CSIC.
Departamento de Fisicoquímica, Facultad de Farmacia, Universidad de Barcelona.

Cristina Larios, Marta Espina, M.Asunción Alsina and Isabel Haro, *Interaction of three beta-interferon domains with liposomes and monolayers as model membranes* Biophys. Chem., **11**, 123-133 (2004)

Resumen

En este trabajo fueron analizadas las propiedades fisicoquímicas de tres péptidos pertenecientes a la molécula del β-interferón (β-IFN), [β-IFN(13-20), β-IFN(40-47) y β-IFN(109-116)] y sus derivados palmitoilados, los cuales han sido descritos como epítopos antigénicos de los anticuerpos neutralizantes responsables del fallo en la terapia de múltiple esclerosis. Los péptidos fueron sintetizados por metodología en fase sólida y caracterizados por análisis de aminoácidos, cromatografía líquida de alta eficacia a escala analítica y espectroscopia de masas por electrospray. Se determinó la actividad de los péptidos libres y derivatizados. Se realizaron estudios de cinéticas de penetración a área constante e isotermas de compresión para conocer si los péptidos sintetizados eran capaces de interaccionar con modelos de membrana. Además, la calorimetría diferencial de barrido (DSC) fue utilizada para investigar las propiedades de fase termotrópica de mezclas binarias de dipalmitoilfosfatidilcolina (DPPC) o dipalmitoilfosfatidilglicerol (DPDG) con los péptidos en estudio.

ELSEVIER

Biophysical Chemistry 111 (2004) 123–133

Biophysical Chemistry

www.elsevier.com/locate/bpc

Interaction of three β-interferon domains with liposomes and monolayers as model membranes

Cristina Larios[a,b], Marta Espina[b], María A. Alsina[b], Isabel Haro[a,*]

[a] *Department of Peptide and Protein Chemistry, IIQAB-CSIC, Jordi Girona 18-26 08034 Barcelona, Spain*
[b] *Department of Physical Chemistry, Faculty of Pharmacy, University of Barcelona, Avda. Joan XXIII s/n 08028 Barcelona, Spain*

Received 5 April 2004; received in revised form 13 May 2004; accepted 17 May 2004
Available online 9 June 2004

Abstract

The physicochemical properties of three peptides belonging to the β-interferon (β-IFN) molecule, -β-IFN(13–20), β-IFN(40–47) and β-IFN(109–116)-, which have been described to be antigenic epitopes of the neutralising antibodies responsible of the failure of the Multiple Sclerosis therapy, and their palmitoylated derivatives were analysed. Peptides were synthesised by solid-phase methodologies and characterized by amino acid analysis, analytical high-performance liquid chromatography and electrospray mass spectrometry. The activity of free and derivatized peptides was determined. In order to know how the synthesised peptides were able to interact with membrane models, studies of kinetics of penetration at constant area and compression isotherms were carried out. Moreover, differential scanning calorimetry (DSC) was used to investigate the thermotropic phase properties of binary mixtures of dipalmitoylphosphatidylcholine (DPPC) or dipalmitoylphosphatidylglicerol (DPPG) with the peptides.

Keywords: β-Interferon; Synthetic peptides; Phospholipids; Monolayers; Liposomes; Differential scanning calorimetry

1. Introduction

Multiple Sclerosis is an autoimmune disease associated with immune activity directed against central nervous system antigens. The most effective treatment available is β-interferon (β-IFN), as a result of its immunomodulatory effect. β-IFN decreases the frequency of relapses and the number of lesions in magnetic resonance imaging as well as it causes a slow disease progression [1]. However, patients treated with β-IFN develop neutralising antibodies against the drug, this fact being a failure of β-IFN therapy [2].

Previous studies have indicated that three main antigenic epitopes on the β-IFN molecule do exist. The molecule of β-IFN contains five α-helices: A (residues 2–22), B (residues 51–71), C (residues 80–107), D (residues 118–136), and E (residues 139–162). These helices are connected by loops designated AB, BC, CD and DE [3]. Mapping the locations of the major observed linear epitopes onto the three-dimensional structure of β-IFN have resulted that most antibodies detected in the ELISA analysis recognise regions of the molecule close the N-terminus, the AB or CD loops, or D helix. These regions possess an extended linear structure in the native, folded molecule [4]. Consequently, antibodies that bind to these regions of the native structure would also bind to linear peptides of the same sequence.

Having in mind that synthetic peptides have been shown to be a valuable tool to mimic the action at the lipid membrane level [5,6], the main aim of the present study was to get insight into the interaction of three putative antigenic synthesised peptides belonging to (13–20), (40–47) and (109–116) portions of β-IFN molecule and its derived lipopeptides with lipid bilayers.

Phosphatidylcholines (PC) are the most abundant lipids in mammalian membranes and a major membrane component in eukaryotic organism. Dipalmitoylphosphatidylcholine (DPPC) has a well-defined transition temperature that facilitates the study of the effect of peptides in its thermotropic properties.

The amphipatic character of these peptides could make them surface active products and as their biological activity

* Corresponding author. Tel.: +34-93-4006109; fax: +34-93-2045904.
E-mail address: ihvqpp@iiqab.csic.es (I. Haro).

0301-4622/$ - see front matter © 2004 Elsevier B.V. All rights reserved.
doi:10.1016/j.bpc.2004.05.004

occurs at lipid membrane interfaces, the monolayer technique is entirely suitable to study their physicochemical and biological properties [7]. Interactions of molecules, in our case peptides, with a bilayer-ordered structure can influence vesicle transition thermotropic parameters according to their own physicochemical properties [8,9]. In this sense, we have used the differential scanning calorimetry (DSC) technique to analyse the effect of increasing amounts of the β-IFN belonging peptides on the thermotropic properties of multilamellar vesicles composed of the zwitterionic lipid DPPC. Moreover, we have studied the effect of 10% of β-IFN lipopeptides with an anionic lipid such as dipalmitoylphosphatidylglicerol (DPPG).

2. Experimental section

2.1. Materials

DPPC and DPPG were obtained from Sigma. Chloroform, methanol and acetonitrile solvents were from Merck. Dimethylformamide (DMF) was purchased from Sharlau. Water was double distilled and deionized (Milli-Q system, Millipore) The resistivity of water was 18.2 MΩ cm and pH was 5.8. Rink Amide MBHA resin and amino acids were obtained from Novabiochem. Coupling reagents were obtained from Fluka and Novabiochem. Trifluoroacetic acid (TFA) was supplied by Merck and scavengers such as ethanedithiol (EDT) or triisopropylsilane (TIS) were from Sigma-Aldrich.

2.2. Methods

2.2.1. β-IFN peptides syntheses

The studied peptide sequences were chosen according to the semiempirical method of Chou and Fasman [10] that theoretically predicts the secondary structure of peptides. This method was applied by using the Peptide Companion version 1.24 (Coshisoft/Peptide Search) computer program. Then, the peptides were synthesised by a solid-phase methodology following an Fmoc/tBut strategy. β-IFN(13–20) (SNFQCQKL), β-IFN(40–47) (IPEEIKQL) and β-IFN(109–116) (EDFTRGAL) were obtained manually on a Rink Amide MBHA (functionalization 0.65 meq/g) by means of a diisopropylcarbodiimide/hydroxybenzotriazole (DIPCD/HOBt) activation. Threefold molar excesses of Fmoc-amino acids were used throughout the synthesis, the yield of each coupling being at least 95% according to Kaiser et al.'s [11] test. At the completion of the introduction of Fmoc-Leu, the peptide resin was removed from the reaction column, washed with DMF, isopropyl alcohol, and ether, dried in vacuum, and divided into three parts. Each part of the amino resin was elongated in order to obtain the about-described peptides. During the synthetic process carried out to obtain the β-IFN(109–116) peptide, repeated couplings for the incorporation of Thr^{112} and Arg^{113} were needed. Final deprotection and cleavage of peptides from the resin was achieved by an acid treatment with TFA containing appropriate scavengers (H_2O, EDT and TIS) at room temperature for about 2 h with occasional agitation. The crude peptides were then precipitated with diethyl ether, the samples were sonicated and centrifuged, and the supernatants were decanted off. This last step was repeated until the total removal of scavengers. Finally, the peptides were dissolved in water and lyophylized.

The synthesised peptides were successfully characterised by analytical HPLC, amino acid analysis and Maldi-Tof mass spectrometry (Table 1).

HPLC analyses were performed on a C-18 silica column eluted with acetonitrile (A)/water (W) (0.05% TFA) mixtures. Conditions used for the three deprotected peptide sequences, were 30 min by a gradient from 85%W to 65%W. Eluted substances were detected spectrophotometrically at 215 nm. A single peak for β-IFN(13–20), β-IFN(40–47) and β-IFN(109–116) with capacity factor values (K') of 6.6, 12.6 and 12.0 respectively, were obtained.

Satisfactory amino acid analyses were obtained. The analyses were carried out in a Pico-Tag system (Waters). Samples of 1 mg of the peptides were hydrolysed in 6 N HCl at 110 °C over 24 h.

2.2.2. Lipopeptides syntheses

Dry peptide resins were swollen in DMF for 30 min and the solvent decanted off. Fmoc protecting groups were removed from protected peptide resins, and palmitic acid was attached to the N-terminus as follows. Palmitic acid was dissolved in a minimum amount of DMF, followed by the addition of DIPCD/HOBT reagents. The solutions were then

Table 1
Peptides characterization

Peptide	aaa[a]	HPLC (K')[b]	Maldi-Tof[c]
β-IFN(13–20): SNFQCQKL	L=1.01 (1), K=1.17 (1), Q=1.98 (2), C=n.d. (1), F=0.75 (1), N=0.84 (1), S=0.84 (1)	6.6	965.9
β-IFN(40–47): IPEEIKQL	L=1.05 (1), $E+Q$=3.23 (3), K=1.21 (1), I=1.51 (2), P=1.07 (1)	12.6	968.0
β-IFN(109–116): EDFTRGAL	L=1.03 (1), A=1.06 (1), G=1.05 (1), R=0.96 (1), T=1.03 (1), F=0.9 (1), D=0.97 (1), E=1.03 (1)	12.0	908.0

[a] Amino acid analysis (theoretical values in parenthesis).
[b] Eluents: (A) H_2O (0.05% TFA), (B) CH_3CN (0.05% TFA); gradient: 85% A to 65% A in 30 min; Detection: λ=215 nm; flow: 1ml/min.
[c] MALDI-TOF mass spectrometry.

poured into the soaked peptide resins. The mixtures were set aside at room temperature and agitated occasionally. Reactions were completed in 2 h as judged by the Kaiser's test. Afterwards, they were rinsed and dried. Finally, palmitoylated peptides were removed from the resins and their identity was confirmed by mass spectrometry.

2.2.3. Monolayer studies

The experiments were performed on a Langmuir film balance KSV5000, equipped with a Wilhemy platinum plate.

2.2.3.1. Surface activity. Surface activity measurements were carried out in a cylindrical trough (volume 70 ml, 30 cm^2) with mechanical stirring. The trough was filled with phosphate-buffered saline (PBS) and increasing volumes of concentrated peptide solutions were injected directly underneath trough a lateral hole. Pressure increases were recorded continuously for 60 min.

2.2.3.2. Insertion of peptides into monolayers. The same methodology was used in the presence of phospholipid monolayers. Monolayers were formed spreading the phospholipids from a 1 mg/ml stock solution in chloroform, directly to the air–water interface, to reach the required initial surface pressure: 5, 10, 20 and 32 mN/m. After pressure stabilisation peptide solution was injected directly underneath the monolayer [12].

2.2.3.3. Compression isotherms. Compression isotherms of peptides or DPPC spread on the aqueous subphase containing peptides were carried in a Teflon trough (surface area 17,000 mm^2, volume 1000 ml) containing 850 ml of PBS. The surface pressure of the monolayers was measured by a Wilhelmy plate pressure sensor and it was calibrated periodically with the π–A curve of the stearic acid monolayer. The uncertainty in the area per molecule obtained from the isotherms was about $\pm$ 5%. Films were spread from chloroform/methanol solutions and at least 10 min was allowed for solvent evaporation. The monolayer was compressed with an area reduction rate of 20 mm^2/min and was compressed up to their collapse pressure. Stability of the monolayers was assessed by compressing them and stopping the barrier at different pressures, and observing that no pressure decay occurred after 30 min. All experiments were performed at 21 $\pm$ 1 °C. Each run was repeated three times.

2.2.4. Differential scanning calorimetry

Multilamellar vesicles (MLVs) of DPPC or DPPG were prepared as follows. Briefly, the lipid was dissolved in a glass tube with a mixture of chloroform/methanol (2/1 v/v) and dried by slow evaporation under constant flow of nitrogen. The residual solvent was removed by storing the samples overnight under high vacuum in a vacuum oven at room temperature. MLVs were obtained by hydrating the lipid film with HEPES buffer, pH 7.4 alone or containing the different peptides at increasing proportions (0%, 3%, 5%, 10%, 20% and 30 %) and vortexing at 50 °C. Final lipid concentration was quantified by phosphorous analysis [13] and was around 4 mM.

DSC experiments of MLVs were performed using a DSC 821E Mettler Toledo (Greifensee, Switzerland) calorimeter. Hermetically sealed aluminium references and samples containing pans were used. Sample pans were loaded by adding 30 μl of DPPC vesicle suspension, corresponding to approximately 0.13 mg of phospholipid. Differences in the heat capacity between the sample and the reference cell were obtained by raising the temperature at a constant rate of 5 °C min^{-1} over a range from 0 to 60 °C. All samples were submitted to three heating/cooling cycles. Data from the first scan was always discarded to avoid mixing artefacts. The endothermic peak coming from the second scan of the control sample was used as a reference template. The calorimeter was calibrated with Indium. To ensure scan-to-

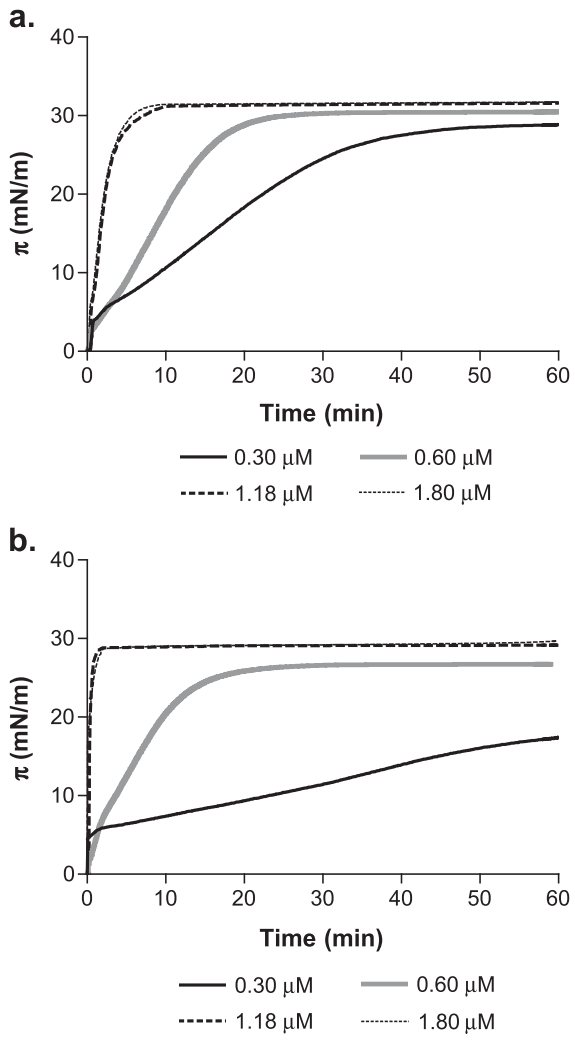

Fig. 1. Surface activity of (a) Palm-β-IFN(40–47) and (b) Palm-β-IFN(109–116) at 0.3, 0.6, 1.18 and 1.8 μM concentrations.

scan reproducibility three consecutive scans of the same sample were performed. DSC runs were carried out within the same day of liposome preparation. Molar enthalpies of transition (ΔH) were calculated from peak areas by means of a STARTe Mettler Toledo system.

3. Results and discussion

3.1. Peptides characterization

The synthesis of free peptides -β-IFN(13–20), β-IFN(40–47), β-IFN(109–116)-, and their derived lipopeptides, -Palm-β-IFN(13–20), Palm-β-IFN(40–47), Palm-β-IFN(109–116)-, was accomplished by using Fmoc/tBu strategy, as described in the experimental section. As shown in Table 1, the synthesised peptides were well characterised by analytical HPLC, amino acid analysis and Maldi-Tof mass spectrometry. Analytical HPLC results indicated that the β-IFN(13–20) peptide sequence is clearly more hydrophilic than β-IFN(40–47) and β-IFN(109–116) peptides, being its K' value two times lower. The mass spectrometry analysis for the Palm-β-IFN(13–20), Palm-β-IFN(40–47), Palm-β-IFN(109–116) confirmed that the syntheses were successfully carried out.

3.2. Surface activity

The surface activities of the peptides were determined by injecting different peptide concentrations into the PBS-buffered surface and recording the surface pressures, π, that were achieved. The experimental curves were used to determine the peptide concentration to be employed in the kinetics of penetration experiments. The chosen concentration, 0.6 μM, was slightly lower than the saturation concentration.

β-IFN(13–20), β-IFN(40–47) and β-IFN(109–116) did not present surface activity as a consequence of their solubilization in the subphase. Due to the high hydrophilicity of β-IFN(13–20) sequence, that has five polar amino acids at the N-terminus, its lipophilicaly derivative neither presented surface activity. Contrarily, the adsorption of Palm-β-IFN(40–47) and Palm-β-IFN(109–116) peptides into the interface was gradual at low concentrations. However, the adsorption at saturation concentrations was achieved very quickly and before 5 min (Fig. 1a and b).

3.3. Penetration kinetics at constant area

The interaction of the peptides that had surface activity with monolayers composed of a zwitterionic phospholipid (DPPC) was studied trough penetration kinetics at constant area at different initial surface pressure: 5, 10, 20 and 32 mN/m. At 32 mN/m, there was not an increase in the pressure when the peptide was incorporated. Peptide concentration in the subphase was 0.6 μM. Fig. 2 shows the pressure change versus time. The maximum pressures were achieved at around 25 min for all initial pressures assayed. The inset of the figure shows the values obtained after 1 h at different initial pressures. In this diagram is shown the effect of the initial surface pressure in the increase induced for the peptides. The greater was the initial pressure the lower was the effect of the peptide. This is a common behaviour for

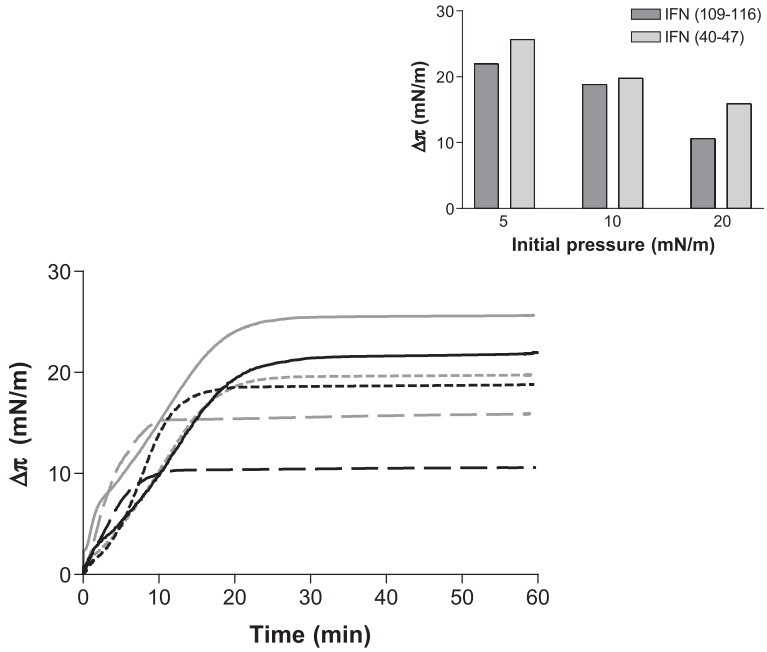

Fig. 2. Pressure increase produced by Palm-β-IFN(40–47) at (▬) 5 mN/m, (▪▪▪) 10 mN/m, (▬ ▪) 20 mN/m and Palm-β-IFN(109–116) at (▬) 5 mN/m, (▪▪▪) 10 mN/m, (▬ ▪) 20 mNm. Peptide concentration was 0.6 μM. The inset reports the pressure increase (mN/m) obtained after 1 h for Palm-β-IFN(40–47) and Palm-β-IFN(109–116) injected under DPPC membrane at different initial pressures.

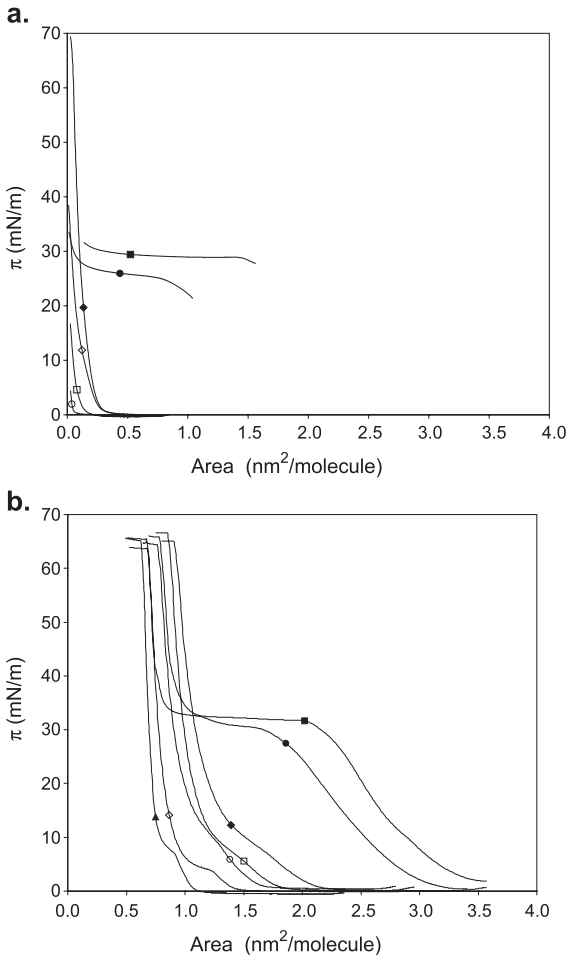

Fig. 3. (a) Compression isotherms of ◇ β-IFN(13–20), □ β-IFN(40–47), ○ β-IFN(109–116), ◆ Palm-β-IFN(13–20), ■ Palm-β-IFN(40–47), and ● Palm-β-IFN(109–116). (b) Compression isotherms of ▲ DPPC and DPPC spread on subphases containing the peptides at 1.8 μM.

hydrophobic molecules [14]. The contribution of the Palm-β-IFN(40–47) to the surface pressure increase is greater than the obtained for Palm-β-IFN(109–116), thus agreeing with the greater surface activity of Palm-β-IFN(40–47).

The interaction with DPPC could be related with the different hydrophobicity of the molecules studied. Accordingly, Palm-β-IFN(40–47) has a higher aliphatic index, having a value of 146.12. This index is defined as the relative volume of a peptide or a protein occupied by the aliphatic side chains (alanine, valine, isoleucine, and leucine) [15]. On the other hand, Palm-β-IFN(109–116) has a value of 61.25. Moreover, the Grand Average of Hydropathicity (GRAVY) parameter, calculated as the sum of hydropathy values of all the amino acids, divided by the number of residues in the sequence [16], was also higher for Palm-β-IFN(40–47) than for Palm-β-IFN(109–116).

3.4. Compression isotherms

In order to have a more complete knowledge of the physicochemical properties of β-IFN peptides, compression isotherms were studied. Fig. 3a shows the obtained isotherms of the different peptides. All free peptides showed very low area/molecule values that suggested a solubilization of the peptides into the subphase after being spread on the interface, this fact being in agreement with their lack of surface activity. As in previous experiments of surface activity and penetration kinetics, Palm-β-IFN(13–20) had a similar behaviour to free peptides. On the contrary, Palm-IFN(40–47) and Palm-IFN(109–116) formed a stable monolayer at the air/water interface. The peptide concentration used was 1.8 μM for all peptides, the hydrophobic peptides Palm-β-IFN(40–47) and Palm-β-IFN(109–116) presented elevated initial pressures but without all the ordered states being presented. Since the monolayers in these conditions were totally collapsed the isotherms of Palm-β-IFN(40–47) and Palm-β-IFN(109–116) were repeated with a lower concentration, 0.6 μM. Fig. 3b shows the obtained isotherms of surface pressure versus mean area for the pure lipid DPPC and DPPC with peptides in the subphase. Fixed amounts of DPPC (50 μl solution of 1 mg/ml in $CHCl_3$/MeOH 2/1 v/v, aprox. 4.10^{16} lipid molecules) were spread on the aqueous subphase containing the peptides under study at 1.8 μM.

The isotherm taken from pure DPPC shows the well-known phase transition from liquid-expanded (LE) to liquid-condensed (LC) phases around 7 mN m^{-1} and 0.9 nm^2 $molecule^{-1}$ of molecular area. DPPC monolayers spread onto the surface of peptide solution were shifted to higher areas compared to the isotherm obtained in the absence of peptide. All free peptides and Palm-β-IFN(13–20) did not change the ordered states; however, Palm-β-IFN(40–47) and Palm-β-IFN(109–116) showed higher area values at

Table 2
Surface compression modulus (mN/m) of monolayers of DPPC and DPPC with peptides in the subphase PBS

π (mN/m)	DPPC	DPPC β-IFN(13–20)	DPPC β-IFN(40–47)	DPPC β-IFN(109–116)	DPPC Palm-β-IFN(13–20)	DPPC Palm-β-IFN(40–47)	DPPC Palm-β-IFN(109–116)
5	26.55	8.24	22.09	25.24	25.19	38.06	37.44
10	17.64	31.85	20.37	20.35	18.36	44.53	52.84
20	76.23	61.59	59.52	44.50	46.06	77.11	52.15
30	113.69	94.51	94.64	77.36	85.54	26.94	9.35
40	132.67	95.87	135.31	101.74	106.34	27.54	39.23
50	155.27	141.98	167.67	133.55	151.92	121.87	128.83
60	75.56	81.15	107.58	82.52	101.90	79.18	84.05

pressures smaller than 30 mN/m. On the other hand, Palm-β-IFN(40–47) and Palm-β-IFN(109–116) presented area values smaller than the other peptides at higher pressures, suggesting that these peptides were released from the monolayer [17].

Surface compression modulus (C_s^{-1}) values of monolayers in the presence of DPPC were calculated using the values of Fig. 3b and applying Eq. (1) [18]:

$$C_s^{-1} = -A\left(\frac{\partial \pi}{\partial A}\right)_T \quad (1)$$

Results obtained (Table 2) show that in DPPC monolayers, Palm-β-IFN(40–47) and Palm-β-IFN(109–116) at lower pressures have a higher compressibility than free peptides and Palm-β-IFN(13–20). The maximum surface compression modulus was produced around 50 mN/m for all peptides studied.

The expanding effect caused by the peptides reflect a destabilization of the monolayer packing. The greater effect of the lipopeptides can be attributed to higher hydrophobic interactions as a consequence of its palmitoylated tail. Moreover, the different behaviour between the derivative peptides can be attributed to the different isoelectric point. Palm-β-IFN(40–47) and Palm-β-IFN(109–116) have isoelectric points of 4.5 and 4.4, respectively. Consequently, at pH 7.4 they were negatively charged. On the other hand,

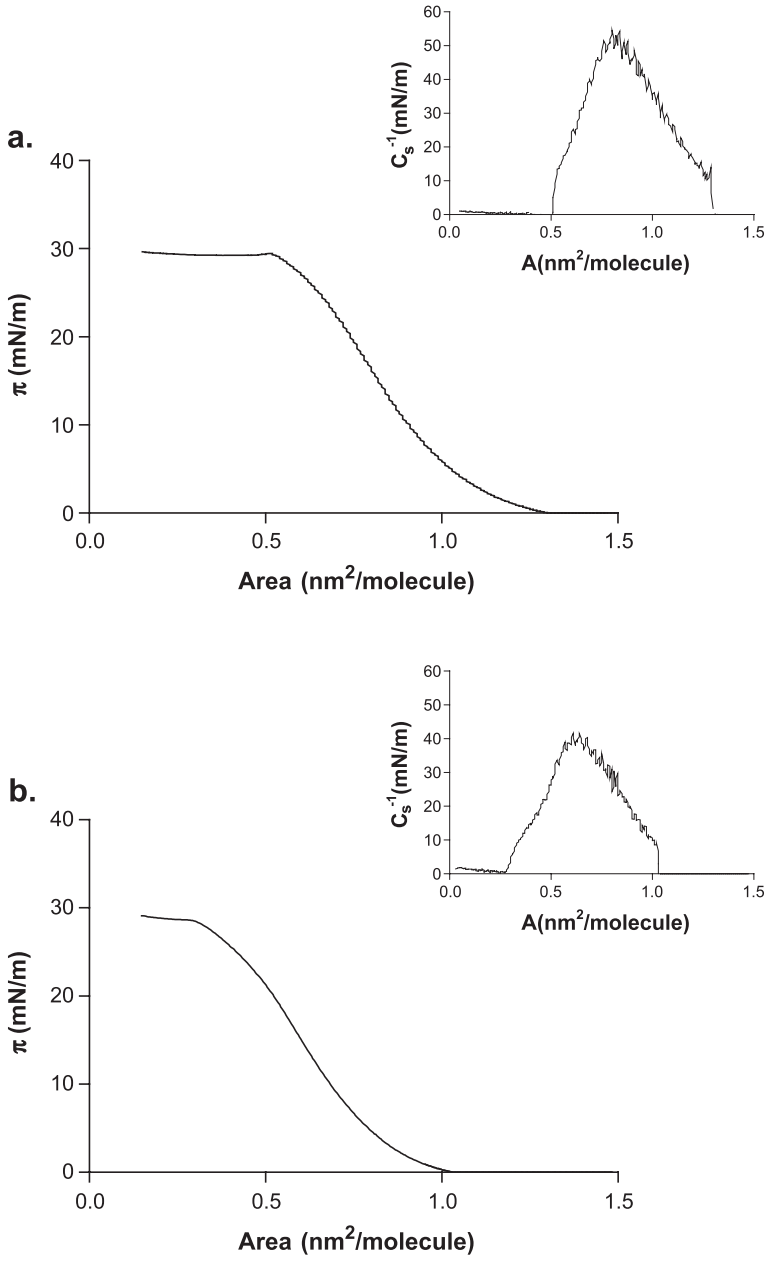

Fig. 4. Compression isotherms of (a) Palm-IFN(40–47) and (b) Palm-IFN(109–116) at 0.6 μM. Inset: surface compression modulus (C_s^{-1}) values as a function of the area/molecule.

Palm-β-IFN(13–20) has an isoelectric point of 7.9; thus, at this pH it would be neutral or positively charged.

The compression isotherms of Palm-IFN(40–47) and Palm-IFN(109–116) spreading 3.5×10^{17} molecules (0.6 μM) is shown in Fig. 4a and b. Palm-β-IFN(40–47) showed an extrapolated area/molecule of 1.05 nm^2/molecule and a lift-off area of 1.3 nm^2/molecule. The inset of the figure represents the compression modulus (C_s^{-1}) (mN/m) versus area (nm^2/molecule). Maximum C_s^{-1} values are around 50 mN/m, which suggests a liquid-expanded character. The Fig. 4b shows the isotherm of Palm-IFN(109–116) with an extrapolated area of 0.85 nm^2/molecule and a lift-off area of 1 nm^2/molecule. The compression modulus was similar to Palm-IFN(40–47) and there was the collapse without con-

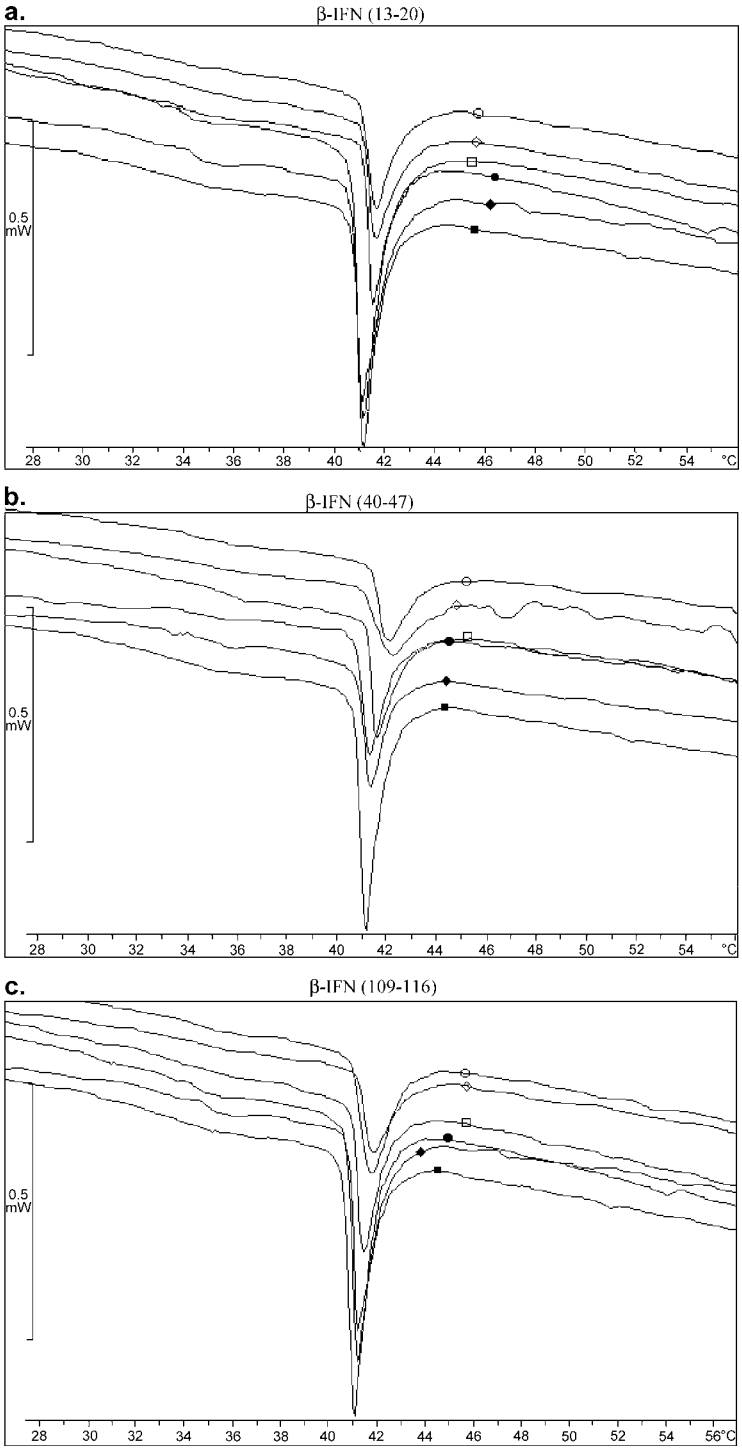

Fig. 5. DSC heating endotherms of DPPC MLVs were obtained in presence of 0 (■), 3 (♦), 5 (●), 10 (□), 20 (◇) and 30 (○) mol% of (a) β-IFN(13–20), (b) β-IFN(40–47) and (c) β-IFN(109–116). The curves refer to the second scan in the heating mode at a temperature scanning rate of 5 °C/min.

densed nor solid state. These values can provide different conformational states [19].

3.5. Differential scanning calorimetry (DSC)

The effect of β-IFN peptides on the gel–liquid crystalline phase transition of DPPC liposomal bilayer membranes was examined by differential scanning calorimetry (DSC). When the transition occurs upon increasing the temperature, several structural changes in the lipid molecules are produced. The principal change associated to the transition is the trans-gauche isomerization in the acyl chains and the average of gauche conformers is related to bilayer fluidity [20]. In Fig. 5 are presented the thermograms of MLV-DPPC alone and in the presence of increasing concentrations of the peptides. The multilamellar bilayers of DPPC alone showed a pretransition at 34.5 °C that is attributed to the transition of two different gel phases: Lβ phase to the rippled gel Pβ phase and a main phase transition (T_m) at 41 °C due to the chain melting transition Pβ to a highly cooperative transition to a lamellar liquid crystalline, Lα. The chain melting transition observed was sharp, the half width at the scan rate used (5 °C/min) being 0.7 °C, similarly to the values described in the literature [21]. The obtained total enthalpy change (36.05 kJ/mol) also agreed with the literature data [22]. When studied the influence of β-IFN peptides, we could observe that they caused a low perturbation in DPPC bilayers. The temperature of the main gel to liquid crystalline phase transition was practically not affected. The little change in the T_m for all peptides could suggest that the interactions of the studied peptides with DPPC vesicles did not alter the packing of the hydrocarbon chains in the gel and liquid crystalline states [23,24]. However, the peak becomes broader suggesting a lower cooperatively on the phospholipid main phase transition in presence of the β-IFN peptides [25]. As described by Ali et al. [26], an enthalpy decrease associated with increasing amounts of peptides (Table 3) could be attributed to a reduction of the intermolecular interactions between the hydrophobic region of the bilayer interiors, caused by the disruption of hydrogen bonding at the lipid/water interface produced by the peptides. In the palmitoylated peptides, the effect on the thermotropic parameters of DPPC MLVs was greater (Fig. 6). Similarly, as occurred with the monolayer technique, Palm-β-IFN(13–20) showed a lower interaction with MLV-DPPC compared to the other palmitoylated peptides. The decrease of enthalpy was about two times lower than the obtained for the other peptides and the peak did not disappear at the higher concentration of the peptide. However, Palm-IFN(40–47) and Palm-IFN(109–116) caused the total disappearance of the transition peak at a percentage of 20% of peptide. As in the other studied techniques Palm-β-IFN(40–47) interacts with a higher extent than Palm-β-IFN(109–116). In Fig. 7, the variation of the transition enthalpy versus the percentage of both free and lipophilically derivatised β-IFN peptides is shown.

Table 3
Thermotropic parameters of the gel to liquid crystalline phase transition of DPPC MLVs prepared in presence of the different peptides

DPPC	T_m (°C)	ΔH (kJ/mol)	$\Delta T_{1/2}$ (°C)
DPPC	41.5	36.0	0.8
β-IFN(13–20)			
3%	41.4	30.8	0.9
5%	41.8	32.5	1.1
10%	41.6	28.4	0.9
20%	41.6	23.3	1.1
30%	41.6	22.0	1.1
β-IFN(40–47)			
3%	41.4	20.8	0.9
5%	41.3	21.1	0.9
10%	41.5	21.7	1.0
20%	42.2	17.5	1.8
30%	42.1	17.5	1.4
β-IFN(109–116)			
3%	41.4	30.6	0.9
5%	41.9	32.7	1.1
10%	41.3	28.9	0.9
20%	41.8	18.3	1.3
30%	41.8	18.1	1.4
Palm-β-IFN(13–20)			
3%	41.2	29.3	1.1
5%	41.1	27.6	1.2
10%	42.2	34.7	1.3
20%	41.7	24.5	2.3
30%	41.2	21.0	1.8
Palm-β-IFN(40–47)			
3%	41.5	29.2	1.5
5%	42.5	24.0	3.7
10%	42.5	8.1	2.7
20%	–	–	–
30%	–	–	–
Palm-β-IFN(109–116)			
3%	41.3	24.9	1.1
5%	41.2	30.6	1.6
10%	41.5	8.4	3.4
20%	–	–	–
30%	–	–	–

To sum up, the studied peptides did not cause any significant change in the transition temperature; nevertheless, they produced a clear decrease in the enthalpy and a broadening of the transition peak. This behaviour is characteristic of molecules with both hydrophobic and hydrophilic interactions with phospholipid membranes being thus mainly situated in the outer part of the bilayer but also having a partial interfacial location [27].

In order to get more insights into the main forces that contribute to peptide–lipid interactions, we tried to evaluate and to compare whether different electrostatic interactions were established between the two negatively charged synthetic lipopeptides [Palm-β-IFN(40–47) and Palm-β-

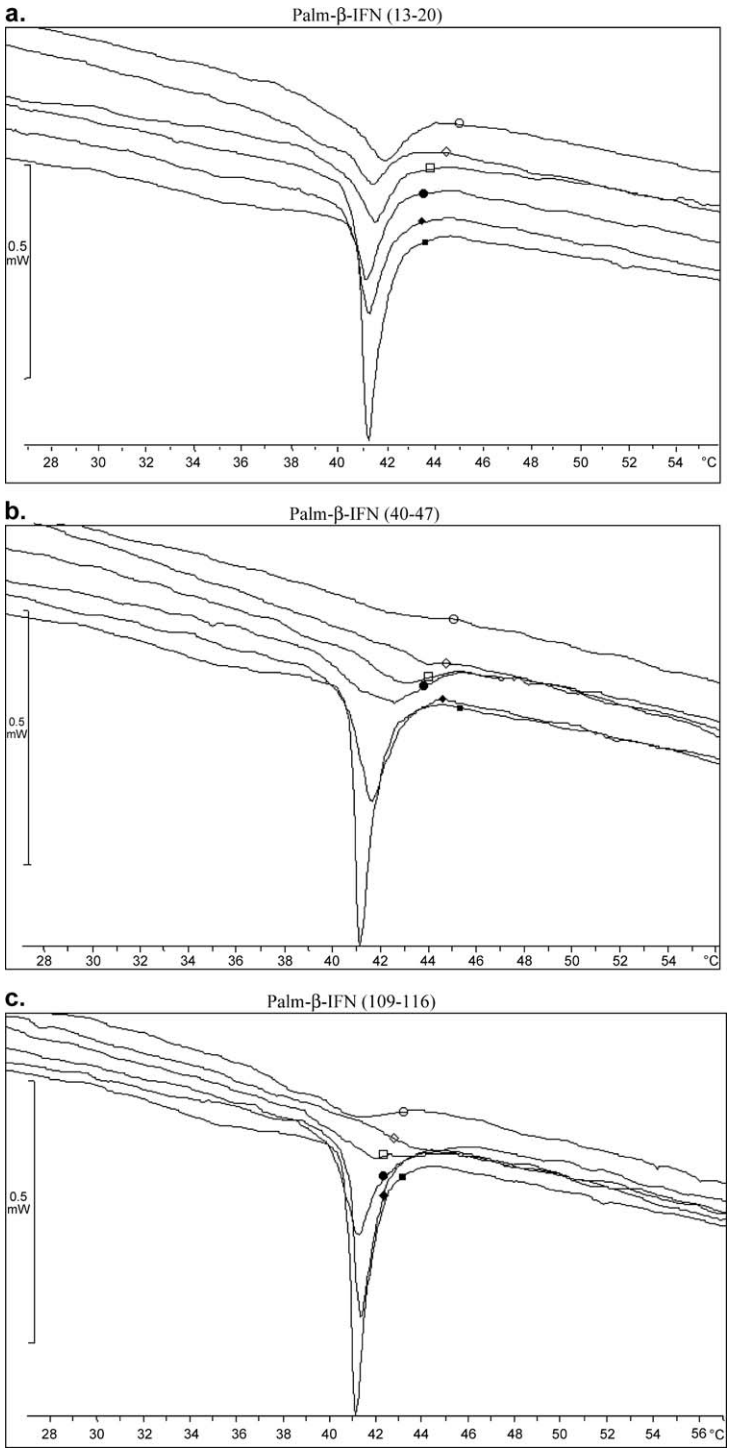

Fig. 6. DSC heating endotherms of DPPC MLVs were obtained in presence of 0 (■), 3 (◆), 5 (●), 10 (□), 20 (◇) and 30 (○) mol% of (a) Palm-β-IFN(13–20), (b) Palm-β-IFN(40–47) and (c) Palm-β-IFN(109–116).

IFN(109–116)] and the positively charged one, Palm-β-IFN(13–20), with a negative phospholipid, such as dipalmitoylphosphatydilglicerol (DPPG). As described in the literature [28], the DSC curve of MLV-DPPG showed an endothermic peak at 40.7 °C due to the main phase transition temperature. Table 4 lists quantitative data from the thermograms studied, in the absence and in the presence of 10% of palmitoylated peptides. MLV-DPPG experimented a light increase in the transition temperature when the peptides were added. Moreover, in all cases, the broadening of the transition profile of DPPG bilayers was considerable. Regarding ΔH values, Palm-β-IFN(13–20) produces a light increase. This result could be explained by a certain rigidification of the bilayer, mainly produced by

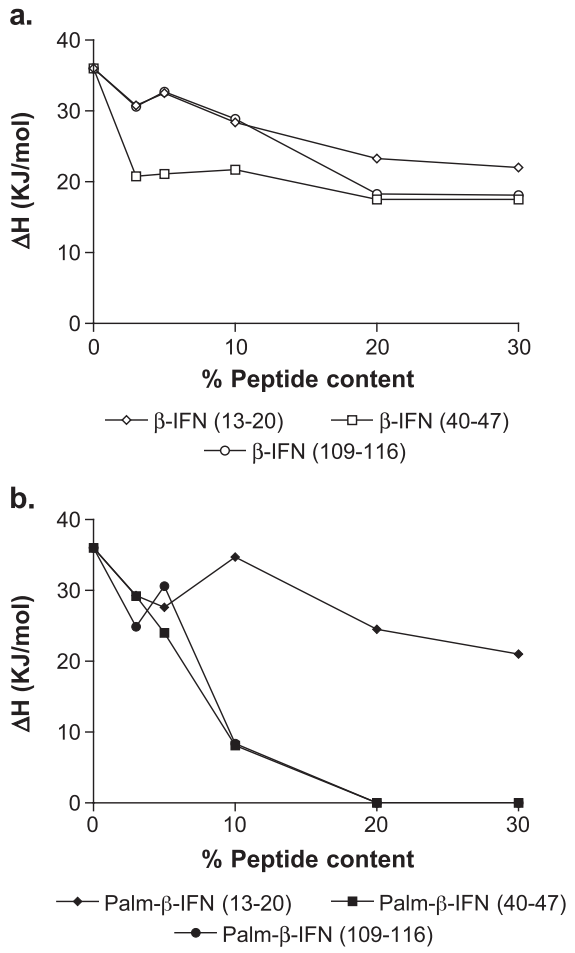

Fig. 7. Dependence of the transition enthalpy (ΔH) of the main gel to liquid crystalline phase transition of DPPC on the percentage of peptides (a) β-IFN peptides and (b) Palm-β-IFN peptides.

electrostatic forces between the positively charged peptide, that could be located at the outer part of the bilayer without penetrating into the bilayer interior, and the negative character of MLVs-DPPG.

On the other hand, the two negatively charged peptides, this is Palm-β-IFN(40–47) and Palm-β-IFN(109–116), produced a notorious effect on ΔH, these values being clearly lower. These results agree with a decrease in acyl chain cooperativity of the bilayer possibly due to a partial penetration of the lipidic chain and the consequent deformation of the packing of the phospholipid acyl chains. In these cases, the interaction peptide/lipid is produced mainly by hydrophobic forces.

4. Conclusions

The present study was undertaken in order to investigate the interaction of peptides belonging to β-IFN with lipid model membranes (monolayers and liposomes). We have used different physicochemical techniques to analyse the properties of peptides and their palmitoylated sequences. The results obtained suggest the following conclusions:

1. β-IFN(13–20), β-IFN(40–47) and β-IFN(109–116) do not have surface activity due to the elevated solubility in the aqueous subphase. Palm-β-IFN(13–20) although bearing a palmitoyl hydrophobic tail, it behaves like a hydrophilic peptide without being detected surface activity. Pressure increase of DPPC monolayers in the presence of Palm-β-IFN(40–47) and Palm-β-IFN(109–116) was studied because they have shown enough surface activity. Palm-β-IFN(40–47) shows a greater effect than Palm-β-IFN(109–116) in all initial pressures studied. Having in mind that the fatty acid that was incorporated in free β-IFN peptides was the same, the different effects observed in the DPPC monolayer could be attributed to the different amino acid sequence within the two peptides and the different conformation adopted.
2. β-IFN(13–20), β-IFN(40–47), β-IFN(109–116) and Palm-IFN(13–20) do not form stable monolayers when spread at an air/water interface due to their high hydrophilicity. However, Palm-β-IFN(40–47) and Palm-β-IFN(109–116) do form stable monolayers, but not showing all the ordered states at the same studied concentrations than the free peptides. On the other hand, at a lower concentration Palm-β-IFN(40–47) and Palm-β-IFN(109–116) presented all the ordered states. The different effect of peptides in monolayers could be attributed to the different isoelectric point.
3. The effects of the free peptides on the thermotropic phase transition properties of MLV DPPC have shown that β-IFN(40–47) shows the greater effect. Although the peptides do not show a significant displacement of the DPPC phase transition midpoint, at 20% β-IFN(40–47) a small shift to lower temperatures was observed. ΔH clearly decreases with an increase in the peptide content, being the decrease observed of 39%, 51% and 50% for β-IFN(13–20), β-IFN(40–47) and β-IFN(109–116), respectively. Moreover, the main transition peak broadens with increasing the amount of peptide present. The change on the thermotropic parameters of the DPPC in the presence of palmitoylated peptides is similar than the one obtained for the free peptides at low concentrations. The phase transition of DPPC disappears at high peptide/

Table 4
Thermotropic parameters of the gel to liquid crystalline phase transition of MLVs DPPG prepared in presence of palmitoylated β-IFN peptides

	T_m (°C)	ΔH (kJ/mol)	$\Delta T_{1/2}$ (°C)
DPPG	40.7	27.0	1.3
DPPG/Palm-β-IFN(13–20)	40.8	29.1	2.4
DPPG/Palm-β-IFN(40–47)	41.6	18.9	3.8
DPPG/Palm-β-IFN(109–116)	41.6	18.1	3.3

The percentage of peptides was 10%.

phospholipid ratios in Palm-β-IFN(40–47) and Palm-β-IFN(109–116); however, at 30% content of Palm-β-IFN(13–20) the transition from the liquid crystalline to the gel phase could still be detected.

4. To evaluate the electrostatic interactions between phospholipids and the studied peptides, an anionic phospholipid such as DPPG, was chosen. As shown, Palm-β-IFN(40–47) and Palm-β-IFN(109–116) could penetrate deeper in the bilayer of MLVs having as a consequence a fluidification of the vesicles. On the other hand, Palm-β-IFN(13–20) could be preferentially located in the outer part of the bilayer.

This paper focused mainly on the physicochemical properties of synthetic β-IFN related peptides and their interaction with lipid model membranes. Future work will be carried out on the use of the described peptides as immunoreagents trying to correlate the properties herein described with their antigenic traits.

Acknowledgements

The excellent technical assistance of Josep Carilla and Amelia López (Laboratori d'Anàlisi Tèrmica IIQAB, CSIC, Barcelona) is greatly acknowledged.

References

[1] G. Antonelli, F. Dianzani, Development of antibodies to interferon beta in patients: technical and biological aspects, Eur. Cytokine Netw. 10 (3) (1999) 413–422.
[2] P. Kivisakk, G.V. Alm, S. Fredrikson, H. LinK, Neutralizing and binding anti-interferon-beta (IFN-beta) antibodies. A comparison between IFN-beta-1a and IFN-beta-1b treatment in multiple sclerosis, Eur. J. Neurol. 7 (1) (2000) 27–34.
[3] M. Karpusas, M. Nolte, C.B. Benton, W. Meier, W.N. Lipscomb, S. Goelz, The crystal structure of human interferon beta at 2.2—a resolution, Proc. Natl. Acad. Sci. U. S. A. 94 (22) (1997) 11813–11818.
[4] M. Briecklmaier, P.S. Hochman, R. Baciu, B. Chao, J.H. Cuervo, A. Whitty, ELISA methods for the analysis of antibody responses induced in multiple sclerosis patients treated with recombinant interferon-beta, J. Immunol. Methods 227 (1–2) (1999) 121–135.
[5] M. García, M. Pujol, F. Reig, M.A. Alsina, I. Haro, Synthesis, lipophilic derivatization and interaction with liposomes of HAV-VP3 (102–121) sequence by using spectroscopic techniques, Analyst 121 (11) (1996) 1583–1588.
[6] P. Sospedra, I. Haro, M.A. Alsina, F. Reig, C. Mestres, Viral synthetic peptide interactions with membranes: a monolayer study, Langmuir 15 (16) (1999) 5303–5308.
[7] A. Shibata, Y. Kiba, N. Akati, K. Fukuzawa, H. Terada, Molecular characteristics of astaxanthin and beta-carotene in the phospholipid monolayer and their distributions in the phospholipid bilayer, Chem. Phys. Lipids 113 (1–2) (2001) 11–22.
[8] T.B. Pedersen, M.C. Sabra, S. Frokjaer, O.G. Mouritsen, K. Jorgensen, Association of acylated cationic decapeptides with dipalmitoylphosphatidylserine-dipalmitoylphosphatidylcholine lipid membranes, Chem. Phys. Lipids 113 (1–2) (2001) 83–95.
[9] A. Grau, J.C. Gomez Fernandez, F. Peypoux, A. Ortiz, A study on the interactions of surfactin with phospholipid vesicles, Biochim. Biophys. Acta 1418 (2) (1999) 307–319.
[10] P.Y. Chou, G.D. Fasman, Prediction of the secondary structure of proteins from their amino acid sequence, Adv. Enzymol. Relat. Areas Mol. Biol. 47 (1978) 45–148.
[11] E. Kaiser, R.L. Colescott, C.D. Bossinger, P.I. Cook, Color test for detection of free terminal amino groups in the solid-phase synthesis of peptides, Anal. Biochem. 34 (2) (1970) 595–598.
[12] M. García, I.B. Nagy, M.A. Alsina, G. Mezö, F. Reig, F. Hudecz, I. Haro, Analysis of the interaction with biomembrane models of the HAV-VP3(101–121) sequence conjugated to synthetic branched chain polypeptide carriers with a poly[L-lysine] backbone, Langmuir 14 (7) (1998) 1861–1869.
[13] C.S.F. Böttcher, C.M. Gent, C. Fries, A rapid and sensitive sub-micro phosphorus determination, Anal. Chim. Acta 24 (1961) 203–204.
[14] P. Sospedra, C. Mestres, I. Haro, M. Muñoz, M.A. Busquets, Effect of amino acid sequence change on peptide–membrane interaction, Langmuir 18 (4) (2002) 1231–1237.
[15] A. Ikai, Thermostability and aliphatic index of globular proteins, J. Biochem. 88 (6) (1980) 1895–1898.
[16] J. Kyte, R.F. Doolittle, A simple method for displaying the hydrophatic character of a protein, J. Mol. Biol. 157 (1982) 105–132.
[17] S. Taneva, K.M.W. Keough, Cholesterol modifies the properties of surface films of dipalmitoylphosphatidylcholine plus pulmonary surfactant-associated protein B or C spread or adsorbed at the air–water interface, Biochemistry 36 (4) (1997) 912–922.
[18] J.T. Davis, E.K. Rideal, Interface Phenomena, 2nd ed., Academic Press, New York, 1963, p. 265.
[19] R. Maget-Dana, D. Lelièvre, A. Brack, Surface active properties of amphiphilic sequential isopeptides: comparison between alpha-helical and beta-sheet, Biopolymers 49 (1999) 415–423.
[20] W. Nerdal, S.A. Gundersen, V. Thorsen, H. Hoiland, H. Holmsen, Chlorpromazine interaction with glycerophospholipid liposomes studied by magic angle spinning solid state (13)C-NMR and differential scanning calorimetry, Biochim. Biophys. Acta 1464 (1) (2000) 165–175.
[21] E. Wachtel, N. Borochov, D. Bach, Effect of dehydroepiandrosterone on phosphatidylserine or phosphatidylcholine bilayers: DSC and X-ray diffraction study, Biochim. Biophys. Acta 1463 (1) (2000) 162–166.
[22] R. Koynova, M. Caffrey, Phases and phase transitions of the phosphatidylcholines, Biochim. Biophys. Acta 1376 (1) (1998) 91–145.
[23] N. Rojo, M.J. Gómara, M.A. Busquets, M.A. Alsina, I. Haro, Interaction of E2 and NS3 synthetic peptides of GB virus C/Hepatitis G virus with model membranes, Talanta 60 (2003) 395–404.
[24] N. Poklar, J. Fritz, P. Mazek, G. Vesnaver, T.V. Chalikian, Interaction of the pore-forming protein equinatoxin II with model lipid membranes: a calorimetric and spectroscopic study, Biochemistry 38 (45) (1999) 14999–15008.
[25] A.B. Hendrich, O. Wesolowska, K. Michalak, Trifluoperazine induces domain formation in zwitterionic phosphatidylcholine but not in charged phosphatidylglycerol bilayers, Biochim. Biophys. Acta 1510 (1–2) (2001) 414–425.
[26] S. Ali, S. Minchey, A. Janoff, E. Mayhew, A differential scanning calorimetry study of phosphocholines mixed with paclitaxel and its bromoacylated taxanes, Biophys. J. 78 (1) (2000) 246–256.
[27] D. Papahadjopoulos, M. Moscarello, E.H. Eylar, T. Isac, Effects of proteins on thermotropic phase transitions of phospholipid membranes, Biochim. Biophys. Acta 401 (3) (1975) 317–335.
[28] P. Garidel, A. Brume, Miscibility of phosphatidylethanolamine–phosphatidylglycerol mixtures as a function of pH and acyl chain length, Eur. Biophys. J. 28 (8) (2000) 629–638.

ANEXO II: Perturbaciones inducidas por péptidos sintéticos pertenecientes a la proteína estructural E2 del virus de la hepatitis G (GBV-C/HGV) en modelos de membrana: estudio de calorimetría diferencial de barrido

Cristina Larios, Josep Carilla, M.Antònia Busquets, M.Asunción Alsina e Isabel Haro

Departamento de Química de Péptidos y Proteínas, Instituto de Investigaciones Químicas y Ambientales de Barcelona, IIQAB-CSIC.
Departamento de Fisicoquímica, Facultad de Farmacia, Universidad de Barcelona.

Cristina Larios, Josep Carilla, M.Antònia Busquets, M.Asunción Alsina and Isabel Haro, *Perturbations induced by synthetic peptides belonging to the E2 structural protein of Hepatitis G virus (GBV-C/HGV) in lipid membranes: a differential scanning calorimetry study* J. Phys. IV, **113**, 31-34 (2004)

Resumen

En este trabajo se muestran las perturbaciones inducidas en liposomas multilamelares (MLVs) de diferentes composiciones fosfolipídicas (DPPC, DMPC, DMPC/DMPG) con péptidos que pertenecen a la proteína E2 del virus de la hepatitis G (GBV-C/HGV). Se realizó un estudio de calorimetría diferencial de barrido (DSC) con los MLVs en presencia de concentraciones crecientes de tres péptidos solapantes del GBV-C/HGV, E2(17-26), E2(12-26) y E2(7-26).

J. Phys. IV France **113** (2004) 31-34

DOI: 10.1051/jp4:20040007

Perturbations induced by synthetic peptides belonging to the E2 structural protein of hepatitis G virus (GBV-C/HGV) in lipid membranes: A differential scanning calorimetry study

C. Larios[1,2], J. Carilla[1], M.A. Busquets[2], M.A. Alsina[2] and I. Haro[1]

[1] *Institute for Chemical and Environmental Research (IIQAB-CSIC), Jordi Girona 18-26, 08034 Barcelona, Spain*
[2] *Department of Physical Chemistry, Faculty of Pharmacy (UB), Avda. Joan XXIII, s/n, 08028 Barcelona, Spain*

Abstract: In the present work we report the perturbations induced on multilamellar liposomes (MLVs) of different phospholipid composition (DPPC, DMPC, DMPC/DMPG) by peptides that belong to hepatitis G virus (GBV-C/HGV). A differential scanning calorimetry (DSC) study was performed with MLVs in the presence of increasing amounts of the three synthetic overlapping peptides from GBV-C/HGV, namely E2(17-26), E2(12-26) and E2(7-26) sequences.

1. INTRODUCTION

Lipid membranes are characterised by a main phase transition between an ordered gel state and a disordered liquid-crystalline phase. The investigation of the thermotropic changes in liposome behaviour in presence of peptide molecules provides useful data on the nature, depth of their interactions and localization within the membrane model [1,2]. In the present work the thermotropic behaviour of dipalmitoyl phosphatidylcholine (DPPC), dimyristoyl phosphatidylcholine (DMPC) and dimyristoyl phosphatidylcholine / dimyristoyl phosphatidylglycerol (DMPC / DMPG) multillamelar vesicles was studied by differential scanning calorimetry (DSC), in the absence and in the presence of increasing concentrations of three overlapping E2 (GBV-C/HGV) belonging peptides. A comparison of the effect of the 10-, 15- and 20-mer peptides on the thermotropic parameters of the lipid vesicles is reported.

2. EXPERIMENTAL PART

2.1 Chemicals

DPPC, DMPC, and DMPG were from Avanti Polar Lipids. Chloroform and methanol were from Merck and Carlo Erba, respectively. Water was double distilled. The buffer used was 5 mM HEPES pH 7.4.

2.2 Peptide Synthesis

The synthesis and analytical characterization of peptides will be described elsewhere. Crude peptides were purified by semi preparative HPLC. Purified compounds were characterized by analytical HPLC, amino acid analysis and electrospray mass spectrometry.

2.3 Differential scanning calorimetry (DSC) measurements

DPPC, DMPC, DMPC/DMPG (2/1) were dissolved in a chloroform/methanol (2:1) mixture and the lipid solution was dried under nitrogen. The samples were stored in a vacuum oven overnight at room temperature to eliminate the residual solvent. The lipid films were hydrated with Hepes buffer (5mM, pH 7.4). MLVs were obtained by vortexing the mixture, always keeping the temperature above the highest gel to liquid-crystalline phase transition of the sample. Multilamellar vesicles containing 6.10^{-4} mmol of DPPC or 3.10^{-3} mmol of DMPC and DMPC/DMPG (2:1) were analysed by DSC alone or with peptides at different lipid/peptide molar ratios (100/0, 98/2, 95/5, 90/10, 80/20, 70/30).
30 µl of MLVs were sealed in small aluminium calorimetry pans and submitted to heating/cooling cycles. Scans were carried out in a DSC 821E Mettler Toledo calorimeter, at heating and cooling rates of 5° C min^{-1}over the sample from 0°C to 60°C. The calorimeter was calibrated with Indium.

3. RESULTS AND DISCUSSION

In Table I is shown the effect on the thermotropic parameters of MLVs of different lipid composition after the addition of 20% of the three studied peptides. The chain melting transition (Tm) of DPPC and DMPC was not significantly affected by the peptides. This observation suggests that the interactions of the peptides with these phospholipids do not alter significantly the packing of hydrocarbon chains in the gel and liquid crystalline states [3]. The melting profile for the 2:1 binary mixture of DMPC/DMPG vesicles shifted to higher temperatures for the three peptides showing a higher displacement working with the E2(7-26) peptide sequence. The enthalpy (ΔH) at 20% molar ratio decreased in all cases showing a higher effect when the peptide chain length increased.

Table I. Thermotropic Parameters of the gel to liquid crystalline phase transition of DPPC, DMPC and DMPC/DMPG (2:1) MLVs were prepared in presence of different peptides, E2 (17-26), E2 (12-26) and E2 (7-26), at a 20% mol.

	Tm[a] (°C)	ΔH (KJ/mol)	$\Delta T_{1/2}$[b] (°C)
DPPC	41.5	34.8	0.7
E2(17-26)	41.7	27.9	1.1
E2(12-26)	41.6	25.5	1.0
E2 (7-26)	41.3	25.2	0.7
DMPC	23.4	18.8	0.7
E2(17-26)	23.6	17.2	1.3
E2(12-26)	23.2	11.2	1.8
E2 (7-26)	23.7	10.9	2.0
DMPC/DMPG(2:1)	23.8	20.5	2.2
E2(17-26)	24.4	16.7	2.6
E2(12-26)	25.8	13.0	4.3
E2 (7-26)	27.6	9.4	5.9

[a]Main transition peak temperature. [b]Temperature width at half-height of the heat absorption peak.

The width ($\Delta T_{1/2}$) of the transitions did not change significantly in DPPC MLVs, however in presence of DMPC and DMPC/DMPG the transition broadened with the incorporation of the peptides, showing a greater effect the E2(7-26) peptide sequence.
The different behaviour between the three peptides could be attributed to the length of the chain as well as the different net charge of the peptides that would favour hydrophobic interactions [4]. E2(17-26) and E2(7-26) are positively charged peptides, while E2(12-26) is neutral, so as expected, electrostatic interactions between the positive peptides and the DMPG have probably been established. Nevertheless, we expected more interaction in positively peptides, but E2(12-26) interacted in a higher extent than did E2(17-26). For this reason, we can conclude that electrostatic interactions seem to play a minor role for the mixing of MLVs composed of DMPC/DMPG with the peptides.
As an example, in figure 1 the DSC profiles of mixtures of E2(7-26) with DMPC/DMPG MLVs are shown. As can be observed, the endothermic peak of the main transition decreased with the incorporation of the peptide and broadened significantly. At 30% peptide concentration the chain melting transition disappeared.

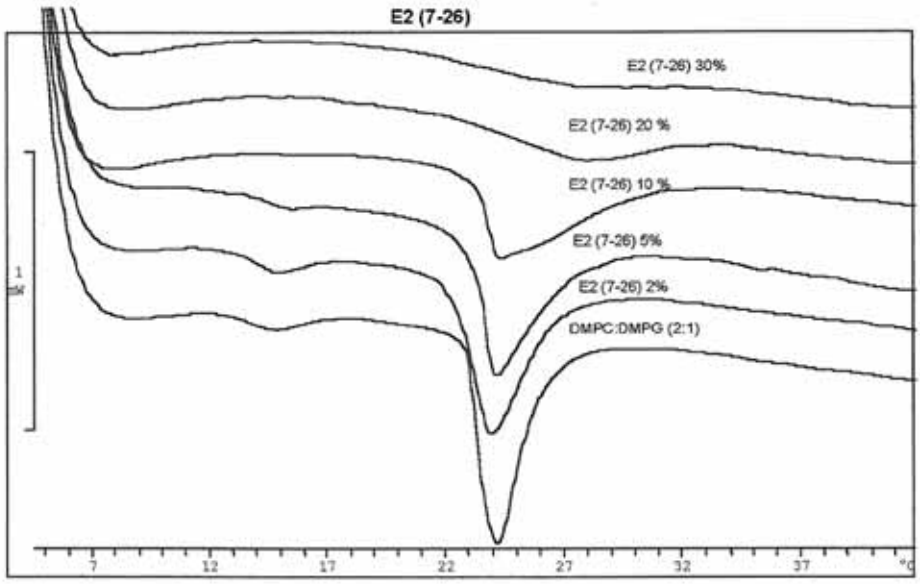

Figure1. DSC heating endotherms of DMPC/DMPG (2:1) MLVs were obtained in presence of 0, 2, 5,10, 20 and 30 mol % of E2 (7-26). The curves refer to the second scan in the heating mode at a temperature scanning rate of 5° C/min.

4. CONCLUSION

The main conclusion of this work is that the larger peptide chain the greater peptide-MLVs interaction measured by differential scanning calorimetry. Moreover, there is a stronger interaction with MLVs composed of DMPC/DMPG probably due to a combination of electrostatic and hydrophobic interactions. At high peptide/lipid ratios, the gel/liquid-crystalline phase transition disappears. This fact can be related with the perturbation and consequently the opening of the structure of MLVs caused by GBV-C/HGV peptides.

Acknowledgements

This work was funded by Grants BQU2000-0793-CO2-01/-02 from the Ministerio de Ciencia y Tecnología (Spain)

References

1. Pedersen, T.B., Sabra, M.C., Frokjaer, S., Mouritsen, O.G., Jorgensen, K., Chem. Phys. Lipids **113**, 83 (2001)
2. Shobini, J., Mishra, A.K., J. Colloid Interf. Sci. **240**, 24 (2001)
3. Rojo,N., Gómara,M.J, Busquets M.A., Alsina M.A and Haro I., Talanta **60**, 395 (2003)
4. P. Sospedra, C. Mestres, I. Haro, M. Muñoz, and M.A. Busquets, Langmuir **18**, 1231 (2002)

ANEXO III: Interacción con modelos de membrana de posibles péptidos de fusión de la proteína E2 del virus de la hepatitis G

Cristina Larios, Jordi Casas, M.Asunción Alsina, Conxita Mestres e Isabel Haro

Departamento de Química de Péptidos y Proteínas, Instituto de Investigaciones Químicas y Ambientales de Barcelona, IIQAB-CSIC.
Departamento de Fisicoquímica, Facultad de Farmacia, Universidad de Barcelona.

Cristina Larios, Jordi Casas, M.Asunción Alsina, Conxita Mestres and Isabel Haro, *Interaction with membrane model systems of synthetic putative fusion peptides derived from hepatitis G virus E2 Protein*, Luminiscence, **20**, 279-281, (2005).

Resumen

En este trabajo se seleccionaron dos secuencias derivadas de la proteína estructural E2 del virus de la hepatitis G [(E2(267-284) y E2(279-298)] mediante métodos semiempíricos y se sintetizaron mediante metodología en fase sólida. La capacidad de interaccionar y perturbar modelos de membrana fue analizada midiendo la penetración de los péptidos en monocapas lipídicas y realizando experimentos basados en la emisión de fluorescencia del triptófano. Se realizaron además experimentos de liberación de contenidos vesiculares de las sondas ANTS/DPX en liposomas zwiteriónicos a diferentes temperaturas.

Luminescence 2005; 20: 279–281
Published online in Wiley InterScience (www.interscience.wiley.com). DOI: 10.1002/bio.850

ORIGINAL RESEARCH

Perturbations induced by synthetic peptides from hepatitis G virus structural proteins in lipid model membranes: a fluorescent approach

Cristina Larios,[1,2] Jorge Casas,[1,2] Concepció Mestres,[2] Isabel Haro[1] and M. Asunción Alsina[1]*

[1]Department of Peptide and Protein Chemistry, IIQAB-CSIC, Jordi Girona 18–16, E-08034 Barcelona, Spain
[2]Unidad Asociada CSIC, 'Péptidos y Proteinas, Propiedades Fisicoquímicas', Department of Physicochemistry, Faculty of Pharmacy, Universitat de Barcelona, Avda. Joan XXIII s/n, E-08028 Barcelona, Spain

ABSTRACT: The name HGV/GBV-C remains as an acronym for hepatitis G virus (HGV) and GB virus-C (GBV-C), strain variants of this enveloped RNA virus independently but simultaneously discovered in 1995. Nowadays there is no evidence that it causes hepatitis in humans either during initial infection or after long-term carriage, but it has been recently related with HIV regarding the inhibition of progression to AIDS.

The overall genomic organization of HGV/GBV-C is similar to that of hepatitis C virus (HCV) and other members of the Flavivirus family in *Hepacivirus* genus. Although a stretch of conserved, hydrophobic amino acids within the envelop glycoprotein of HCV has been proposed as the virus fusion peptide, the mode of entry of GBV-C/HGV into target cells is at present unknown. In the present work, sequences derived from the structural E2-protein of HGV/GBV-C have been selected by means of semiempirical methods and then synthesized manually following solid-phase methodologies. Their ability to induce perturbations in model membranes has been analysed by measuring the penetration of such peptides in lipid monolayers and by a series of experiments based on tryptophan peptide fluorescence emission spectra. Besides, release of vesicular contents to the medium was monitored by the ANTS/DPX assay. The membrane destabilization properties of these peptides was found very related with the lenght of the sequence. Copyright © 2005 John Wiley & Sons, Ltd.

KEYWORDS: hepatitis G; fluorescence; hemolysis.

INTRODUCTION

Infection of eukaryotic cells by enveloped viruses requires the fusion of the viral and plasma or endosomal membranes. The interaction with the target membrane has been thought to involve a hydrophobic stretch of about 15 residues called 'the fusion peptide' (1).

The name 'HGV/GBV-C' is an acronym for hepatitis G virus (HGV) and GB virus-C (GBV-C), strain variants of this enveloped RNA virus independently but simultaneously discovered in 1995. Nowadays there is no evidence that it causes hepatitis in humans, either during initial infection or after long-term carriage. However, HGV has recently been related with HIV regarding inhibition of the progression of AIDS (2).

The overall genomic organization of HGV/GBV-C is similar to that of hepatitis C virus (HCV) and other members of the family Flaviviridae in the genus *Flavivirus*. Although a stretch of conserved hydrophobic amino acids within the envelope glycoprotein of HCV has been proposed as the virus fusion peptide, the mode of entry of HGV/GBV-C into target cells is at present unknown. Therefore, we have initiated the first steps towards the definition of putative sequences of HGV/GBV-C structural proteins that will be able to insert into the target cell membrane, causing local destabilization of the lipid bilayer, necessary to catalyse the fusion process.

In the present work, two overlapping sequences, E2(267–284) and E2(279–298), sharing a 6-mer common region, AGLTGG, derived from the structural E2-protein of HGV/GBV-C, have been selected by semiempirical methods and then synthesized manually following solid-phase methodologies. Their ability to induce perturbations in model membranes has been analysed by measuring the penetration of such peptides in lipid monolayers and by a series of experiments based on tryptophan peptide fluorescence emission spectra. In addition, the release of vesicular contents to the medium was monitored by ANTS/DPX assay (3).

MATERIALS AND METHODS

Peptides were synthesized manually following procedures previously described (4). Crude peptides were purified by semipreparative HPLC on a Perkin-Elmer chromatograph equipped with a C18-silica column. Both

*Correspondence to: M. A. Alsina, Unidad Asociada CSIC, 'Péptidos y Proteinas, Propiedades Fisicoquímicas', Department of Physicochemistry, Faculty of Pharmacy, Universitat de Barcelona, Avda. Joan XXIII s/n, E-08028 Barcelona, Spain.
Email: alsina@farmacia.far.ub.es

Contract/grant sponsor: Ministerio de Ciencia y Tecnología, Spain; Contract/grant number: BQU2003-0709-C02-01/02.

purified peptides were characterized afterwards by analytical HPLC amino acid analysis and electrospray mass spectrometry. Aliquots of lyophilized peptides were quantified by absorbance measured using an LKB-Biochrom Ultrospec II Spectrophotometer at 280 nm and then stored at –20°C until use.

Vesicle preparation

Lipid vesicles of different lipid composition were prepared for fluorescence measurements: DMPC and DMPC:DMPG (2:1) were separately dissolved in a chloroform:methanol (2:1, v/v) mixture and the lipid solutions were evaporated to dryness *in vacuo*. Then, the lipid films were hydrated with Hepes buffer (5 mmol/L, pH 7.4). Large unilamellar vesicles (LUVs) of DMPC and DMPC:DMPG (2:1 were prepared by 10 freeze–thaw cycles and extrusion of the lipid suspension using two 100 nm polycarbonate filters (Nucleopore, Pleasanton, CA) in a high-pressure extruder (Lipex, Biomembranes, Vancouver, Canada), above the transition temperature of the phospholipids. The phospholipid concentration was determined by phosphorus quantification, as previously described (5). The liposome size was measured by the sample diffusion coefficient by photon correlation spectroscopy (Coulter N4 MB, Luton, UK) up to a size of 100 nm.

Trp fluorescence titrations

Fluorescence experiments were performed on a Perkin-Elmer (Beaconsfield, UK) spectrofluorimeter LS50, using 1 cm path-length quartz cuvette. The excitation and emission bandwidths were set at 5 nm each, the wavelengths used being 285 and 340 nm, respectively. Emission fluorescence spectra were recorded for each peptide at 1 μmol/L in Hepes 5 mmol/L, pH 7.4, at room temperature, at increasing lipid:peptide ratios ranging from 1:25 to 1:1000. The suspensions were continuously stirred and they were left to equilibrate for 45 min before recording the spectrum. Fluorescence intensities were corrected for light scattering contribution by subtraction of the appropriate vesicle blank and a parallel lipid titration of N-acetyltriptophanamide (NATA).

Leakage assay

LUVs were prepared as described above. ANTS/DPX was encapsulated in LUVs when dried lipid films were hydrated in Hepes buffer, pH 7.4, containing 20 mmol/L NaCl, 12.5 mmol/L ANTS and 45 mmol/L DPX. In order to avoid spontaneous leakage, the osmolarity of both buffers was adjusted using a cryoscopic osmometer (Fiske 1–10). Afterwards, non-encapsulated ANTS/DPX was removed by gel filtration on a Sephadex G-75 column. ANTS/DPX leakage out of LUVs (100 μmol/L lipids) was measured after 30 min incubation at room temperature, 37°C and 43°C, in the same buffer as was used for fluorescence titration. Leakage was monitored by measuring the increase in ANTS/DPX fluorescence intensity at 520 nm, with an excitation of 355 nm and slit of 6 nm. Peptide:lipid molar ratios were 1:5, 1:10, 1:25 and 1:100. The percentage of leakage was calculated as: % leakage = 100 $(F - F_0)/(F - F_{triton})$, where F_0 is the fluorescence of LUV, F is the fluorescence intensity after incubation with the peptide, F_{triton} is the fluorescence intensity after addition of 10 μL 10% (v/v) Triton-100 solution (complete lysis of the LUV).

RESULTS AND DISCUSSION

Binding of the E2 envelope peptides to lipid vesicles: intrinsic emission fluorescence measurements

Peptide binding to lipid vesicles was investigated by intrinsic Trp fluorescence emission measurements. E2(279–298) and E2(267–284) peptides were incubated with lipid vesicles consisting of DMPC and DMPC:DMPG(2:1).

The maximal emission wavelengths (λ_{max}) of E2(279-298) and E2(267–284) were 359 and 362 nm, respectively, in buffer, thus indicating that the Trp is exposed to the medium (6). Addition of DMPC to E2(278–298) vesicles only decreased the fluorescence intensity, but had no effect on the λ_{max}. In contrast, the addition of mixed DMPC:DMPG shifted the λ_{max} to shorter wavelengths (blue shift of 23 nm; Fig. 1) and decreased the

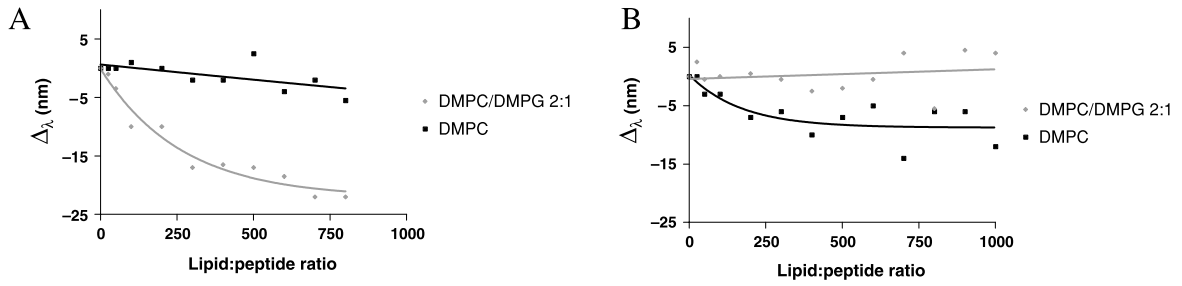

Figure 1. Shifts-partition isotherms corresponding to (A) E2(279–298); (B) E2(267–284).

fluorescence intensity. These values indicate that the Trp residue is located in a less polar environment, showing on interaction and partial penetration of the peptides into the hydrophobic tail of the bilayer without being completely buried (6).

The addition of DMPC to E2(267–284) slightly decreased the λ_{max} while the mixture DMPC:DMPG had no effect, probably due to the electrostatic repulsion between the anionic phospholipids and the negatively charged residues of the peptide.

Leakage assay

This study was performed in order to measure the ability of such peptides to promote the leakage from vesicles. We tested both peptides, but E2(279–298) seemed to induce a higher effect in bilayers than E2(267–284). In a first step, zwitterionic phosphocholines were tested, and especially the effect of temperature. E2(279–298) only induced a 3.5% ANTS/DPX leakage at peptide:lipid ratios between 0.01 and 0.2. Increasing the temperature of work to 37°C (beneath the transition temperature of the phospholipids used) increased the percentage of leakage to 15% at 0.2 ratio. The leakage above the melting temperature (43°C) was really increased, and at 0.2 molar ratio there was a complete lysis of the LUVs (Fig. 2).

Further studies with anionic and cationic phospholipids are being carried out to study the possible mechanism of the perturbations that such peptides promote in model membranes.

Acknowledgements

This work was funded by CICYT, Project BQU2003-0709-C02-01/02.

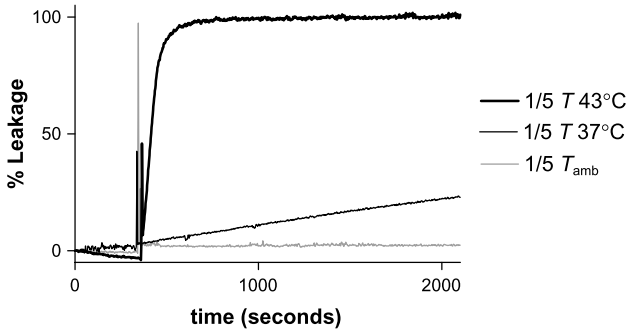

Figure 2. Leakage of ANTS/DPX from zwitterionic phosphatidylcholine-LUVs induced by E2(279–298) at a peptide ratio of 1/5 at different temperatures.

REFERENCES

1. Peisajovich SG, Shai Y. Viral fusion proteins: multiple regions contribute to membrane fusion. *Biochim. Biophys. Acta* 2003; **1614**: 122–129.
2. Polgreen PM, Xiang J, Chang Q, Stapleton JT. GB virus type C/hepatitis G virus: a non-pathogenic flavivirus associated with prolonged survival in HIV-infected individuals. *Microbes Infect*. 2003; **5**: 1255–1261.
3. Ellens H, Bentz J, Szoka FC. pH-induced destabilization of phosphatidylethanolamine-containing liposomes: role of bilayer contact. *Biochemistry* 1984; **23**: 1532–1538.
4. Rojo N, Gómara MJ, Alsina MA, Haro I. Lipophilic derivatization of synthetic peptides belonging to NS3 and E2 proteins of GB virus-C (hepatitis G virus) and its effect on the interaction with model lipid membranes. *J. Pept. Res.* 2003; **61**: 318–330.
5. McClare CW. An accurate and convenient organic phosphorus assay. *Anal. Biochem*. 1971; **39**: 527–530.
6. Wimley WC, White SH. Designing transmembrane α-helices that insert spontaneously. *Biochemistry* 2000; **39**: 4432–4442.

ANEXO IV: Miscibility and Langmuir studies of the interaction of the E2(279-298) peptide sequence of GBV-C/HGV with DPPC and DMPC phospholipids.

C. Larios, J. Jr. Miñones, I. Haro, M.A. Busquests y M.A. Alsina

Departamento de Química de Péptidos y Proteínas, Instituto de Investigaciones Químicas y Ambientales de Barcelona, IIQAB-CSIC.
Departamento de Fisicoquímica, Facultad de Farmacia, Universidad de Barcelona.
Departamento de Química Física, Facultad de Farmacia, Santiago de Compostela.

Cristina Larios, José Jr. Miñones, Isabel Haro, M. Antònia Busquets and M. Asunción Alsina, *Miscibility and Langmuir studies of the interaction of the E2(279-298) peptide sequence of GBV-C/HGV with DPPC and DMPC phospholipids,* en preparación

Resumen

En este trabajo se describe el comportamiento de un péptido sintético E2(279-298) que pertenece a la proteína estructural E2 del virus de la hepatitis G (GBV-C/HGV) en presencia de monocapas fosfolipídicas. Con tal de analizar la influencia de la longitud de la cadena en la interacción, se escogieron fosfolípidos zwiteriónicos, la dipalmitoilfosfatidilcolina (DPPC) y la dimiristoilfosfatidilcolina (DMPC). Se analizó también el efecto de la fuerza iónica utilizando agua y PBS en la subfase. La realización de las isotermas mixtas puso de manifiesto que había interacción entre el péptido y los fosfolípidos con un comportamiento no ideal. Las isotermas presentaron desviaciones respecto a la idealidad tanto en el area molecular como en la energía libre de Gibbs, y éstas fueron siempre mayores cuando se trataba del fosfolípido DMPC.

Miscibility and Langmuir studies of the interaction of the E2(279-298) peptide sequence of GBV-C/HGV with DPPC and DMPC phospholipids.

Larios, C.[1,2], Miñones J. Jr.[3], Haro, I[2], Busquets, M.A[1], Alsina M.A[1*].

[1]Associated Unit CSIC, Department of Physical Chemistry, Faculty of Pharmacy, University of Barcelona, Av. Joan XXIII s/n 08028 Barcelona, Spain;
[2]Department of Peptide & Protein Chemistry, IIQAB-CSIC, Jordi Girona 18-26 08034 Barcelona, Spain;
[3]Department of Physical Chemistry, Faculty of Pharmacy, University of Santiago de Compostela, Campus Sur, 15706 Santiago de Compostela, Spain.

Keywords: Brewster angle microscopy, mixed monolayers, HGV/GBV-C, lipid-peptide miscibility.

Title running head: E2(279-298) miscibility with DPPC and DMPC phospholipids.

Abstract

Mixed Langmuir monolayers of E2(279-298), a synthetic peptide belonging to the structural protein E2 of the hepatitis G virus (GBV-C/HGV), and phospholipids were studied performing pressure-area (π-A) isotherms together with Brewster angle microscopy (BAM). In order to analyze the influence of acyl chain length on the interaction, the chosen phospholipids were the zwitterionic dipalmitoyl phosphatidyl choline (DPPC) and dimyristoyl phosphatidyl choline (DMPC). Furthermore, the effect on ionic strength was measured using water and PBS substrate in the subphase. Analysis of the mixed monolayers indicated that the peptide interacted with both phospholipids with a non ideal behavior. The mean molecular area and the excess free energy of Gibbs deviated from ideality being greater for DMPC/E2 mixed monolayers. The presence of a higher ionic strength in the subphase resulted in an expansion of the isotherms at all compositions. The results indicate an interaction with a formation of complexes of peptide/phospholipids.

* To whom the correspondence should be sent.
Department of Physical Chemistry, Faculty of Pharmacy, University of Barcelona.
Av. Joan XXIII s/n 08028 Barcelona, Spain
Tel:+34934024553
Fax:+34934035987
aalsina@ub.edu

1. Introduction

The molecular mechanism involved in the fusion process between a virus and a cell is not at all known. Hepatitis G virus (GBV-C/HGV) belongs to the F*laviviridae* family. The viruses of this family have a fusion protein which has in its structure an internal fusion peptide (IFP). This IFP is the responsible of the beginning of the fusion events.

The internal fusion peptide of some members of the *flaviviridae* family, such as the tick-borne encephalitis virus is known (1). The sequences of the IFP between the viruses are different but they have similar features. The fusion peptides have a sequence approximately of 20 amino acids having an elevated content of alanine and glycine that gives plasticity to the sequence and hydrophobic amino acids (2). Furthermore, the IFP have a Proline in its sequence that seems to play an important role in the fusion process.

In a previous work we have selected the sequence (279-298) of the E2 protein of the GBV-C/HGV virus and we have performed biophysical assays such as fluorescence using phospholipid bilayers as model membranes. The results indicated a higher interaction with phospholipids negatively charged (3). Furthermore, we studied the secondary structure of this peptide with mimetic membrane solvents or with liposomes. E2(279-298) increased its secondary structure to an α-helix conformation when bounded to liposomes confirming the interaction of this model membrane.

In the present work, in order to better analyse the molecular interactions between the peptide and different phospholipids we have investigated by applying the Langmuir film balance technique, which uses the lipid monolayer at the air-water interface as model membrane (4). This is a simpler model than the bilayer model membrane, but it could confirm our results previously obtained. A first study at the air-water interface of E2(279-298) by surface pressure measurements showed that the peptide could be adsorbed at the air-water interface and penetration experiments demonstrated a higher interaction of the peptide with shorter acyl chain phospholipids, dimyristoylphosphatidylcholine (DMPC) instead of dipalmitoylphosphatidylcholine (DPPC). As these phospholipids are differentiated from each other by chain length, the structural difference of the lipids can have important effects on peptide-lipid interaction (5). Moreover, we have studied these interactions performing a microscopic study using the Brewster angle microscopy (BAM) to visualize the structure and morphology of the monolayers (6).

2. Materials and methods

2.1. Materials

DPPC (1,2-dipalmitoyl-sn-glicero-3-phosphocholine, C16:0) and DMPC (1,2-dimyristoyl-sn-glycero-3-phosphocholine, C14:0) were purchased from Avanti Polar Lipid, Inc. (Alabaster, AL, USA). E2(279-298) was synthesised by manual methodology as described previously (*1*). Chloroform and methanol were supplied by Merck. Water was purified by a Milli-Q system (Millipore Corp) (18.2 MΩ, pH 5.8). Phosphate buffered saline (PBS) was used for the subphase (16 mM $NaH_2PO_4 \cdot 12\ H_2O$, 81 mM Na_2HPO_4, 48 mM NaCl). Spreading solutions (0.3 mg/ml) were prepared by dissolving each compound in a chloroform:ethanol (2:1) solution. Mixed solutions were prepared from the respective stock solutions of the compounds. The number of molecules spread on subphase ($1{,}43 \cdot 10^{16}$ molecules) (Microman Gilson microsyringe, precision ± 0.2µl), was kept constant in all experiments.

2.2. Methods

Mixed monolayer π-A isotherms

A Langmuir-Blodgett trough (surface area 500 cm^2) equipped with a Teflon barrier, was used to record the surface pressure/area (π-A) isotherms (Nima 601, Coventry, U.K). Surface pressure was measured with the accuracy of ±0.1 mN/m using a Wilhelmy plate made from chromatography paper (Whatman Chr1) as the pressure sensor. After 15 min for solvent evaporation and equilibration, the monolayers were compressed at a rate of 25 $Å^2$/molec·min. Stability of the monolayers was assessed by compressing them, stopping the barrier at different pressures, and observing that no pressure decay occurred after 30 min. Each run was repeated three times and the accuracy of the measurements was 0.01 mm^2/ residue. Temperature was 21±1ºC.

Brewster angle microscopy

Brewster angle microscopy images and ellipsometric measurements were performed with BAM 2 Plus (NFT, Göttingen, Germany) equipped with a 30 mW laser emitting *p*-polarized light at 532 nm wavelength which was reflected off the air/water interface at approximately 53.1º (Brewster angle), as described by Rodriguez Patino et al.(7). The shutter speed used was 1/50s. In measuring the relative reflectivity of the film, a camera calibration was necessary. The intensity at each point of the BAM image depends on the local thickness and film optical properties. The expected signal at a certain angle is given by the Fresnel equation. A comparison of this theoretical intensity (Ip), with the measured gray value (G) should allow to generate a calibration curve Ip(G), relating any measured G value to it's corresponding Ip value. Provided that the camera and digitizer response is linear, this is a straight line:

$$I = |Rp|^2 = Cd^2 \qquad [1]$$

Where *C* is a constant, *d* is the film thickness and *Rp* is the *p*-component of the light. The reflected light intensity may be calculated from a single layer optical model as a function of the film thickness *d* and the refractive index *n.* This is the concept:

$$G \xrightarrow{\text{calibration}} Ip \xrightarrow{\text{opt. Model, } n} d$$

The lateral resolution of the microscope was 2 μm, and the images were digitalized and processed to optimise image quality; in our case corresponds to 768 x 572 pixels.

3. Results

3.1. Monolayers of pure components.

To better understand peptide-lipid interaction it is important to compare the isthoerms of the pure components with those of the lipid-peptide mixtures. In our case, isotherms of E2(279-298), DPPC and DMPC, have been extensively described in a previous work (submitted) and for that reason they are shown together with the lipid-peptide mixtures (Figures 1 and 2). Briefly, E2(279-298) the π–A curve for E2 monolayer spread on water exhibits three regions of different slope. At low surface pressures, the monolayer is in the liquid expanded state (LE) with a value of the compressional modulus, below 13 mN/m. Upon compression, the monolayer undergoes a phase transition at $\pi \approx 5$ mN/m, which is seen as a pseudo-plateau in the course of the compression isotherm and as minimum in the C_s^{-1}-π curve. This liquid expanded-liquid condensed (LE-LC) phase transition spans over the areas of approximately 196 $Å^2$/molecule to 124 $Å^2$/molecule. Beyond this transition, at low molecular areas, the surface pressure rises due to the increase of molecular packing. The monolayer reaches the LC state without a net collapse.

DPPC monolayer shows a (LE-LC) phase transition at about 5 mN/m also observed in the compressional modulus (C_s^{-1}) as a minimum (Figure 1). The thickness of the monolayer, d (nm) remains constant up to the LE-LC phase transition and then there is a jump of 0.5 nm. From this point the thickness increases monotonically until reaching a maximum at 2.5 nm (Figure 5).

DMPC monolayer does not present a LE-LC phase transition as confirmed by the compressional modulus that does not show a minimum (Figure 2). The thickness curve vs time shows a change around 900 s which doubles the thickness. From this point there is a consecutive increase of the thickness until 4 nm (Figure 6).

Isotherms of pure components in PBS appear at higher molecular areas as a consequence of an stabilization due to the increase in ionic strength (figure not shown).

3.2. Mixed monolayers

Mixed monolayers of DPPC with 0.2, 0.5 and 0.8 molar fraction of E2(279-298) are shown in Figure 1. DPPC LE-LC phase transition smoothes and shifts to higher molecular areas when 0.2 molar fraction (X_{E2}= 0.2) of E2(279-298) is added. The compressional modulus (inset figure 1) shows a minimum similar to the one observed for LE-LC phase transition of pure E2(279-

298). This could indicate that this phase transition of DPPC monolayer disappears with the presence of the peptide and that the LE-LC transition observed corresponds to the peptide. The influence of peptide on the shape of the pure DPPC isotherm is already noticed at the lowest peptide molar fraction added (X_{E2}= 0.2) as measured from the compressibility modulus. In this way, the observed maximum for DPPC characteristic of a LC state at 160 mN/m changes towards a LE phase (below 100 mN/m) (Inset Figure 1).

DMPC/E2(279-298) mixed monolayers give intermediate curves between the isotherms of the pure components (Figure 2). At X_{E2}=0.2 appears a phase transition at 12mN/m not present in pure DMPC monolayer, also similar to the phase change observed in the peptide monolayer. The isotherm at X_{E2}=0.5 is more expanded and similar to the pure peptide one. The curve obtained at the highest molar fraction of the mixed monolayer is more expanded than the curve of the peptide alone probably as a consequence of a strong interaction with the phospholipid at this molar fraction. Inset of Figure 2 shows the compressional modulus-surface pressure curves. DMPC monolayer has its maximum below 100mN/m indicative of the fluid character of the phospholipid. At x_{E2}=0.2 the minimum characteristic of the phase transition of E2(279-298) is observed. At higher molar fractions of the peptide, the curves are practically the same than the obtained for the pure E2(279-298).

As in the case of the pure components, isotherms of mixed monolayers of DPPC/E2 and DMPC/E2 shift to higher molecular areas when the substrate is PBS.

On another hand, film stability was studied by analyzing the values of the collapse pressure. At x_{E2}=0.2 DPPC isotherm does not show the typical collapse observed in pure DPPC being the final pressure similar to the observed for E2(279-298), indicating a decrease in stability. For DMPC/E2(279-298) mixed monolayers, collapse pressure is similar to the DMPC curve until x_{E2}=0.5. For x_{E2}=0.8 the isotherm breaks down at 22 mN/m in a similar way as observed for the pure peptide isotherm.

The DPPC/E2 and DMPC/E2 mixed monolayers reach a higher collapse pressure when they are in PBS buffer confirming a higher stability of the monolayers in this substrate.

The lift-off areas of the mixed monolayers increase with the molar ratio of the peptide incorporated into the monolayer, being greater for DMPC than for DPPC isotherms (Table 1). This increase could be due to intermolecular interactions between the peptide and the phospholipids.

The limiting area increases with the content of peptide in the subphase and as with all the other parameters, it is greater in PBS buffer (Table 2).

3.2. Miscibility and mixing ideality

In order to find out the kind of molecular interactions between the phospholipids and E2(279-298), we studied the miscibility of our peptide with the above described lipid compositions.

We can determine the miscibility at the interface with the collapse pressure of the mixed monolayers. Each pure component, peptide or phospholipid, have its own collapse pressure. If

the two components of the monolayer are miscible, then there is only one collapse pressure that is different of the collapse of pure components and depends on the composition (8).
The mixed isotherms had a tendency to breakdown before collapsing, in a different peptide content in the lipid compositions studied, being x_p>0.2 for DPPC and x_p>0.8 for DMPC. This tendency to break down before collapsing is a general trend in mixed monolayers, as well as the flattening of the monolayer when increasing the content of peptide (9).

The mixed monolayers can be treated as two-dimensional solutions. The ideality of mixing is another parameter to understand the behaviour of the monolayer. With this aim, the isotherms were analysed by examining the variation of the mean molecular area as a function of the molar fraction of the peptide at different surface pressures (Figure 3a and 3b). The dotted lines illustrate the additive relationship for the ideal system: $A_{12}=A_1X_1+A_2X_2$, where A_{12} is the mean molecular area of mixed monolayer, X_1 and X_2 are the mole fractions of components 1 and 2; A_1 and A_2 indicate molecular areas of pure components at the same surface pressure as A_{12} is determined. The variations for DPPC/E2(279-298) mixed monolayers are reported in the Figure 3a. At all molar fractions and surface pressures measured there are positive deviations, being greater at 5 mN/m. On another hand, DMPC/E2 mixed monolayers (Figure 3b) showed higher positive deviations or an expansion from additively of E2(279-298), being stronger at low surface pressures and at x_{E2}=0.8 molar fraction. These plots suggested miscibility with non ideal mixing of E2(279-298) in the monolayers (10). The deviations between DPPC/E2(279-298) monolyares are lower than the observed for DMPC/E2(279-298), it seems that the last composition has a higher degree of interaction (11).
At both mixed monolayers studied, the presence of PBS buffer increases the positive deviations at all molar fractions and pressures studied.

3.3. Stability analysis

The interaction between the two components and the thermodynamic stability of a mixed monolayer can be studied analyzing the excess free energy of mixing (?G^{EX}_M). The ?G^{EX}_M was calculated applying Goodrich (12) and Pagano (13) approaches.

$$\Delta G_M^{EX} = \int_{\pi\to 0}^{\pi} A_{12}\,d\pi - X_1 \int_{\pi\to 0}^{\pi} A_1\,d\pi - X_2 \int_{\pi\to 0}^{\pi} A_2\,d\pi \qquad (2)$$

where A_{12} is the mean molecular area per residue in the mixed film, A_1 and A_2 are the molar areas per residue in the pure films (in nm^2/molecule), X_1 and X_2 are the molar fractions of monolayer components 1 and 2, and π is the surface pressure in mN/m.

Figure 4 shows ?G^{EX}_M values at surface pressures within the range of 5-20 mN/m for the different lipid composition studied, as a function of E2(279-298) content in mixed monolayers. It can be seen that the stability of the monolayers is influenced by the acyl chain length of the lipid.

For DPPC monolayers, the larger acyl chains, there is a different behaviour depending on the surface pressure. Up to 10 mN/m, at almost all molar fractions of peptide there are negative excess free energies, thus indicating that the isotherms are more stable than the isotherms of pure components. At 20 mN/m there are positive excess, so at this pressure the isotherms are less stable. The excess free energy of DPPC mixed monolayers in PBS buffer induces higher negative deviations at 0.2 molar fraction but higher positive deviations at 20 mN/m at x_{E2}>0.2.

Different behaviour is observed for the shorter and fluid phospholipid DMPC. The mixed monolayer at X_{E2}=0.2 have the highest positive excess free energies, which are increased with surface pressures. This high positive values indicate that the interactions between the two components are lower than the interactions occurred between molecules of the same component in pure monolayers. At x_{E2}=0.5 and x_{E2}=0.8 the isotherms have lower values of excess, but always positive, indicating a repulsive interaction between the two components in the mixed monolayer. It is worth noting that, the stability of mixed monolayers increases with the more rigid phospholipid tested.

The excess free energy of DMPC mixed monolayers in PBS is similar than the obtained in water.

The increase in area/molecule and the positive excess in DMPC mixed monolayers inform us about the formation of complex clusters(14).

3.4. Curves of monolayer thickness (d) versus time (t)

The thickness observed in mixed monolayers of DPPC/E2(279-298) is quite similar to DPPC thickness alone until X_{E2}=0.5. At x_{E2}=0.8 the increase in thickness occurs before than the curves with lower content of peptide and is similar than the thickness present in E2(279-298).

The curve of mixed DMPC/E2(279-298) at x_{E2}=0.2 is quite similar than the observed for pure DMPC. At higher molar fractions, the thickness curves are more similar than the pure E2(279-298). In x_{E2}=0.5 and X_{E2}=0.8, there is a first change at 200 s where the thickness increases until 600 s (from 0.5 to 1.5 nm). Then, the curve is maintained constant and finally increases abruptly.

4. Discussion

DPPC-E2 and DMPC-E2 mixtures exhibit a phase transition at approximately 10mN/m and it is due to the presence of E2(279-298). This phase transition of the peptide is attributed to a higher structuration of the peptide in loops and tails. The fact that the phase transition appears at higher surfaces pressures than the observed for pure E2(279-298) is as a consequence of the interactions between the peptide and the phospholipids. These interactions between the components (DPPC/E2 and DMPC/E2) is also seen in the mean molecular area vs. molar fraction curve.

Both mixed monolayers induced a positive increase in area/residue being greater at 0.8 molar fraction and in DMPC mixed monolayers, indicating that the peptide is miscible and interact with both phospholipids with repulsive interactions. In the case of DMPC/E2(279-298) mixed monolayers the increase in the free energy of mixing at all compositions and pressures, together with the increase in molecular area indicates the presence of clusters in which the excess of molecules of phospholipid ($x_{E2}<0.5$) or peptide ($x_{E2}>0.5$) depends on the molar fraction of the peptide.

As it is described for mixed monolayers of DPPC/AmbB, positive deviations in molecular area is due to the reduction of the desorption of molecules of peptide due to the interaction with phospholipids being this interaction greater in mixtures of DMPC/E2.

Acknowledgements

This work was supported by Grants BQU2003-05070-CO2-01/02 from the Ministerio de Ciencia y Tecnología (Spain) and a predoctoral grant awarded to C. Larios.

Table 1. Lift off area (nm^2/molecule) for DPPC, DMPC, E2(279-298) and their mixtures in water and in PBS subphase.

Lipid/peptide content	Lift off area (nm^2/molec) water		Lift off area (nm^2/molec) PBS	
	DPPC	DMPC	DPPC	DMPC
1.0	1.3	1.2	1.04	1.1
0.8	1.5	2.2	2.3	2.2
0.5	2.4	3.0	2.9	2.9
0.2	3.3	3.5	3.3	3.3
0.0	3.5	3.5	4.0	4.0

Table 2. Limiting area obtained from p-A isotherms of DPPC, DMPC, E2(279-298) and their mixtures in water and in PBS buffer.

Lipid /Peptide content	Limiting area water		Limiting area PBS	
	DPPC	DMPC	DPPC	DMPC
1.0	0.6	0.7	0.5	0.5
0.2	0.6	0.6	1.0	1.1
0.5	0.6	0.5	1.0	1.2
0.8	1.0	1.0	1.3	1.2
0.0	0.9	0.9	1.0	1.0

Figure legends

Figure 1. π-A isotherms for DPPC/E2(279-298) mixed monolayers spread on water. Monolayer composition: ●, DPPC; ○, DPPC/E2(279-298) 0.8/0.2; ▲, DPPC/E2(279-298) 0.5/0.5; △, DPPC/E2(279-298) 0.2/0.8; ■, E2(279-298). Inset: The elastic compressibility modulus versus surface pressure (C_s^{-1}-π) for DPPC/ E2 (279-298) mixed monolayers.

Figure 2. π-A isotherms for DMPC/E2(279-298) mixed monolayers spread on water. Monolayer composition: ●, DPPC; ○, DPPC/E2(279-298) 0.8/0.2; ▲, DPPC/E2(279-298) 0.5/0.5; △, DPPC/E2(279-298) 0.2/0.8; ■, E2(279-298). Inset: The elastic compressibility modulus versus surface pressure (C_s^{-1}-π) for DPPC (a), DMPC (b) / E2 (279-298) mixed monolayers.

Figure 3. Plot of mean molecular area (A_{12}) vs the molar fraction of E2(279-298) in mixed films with DPPC (a) and DMPC (b) spread at aqueous subphase.

Figure 4. Excess free energies of mixing (AG^{EX}_M) as a function of mole fraction of E2(279-298) in mixed films with DPPC (a) and DMPC (b) spread at aqueous subphase at 2.5, 5, 10 and 20 mN/m.

Figure 5. The thickness (nm) vs time (s) of DPPC, E2(279-298) and DPPC/E2(279-298) mixed monolayers at 0.2, 0.5 and 0.8 spread on water.

Figure 6. The thickness (nm) vs time (s) of DMPC, E2(279-298) and DMPC/E2(279-298) mixed monolayers at 0.2, 0.5 and 0.8 spread on water.

Figure 1.

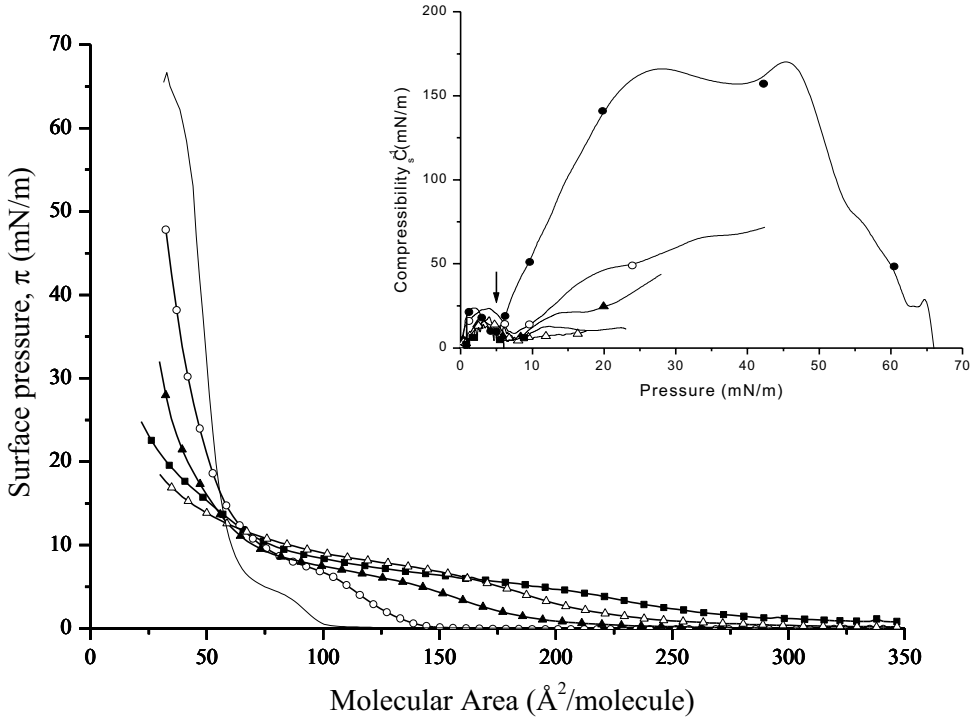

Figure 2.

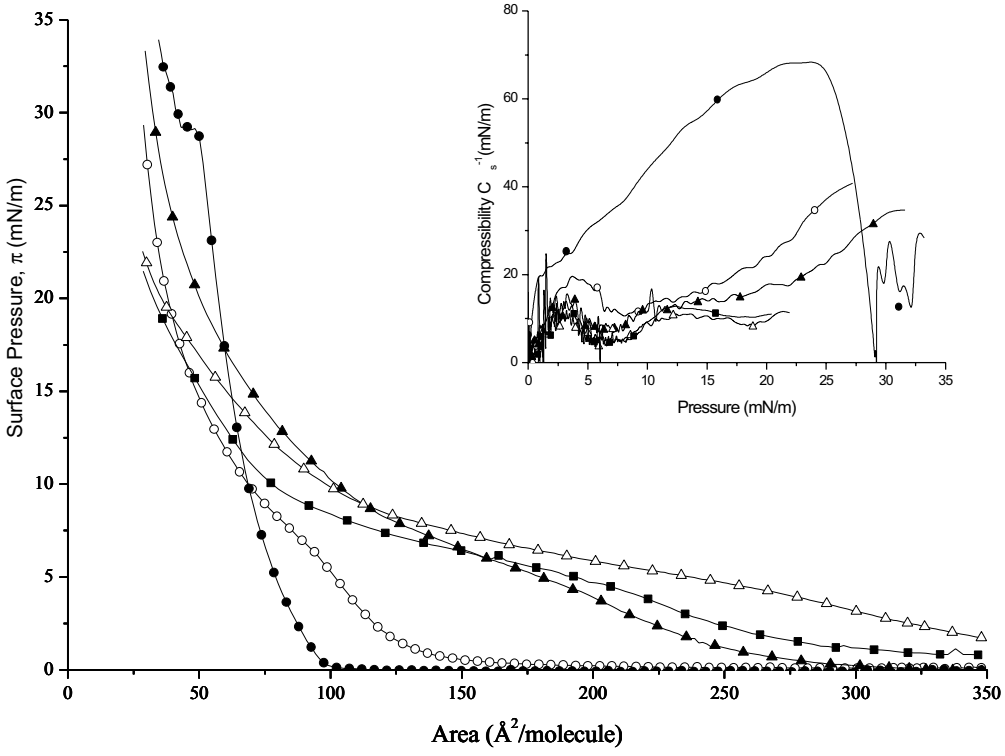

Figure 3.

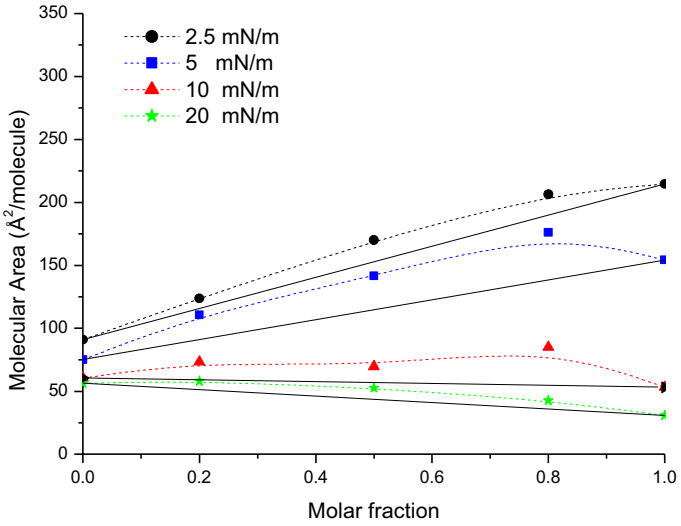
2.5 mN/m
5 mN/m
10 mN/m
20 mN/m
Molecular Area (Å²/molecule)
Molar fraction
0
50
100
150
200
250
300
350
0.0
0.2
0.4
0.6
0.8
1.0

a.

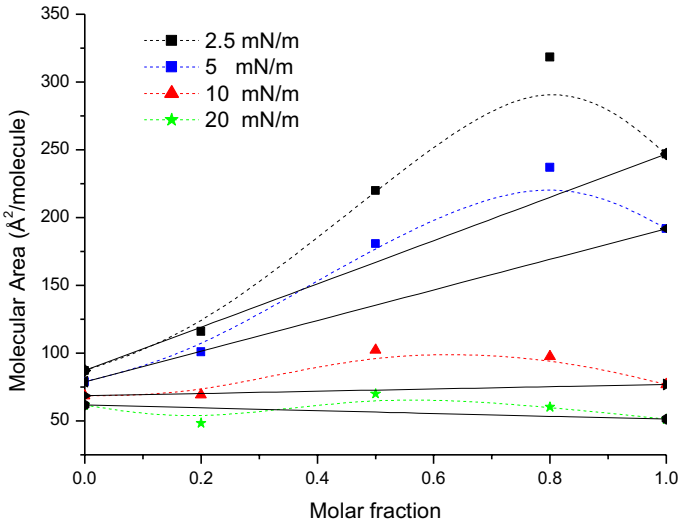
2.5 mN/m
5 mN/m
10 mN/m
20 mN/m
Molecular Area (Å²/molecule)
Molar fraction
50
100
150
200
250
300
350
0.0
0.2
0.4
0.6
0.8
1.0

b.

Figure 4.

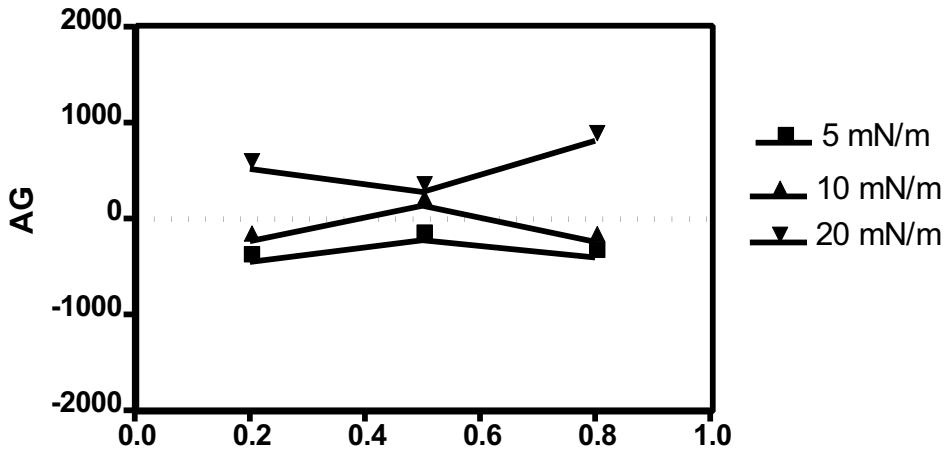
2000
1000
0
-1000
-2000
AG
0.0
0.2
0.4
0.6
0.8
1.0
5 mN/m
10 mN/m
20 mN/m

a.

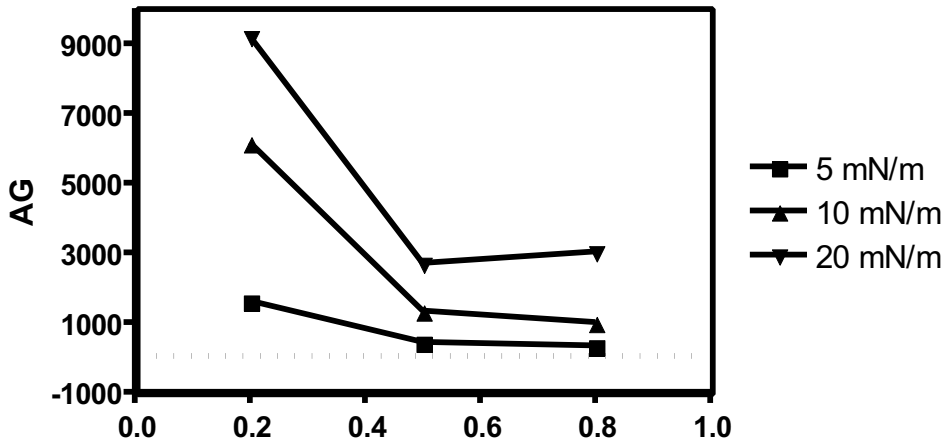
9000
7000
5000
3000
1000
-1000
AG
0.0
0.2
0.4
0.6
0.8
1.0
5 mN/m
10 mN/m
20 mN/m

b.

Figure 5.

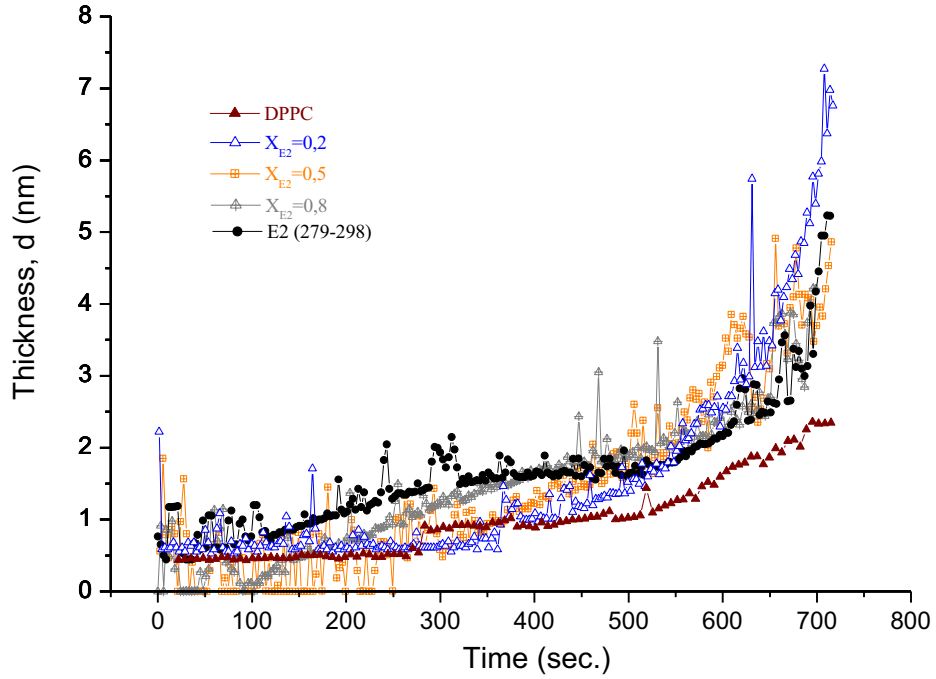

Figure 6.

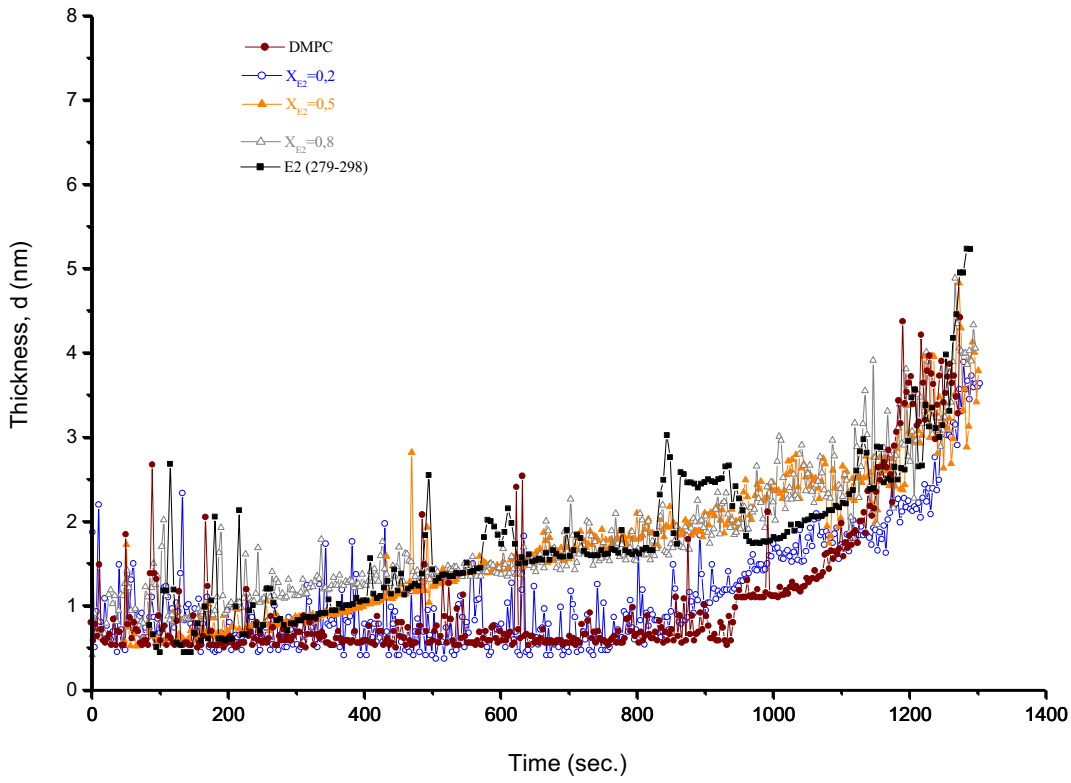

References

1. Allison, S. L., Schalich, J., Stiasny, K., Mandl, C. W., and Heinz, F. X. (2001) *J. Virol. 75*, 4268-4275.
2. Del Angel, V. D., Dupuis, F., Mornon, J. P., and Callebaut, I. (2002) *Biochem. Biophys. Res. Commun. 293*, 1153-1160.
3. Larios, C., Christiaens, B., Gómara M.J, Alsina, M. A., and Haro, I. (2005) *Eur. J Biochem. 272*, 2456-2466.
4. Maget-Dana, R. (1999) *Biochim. Biophys. Acta 1462*, 109-140.
5. Zhao, L. and Feng, S. S. (2004) *J Colloid Interface Sci. 274*, 55-68.
6. Volinsky, R., Kolusheva, S., Berman, A., and Jelinek, R. (2004) *Langmuir 20*, 11084-11091.
7. Rodriguez Patino J., Sánchez, C.C., Rodríguez Niño, M.R. (1999), Langmuir 15, 2484-2492.
8. Ambroggio, E. E., Separovic, F., Bowie, J., and Fidelio, G. D. (2004) *Biochim. Biophys. Acta 1664*, 31-37.
9. Maget-Dana, R. and Lelievre, D. (2001) *Biopolymers 59*, 1-10.
10. Gaines, G. L. Jr. (1966) *Insoluble monolayers at liquid-gas interfaces* Wiley, New York.
11. Taneva, S. and Keough, K. M. (1994) *Biophys. J 66*, 1137-1148.
12. Goodrich, F. C. (1957) *Proc. 2nd Int. Congress on Surface activity* Butterworth, London.
13. Pagano, R. E. and Gershfeld, N. L. (1972) *J Phys. Chem 76*, 1238-1243.
14. Matuo, Motomura, Matuura. (1981) Chem. Phys. Lipids, 28, 385-397.